On kinetics of small fatigue crack growth

Thesis

UNRESTRICTED

ON KINETICS OF SMALL FATIGUE CRACK GROWTH

A THESIS SUBMITTED TO THE
MATERIALS DISCIPLINE OF
THE OPEN UNIVERSITY
FOR THE DEGREE OF
DOCTOR OF PHILOSOPHY

Date of submission: 12 February 1996
Date of award: 9 May 1996

by XU-DONG LI

(B.Engng, M.Engng, Engneer, M.CSTAM)

February, 1996

ABSTRACT

This work presents a systematic model which predicts the kinetics of small fatigue crack growth in polycrystalline materials. The dislocation-based micromechanical model covers the entire process of small crack propagation from Stage I growth, Stage I to Stage II crack growth transition, Stage II growth, to the convergence into long cracks. Two fatigue thresholds that specifically relate to small fatigue crack propagation are also modelled.

Beginning with a detailed review of the historic development of small crack research, this work aims to (1) seek a unified parameter that can kinetically correlate small fatigue crack growth and then a unified small crack growth rate law; (2) establish a coherent micro-macro mechanical relationship that connects microscopic cracking in solids with bulk fatigue properties; and (3) predict fatigue crack growth thresholds on the basis of physical phenomena rather then any crack closure argument; (4) achieve overall *da/dN* predictions.

Typical 7×××series aluminium alloys plus a 8090 aluminium-lithium alloy were the materials selected for testing. Small fatigue crack growth and low-cycle fatigue tests were carried out to investigate small crack behaviour, typical crack growth characteristics, cyclic stress-strain responses and low-cycle fatigue properties. Fatigue damage mechanisms for both alloys were also studied using SEM and TEM for proper simulation of microstructure.

By proposing a microstructurally-affected-zone, this work considers a polycrystalline material to be build up of microstructurally-affected-zones. The local microstructure affecting crack front advancing is interpreted in terms of slip band orientation and crack tip orientation. The local microstructural effect is characterised by the microstructurally-affected-zone size ρ^*. By defining a process zone at the advancing small crack front, it is found that the process zone size d^* is a novel unified physical parameter that can be used to kinetically correlate small fatigue crack growth rates. Further, a micro-macro mechanical relationship associated with growth of small fatigue cracks is established that describes the coherent connection of microscopic plastic deformation to local microstructure. The Stage I to Stage II crack growth transition is modelled to be due to the severe blockage to small fatigue crack growth caused by barriers. By using a pile-up simulation of continuous dislocations, the blockage is modelled as dislocations against grain boundaries. The transition crack size $2a_0$ is thus determined using the function $2a_0 = f(\varphi, \Phi, \sigma, l_0)$. As a result, a unified dislocation-based micromechanical model is established that predicts kinetics of overall small fatigue crack growth whose notable advantage is that the microscopic small crack growth can be directly predicted using macroscopic bulk fatigue properties without tedious fatigue tests for each load level.

Modelled are two fatigue threshold parameters, K^*_{max} and ΔK^*_{th}, that are coherently related to fatigue limit and describe fatigue threshold behaviour at any load ratio without invoking crack closure. The fatigue limit is determined in terms of a critical condition at which a fictitious microcrack associated with dislocation pile-up just begins to propagate. These two fatigue threshold parameters constitute two novel fatigue criteria that demarcate safety zones and predict fundamental fatigue threshold curves at any load ratio. Microstructure is incorporated into the model to account for its effect on fatigue threshold behaviour. Quantitative assessment of the two fatigue criteria requires only knowledge of the conventional material properties. The convergence of small fatigue crack growth into long fatigue crack growth is also modelled in terms of Lankford's criteria by using a simulation where the controlling microstructural dimension ρ^* rather than the grain size controls small to long crack growth transition. All model predictions in this work are in good agreement with experimental results. Generally, a series of computer-assisted simulations for predicting realistic small crack growth are developed which lays a foundation for fatigue lifetime predictions that are based on fatigue crack growth tolerance techniques.

ACKNOWLEDGEMENTS

The present research work for PhD was supervised by Dr. Lyndon Edwards and then further supervised by Prof. W. J. Plumbridge. Prof. W. J. Plumbridge made great effort and spent considerable time doing the final revision of the thesis. I would like to express my sincere gratitude to both supervisors for their supports throughout this research work. Without those supports in computing facilities and finance, it was difficult for me to get through this thesis and demonstrate research results in two international conferences. I am also indebted to Prof. W. J. Plumbridge for the provision of laboratory facilities.

I would like to offer my deep gratitude to Mr. Jim Moffatt, Mrs. Naomi Williams for their patient and careful instructions in using fatigue testing facilities as well as Electron Microscopes throughout this research work.

I also deeply appreciate the generous technical assistance supplied by all the members of research laboratories and workshop at the Materials Discipline, particularly to Mr. Peter Ledgard, Mr. Richard Black, Mr. Gordon Imlach and Mr. John Bandy for wonderful assistance that they did for me over past three years. Of particular thanks go to Mr. John Bandy and Alistair Cree for teaching me English.

Many thanks to Jennifer Seabrook and Tracey Bartlett for their warm receptions that I really felt every time when I ask them for help.

It is worth pointing out here that I do value the motivated academic environment that I experienced in the Materials Discipline to openly hold technical discussions or exchange research opinions which were much helpful in freshening mind for this research work.

Finally, I wish to express my heart felt gratitude to my wife, Li Sun. It was her persistent support and encouragement in spirit over past three years that get me over the difficult period in my life. Without her precious love, I was hardly to concentrate attention to this thesis.

Xu-Dong Li, (February, 1996)

PREFACE

This thesis is submitted for the degree of doctor of philosophy of The Open University. It is an accounted of the research program performed in the Materials Discipline of the Faculty of Technology between August 1992 and August 1995. This research work reported here is original and has been performed without collaboration. None of this work has been submitted for a degree or other qualification at this or any other university. Where the work of other authors has been included in the text, this has been acknowledged and its source is given in the References at end of the thesis. Some parts of the work conducted for this thesis were presented as conference papers to two international conferences. Following six articles have been published or accepted for publication that draw from the research work and other studies. These articles deal with small fatigue cracks, along with fatigue crack growth threshold in a systematic manner and show analyses together with engineering approaches in a different way.

(1) Xu-Dong Li and L. Edwards, Analysis Of Short Crack Growth From Macroscopic Fatigue Properties. *Theoretical & Applied Fracture Mechanics,* **23** 187-198 (1995)

(2) Xu-Dong Li, Dislocation Pile-Up Model Of Fatigue Thresholds For 2024- And 7075-Alike Aluminium Alloys. *Theoretical & Applied Fracture Mechanics,* **24** 165-179 (1996)

(3) Xu-Dong Li, Micromechanical Model Of Stage I To Stage II Crack Growth Transition For Aluminium Alloys. *Theoretical & Applied Fracture Mechanics,* **24** 217-231 (1996)

(4) Xu-Dong Li and L. Edwards, Theoretical Modelling Of Fatigue Threshold For Aluminium Alloys. *Engineering Fracture Mechanics,* **54** 35-48 (1996)

(5) Xu-Dong Li, On Upper Limit For Small Crack Growth. *Engineering Fracture Mechanics,* accepted for publication.

(6) Xu-Dong Li, On Kinetics Of Small Fatigue Crack Growth. *Engineering Fracture Mechanics*. accepted for publication.

Before rushing to contents of the thesis straitforwards, I connect in my mind a series of factors that affect scientific research. Some factors seem inevitable to be concerned when someone reads the thesis along with cited publications. What is the relevance of conducting experiment with model developing? As the results of my knowledge and experienced facts in the past research period, I have been aware of the relevance that I would like to expressed it in following three paragraphs in this preface. I dedicate them to all readers to this thesis before they are starting each chapter or reading other relevant publications.

If you show people a model, nobody really believes you before your explanations except yourself. If you show people an experiment, nobody really knows how you did it from your displayed experimental data except yourself.

Theoretical predictions may lead you to fantasy because they might ignore vital facts while displayed experimental data may lead you to misconception because they might have concocted the facts.

A fantasy may occur when someone tries to illustrate consistency of developed theories with experimental data. On the contrary, a paradox may occur when someone attempts to prove consistency of experimental data with predetermined theories.

List Of Tables

List Of Figures

List Of Symbols

$\tilde{a}$	crack depth;
a	half surface crack length;
a_o	half transition crack length at which small fatigue crack shifts from Stage I growth to Stage II growth;
a_{th}	half crack length at fatigue threshold;
A_p	plastic zone area;
A_1, A_2, A_3	constants;
b	Basquin fatigue strength exponent;
B_1, B_2	constants;
B	Burger´s vector;
c	Coffin-Manson fatigue ductility exponent;
CTOD	crack tip opening displacement;
D	grain size;
$\frac{da}{dN}$	fatigue crack growth rate;
d^*	process zone size;
$(d^*)_o$	process zone size at Stage I to Stage II crack growth transition;
E	Young´s modulus;
G	shear modules;
ΔJ	cyclic range of J-integral;
K'	cyclic strength coefficient;
K_T	stress concentration factor;
ΔK	stress intensity factor range;
ΔK_e	strain intensity factor range;
ΔK_{eff}	effective stress intensity factor range;
ΔK_{effth}	effective range of stress intensity factor at fatigue threshold;
K_{max}	maximum stress intensity factor;
K_{min}	minimum stress intensity factor;

ΔK_{con}	stress intensity factor range corresponding to the convergence of small into long fatigue crack;
$[K_{max}]_{con}$	maximum stress intensity factor corresponding to the convergence of small into long fatigue crack;
K_{op}	stress intensity factor corresponding to crack tip opening loading;
K_{opmax}	stress intensity factor corresponding to crack tip maximum opening loading;
ΔK_t	stress intensity factor range at transition point from small crack growth into long crack growth;
ΔK_{th}	fatigue threshold stress intensity range;
K_{th}^{max}	maximum stress intensity at fatigue threshold;
ΔK_{th}^{*}	a parameter that is a critical value in cyclic amplitude;
K_{max}^{*}	a parameter that is a critical maximum stress intensity;
l_0	pile-up length of dislocations ahead of a growing small fatigue crack;
L	length of slip band;
n'	cyclic strain hardening exponent;
N_f	fatigue cycles to failure;
P	applied load;
r_p	plastic zone size;
R	load ratio;
R_p	radius of the plastic zone ahead of a fatigue crack tip;
R^*	a defined ratio to demarcate low-R region from high-R region;
CTSD	crack tip sliding displacement;
u	displacement in x–direction;
v	displacement in y–direction;
Y	crack shape–related parameter;
υ	Poisson's ratio;
δ	opening displacement;
Φ	an angle subtended by the slip plane with the crack plane;
ε_f'	fatigue ductility coefficient;
ε_{max}	maximum strain;

ε_{min}	minimum strain;
$\Delta\varepsilon$	total strain range;
ε_a	strain amplitude;
$\Delta\varepsilon_e$	elastic strain range;
$\Delta\varepsilon_p$	plastic strain range;
ε_{th}	strain at fatigue threshold;
$\Delta\gamma$	shear strain amplitude;
ΔE_p	generalised strain amplitude for the plastic strain range and the shear strain amplitude respectively;
η	deformation in a yielded zone just at crack tip;
φ	an angle between loading direction and crack plane;
θ	an angle between the point of interest and the major axis of the ellipse;
β	an angle between the point of interest in plastic zone and the crack plane;
ρ	crack tip radius;
ρ^*	elementary block size/microstructurally-affected-zone size;
σ	stress;
σ_a	stress amplitude;
σ_f'	cyclic fracture stress;
σ_m	mean stress;
σ_{max}	maximum stress;
σ_{min}	minimum stress;
σ_y	yield strength;
σ_y'	cyclic yield stress;
τ	shear stress;
τ_{comp}	an appropriate comparison stress greater than the applied stress τ;
τ_{Li}	shear stress corresponding to fatigue limit;
ω	triaxiality factor.

Chapter 1 INTRODUCTION

Fatigue damage in polycrystalline materials is strongly associated with microcrack growth. Fatigue design of engineering components entails evaluation of fatigue damage accumulation. As we have known, linear fatigue damage accumulation rule (Miner rule) is widely adopted by industries today for fatigue damage tolerance design. However, Miner's rule was established on a base of intuitive sense that counts fatigue cycles to evaluate fatigue damage in materials. Although some approximate remedies were proposed by extending the linear fatigue damage accumulation rule to double linear fatigue damage accumulation rule and then to triple linear fatigue damage accumulation rule to correct inaccuracy, these rules fail to account for load sequencing effects and fail to properly explain fatigue damage mechanism because Miner's rule is totally empirical. People have no option but to use Miner rule. Therefore, replacing the linear fatigue damage accumulation rule by crack growth tolerance rule seems an attractive way to properly measure fatigue damage in materials.

Basic ideas for fatigue research of small crack propagation have been established over the past twenty years. Most technical advances and academic achievements (including fatigue data, mechanisms, models, application of statistics) in this mechanics-material overlapping research field of small fatigue cracks successfully impressed people within last fifteen years. Hundreds and hundreds of experimental data of a — N characterisation curves have been well established that cover a wide range of metal materials, and metal-matrix

composites. However, in recent years, financial investments on further development of research of small fatigue cracks are reducing because industries seem to take such an attitude that small crack research may be a high risk business without economic outcomes even though industries still have engineering demands to improve fatigue damage assessment method to insure safety of crucial components for the purpose of structural integrity. The basic cause for this situation can be frankly outlined that today's research achievements in the domain of small fatigue cracks are still unable to properly predict fatigue lifetime for engineering components in service conditions. This is due to the reality that several fundamentals of engineering significance regarding small fatigue cracks are still in the vague. Therefore, any investment may be in danger, being put in vain unless these fundamental problems are cleared.

It is well known that ΔK (or ΔK_{eff}) is an effective physical parameter to correlate long fatigue crack growth. The Paris law in the form of $\frac{da}{dN} = A_{long}\Delta K^m$ is applicable to most engineering materials. A_{long} is a material constant dependent on loading rate but independent of load levels. In the case of small fatigue cracks, almost all proposed crack growth rate laws can be generally simplified as $\frac{da}{dN} = A_{small}\,\Pi^M$ in which Π stands for a physical parameter (or a term containing physical parameters) to correlate small fatigue crack growth and M is a constant. The crack size a, the J-integral, the plastic displacement δ_p, the modified stress intensity factor range ΔK_ε, or the combinative parameter of stress item σ with crack size item a were usually taken as the physical parameter.

However, using these parameters fails to describe the evolution of the plastic zone associated with a growing small fatigue crack and fails to take account of the local effect of microstructure. Moreover, the material-related quantity A_{small} is not a constant but depends upon load levels which has to be determined from each fatigue test for a given load level. Additionally, some parameters values, that relate to microstructural dimensions, used in those laws seem to be either adjustable or fixed to a specified grain size without reflecting the kinetic growth of small fatigue cracks. This makes the application of those crack

growth laws more difficult. In summary, people did not find an appropriate physical parameter, such as ΔK for long fatigue cracks, for small fatigue cracks.

- There is still a lack of a sound physical parameter that can be used to correlate small fatigue crack growth.

- There is still a lack of a unified model to predict small fatigue crack growth kinetics.

These are two main objectives that the present work tries to achieve. Despite the fact that small fatigue crack growth behaviour has been studied for the past twenty years, there has been little effort to connect microscopic cracking behaviour with macroscopic bulk fatigue properties. The ability to use simple material parameters to predict small crack growth would be of considerable engineering utility and thus one of purposes of the present research work is to reveal the coherent connection of microscopic crack growth with macroscopic bulk fatigue behaviour.

As recognised widely, fatigue cracks can be generally classified into three regimes: (1) *microstructurally small fatigue cracks* (Stage I cracks); (2) *physically small fatigue cracks* (Stage II cracks); (3) *long fatigue cracks* as shown in Figure 1-1. There are two transitions between the three regimes, *i.e.*, (1) Stage I to Stage II crack growth transition; (2) convergence of small fatigue crack growth into long fatigue crack growth.

To predict kinetics of small fatigue crack growth, one really needs a systematic simulation/model that covers the whole process of small crack propagation because small crack growth constitutes most of the fatigue lifetime of polycrystalline materials. In addition, two threshold phenomena, *i.e.*, *a microstructural fatigue threshold* and *a mechanical fatigue threshold*, have been recognised for polycrystalline materials. The microstructural fatigue threshold reflects an intrinsic resistance of polycrystalline materials to small fatigue crack propagation while the mechanical fatigue threshold reflects an inherent mechanical resistance of polycrystalline materials to fatigue crack growth. Therefore, one has to model/predict the two thresholds in favour of fatigue life predictions.

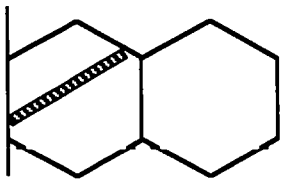

STAGE I SMALL CRACK

a/r_p RATIO LOW (< 1)

$2a$ < 1 grain or a few grains

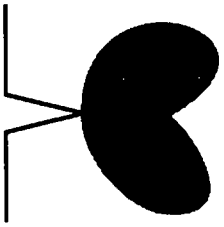

STAGE II SMALL CRACK

a/r_p RATIO INTERMEDIATE VALUES

$2a \lesssim 10$ grains

Long Crack

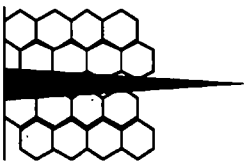

MODE I (TENSILE) CRACK

a/r_p RATIO HIGH ($\gg$ 1)

$2a$ > 100 grains

Figure 1-1 Three Distinct Regimes Of Microstructurally Small Cracks, Physically Small Cracks And Long Cracks

Given the wealth of published information on small fatigue crack research in the past, the author of this thesis has realised that it is no longer conventional material testing results of small fatigue crack growth that one really needs, but critically, the methodology to simulate realistic small fatigue crack propagation. Challenged by the kinetic nature of small fatigue crack growth, this thesis describes novel approaches in a comprehensive way which would enable a perceived improvement in predicting small fatigue crack growth kinetics. Therefore, the present work attempts to:

- Simulate microstructure of polycrystalline materials;
- Seek a unified physical parameter that can correlate small fatigue crack growth rates;

- Find a coherent micromechanical relationship linking microscopic small fatigue crack growth with macroscopic bulk fatigue behaviour;
- Model Stage I to Stage II crack growth transition that is related to microstructural barriers to small crack propagation;
- Model/predict fatigue crack growth threshold ΔK_{th};
- Predict kinetics associated with Stage I, Stage II small fatigue crack growth and the convergence of small crack growth into the long crack growth.

The following chapter provides a detailed survey of small fatigue crack research conducted in the past. The contents of the chapter cover most aspects of historical developments relating to small crack growth which are reviewed in detail. Various models developed in the past are outlined either theoretically or graphically and some techniques used to quantify small crack behaviour are introduced.

Chapter 3 introduces materials used in relevant fatigue tests, heat treatment for the materials before testing, specimens, polishing techniques for specimen preparation and microstructure examinations of the specimens. Experimental procedures for different types of fatigue tests are also detailed in the chapter.

Chapter 4 outlines experimental observations and fatigue test results of small crack growth in 7××× aluminium alloys. Microcrack initiation under different circumstances, subsequent irregular growth behaviour of small fatigue cracks, as well as the convergence of small crack growth into the long crack growth is described respectively in detail. This chapter explains observed results, analyses and possible factors causing discrepancies in small crack growth rates.

Experimentally-determined low-cycle fatigue properties, obtained through testing 7150-T651 aluminium alloy and 8090-T6 aluminium-lithium alloy, are displayed in Chapter 5.

Observed cyclic deformation behaviour and fracture characteristics associated with the two alloys are carefully studied and illustrated by way of SEM and TEM observations.

Chapter 6, Chapter 7, Chapter 8 and Chapter 9 constitute the core content of this thesis. Kinetic growth of small fatigue cracks is thoroughly analysed in Chapter 6, Chapter 7, Chapter 9 and then modelled using elastic-plastic fracture mechanics and dislocation theories. Simulation of microstructure for polycrystalline materials, proposing a unified physical parameter to correlate small fatigue crack growth along with predictions of two crack growth transitions are the prominent features of the thesis. Chapter 8 presents in detail novel model predictions of fatigue crack growth thresholds by using two fatigue threshold criteria. This chapter demonstrates an idea/method of modelling the fatigue crack growth threshold in terms of the physical phenomenon rather than crack closure arguments. A series of conclusions is drawn from these chapters.

Micromechanical modelling of the whole process of small fatigue crack growth kinetics will be the emphasis of this thesis. Relevant fatigue tests, fractography of fatigued specimens, along with microstructure examinations, play such a role to provide not only necessary material information but also collateral evidence for proper microstructure simulations and modelling kinetics of small fatigue crack growth.

Chapter 2 REVIEW OF SMALL FATIGUE CRACKS

2.1 INTRODUCTION

A large number of experimental investigations on the behaviour of small fatigue cracks have been carried out over the past twenty years. Despite the fact that loading can change deformation response of a metal and its microstructure, metal fatigue damage can now be equated to crack length and the rate of damage accumulation to the rate of fatigue crack growth [1]. Small fatigue cracks typically exhibit the following anomalous behaviour when compared with conventional long fatigue cracks:

- Small fatigue crack growth can occur even when the value of stress intensity factor is below the long crack fatigue threshold ΔK_{th};
- Small crack growth rate is higher than that of long cracks at the same driving force;
- Small fatigue crack propagation is affected by local microstructure;
- Small crack growth can dominate fatigue lifetime of many structures and components.

These features are schematically summarised and interpreted in Figure 2-1.

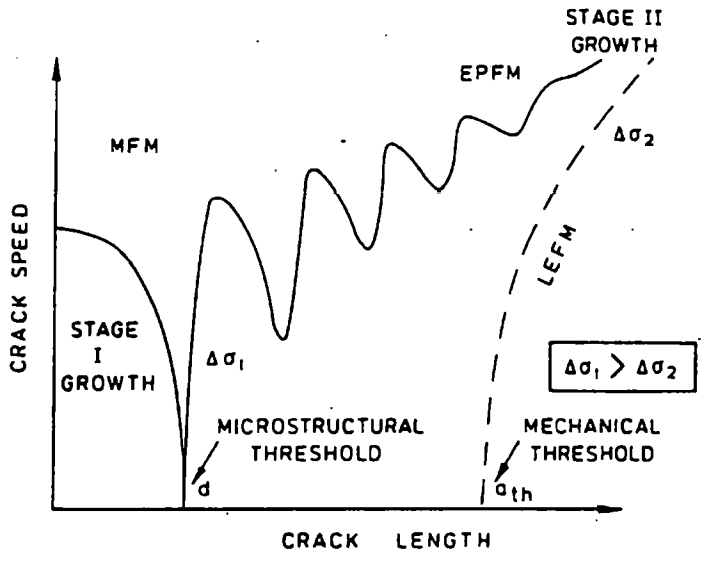

Figure 2-1 A Schematic Presentation Of Small Fatigue Crack Nature, Crack Propagation Features And Possible Crack Arrest [1]

2.2 WHY ARE SMALL FATIGUE CRACKS SO IMPORTANT

Fatigue cracks have been classified into three types [2-4]: (1) microstructurally small fatigue cracks in which the crack length is of same order of a microstructural dimension, *i.e.*, Stage I crack; (2) physically small fatigue cracks that typically have crack lengths in the range of 50-500 μm; and (3) long fatigue cracks where the crack length is typically longer than 0.5 mm and which can be well described by linear-elastic fracture mechanics analysis.

The use of LEFM has been questioned for small cracks. Experiments on the growth of small fatigue cracks have clearly shown that small fatigue cracks grow at rates that are higher than those of long fatigue cracks. therefore, for small cracks, similitude breaks down and the crack growth rate is no longer a unique function of the stress intensity factor. The reasons for this are:

(1) Breakdown of microstructural similitude When the crack length is on the order of the material microstructure, e.g. the grain size, plastic deformation near crack tip is

influenced very much by local microstructure, e.g., grain boundaries may block small crack growth.

(2) Breakdown of the mechanical similitude When the crack tip plastic zone size is large compared with its length, that is, the crack tip yielding is of large scale, the use of ΔK is questionable.

Knowledge of the smallest cracks to which LEFM is applicable is important for many engineering applications. J. Lankford [5-6] concluded that the growth rates of small and long cracks merge when the plastic zone size is equal to a relevant microstructural dimension.

Fast, irregular growth of small fatigue crack in smooth specimens has been reported for many metals including Al-alloys [7]. Plastic deformation at the crack tip is assumed to occur as one or two localised slip bands that are inclined to the direction of the applied stress and are confined. Accelerations and decelerations of crack growth rate are the result of the interaction of the crack tip plastic zone with barriers to plastic flow (*i.e.*, grain boundaries). Initial accelerated growth occurs when the crack is smaller than the grain size or barrier spacing. As the crack approaches the grain boundary or barrier the rate of propagation is reduced if the barrier is strong or the slip systems in the neighbouring grains are unfavourably oriented. Whether or not a grain boundary constitutes a barrier depends upon the relative misorientation [5], *i.e.*, upon how hard it is to get a crack to grow in the next grain. In the case of higher barrier strength or unfavourable misorientation, crack growth may be critically reduced leading to crack arrest. On the other hand, if the barrier is easily overcome or there is little mismatch, then growth continues unhindered. It should be noted that retardation in crack growth need not occur only at the first grain boundary encountered. A statistical survey of the positions of microcracks growing in 7075-T6 [8] showed that on average, crack tips were clustered around the first three grain boundaries crossed by each crack.

Small fatigue cracks nucleated in smooth specimens initially grow in a very irregular manner because of microstructural inhomogeneities. Actually, it is not realistic to expect continuous crack growth right after initiation, unaffected by microscopic discontinuities. The phenomenon of irregular microcrack growth always occurs at a crack length of just a few grain diameters. Figure 2-2 illustrates such small crack behaviour.

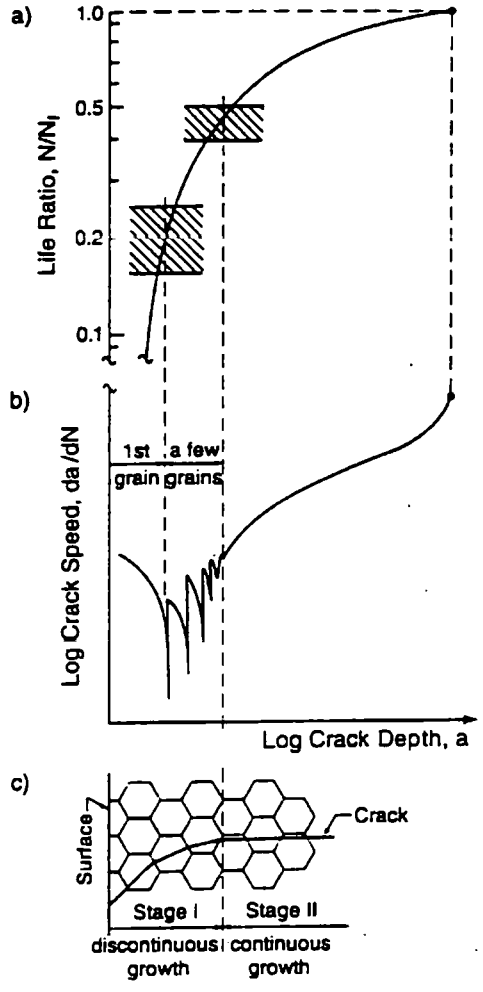

Figure 2-2 Schematic Illustration Of Small Fatigue Crack Behaviour [210]

The criterion for anomalous rapid growth of such microcracks is a joint one, the appropriate conditions being [5] that (1) the ratio of plastic zone size to surface crack length is greater than 0.05 and (2) the ratio of plastic zone size to the size of a controlling microstructure is less than 1. The relation between the crack growth rate and the crack length at this stage varies greatly depending on individual cracks. Upon further crack

growth, the variability in crack growth rate becomes negligible and this is effectively the transition from small to long crack growth.

In commercial Al-alloys, crack nucleation is generally associated with intermetallic particles (1 to 10 μm). For steels and Al-bronze inclusions are significant, whereas for ferrite, Cu- and Ni-alloys slip band cracking is the source of crack nucleation. Crack nucleation in grain boundaries is sometimes mentioned. An intermetallic particle in a grain will affect the local stress concentration, indicating that "microscopic stress concentrations" can not be ignored. With respect to intermetallic particles, there has been some debate on the question whether nucleation starts at the interface between the particle and the matrix material, or as a crack in a particle, or in a slip band impinging on the particle. Actually, it can not be ruled out that a crack in the particle was already present as a result of the material processing. It is very difficult to study the very beginning of microcrack nucleation. The mechanism at that stage is not really known, while it will probably be different for different materials [7]. But crack nucleation is generally associated with the material surface. At the surface the restraint on cycle slip is relatively low.

The initial and final crack lengths are so important in engineering that it is not possible to make a satisfactory fatigue life prediction without accurate values for them because the integration of a small crack growth law from initial to final crack length should yield a S–N curve [4]. However, whatever we do in defining the initial crack length, it seems to be an adjustable parameter and may not have a precise physical meaning. For the purpose of working out reasonable predictions of fatigue lifetime, we have to judge whether or not a small fatigue crack nucleates at a surface inclusion. If the surface inclusion becomes a fracture origin, the inclusion size should be taken as the initial surface crack length which can be expressed by the square root of surface area, $\sqrt{area_S}$, of the inclusion otherwise we have to determine an absolute critical length and take this crack length as the initial crack length. The anomalous growth of small cracks, of the order of one to three grain sizes, and the coalescence behaviour of microcracks must be modelled to derive a better method for life prediction if the linkage process of small cracks is apparently significant.

Statistical analyses are useful for both irregular growth and coalescence of small cracks. The distribution of crack length at a certain number of cycles in constant-amplitude fatigue can be expressed by a Weibull distribution having three parameters (shape, scale, and location parameters). A method to estimate the distribution of crack length as a function of number of stress cycles could be obtained by combining the statistics of crack nucleation with those of crack growth.

2.3 RELEVANT MODELS

There have been a number of models developed for small crack growth rate $\frac{da}{dN}$. However, they all use parameters that can only be obtained by characterisation of a – N curves.

2.3.1 Empirical Models

Being introduced in [4], Kitagawa, *et al* developed the strain intensity range, ΔK_e, as an analogy of stress intensity range that is given by $\Delta\varepsilon\,(\pi a)^{1/2}$ or $\Delta\,\varepsilon_p\,(\pi a)^{1/2}$ to correlate small crack growth data. The crack growth rate law is then:

$$\frac{da}{dN} = C_e\,(\,\Delta K_e\,)^m. \qquad (2\text{-}1)$$

Also being introduced in [4], Nisitani [4] proposed that da/dN is proportional to the crack length, *i.e.*,

$$\frac{da}{dN} = C\,\sigma_a^m\,a\ . \qquad (2\text{-}2)$$

The effects of crack shape and crack closure are not taken into account in these formulae. Several investigators showed that ΔK_e was roughly proportional to the square root of cyclic range of J-integral, ΔJ, [4] [10]. ΔJ can be estimated from measurements of the cyclic hysteresis loop and crack closure [9].

2.3.2 Chan-Lankford Model

K. S. Chan and J. Lankford studied small crack growth behaviour in 7075-T6 aluminium alloy and proposed a model [11] that was based upon the concept of greater plastic strain at crack tips of small cracks. In their model, a physically small crack, on the order of a few micrometres in length, was assumed to nucleate at an inclusion within a grain 'A'. Plastic deformation at the tips of the small fatigue crack occurs in the form of one or two localised slip bands that are inclined to the nominal stress axis and are confined to the region where the crack tip stress field dominates. General yielding does not occur within the grain A containing the small crack, nor in any neighbouring grains. The size of crack tip plastic zone, however, is of the order of half the crack length. As the small crack grows, the rate of crack propagation will be reduced if crack tip slip is restricted by the presence of grain boundary. The continued growth of a small crack requires the propagation of crack tip slip into neighbouring grains.

In order to relate plastic deformation to stress intensity range ΔK, they further assume that the plastic strain range, $\Delta\varepsilon_p$, associated with a small crack can be described by a power-law formulation, *i.e.*,

$$\Delta\varepsilon_p = C\,\Delta K^n . \qquad (2\text{-}3)$$

where C and n are constants.

Small crack studies of 7075-T6 aluminium by J. Lankford [6] reveal that near threshold stress intensity range ΔK_{th} for a long crack, the crack tip opening displacement (CTOD) is larger for a growing small crack than for an equivalent long through crack, suggesting that the plastic strain range associated with a small crack is also higher than that of long cracks. This is a critical assumption in their analysis.

The influence of grain boundaries on the crack tip plastic strain range should depend on the crystallographic orientations of the neighbouring grains, as well as the distance of the crack tip from the nearest grain boundary. To account for the grain boundary effects, the fractional change of the crack tip plastic strain due to the grain boundary blocking of crack tip slip was postulated as follows:

$$\frac{d\Delta\varepsilon_p}{\Delta\varepsilon_p} = -\kappa(\phi)\left(\frac{D-2X}{D}\right)^m \tag{2-4}$$

where X — distance from crack tip to a nearest grain boundary;

m — a constant.

In Equation 2-4, $\kappa(\phi)$ is a function which depends on the crystallographic orientation of the neighbouring grain, and can be expressed by shear stresses of particular slip system in grain A, τ_A , and grain B, τ_B , as $\kappa(\phi) = 1 - \frac{\tau_B}{\tau_A}$. By combining Equations 2-3 and 2-4 , the plastic strain range associated with a small crack in the proximity of a grain boundary becomes:

$$\Delta\varepsilon_p = C\,\Delta K^n\left(1 - \left(1 - \frac{\tau_B}{\tau_A}\right)\left(\frac{D-2X}{D}\right)^m\right) \tag{2-5}$$

Certainly, if $\frac{\tau_B}{\tau_A} > 1$, $\Delta\varepsilon_p$ will increase as the small crack approaches a grain boundary and conversely will decrease with decreasing of X if $\frac{\tau_B}{\tau_A} < 1$.

A crack growth rate expression can be established by a cumulative plastic strain criterion using the local plastic strain range at the crack tip as a measure of fatigue damage. Crack advance by the failure of a crack tip element of size ΔX occurs when the accumulated local plastic strain exceeds a critical value, ε_p^*. The number of cycles ΔN required for failure of the crack tip element is given by

$$\Delta N = \frac{\varepsilon_p^*}{\Delta\varepsilon_p} \tag{2-6}$$

The crack growth rate law thus becomes

$$\frac{da}{dN} = \frac{\Delta X}{\Delta N} = C_1\,\Delta K^n\left(1 - \left(1 - \frac{\tau_B}{\tau_A}\right)\left(\frac{D-2X}{D}\right)^m\right) \tag{2-7}$$

where $C_1 = \frac{\Delta X\, C}{\varepsilon_p^*}$.

This simulated behaviour indicates that crack arrest occurs when crack tip slip is completely blocked by a grain boundary, such that the crack tip strain range is reduced to zero. This occurs when the resolved shear stress in the neighbouring grain is zero (*i.e.*, $\tau_B = 0$). In cases where $\frac{\tau_B}{\tau_A}$ is smaller but finite, the crack propagates away from the boundary.

In terms of their model, the reduction of crack-tip strain at boundaries will be responsible for a transient deceleration of microcrack growth rate. In addition, the determination of the crack-tip plastic strain range at the tips of large and small cracks as they approach grain boundaries will be critical to the application of the proposed model.

2.3.3 Hobson-Brown Model

P. D. Hobson, *et al* [12] found that cracks were arrested at triple points in dual phase steels after propagation in the ferrite phase along prior austenite grain boundaries. E. R. de Los Rios and A. Navarro [13] have observed that grain boundaries frequently become barriers to propagation in a range of metals. Z. Shaikh [14] also observed that small cracks initiated very rapidly in 316 stainless steel both at room temperature and at 550°C. Then growth rate slowed down significantly on trying to penetrate a grain boundary before propagating across an adjacent grain. For these reasons, P. D. Hobson and M. M. Brown suggested that small crack growth occurs by a Stage I mode II process. They also assume that slip bands extend right across the grains and are blocked by the grain boundaries [12]. Thus, the Stage I crack growth rate can be predicted to be

$$\frac{da}{dN} = A \Delta \varepsilon^q (d - a) \tag{2-8}$$

for the microstructural small crack (Stage I) growth regime. In Equation 2-8, A and q are material constants. For the physically small crack growth regime (Stage II)

$$\frac{da}{dN} = B \Delta \varepsilon^p a - H \tag{2-9}$$

where B, p — material constants;

H — a parameter determined by long fatigue crack growth threshold condition.

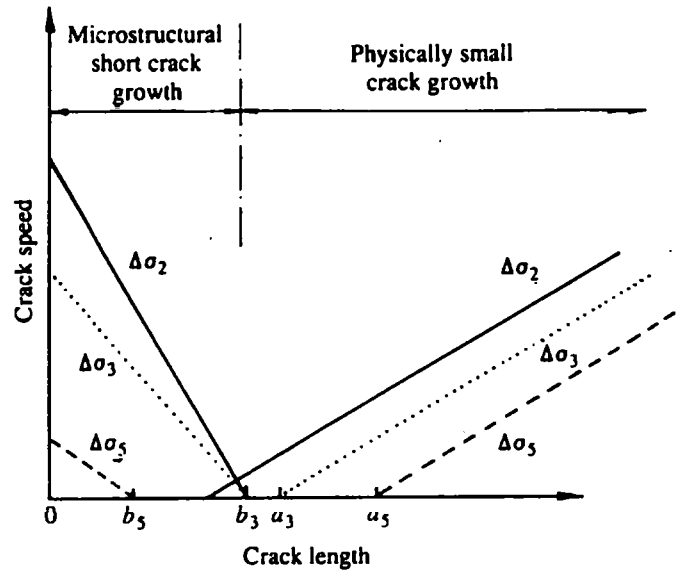

Figure 2-3 Effect Of Cyclic Stress Level And Barrier Strength On The Propagation Or Non-Propagation Of A Fatigue Small Crack [1]

These two stage equations plus stress level effect are illustrated in Figure 2-3. According to this model, although Stage I shear mode cracks initiate and grow rapidly, their development is stunted as they meet barriers since these barriers inhibit the free movement of dislocations along the slip system. This effect must be incorporated in crack propagation equations, by inclusion of a parameter to present this barrier to growth. Additionally, it is important to include the threshold term, otherwise the fatigue limit will not be correctly modelled.

The above two equations can be added together to predict the growth domain of a small crack. In high strain fatigue there will be considerable overlap of the equations. The threshold value a_{th} in Equation 2-8 will be substantially smaller than the value d in Equation 2-9. However at low strain levels the overlap will be considerably reduced. Below the fatigue limit, $a_{th} > d$ and fatigue crack propagation will cease when $a = d$. The transition size for cracks from Stage I to Stage II is determined by plotting a versus. N when the slope of the $a-N$ curve reaches zero.

In most cases, Stage I is of negligible proportions, and for finite fatigue lives the Stage I regime can be regarded as negligibly small [1]. But when a_{th} is of the same order as d the crack will be temporarily arrested at the dominant barrier, the transition period between Stage I to Stage II growth can be the dominant phase in the fatigue lifetime.

The main problem with this model is that it is hard to determine the transition crack size between Stage I to Stage II from experimental data. The model was first applied to a low carbon steel with success and then to other materials. However, the suggested explanations for fast initial crack growth has been debated by J. Schijve [7]. He considered that although observations were made by several investigators mostly in Al-alloys, that inhomogeneous microcrack growth has been taken as fast initial crack growth which then slows down later on, sometimes observations on initial fast microcrack growth could be the result of subsurface crack nucleation at an inclusion, followed by a break though to the material surface [7].

2.3.4 Navarro And de Los Rios Model

By modifying Bilby's solution for continuous distribution of infinitesimal dislocations, A. Navarro and E. R. de los Rios developed an attractive model [15,16] to describe the progressive evolution of the plastic zone for a shear small fatigue crack. The model describes small crack behaviour on the basis of grain boundary blocking and dislocation distribution [15]. In the model, the driving force for crack growth is provided by the energy of the slip bands which abut and collide with the barriers. In this case, the growth rate of small crack is dependent upon the effective slip band length which, in turn, depends on the proximity of the crack tip to a barrier and orientation of the neighbouring slip system. Figure 2-4 gives a general ideal of their simulations.

The observed phenomenon of crack arrest, crack retardation followed by crack acceleration or constant crack growth rate may be accounted for by the plastic displacement δ_p at the tip of crack [16], representing the barrier strength or misorientation between neighbouring grains. The model is based on the idealisation of a crack and its plastic zone, but with the

elastic-plastic interface coinciding with a grain boundary. The formulation used for the dislocation distribution function is, therefore, unbounded at the end of the array.

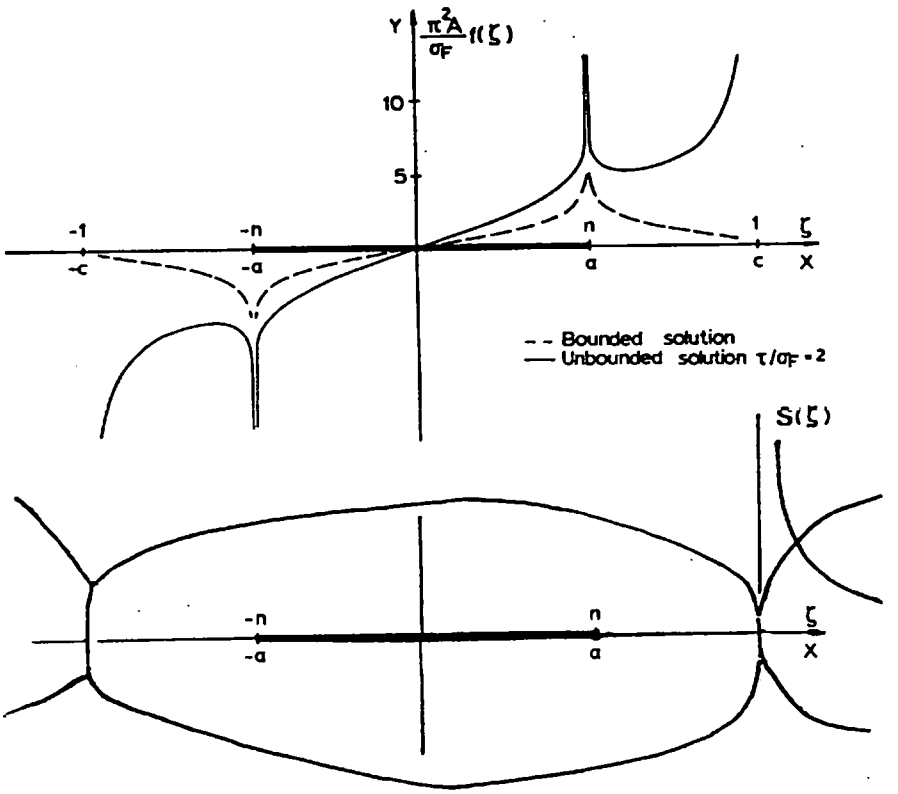

Figure 2-4 Schematic Representation Of The Grain Boundaries Surrounding The Crack And The Stress Distribution Ahead Of The Plastic Zone Together With The Distribution Which Simulates The Crack And Plastic Zone [173]

After solving the equilibrium equations of all the internal and external forces acting on the system, δ_p can be determined for conditions where the applied stress σ is much higher than the friction stress [16]

$$\delta_p = \frac{2\kappa}{G}\frac{\sqrt{1-n^2}}{n}\sigma a . \qquad (2\text{-}10)$$

where $\kappa = 1$ or $1-\upsilon$ depending on whether screw or edge dislocation are considered.

The dimensionless parameter $n = \frac{a}{H}$ (where H is the length segment that incorporates both the crack length and the plastic zone) defines the location of crack tip in relation to the grain boundary on which the leading dislocation is blocked.

The condition for crack propagation in their model is governed by the stress ahead of plastic zone being able to operate dislocation sources in the next grain. For constant applied stress, the stress concentration ahead of the plastic zone depends solely on the parameter n. As the crack grows, but with the plastic zone still being blocked by the grain boundary, the parameter n increases towards a critical value $n = n_c$, at which point the stress concentration reaches a level sufficiently high to activate dislocation sources and consequently the plastic zone extends right across the next grain. When this happens, the stress concentration ahead of the new extended plastic zone decreases, affected by the new lower value of n (n_s) related to the large plastic zone

$$n_s = n_c \frac{i}{i+2} \qquad \text{for } i = 1, 3, 5 \ldots \tag{2-11}$$

which is obtained by relating crack length to the two successive values of H, that is, iD/2 before slip extension and (i+2) D/2 after slip, where i gives the position of the plastic zone in terms of the number of half grain diameters (D/2). This discontinuous character of the slip transfer is repeated grain after grain, giving an oscillating crack growth.

A. Navarro and E. R. de Los Rios derived expressions both for n_c, n_s and plastic displacement δ_p [15] which can be expressed:

$$n_c = \cos\left(\frac{\pi}{2}\frac{\sigma}{\sigma_{comp}}\left(1 - \frac{K_{th}}{K}\right)\right) \tag{2-12}$$

$$n_s = \frac{n_c}{1 + 2\left(\frac{\sigma}{\sigma_{FL}}\right)^2\left(\frac{\Delta K_{th}}{K}\right)^2} \tag{2-13}$$

and δ_p can be expressed as a function of K and K_{th} and takes the form of

$$\delta_p = \frac{\kappa}{G\sigma_{comp}}\left(1 - \frac{K_{th}}{K}\right)K^2 \tag{2-14}$$

Figure 2-5 represents the evolution of normalised plastic displacement as a crack grows. Crack growth rate $\frac{da}{dN}$ is assumed to be proportional to the plastic displacement δ_p at the tip of the crack, that is the number of active dislocations within the plastic zone. The crack

growth rate will depend not only on the applied stress σ and the current crack length but also on the ratio n.

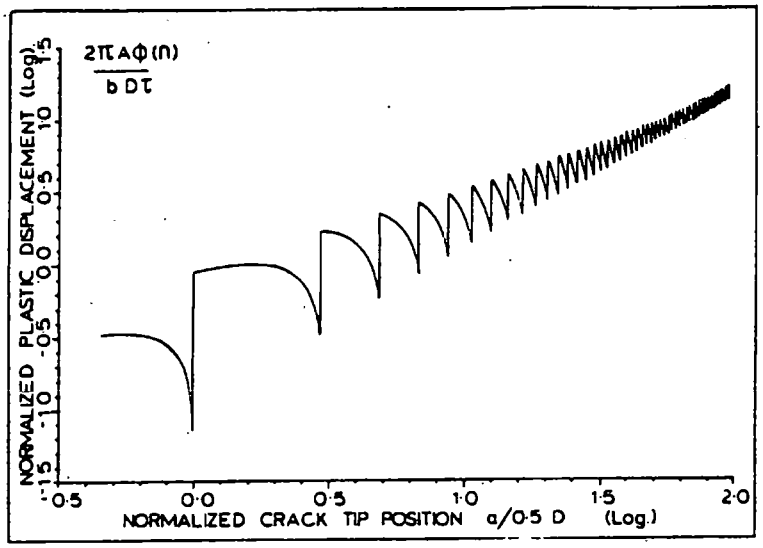

Figure 2-5 Plastic Displacement At The Tip Of The Crack [13]

$$\frac{da}{dN} = \phi\,\delta_p = \phi\,\frac{2\kappa}{G}\,\frac{\sqrt{1-n^2}}{n}\,\sigma a \qquad (2\text{-}15)$$

The factor ϕ has been interpreted as the fraction of dislocations on the slip band that participate in the process of crack extension, and therefore it is expected to depend on the level of applied stress. By rearranging some terms in Equation 2-15 it can be expressed in a dimensionless manner as

$$\frac{dn}{dN} = \frac{\phi(1-\upsilon)\Delta\sigma}{G}\sqrt{1-n^2} \qquad (2\text{-}16)$$

This is the single crack growth law equation describing both microstructurally small and physically small cracks. The upper and lower bound of curves for crack growth are derived by using respectively the minimum and maximum values of the ratio n.

Recently, K. Hassan, E. R. de Los Rios and A. Navarro published a paper [17], reporting that the influence of microstructure on the propagation behaviour of small surface cracks is examined in a simulated HAZ microstructure in C-Mn steel. Their material tests are

conducted under torsional and push-pull loading. The length of ferrite at the prior austenite grain boundaries is characterised as the effective microstructural parameter.

2.3.5 Topper And Plumtree Model

H. Abdel-Raouf, T. H. Topper and A. Plumtree [18] observed small crack growth in 2024-T3 aluminium alloy and suggested a unified model for dealing with small fatigue crack growth which described the strain redistribution with depth from the surface of a specimen, as well as along the surface. The proposed model would be able to predict the kinetics of small fatigue crack growth. There were two physical phenomena involved in their development. First, the strain is a maximum at the free surface of a smooth specimen and decreases with distance from the surface. Secondly, the decay rate of strain concentration is dependent on the microstructure and, in particular, the grain size. Therefore, their model was based on these two physical aspects, namely the nature of the free surface and the microstructure of the material.

The free surface of an annealed polycrystalline metal is typically a section through a large number of randomly oriented grains located at the surface. The operating slip system in each grain will have a different orientation with respect to the loading axis. When the specimen is subjected to a nominal cyclic strain range, *i.e.*, the surface grains deform according to their orientation. The strain in each layer is accommodated by the lack of restraint and this local strain is proportional to the corresponding orientation. Favourably orientated grains experience the largest amount of surface deformation and the greatest amount of localised slip occurs allowing persistent slip bands to develop at the surface of these grains, representing a preferred site for crack initiation. The correspondingly large local strain, ε, decreases with depth as well as distance along surface, eventually, approaching the nominal strain. This decay is due to the increasing constraint and strain compatibility requirements. These ideas can be represented by Figure 2-6.

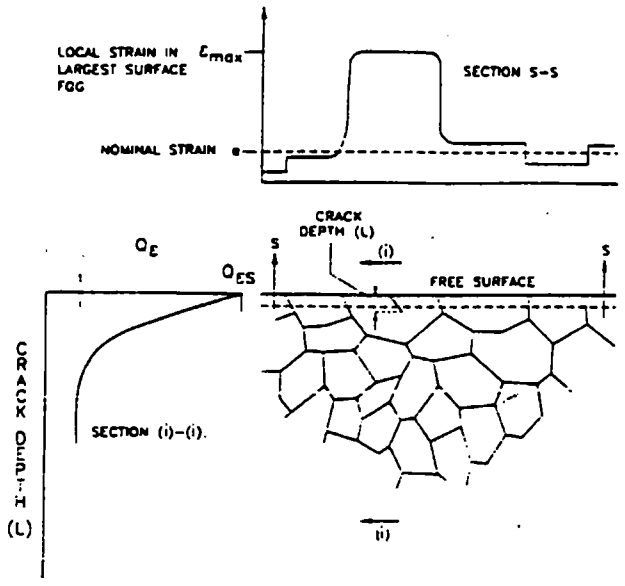

Figure 2-6 Surface Strain Redistribution [18]

If the rate of decay is controlled by the grain size, D, then the larger the grain, the deeper the local resolved shear strain and also less surface area per unit volume of contact between this favourably orientated grain (FOG) and its neighbouring grains. The grain decay gradient is assumed to be proportional to D^{-1}. In order to satisfy the surface and interior conditions, the strain redistribution factor Q_e may be expressed by [18]:

$$Q_e = 1 + q \exp(-\alpha a) \tag{2-17}$$

$$\alpha = b D^{-1} .$$

where q — constant;

α — decay constant;

b — constant depending upon deformation character.

When $a = 0$ at the free surface, Q_{es} is constant ($Q_e = Q_{es} = 1 + q$). For long cracks where a is more than or equal to a critical crack length a_i at which the threshold stress range approaches that of a smooth bar fatigue limit, Q_e approaches unity. But when crack depth is less than the critical value a_i, crack growth behaviour has been found to be highly dependent on the microstructure [9-10] [19-22].

The free surface is not completely constrained and deformation is accommodated at the free surface by intrusion and extrusion formation. To estimate the surface strain redistribution factor Q_{es}, a metal bar is considered as consisting of a row of N randomly orientated grains. For simplicity the bar diameter is less than the grain diameter D. Hence, the bar has a total length of ND. There will be no constraint along the surface of this bar. When the bar is subjected to a nominal strain *i.e.*, each grain will contribute to this strain by an amount of Δ_i, depending on its orientation, defined by the angle θ between the slip plane and the tensile axis. If $N(\theta) = [N/360]d\theta$ is the number of grains with orientation between θ and $(\theta + d\theta)$, then the deformation Δ_q in these grains is given by

$$\Delta_\theta = \gamma (\sin 2\theta)^f \tag{2-18}$$

where γ — deformation in the favourably orientated grains (FOGs);

f — exponent dependent upon the ratio of slipped to unslipped grains.

The total deformation, Δ_T, in all grains can be expressed as

$$\Delta_T = \frac{4N_\gamma}{360} \int_0^{90} (\sin 2\theta)^f \, d\theta \tag{2-19}$$

The nominal strain for the bar of total length ND is then:

$$\varepsilon = \frac{N_T}{360} = \frac{\gamma}{90D} \int_0^{90} (\sin 2\theta)^f \, d\theta \tag{2-20}$$

The deformation in the favourably orientated grains with orientation $45.5^o > \theta > 44.5^o$ is

$$\Delta_{FOG} = \frac{N_\gamma}{360} \int_{44.5}^{45.5} (\sin 2\theta)^f \, d\theta \tag{2-21}$$

The total length of FOGs. is ND/360, hence the total local strain in FOGs is

$$e = \frac{\gamma}{D} \int_{44.5}^{45.5} (\sin 2\theta)^f \, d\theta \tag{2-22}$$

Then the strain redistribution factor of free surface is

$$Q_{\varepsilon s} = \frac{e}{\varepsilon} = \frac{90 \int_{44.5}^{45.5} (\sin 2\theta)^f \, d\theta}{\int_0^{90} (\sin 2\theta)^f \, 2\theta} \tag{2-23}$$

It is apparent that determination of the exponent, f, that is the ratio of slipped to unslipped grains, is essential in estimating strain redistribution factor at free surface.

However, H. Abdel-Raouf, T. H. Topper and A. Plumtree avoided the determination the value of f directly from experiment by examining slipped and unslipped grains. They employed typical values, *i.e.*, 0.01 for the local strain range at the surface within the persistent slip bands, and 25 for the exponent f which were of results of examination in copper single crystals and SB-22 mild steel respectively. With these two values the strain redistribution factor, $Q_{\varepsilon s}$, in the bar specimen at the free surface is then determined to be 6.3 using Equations 2-17, 2-19 and 2-22.

For the purpose of verifying the present model, threshold data of the 2024-T3 alloy was considered by them, for which the relationship between threshold strain amplitude and crack length may be expressed by:

$$\varepsilon_{th}\sqrt{\pi a} = Y \tag{2-24}$$

where Y — crack driving parameter which is constant for the material testing condition.

It is analogous to the strain intensity parameter for correlating crack growth rates in elastic and plastic strain field. However, care must be exercised in extrapolating Equation 2-24 to a value approaching zero, since the threshold strain amplitude at the free surface must be finite [21]. The strain redistribution is then estimated using Equation 2-17 with a finite local strain range at the surface limited to a maximum value of 0.01.

The nominal stress amplitude at threshold ($\Delta\sigma_{th}$) is now able to be calculated using the familiar expression for the threshold stress intensity factor amplitude (ΔK_{th}) modified for strain redistribution:

$$\Delta\sigma_{th} = \Delta K_{th} \left(Q_e F\sqrt{\pi a}\right)^{-1}$$

$$= \Delta K_{th} \left([1 + q\exp(-\alpha a)]\, F\sqrt{\pi a}\right)^{-1} \qquad (2\text{-}25)$$

where F — crack shape factor.

Using the relationship between crack growth rate and applied stress intensity for long cracks given by A. F. Blom, *et al* [23] together with above equation, the propagation rates at various stress levels for small cracks could be predicted. Since the model is based on the condition of free surface, any change in its nature or microstructure will affect small fatigue crack behaviour.

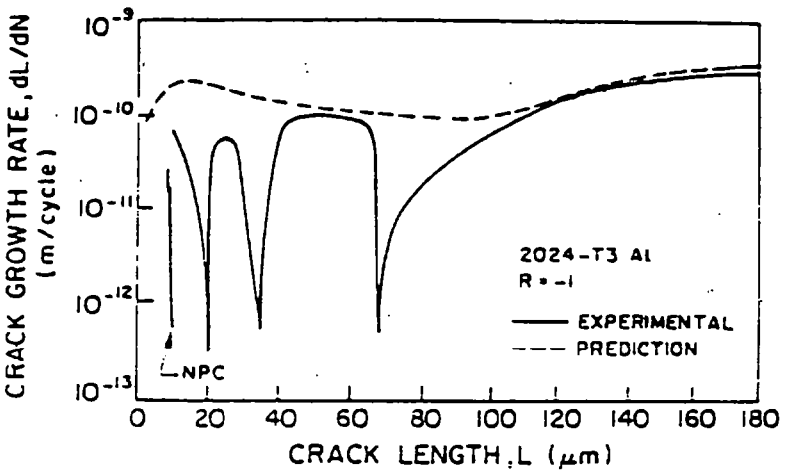

Figure 2-7 Predicted And Experimental Short Fatigue Crack Growth Rates. NPC Indicates Non propagation Crack [18]

This fracture mechanics model seems to be capable of predicting both the behaviour of small fatigue cracks and fatigue limits by accounting for the non-uniform strain distribution at the surface and relating it to the microstructure, although the determination of strain redistribution factor is difficult. The validation of the proposed method to predict small crack growth rate was confirmed through a comparison between predicted experimental results on 2024-T3 aluminium alloy as shown in Figure 2-7. H. Abdel-Raouf, T. H. Topper and A. Plumtree also extended the model to predict fatigue limits, size of non-propagating cracks and growth rates of small fatigue cracks in smooth specimens [24].

2.3.6 Modified Linear Elastic Approach

A. J. McEVILY introduced a number of modifications to linear elastic approach [25] [26] to establish a new parameter which was capable of correlating both long crack and small fatigue crack growth data. By a fairly straightforward extension of the linear elastic approach, a formalism has been developed to deal with small crack behaviour. His modifications include use of material constant, r_e ; an allowance for large scale plasticity effects; an allowance for the development of crack closure; and the incorporation of the fatigue crack growth threshold.

Small fatigue crack propagation is associated with a larger crack tip plastic zone, compared to that of long cracks. In order to make use of a modified elastic analysis to characterise fatigue crack growth for small cracks, the Irwin expression for stress intensity factor, K was used as a starting point in the analysis.

$$K = \lim_{\rho \to 0} K_T \sigma \sqrt{\frac{\pi \rho}{4}} \quad . \tag{2-26}$$

where ρ — radius of a stress raiser.

Irwin has shown that it is possible to develop a variety of stress intensity factors appropriate to large cracks from a knowledge of the corresponding stress concentration factor when the radius ρ is allowed to approach zero. However, instead of allowing ρ to approach zero in the limit, A. J. McEVILY allows it to approach a finite value ρ_e in his analysis. This modification will have a negligible effect on the stress intensity factor of a long crack and is of significance in dealing with small cracks. The justification for the modification is that:

- the fatigue crack tip is not of zero radius even at the minimum load of a cycle;
- the large plastic zone to length ratio of a small crack requires modification of the LEFM approach;

- the stress range required to propagate a crack must remain finite rather than go to infinity when the length of small crack is extremely small.

The value of ρ_c is determined by experimental results and as such is an empirical constant. The need for dealing with small crack behaviour has been demonstrated by M. H. Elhaddad, T. H. Topper & K. N. Smith [27] as well as K. Tanaka [4]. So, his expression for the stress intensity factor becomes:

$$K = \left(\sqrt{\frac{\pi \rho_e}{4}} + F \sqrt{\pi a} \right) \sigma . \tag{3-27}$$

In which F is a factor which reflects the usual dependence of the stress intensity factor on the geometry involved. Since the local stress at a crack tip for a linear elastic body is given by

$$\sigma_{yy} = \frac{K}{\sqrt{2\pi\rho_y}} \tag{2-28}$$

The parameter ρ_e can be expressed as a length unit r_e by the following relationship, with $\sigma_{yy} = \sigma_m$, and $\sigma_m = K_T$, and $r = r_e$

$$\sigma_m \sqrt{2\pi r_e} = \sigma_m \sqrt{\frac{\pi \rho_e}{4}} \tag{2-29}$$

Consequently, the parameter ρ_e can also be expressed as a length unit by

$$r_e = \frac{\rho_e}{8} . \tag{2-30}$$

In the following analysis, the crack length, *a*, is assumed to approach the value of r_e in the limit. The value of r_e will be shown to be of the order of a micron. Implicitly, A. J. McEVILY therefore assumes that below this size of crack, inherent defects in the material are more severe as stress raisers than is the crack itself. The expression for the stress intensity factor therefore becomes

$$K = \left(\sqrt{2\pi r_e} + F\sqrt{\pi a}\right)\sigma \tag{2-31}$$

In order to propagate a small crack, the applied stress levels are often high with respect to the yield strength level. As a result the plastic zone size will be larger than predicted by EPFM. To deal with this situation, A. J. McEVILY makes use of Irwin's suggestion that the effective length of the crack, a_{eff}, is increased by one-half of the plastic zone size to account for the effective length of the relaxation of stress within the plastic zone on the surrounding elastic stress field. If the expression for the plastic zone size is taken to be:

$$r_p = \left(\sec\frac{\pi\sigma_{max}}{2\sigma_y} - 1\right)a \tag{2-32}$$

then the effective crack length becomes

$$a_{eff} = \frac{a}{2}\left(\sec\frac{\pi\sigma_{max}}{2\sigma_y} + 1\right) \tag{2-33}$$

and stress intensity factor K can be written in the form of

$$K = \left(\sqrt{2\pi r_e} + F\sqrt{\frac{\pi a}{2}\left(\sec\frac{\pi\sigma_{max}}{2\sigma_y} + 1\right)}\right)\sigma \tag{2-34}$$

Since A. J. McEVILY was dealing with the growth rates of small fatigue cracks, an expression for the growth rate law is needed. The following expression was deduced

$$\frac{da}{dN} = A\,(\Delta K_{eff} - \Delta K_{effth})^2 \tag{2-35}$$

where A — material constant;

$\Delta K_{eff} = K_{max} - K_{op}$.

In this expression the second power relationship is taken to indicate a relationship between advance of the crack per cycle and the crack tip opening displacement, taking into account the existence of a threshold level.

Since the extent of crack closure in the wake of a newly formed crack increases from zero up to the level associated with a long crack as the crack increases in length, the effective stress intensity factor is gradually reduced as this closure develops. The transition distance involved has been found to be the order of a millimetre in length. The expression takes the form of

$$K_{op} = (1 - e^{-2\chi a}) K_{opmax} \tag{2-36}$$

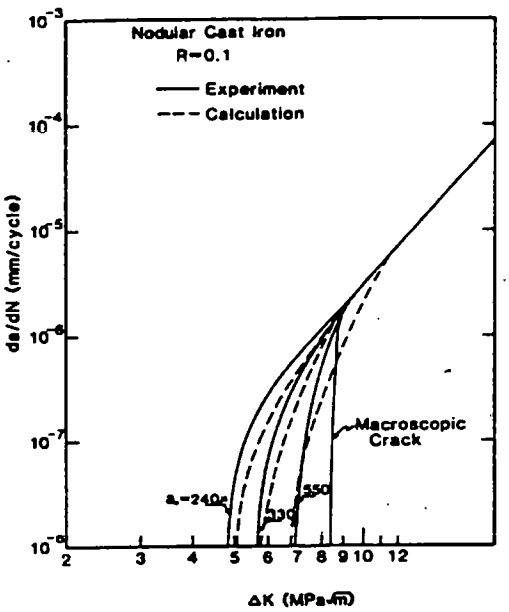

Figure 2-8 A Comparison Of Experimental And Predicted Crack Growth Rates For Different Initial Crack Sizes [25]

with $0 \le K_{op} \le K_{opmax}$ which provides a means for taking into account the development of closure during the transition period [28]. K_{op} is the crack opening level in the transition region. χ is a material constant expressed in reciprocal millimetre unit (mm^{-1}). K_{opmax} is the crack opening level for a long crack which is a function of R, the ratio of the minimum to the maximum stress in a cycle. with these modifications the expression for the rate of fatigue crack growth becomes

$$\frac{da}{dN} = A \left([\Delta K - (1 - e^{-2\chi a}) K_{opmax}] - \Delta K_{effth} \right)^2 \tag{2-37}$$

and using the expression for K given in Equation 2-34,

$$\frac{da}{dN} = A\left\{\left(\sqrt{2\pi r_e} + F\sqrt{\frac{\pi a}{2}\left(\sec\frac{\pi\sigma_{max}}{2\sigma_y} + 1\right)}\right)\Delta\sigma - (1 - e^{-2\chi a})\,K_{opmax} - \Delta K_{effth}\right\}^2 \qquad (2\text{-}38)$$

This is the general expression applicable to both long and small cracks. Typical small crack growth rate predictions is illustrated in Figure 2-8.

2.3.7 Other Models

(1) On the basis of discussions of micromechanisms and effective plastic strain energy involved in fatigue crack initiation, an analytic model of Stage I fatigue crack initiation and subsequent Stage II crack propagation that was based on plastic strain intensity factor, K_p, was proposed by J. W. Provan and Z. H. Zhai [29-30]. The growth rate law took the form

$$\frac{da}{dN} = C_p(\Delta K_p)^{\Psi} \qquad (2\text{-}39)$$

where C_p, ψ — constants.

(2) On the basis of governing local plastic strain and stress state a model for small fatigue crack growth was proposed [31] by D. Kuiawski and F. Ellyin which incorporated the bulk fatigue properties of 7075-T6 aluminium alloy as well as the mechanical properties of a surface layer of near the free surface. D. Kuiawski and F. Ellyin considered that the material thickness could be subdivided into a series of strips whose thickness, δ^*, is equal to the process zone size. In their work the process zone size, δ^*, in front of crack , is of the order of grain size of material and the growth rate of long cracks could be described in terms of δ^*/N^*. The failure criterion in their model is based on the governing local plastic strain and stress states within the process zone. Their products are proportional to the plastic strain energy density that is related to the crack tip intensity. Once a crack is initiated

in the surface layer, its growth will depend on the combined plastic deformation of the subsequent layer and the crack tip plasticity.

(3) Small fatigue crack growth in a high strength aluminium alloy of 7000 series has been studied by Y. Zhang and L. Edwards [32]. It was found that the plastic zone and its shape were dependent on both crack length and growth morphology. Naturally, initiated Stage I fatigue cracks were predominantly crystallographic in nature and were accompanied by a relatively long slender plastic zone shape. They concluded that the growth rates of small cracks coincide with that of long cracks when their plastic zone size approached the grain size. By comparing measured plastic zone size r_p and crack growth rates, it was proposed that the crack growth rates were proportional to plastic zone size independent of whether they were blocked by grain boundaries, which is in accordance with the same assumption made by H. Nisitani, *et al* [33]. So the following relationship exists between crack growth rate $\frac{da}{dN}$ and the plastic zone size measured ahead of small fatigue cracks [32]:

$$\frac{da}{dN} = C\, r_p^m \,. \tag{2-40}$$

2.4 OTHER SIMULATIONS FOR SMALL FATIGUE CRACK BEHAVIOUR

2.4.1 Energy Consideration.

The problem of nucleation and growth of small fatigue crack was addressed from an energetic point of view by F. Guiu and R. N. Stevens [35]. It is explained by their theory that vanishing small cracks can only nucleate and grow at the expense of the release of some locally stored energy during the fatigue deformation. This is necessary because an external loading system alone can not provide a positive driving force for the growth of a crack whose length is below an absolute critical value. On the basis of an energy analysis, A. N. Vasjutin [36] tried to present a new interpretation for the fracture mechanics energy

approach to physically small fatigue crack growth. Using his criterion an expression for the fatigue crack growth rate was proposed. Observed and predicted results of small fatigue crack propagation rate are presented. However, his theory as well as the criteria for small crack growth seems to be a somewhat idealised analysis because it is difficult to apply his model to practical applications. M. L. Bartlett and A. Saxena found that the growth rate of small fatigue cracks, $\frac{da}{dN}$, in mild steel correlated with $\sqrt{E\Delta J}$ under fully plastic conditions. This observation is consistent with the proposal that energy release rate G is a parameter for characterising the growth rate of small cracks [37]. However, no more details are available in this aspect.

2.4.2 Shape Varying Of Small Fatigue Cracks.

The influence of microstructure and processing method on the initiation and growth of fatigue cracks in an aluminium-magnesium-silicon alloy has been studied by A Plumtree and B. P. D. O'Connor [39]. Surface small crack lengths at various intervals of the fatigue life were measured for imposed strain amplitudes, ε_a, ranging between 0.15 and 1.0%. The small crack profile was examined optically and was observed to be slightly curved, approximating a semi-ellipse. This shape was found to exist over the full range of strains examined up to cracked areas of 50%, which was used as the life criterion in their study.

The resulting data from their experiment showed that the crack depth, $\tilde{a}$, was related to the surface crack length, a, (for $a > 1$ mm) by the equation

$$\tilde{a} = 0.384 \times (a - 0.7) \qquad \text{mm} \tag{2-41}$$

Crack depths associated with the crack length less than about 1 mm were related by

$$\tilde{a} = 0.2 \times a \qquad \text{mm} \tag{2-42}$$

They concluded that the microstructural features which impaired small crack growth were dependent on the stress or strain level. Initiation and early growth of small cracks were also found to be dependent upon the applied stress and strain level. At high strains, small

cracks could traverse most grain boundaries and break through second phase particles easily, both particle cracking and decohesion at the particle/matrix interface were observed, whereas at low strains these presented barriers to crack growth and only decohesion occurred. Triple points and other high misorientation boundaries represented the greatest impediments to growth.

N. M. Grinberg, *et al* [40] conducted an experiment to investigate nucleation and growth of small surface cracks in a aluminium alloy. They reported that small cracks have an elliptical form and the relation between depth ã of a microcrack extending beyond the grain boundaries and its length, a, equals to 0.32 and remains same at all stages of small crack growth. This axial ratio under all load levels investigated is independent of the stress amplitude and the environment [40]. C. Kaynak and A. Ankara [41] investigated small fatigue crack growth in aluminium alloys 2024-T3 and 7075-T6. The employed relationship between the crack depth ã, surface crack length (a) and specimen thickness (t) had the form

$$\frac{\tilde{a}}{a} = 0.9 - 0.25\left(\frac{a}{t}\right)^2 \tag{2-43}$$

which was decrived from results an experimental programme [42] for a/t ratios greater than 0.05. However, no information was given in this programme on the shape of cracks with an a/t ratio less than 0.04. N. H. Carvalho and M. de Freitas [43] determined crack shape in 2090-T8E41 aluminium-lithium alloy specimens. They put forward a relationship

$$\frac{\tilde{a}}{a} = 1.18 + 0.51\left(\frac{a}{t}\right). \tag{2-44}$$

Swain, *et al* [44] determined the crack shape in AISI 4340 steel SENT specimens. They developed an equation

$$\frac{\tilde{a}}{a} = 1.0 - 0.25\left(\frac{a}{t}\right) \tag{2-45}$$

for a limited range of experimental data.

The effect of changes of crack shapes on the behaviour of small cracks were investigated using single edge crack specimens and small surface crack specimens with different initial crack shapes by Y. Jingiun, P. Hongxun and K. Wei [45]. For surface cracks, the relationship between aspect ratio $\frac{\tilde{a}}{a}$ and normalised crack length $\frac{a}{w}$ could be characterised by the following equation [45], where w is of specimen thickness,

$$\frac{\tilde{a}}{a} = 0.4\left(1 - \left(\frac{0.078}{a/w}\right)^3\right)^{1/3} \tag{2-46}$$

and the crack growth rates in the direction of the minor axis of the semi-elliptic crack, $\frac{d\tilde{a}}{dN}$, as a function of $\frac{da}{dN}$, was derived by differentiating Equation 2-46 deducing finally

$$\frac{d\tilde{a}}{dN} = \left\{ 0.4\,(1 - Q^3)^{1/3} + 0.4\,(1 - Q^3)^{-2/3}\,Q^3 \right\} \frac{da}{dN} \tag{2-47}$$

where $Q = \frac{0.078}{a/w}$.

2.5 THE INFLUENCE OF INCLUSIONS AND DEFECTS

Engineering materials are known to contain various microstructural inhomogeneities (e.g. microscopic casting defects, micropores, non-metallic inclusions, corrosion pits) which may have a deleterious effect on mechanical properties, in particular, on the fatigue behaviour.

The importance of small defects and inclusions on fatigue crack initiation and growth has been noted for a long time. Investigations about the influence of inclusions on the fatigue strength of materials, especially on high strength or high hardness materials, have shown that the fatigue strength may be affected by very small defects or inclusions. Origins of fatigue failure in such materials are mostly from defects or inclusions rather than from slip bands or grain boundaries. However, the complication of dominant mechanisms and inclusion configurations has prevented the establishment of a reliable quantitative method for evaluating the effects of small defects and inclusions. Experiments have shown that

fatigue strength of metals is in some cases determined by one crucial defect or inclusion. The effects of similar size inclusions can be different depending on their location, especially on the surface of the specimen. Also that defects or inclusions less than a certain size do not affect the fatigue strength of metals. Furthermore, the same defect or inclusion can cause different effects on the fatigue strength depending on the loading direction. Some experimental results indicate that the shape and the size of defect or inclusions are the important factor. All these factors are related to the stress concentration factors and the stress distribution around the defect or inclusion. Much effort have been made to quantitatively evaluate the stress concentration factors of inclusions by assuming their shapes were spherical or ellipsoidal, but these assumptions are just rough estimations.

In order to study the effect of small surface defects or inclusions, it is extremely important to note that their effect on fatigue strength is essentially a small crack problem, and therefore, the effect can be evaluated quantitatively and also can be unified only by regarding small defects and inclusions as small cracks [49-51]. Therefore, it is reasonable to seek a representative geometrical parameter by which the shape and size of the crack-like defects or inclusions may be correlated in terms of stress intensity factors, especially the maximum stress intensity factor. Such a parameter should enable one to analyse quantitatively the influence of inclusions on fatigue strength.

2.5.1 Murakami's Consideration

To overcome difficulties of correlating the size and shape of different defects, Y. Murakami, *et al* [50]. proposed that the parameter which describes different geometrical shapes is best expressed by the square root of the defect area projected onto a plane normal to the stress direction [50] although they did not take into account the contribution of the non-propagating cracks and the influence of closure. They proposed that for the region $\sqrt{area_s} \leq 1000$ mm, the relationship between ΔK_{th} and $\sqrt{area_s}$ is linear, and the following equation holds regardless of the nature of material

$$\Delta K_{th} \propto (\sqrt{area_s})^{1/3} \tag{2-48}$$

The above equation indicates that the dependence of fatigue limit σ_l on defect or inclusion size can be expressed as

$$\sigma_l \propto \frac{1}{(\sqrt{area_s})^{1/6}} \tag{2-49}$$

If $\sqrt{area_s} \rightarrow 0$, we have $\sigma_l \rightarrow \infty$. But this is not realistic because the lower limit of $\sqrt{area_s}$ over which Equation 2-49 is valid is related to the maximum size of nonpropagating crack a_n observed in an unnotched specimen. Therefore, it may be concluded that $\sqrt{area_s}$ is promising as the representative geometrical parameter.

Since the defects have been regarded as small cracks, it may be considered that the fatigue limit is not the critical condition for crack initiation but a condition for the propagation of a crack emanating from defects or inclusions. For example, the fatigue limit of a structure or component containing a small defect or inclusion must not be treated as a notch problem in which the critical condition is that for crack initiation, but should be understood as a problem of a crack that emanates from the defect and stops propagating. Only this interpretation of the problem leads one to find the geometrical parameter for inclusions.

It should be mentioned here that a small fatigue crack can initiate either from the surface or from the subsurface of a specimen at a site where a defect is located. In the former case, as stated above, the value of $\sqrt{area_s}$ of the defect or inclusion can be regarded as an initial surface length of a small crack to be used in life prediction. In the latter case, where the defect or inclusion is not at the free surface of specimen. It may be very hard to observe small crack propagation during its early growth period until the crack extends and breaks through the subsurface to the free surface.

2.5.2 Weiss´s Consideration

A qualitative explanation [52] was proposed for the existence of small non-damaging surface notches to describe their critical sizes. The analysis proposed requires only the knowledge of geometric factors (notch geometry, notch size) and intrinsic material

parameters (fatigue strength of unnotched materials, effective threshold stress intensity for fatigue crack propagation). Recently, a new understanding about the effect of surface inclusions on fatigue behaviour has been reached which takes into account non-propagating cracks and closure effects. An attractive model derived on the basis of magnitude and extent of the stress concentration associated with small artificial hemispherical micro-pits or cylindrical blind-bottom holes allows the prediction of the size of defects that do not affect the fatigue limit of defect-free specimens. B. Weiss, *et al* concluded that [53]:

- Non-propagating microcracks are associated with artificial micro-pits. The maximum size of the microcracks was found to correlate with the extent of the stress-concentration field.
- The extent of the field of stress concentration around an isolated micro-pit was found to amount to approximately twice the radius of the micro-pit.
- The fatigue strength of specimens with micro-pits is related to the factors governing propagation of a small crack formed at the perimeter of most of these pits.
- A prediction of the effects of micro-pits can be determined on the basis of the appropriate Kitagawa diagram [211], with the effective threshold value for fatigue crack growth and the fatigue limit as material-related parameters. The geometry of the notch has to be taken into account which determines the magnitude of stress-concentration at the edge of the micro-pit.

Generally, surface defects have a more harmful effect than interior ones. Only those defects larger than a critical size a_c influence the fatigue strength of metals.

2.6 PROBLEMS RELATING TO THE PREDICTION OF FATIGUE LIFETIME

A quantitative estimation of the reliability of any predicted fatigue life is important since experimental fatigue data invariably exhibit large scatter. In order to perform a reasonable evaluation of the scatter characteristics of fatigue life, one must clarify the physical basis of such scatter. It follows that the relation between scatter in fatigue life and the behaviour of small cracks must be investigated so as to predict fatigue lifetimes with high confidence levels because the fatigue life of a specimen is controlled mainly by the period of small crack development. In many studies on small fatigue crack growth, the influence of microstructure been shown to play a dominant role, especially on cracks that are of a size comparable to the scale of the microstructure features so it is a good idea to incorporate a proper microstructural dimension into the life prediction model. In addition, the transition behaviour of small cracks to long cracks is very important in engineering applications [54-55].

2.6.1 Statistical Approach To Fatigue Lifetime Prediction

The initial growth of small cracks is affected by microstructure, e.g. grain boundaries, inclusions, triple points, texture, etc., and these factors are randomly distributed in the material. Any quantities pertaining to the mechanical state of a micro-element is either a random variable, or a stochastic process. Any deterministic description only represents the growth of an individual crack, but does not cover the collective behaviour, *i.e.*, the intrinsic stochastic nature of the small crack growth process. Recent research on this topic has identified several points:

- Grain boundaries temporarily constrain crack growth. Sudden change in crack growth occurs periodically, *i.e.*, the crack length versus number of cycles curve is not a continuously smooth line.
- The crack growth mode is not a simple one. Most of cracks are of mixed mode character, so the relation between ΔK and $\frac{da}{dN}$ is no longer a monotonic function.

- The time interval for which a crack tip is arrested by a grain boundary decreases with increasing crack length.
- The stress state and the crack length are not sufficient state parameters to describe small crack growth because of the interaction of a small crack with microstructural inhomogeneities which are randomly distributed.

Y. Akiniwa, *et al* [56] put forward a method using a three parameter Weibull distribution, to simulate statistical distribution of crack propagation rate. The cumulative probability function is plotted *vs.* the crack growth rate for cracks whose lengths are within each predetermined interval. The intervals are taken nearly equal on the logarithmic scale to the square root of the crack length. The cumulative probability function $F\left(\frac{da}{dN}\right)$ is given as

$$F\left(\frac{da}{dN}\right) = 1 - \exp\left(-\left(\frac{t-\vartheta}{\zeta}\right)^{M}\right) \tag{2-50}$$

where the mean value μ and the standard deviation SD are given by

$$\mu = \zeta\,\Gamma\left(1+\frac{1}{M}\right)+\vartheta \tag{2-51}$$

$$SD = \zeta\left(\Gamma\left(1+\frac{2}{M}\right)-\left(\Gamma\left(1+\frac{1}{M}\right)\right)^{2}\right)^{1/2}. \tag{2-52}$$

where M — shape parameter;

ζ — scale parameter;

ϑ — a location parameter;

t — a variable;

Γ — gamma function.

The average growth rate of small cracks was obtained using the three-parameter Weibull distribution from the following equation for the central crack length of each interval:

$$\frac{da}{dN} = \frac{10^{-11}n_1 + M(n-n_1)}{n}. \tag{2-53}$$

where n — number of cracks;

n_1 — number of arrested cracks.

and the crack growth rate was assumed to be 10^{-11} mm/cycle for non-propagating cracks.

After investigating small crack growth in 2024-T3 aluminium alloy, they concluded that the probability distribution of the crack propagation rate was approximated by the three parameter Weibull distribution. The scale parameter and the location parameter tended to increase with the increasing crack length. The standard deviation increased with increasing crack length, while the coefficient of variation decreased. M. Goto [57] also applied the three parameter Weibull distribution to sets of his experimental data to analyse the distribution of crack initiation life, propagation life, fatigue life and crack length.

Two years later, Y. Akiniwa and K. Tanaka proposed another model, using Monte Carlo simulation, to simulate small fatigue crack growth rate by assuming that the crack growth rate was controlled by crack-tip opening displacement, *i.e.*, [58]

$$\frac{da}{dN} = C\,(\Delta CTOD)^n. \qquad (2\text{-}54)$$

A continuous distribution of dislocations was used in their development to model the slip deformation ahead of the tip of a small crack. The Monte Carlo simulation was conducted for fatigue crack propagation by giving the grain size and the friction stress within each grain as random variables following a two parameter Weibull distribution. The critical stress intensity required for slip propagation across the grain boundary was also given as an independent random variable of the two parameter Weibull distribution. The shape and scale factor of the Weibull distribution were determined from the prescribed values of the mean and variance. A fatigue crack in their model was assumed to start from the weakest grain having the largest value of the grain size multiplied by the effective stress ($\Delta\sigma - 2\sigma_f$). The amount of crack propagation in ΔN cycle was obtained from Equation 2-54 by making $C = 1$ and was kept smaller than one-tenth of grain size by adjusting ΔN in their simulation.

S. Z. Wang, *et al* [59] developed a statistical model for small crack growth process in the form of a non-stationary Markov chain that could be described with a probabilistic transformation matrix. In their research, assumptions are based on the cumulative damage model developed by J. L. Bogdanoff and F. Kosin [60] who employed a unit jump state dependent process of the Markov chain theory. According to their measured crack growth data, a probabilistic transformation matrix is presented. The matrix can simulate any small fatigue crack growth process by a change in its entry procedure. The initial period, crack acceleration and crack arrest at grain boundaries etc. can be described by the matrix.

2.6.2 Small Fatigue Crack/Long Crack Growth Transition

A. Navarro and E. R. de los Rios, using the concepts developed by Bilby, Cottrell and Swinden, proposed a model [54] to describe the transition of small cracks to long cracks. They put forward a expression for the transition condition which is

$$\Delta K_t = \left(\frac{4\tau_y}{\pi\tau_f}\right)\Delta K_{th} \tag{2-55}$$

where τ_f — shear stress at fatigue limit.

Similarly, K. Hussain and E. R. de los Rios put recently forward an expression [61] to determine the ΔK_t at transition point from small crack growth to long crack growth. P. Hyspecky and B. Stranadel proposed a statistical criterion [62] for the transition which could be used to determine the critical number of cycles needed for the formation of a long fatigue crack. Their work has confirmed that the pattern of crack length follows a Weibull distribution as suggested by K. Tanaka [56].

In their research, the sets of detected crack length at various numbers of cycles N and at both of the applied total deformation amplitude levels, were subjected to statistical analyses. The underlying assumption was that the crack lengths in each set would correspond to the probability density of a two-parameter other than three-parameter Weibull distribution in the form of

$$\rho_{\varepsilon/2}\,[a, \gamma(N), \beta(N)] = \beta(N)\, a^{\beta(N)-1}\, [\gamma(N)]^{-\beta(N)}$$

$$\exp\left(-\left(\frac{a}{\gamma(N)}\right)^{\beta(N)}\right) . \qquad (2\text{-}56)$$

where $\rho_{\varepsilon/2}$ — probability density;

$\gamma(N)$ — size parameter;

$\beta(N)$ — shape parameter.

Their experimental work and the statistical processing of its results have demonstrated that the length of fatigue microcracks, assessed for any given number of cycles by a Weibull probability density, *i.e.*, Equation 2-56, increases with the number of cycles. This naturally entails an increase in size parameter (N), which could be regarded as a normalised microcrack length. An increasing number of cycles also raises the modal value of the microcrack length, a_m, in other words the value at which the probability density function $\rho_{\varepsilon/2}$ attains its maximum. The dependence of a_m on parameters $\gamma(N)$ and $\beta(N)$ is given by the first derivation of Equation 2-54, and assumes

$$a_m(N) = \left(\frac{\beta(N) - 1}{\beta(N)\,[\gamma(N)]^{-\beta(N)}}\right)^{1/\beta(N)} . \qquad (2\text{-}57)$$

When a certain number of cycles has been completed, a long crack is formed, and other cracks cease to grow. It follows that we may define the instant when the initiation and propagation of small fatigue cracks converge into the growth of a long fatigue crack as the moment when a number of cycles is completed at which the modal value of fatigue crack lengths, a_m, remains constant regardless the number of further cycles concluded. Consequently, the first derivation of a_m by the number of cycles must at the instant of convergency be equal to zero:

$$\frac{da_m(N)}{dN} = 0. \qquad (2\text{-}58)$$

Upon inserting Equation 2-57 into Equation 2-58, we can compile the following differential equation expressing the criterion for the convergency of small crack initiation and propagation into the growth of a fatigue crack:

$$\frac{1}{\gamma(N)}\frac{d\gamma(N)}{dN} = \frac{1}{\beta^2(N)}\left(\ln 3\beta(N) - 14 - \ln\beta(N) - \frac{1}{\beta(N)}\right)\frac{d\beta(N)}{dN} \qquad (2\text{-}59)$$

After insertion of the dependence of parameters $\gamma(N)$ and $\beta(N)$ into Equation 2-59 numerical solution of the equation reveals the number of cycles, N_c, at which convergency takes place.

The criterion proposed for the convergency of the small crack initiation and propagation stage into the long crack growth stage is a zero value of the first derivative of the modal value of fatigue crack lengths by the number of cycles. The moment when the convergency takes place is determined by the least number of cycles after which the modal value of fatigue crack lengths remains constant irrespective of the number of further cycles. The size parameter of the Weibull distribution of fatigue crack lengths increases with the number of cycles, while the shape factor diminishes as the number of cycles increases.

2.7 SUMMARY OF THE CHAPTER

Several models that simulate small fatigue crack growth rate have been introduced in this chapter. Each model has its own novel features and adequately predict some experimental data of small fatigue crack propagation. Some of these models were applied to deal with small fatigue crack growth in aluminium alloys, especially 7075-T6 and 2024-T3 alloy, with reasonable success. However, it seems difficult to say, by direct comparison of these models, which one could be taken as a unified crack growth law for practical estimation of growth rate of small fatigue cracks in engineering because, apart from the more complicated behaviour of small fatigue crack growth, those researchers who established the above models either concentrate their attention to several factors, such as crack closure,

threshold condition *etc.*, or relate their models to a certain microscopic dimension, such as average grain size and plastic zone size.

- In all models, prediction of growth rate of small fatigue cracks requires determination of crack growth characterisation for each load level.
- Some parameters used in their models seem adjustable when the models are used to predict small crack growth rates.

It remains a difficult task to properly quantify the effect of local microstructure on small fatigue crack growth. To date, no models have been published that use a unified physical parameter to predict the kinetics of small fatigue crack growth on the basis of local plastic deformation and local microstructure. Most models employ experimentally correlated quantities to reflect crack growth characteristics instead of simple mechanical and fatigue properties of materials. The micro-macro mechanical relationship connecting small fatigue crack growth with bulk fatigue behaviour still needs to be studied.

Chapter 3 MATERIALS AND EXPERIMENTAL PROCEDURES

3.1 MATERIALS

Materials to be tested were 7150-T651, 7475-T651 aluminium alloys and 8090-T6 aluminium-lithium alloy. A great deal of experimental research work on small fatigue crack propagation has been published for 7×××series aluminium alloys, which contributes significantly to understanding small crack behaviour and enables comparison of experimental results with model predictions. It is known that cracking behaviour is more complicated in 8090 aluminium-lithium alloy than that in 7××× series aluminium alloys. Therefore, these alloys were selected for testing to obtain basic growth rate data of small fatigue cracks and conventional low-cycle fatigue properties for model prediction use.

The 7150-T651 studied is a conventionally-cast aluminium alloy 7150 and was received as plate 19-mm thick. The material was solution treated at 460^{o}C for about 4 hours. After solution treatment, the material was quenched in cold water to room temperature and then stretched by 2.5 per cent. All specimens were aged at 121^{o}C for 50 hours. The material was partially recrystallized with the unrecrystallized grains flattened, somewhat elongated along the rolling direction and pancake shaped, which is comparable with the same material reported in [63]. Clustering of coarse constituent particles was seldom observed.

40 Microns (a)

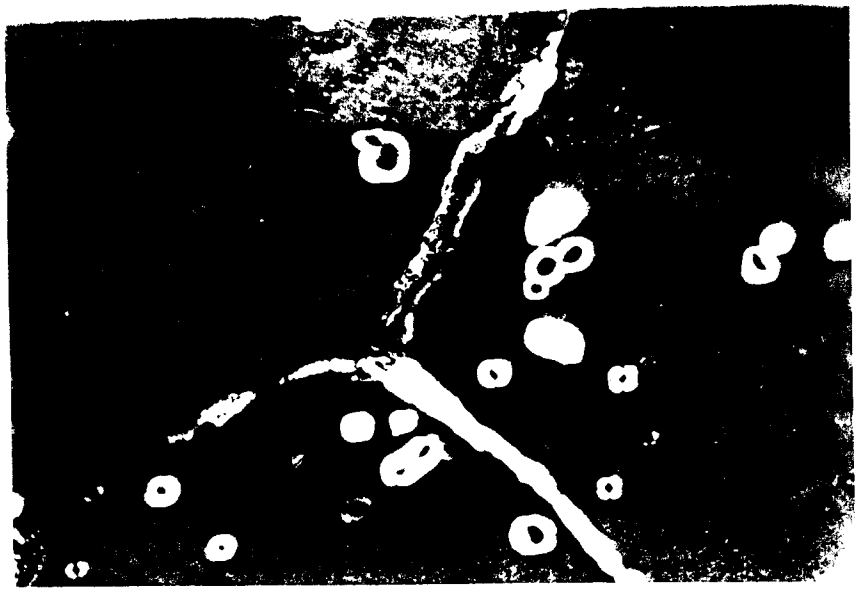

10 Microns (b)

Figure 3-1 Micrographs Of (a) Microstructure Of 7150-T651 Aluminium Alloy; And (b) Grain Boundaries And Triple Point

Figure 3-1(a) is an optical micrograph illustrating the grain structure of the alloy. The nominal chemical composition is shown in Table 1. Etching and anodising were employed to reveal the microstructure of the alloy. A modified Keller's etchant was used to etch two specimens revealing the grain boundaries. Two specimens were anodised by use of 2% fluoroboric acid (HBF4) in distilled water to expose the microstructure. Figure 3-1(b) shows the triple point and grain boundaries.

The 7475 aluminium alloy was supplied in the form of 16-mm thick plate that was in T7351 temper. The material was solution treated firstly in a furnace at 470°C for half hour and then in salt bath at 510°C for another half hour. Then the material was quenched in cold water to room temperature. For a same reason, specimens made of 7475-T651 were aged at 124°C for about 40 hours. Examinations of microstructure revealed an elongated pancake grain microstructure typical of rolled high strength Al-Zn-Mg-Cu alloys. The nominal chemical composition is listed in Table 1.

Table 1. Nominal Chemical Compositions In wt % For Tested Materials

Alloy	Si	Fe	Cu	Mn	Mg	Cr	Ni	Zn	Ti	Zr	Pb	Na	Li
7150–T651	0.07	0.11	2.10		2.16			6.16	0,02	0.13			
7475–T651	0.02	0.04	1.50	44 ppm	2.19	0.21	1.2 ppm	5.75	0.01	1.0 ppm	4.0 ppm	1.0 ppm	
8090–T6	0.05	0.09	1.15		0.62					0.12			2.42

Figure 3-2(a) and Figure 3-2(b) show results of hardness measurement for both aluminium alloys. The aging temperature was 121°C and 124°C for 7150-T651 and 7475-T651 respectively. Higher hardness occurs at about 50 hours for 7150-T651 and 40 hours for 7475-T651 aluminium alloys.

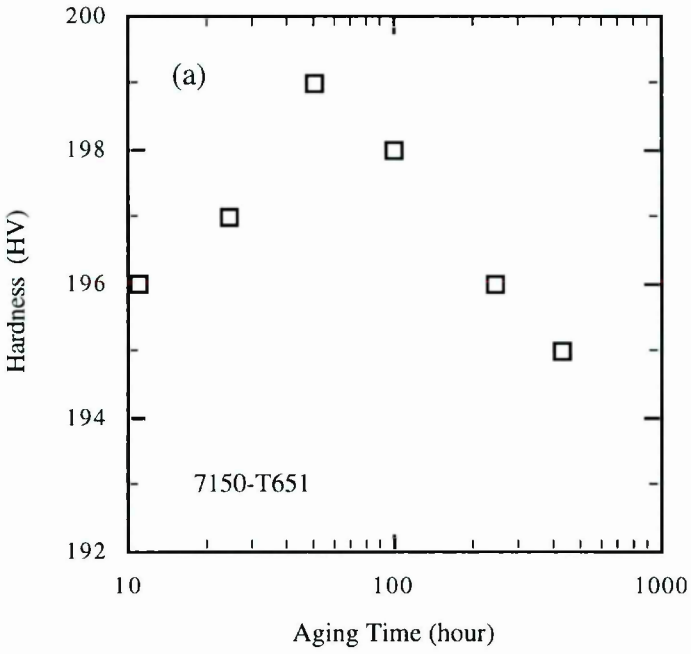
200
198
196
194
192
(a)
7150-T651
Hardness (HV)
10
100
1000
Aging Time (hour)

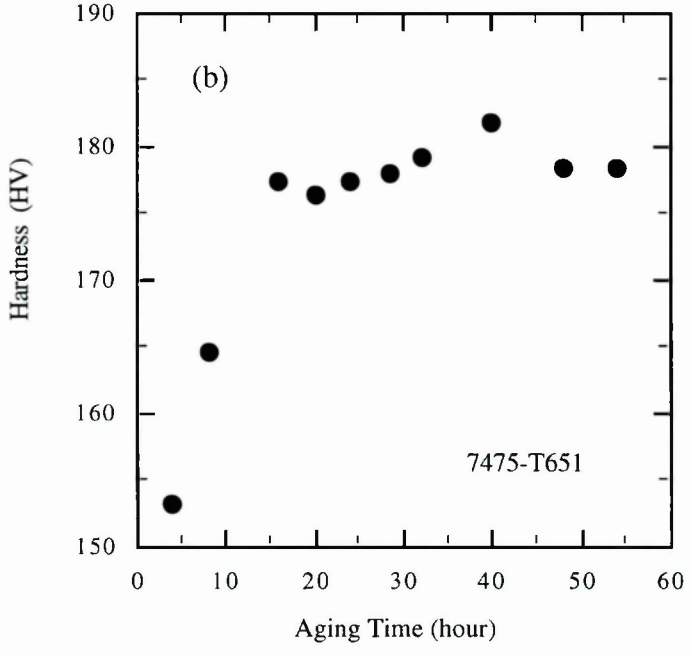
190
180
170
160
150
(b)
7475-T651
Hardness (HV)
0
10
20
30
40
50
60
Aging Time (hour)

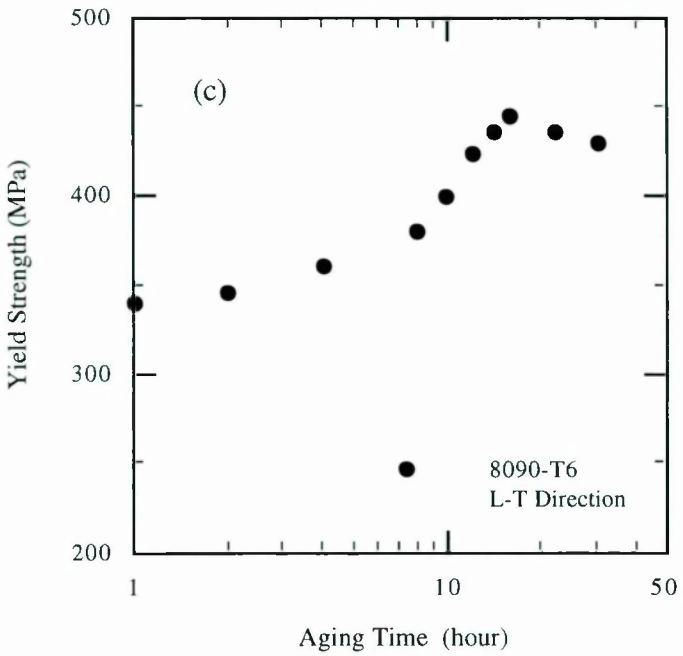

Figure 3-2 Aging Time Effect On Hardness/Strength Of (a) 7150-T651 Aluminium Alloy, (b) 7475-T6 Aluminium Alloy and (c) 8090-T6 Aluminium-Lithium Alloy [201]

The 8090 aluminium-lithium alloy was supplied in T3 temper as 25-mm thick rolled plate in the solution treated, 2% stretched and naturally aged condition. For the modification of microstructure, the material was peak aged at 190^{o}C for 12 hours to form T651 temper condition. The mechanical properties are as follows. Hardness: 171 Hv, 0.2% Proof Stress: 452 MPa, Tensile Strength: 504 MPa, and Elongation(%): 4.2. Aging time effect on the yield strength of the alloy is show in Figure 3-2(c). Maximum yield strength is attainable at about 16 hours.

All micrographs in this study were taken with a Reichert MeF3 optical microscope, a JMS-820 scanning electron microscope and a JEM 2000FX transmission electron microscope.

3.2 SPECIMEN PREPARATION AND EXPERIMENTAL PROCEDURE

3.2.1 Small Fatigue Crack Growth Tests

Fatigue crack propagation tests were conducted in a ESH servo-controlled hydraulic fatigue testing machine under constant amplitude cyclic loading at room temperature. Tests were performed under load control with a frequency of 30 Hz (sine wave) at load ratio ($R = \sigma_{min} / \sigma_{max}$) 0.1. Standard unnotched four-point bending (FPB) specimens (see Figure 3-3) with dimensions of 7×12×60 millimetre were used. The advantage of this type of specimen is that it keeps a constant maximum bending moment between the two small loading arms. The area of the main working surface on the top side of the specimen to be examined is about 7×10 mm^2 where is subjected to a constant maximum tensile stress during bending. Specimen orientation is also indicated in Figure 3-3. Small fatigue cracks propagate on the specimen surface along the normal direction.

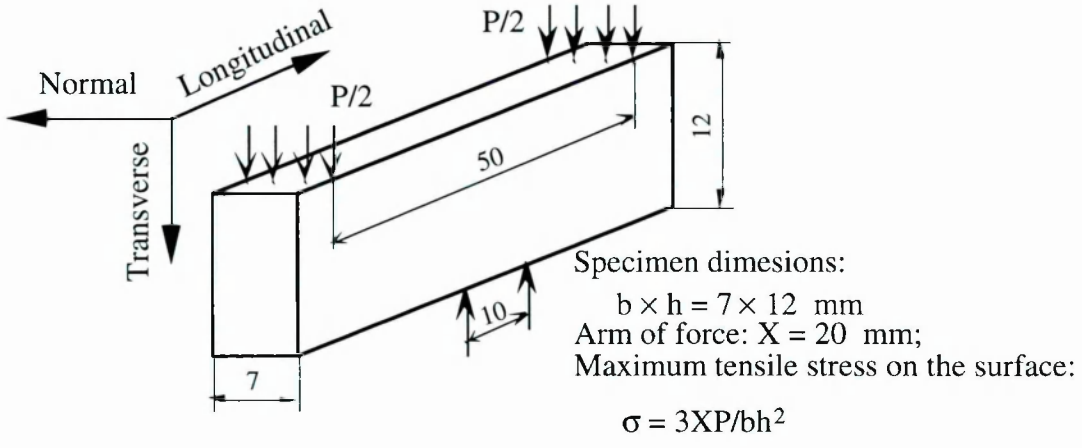

Figure 3-3 Configuration And Orientation Of Four Point Bending Specimen

All specimens were first polished mechanically by wet grinding on emery papers (silicon carbide abrasive papers) ranging from 400 to 1200 grit, and then they were polished, using diamond pastes, starting with 30 microns and ending with 1 micron, on a universal polisher with different sort of Texmet paper cloths step by step. After these two polishing processes, specimens were examined carefully under an optical microscope to make sure that there were no serious scratches remaining on the working surface. The final polishing was finished using diamond slurry oil of 1 micron or a polishing compound of 1 micron to ensure that there were no crack-like scratches or the trace of the last polishing step left on

the working surface. At each polishing step, the polishing direction was always turned 180^{o} to the previous one. The final polishing direction was perpendicular to the load direction to avoid introducing stress concentrations. The edges of all specimens were rounded by abrading and polished in the same way to prevent crack initiation from the edges. Figure 3-4 shows the typical surface texture of a well-polished specimen.

The plastic acetate replication technique was employed in small crack growth tests to measure crack size. Surface replicas were taken periodically during each test. The interval for taking replicas depends upon the fatigue life of the specimen at a prescribed load amplitude as well as a mean stress.

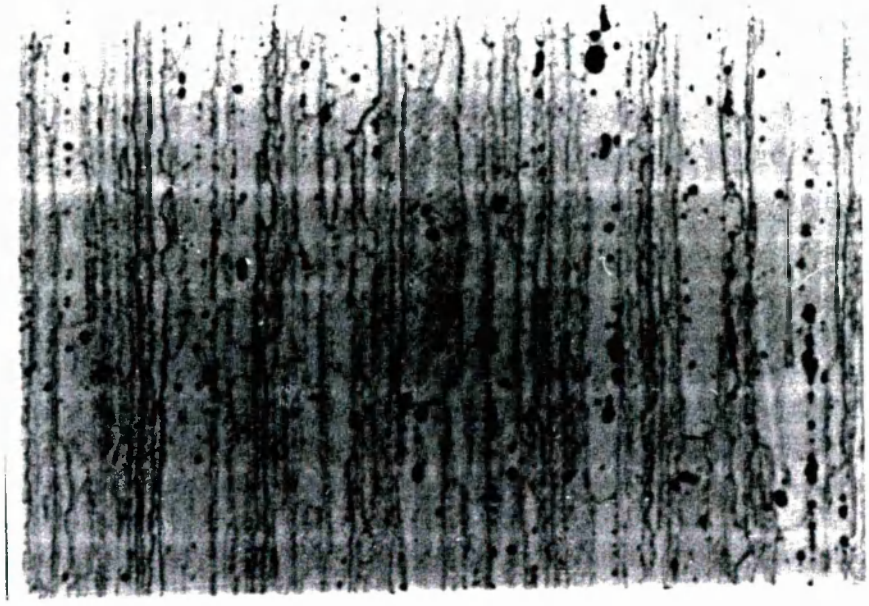

Figure 3-4 Surface Texture Of 7150-T651 Aluminium Alloy

The replication of small fatigue cracks within the main working surface was carried out using a strip of cellulose acetate replicating tape while the specimen surface had been wetted with acetone solution in advance. The solution causes the replica to stick to the surface when it touches the solution and no pressure on the replica is needed. Each replica was laid against the main working surface of a specimen with the crack being open at mean load and left on the surface for about eight minutes to take the configurations of small cracks. When the replica was dry, it was peeled off carefully from the specimen without

damaging the replicating side of the tape. Once the tape was striped off, it was mounted flat on a microscope slide by two pieces of sticky tape as quickly as possible to prevent it from curling. All replicas were collected and stored in identifiable containers for later processing and evaluation. The replication procedure continued until a fatigue crack developed long enough to been seen clearly by eyes. If the crack formed outside the main working area, the specimen was discarded.

Identification of small cracks on replicas was in such a way that each replica was examined from one side to the other side under the optical microscope to identify the location of cracks and measure the crack size. If a microcrack was discovered, the crack was traced back to its first discernible beginning. If a dominant small crack initiated at the edge of the specimen, the crack propagation data was not accepted as effective data. All reported crack growth data are from centrally initiated cracks. For the sake of convenience, the stress intensity factor for small fatigue cracks was estimated by assuming a semi-elliptical surface crack in a finite plate under bending [64-66]. A ratio of depth to surface crack size $\frac{\tilde{a}}{2a}$ = 0.4 was assumed in the K-calculation.

3.2.2 Low-Cycle Fatigue Tests

Fully reversed, total strain-controlled, tension-compression ($R = \varepsilon_{min} / \varepsilon_{max} = -1$) low-cycle fatigue tests were performed at a constant strain rate of 1×10^{-3} s^{-1}. Fatigue specimens made of 7150-T651 aluminium alloy and 8090-T6 aluminium-lithium alloy were taken from the plate with the stress axis parallel to the longitudinal direction (rolling direction) of the plate. The specimens are smooth and cylindrical in the gauge section, which measured 5 mm in diameter and 15 mm in length. The length-to-diameter ratio ensures that the specimen will not buckle under compressive strains.

All fatigue tests were conducted on an Instron 1332 servo-hydraulic testing machine. The strain function exhibited a triangular wave form and the mean strain is zero. All tests were carried out in a laboratory air environment (temperature 16C^{o}, relative humidity of 50%

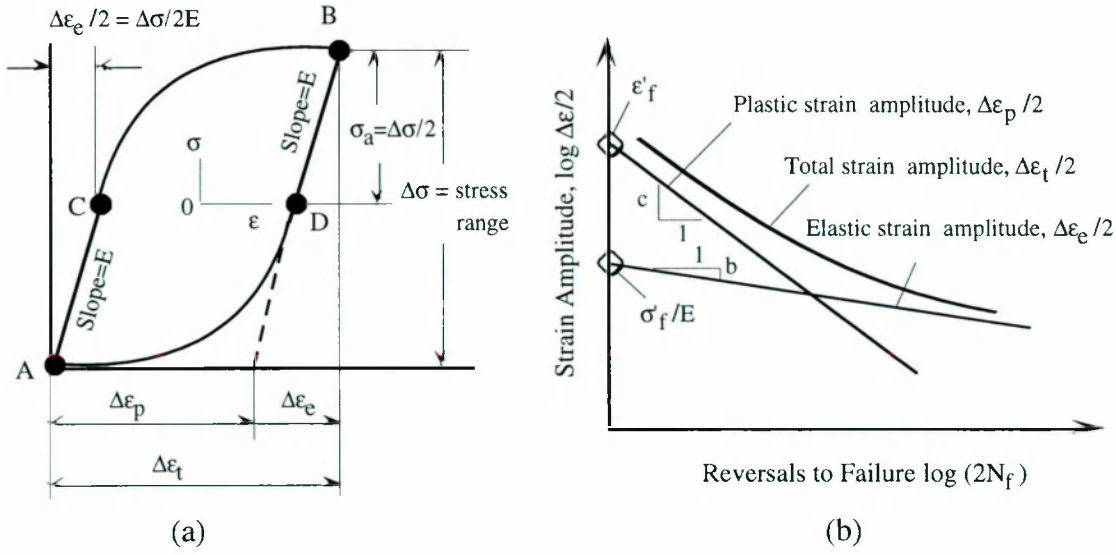

Figure 3-5 Parameters Associated With Strain-Controlled Fatigue. (a) Cycle-Dependent Material Response In Strain Control Fatigue Test; (b) Cyclic Strain-Fatigue Life Response

for 7150-T651 Al-Alloy and temperature 21C^{o}, relative humidity of 48% for 8090-T6 Al-Li Alloy). An axial 10 mm clip-on extensometer was attached to the gauge section of specimen to control the total strain. The stress-strain hysteresis loop was recorded on an X–Y recorder and a Y-t (load-cycle) chart recorder was used to monitor cyclic stress response. The plastic strain range ($\Delta\varepsilon_p$) and the stress range ($\Delta\sigma$) were determined from the width and height of the monitored hysteresis loop during steady-state condition as illustrated in Figure 3-5(a). Figure 3-5(b) illustrates a strain-life curve in low-cycle fatigue tests.

The fatigue failure criterion both for strain-controlled tests and for load-controlled test was defined as complete specimen fracture. Surface inspection for signs of cracking during testing, along with fracture surface examination showed that load instability in load-controlled tests and load drop in strain-controlled tests were due to crack formation and fast growth of fatigue cracks respectively.

Chapter 4 EXPERIMENTAL RESULTS OF SMALL CRACK GROWTH TESTS

4.1 INTRODUCTION

Experimental observations of small fatigue crack propagation in 7150-T651 aluminium alloys and crack growth rates at different load levels are examined in this chapter. There are no published small crack growth data available, to my knowledge, for this aluminium alloy in the T651 condition.

Although it has been extensively suggested that small crack growth rates would fall to a minimum as the small fatigue crack encountered the first grain boundary, there is still a lack of convincing experimental evidence to prove or disprove this expectation. Therefore, the experimental observations in the present work are designed not only to study the small crack behaviour but also to see if the expectation is true.

Besides the observations, the minimum small crack growth rates at different load levels are particularly important because fatigue life of specimens is certainly related to the minimum crack growth rates.

4.2 EXPERIMENTAL OBSERVATIONS AND RESULTS

The initiation sites of microcracks were generally in the middle part of the main working area of FPB specimens, somewhat near, but not at the edge of the specimen. Two sorts of fatigue microcrack initiation were observed for all the load levels investigated.

- Microcracks initiate and develop in the matrix at approximately 45^{o} to the loading direction due to shear band cracking (see Figure 4-1).
- Microcracks emanate from an inclusion as a result of stress concentration there [see Figure 4-2(a)].

The predominant mechanism of fatigue crack initiation is extensive Stage I cracking along slip bands. The early stage propagation of microcracks along grain boundary occurs rarely [see Figure 4-2(a)]. After crack initiation, small fatigue cracks propagate along a somewhat tortuous path that is generally perpendicular to the tensile loading direction. Upon further propagation the crack tip may be deflected by a grain boundary towards a new direction. Fatigue cracking is typically associated with transgranular propagation of small fatigue cracks [see Figure 4-2(b)]. No intergranular cracking was found. Either grain boundaries or inclusions may cause a delay of crack propagation. However, there is no clear evidence from experimental data and observations that indicate

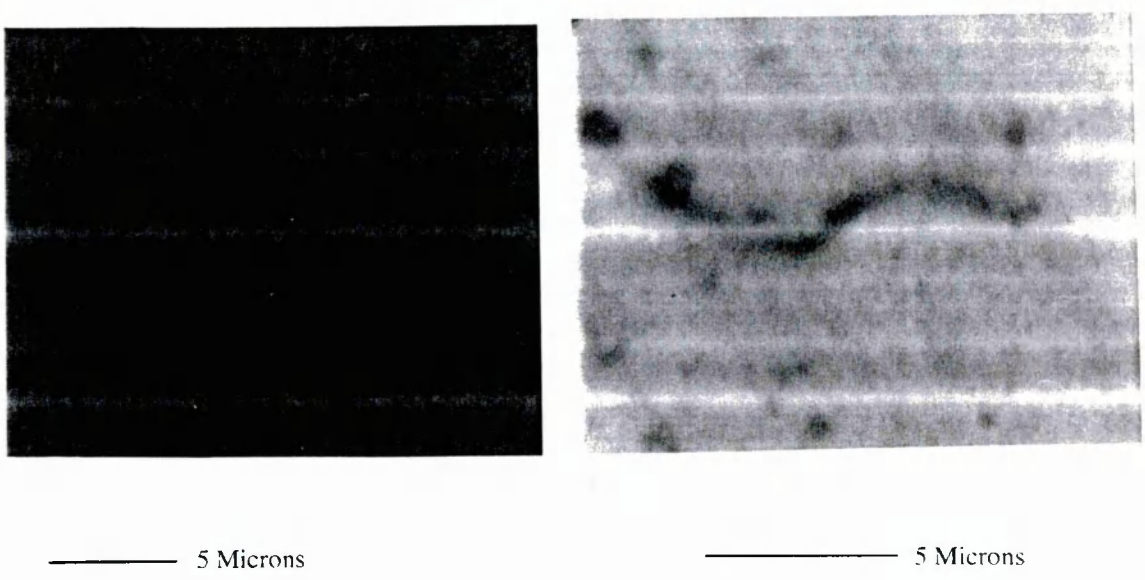

Figure 4-1 Microcracks Initiated At 7150-AA Matrix (Micrographs Taken From Replicas)

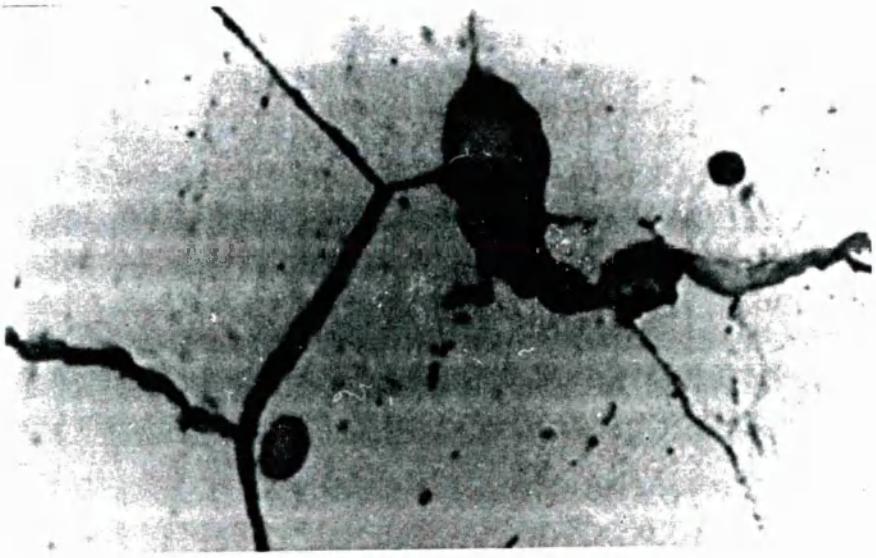

10 Microns (a)

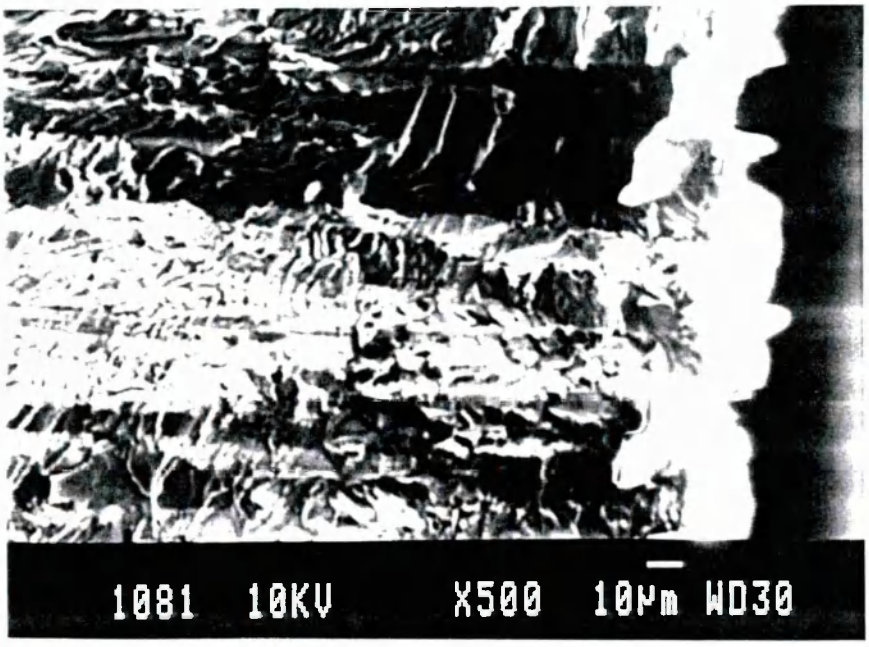

(b)

Figure 4-2 Micrographs Demonstrating (a) Microcracks Initiated At An Inclusion And Early Stage Propagation Along Grain Boundary; And (b) Transgranular Propagation

the severest fall of growth rates as a small fatigue crack penetrates the first grain boundary that it meets.

In the early stage of propagation, small fatigue cracks grew in an anomalous way which is the result of the influence of local microstructure, especially grain boundaries and misorientation between grains. An interaction of the plastic zone with grain boundaries may be a major cause of the irregular manner of small crack propagation [67]. In the low load levels of stress amplitude ranging from 155 to 188 MPa, it was observed that only a single microcrack nucleated from the surface. In the high load level of stress amplitude σ_a = 210 MPa, crack size of nucleated microcracks is relatively bigger and up to three microcracks nucleated from the surface in a few specimen. However, no coalescence of microcracks took place during the early stage of small crack propagation at any load level. Fatigue failure was obviously the result of a dominant small fatigue crack propagation.

Two microcracks emanating from an inclusion/particle on the specimen surface were also observed [see Figure 4-2(a)] in several specimens. The inclusion causes a stress concentration, which facilitates the initiation of microcracks from somewhere around it. If cyclic slip occurs, it will be affected by inclusions. There has been some debate on whether the initial nucleation starts at the interface between an intermetallic inclusion and matrix material, or as a crack in the inclusion, or in a slip band impinging on the inclusion. It can certainly not be ruled out that a microcrack in the inclusion was already present as a result

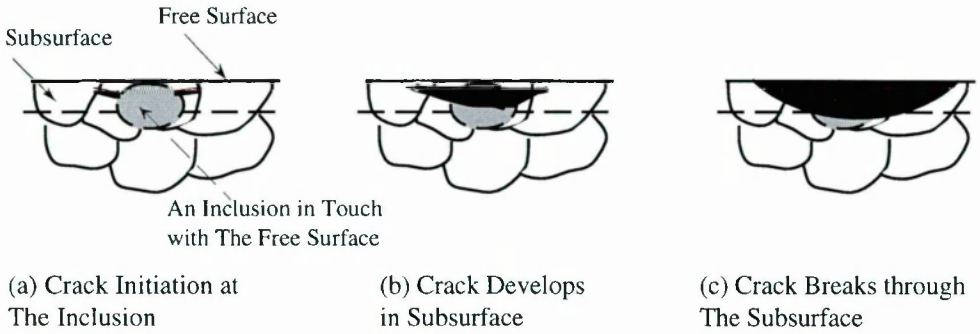

Figure 4-3 A Sketch Of Development of Small Fatigue Cracks That Initiates At An Inclusion In Subsurface

of the material manufacturing. It can also be inferred that a small fatigue crack may nucleate from a subsurface defect, such as an inclusion/particle. It is particularly worth noting that the inclusion may be in contact with but not on the free surface of the specimen. Consequently, the small fatigue crack in the subsurface layer can not be detected until the microcrack breaks through the subsurface layer to the free surface as illustrated in Figure 4-3.

Experimental results of small fatigue crack growth are shown in Figure 4-4 for 7150-T651 aluminium alloy. Irregular crack growth rates are recorded at all load levels. Through examining the specimen surface that had been lightly etched, the blocking effect of grain boundaries to small crack propagation was observed which results in crack path deflection at grain boundaries. More details about the effect has been studied in [78]. This blocking effect remains to take effect even when a small fatigue crack penetrates the first grain boundary, suggesting that the influence of grain boundary blockage should be taken into account. However, a minimum crack growth rate that occurs in the course of small crack propagation is not always in connection with the first grain boundary that the small fatigue crack meets. Upon further development of crack propagation, the convergence of small crack growth into long crack growth occurs as the small fatigue cracks extend to a size ranging from about 90 to 108 microns. Corresponding to 90 and 108 microns, the stress intensity factor range takes values ranging from 2.4 to 3.8 MPa$\sqrt{m}$ at minimum and maximum applied load levels.

It was also found that surface roughness had a dramatic effect on fatigue life of FPB specimens. Specimens polished in the final step with 1 μm slurry oil have longer lifetime than those finished with 1 μm diamond compound. This is due to the fact that the slurry oil as a polishing medium can eliminate very small scratches on specimen surface. Fatigue lives of all specimens versus stress amplitude and applied maximum load are plotted in Figure 4-5. Discrepancy in lifetime caused by the different polishing is quantitatively estimated in terms of maximum stress. The relative error corresponding to the discrepancy

distributes approximately within a range from 50.7% at higher load levels to 165% at lower load levels.

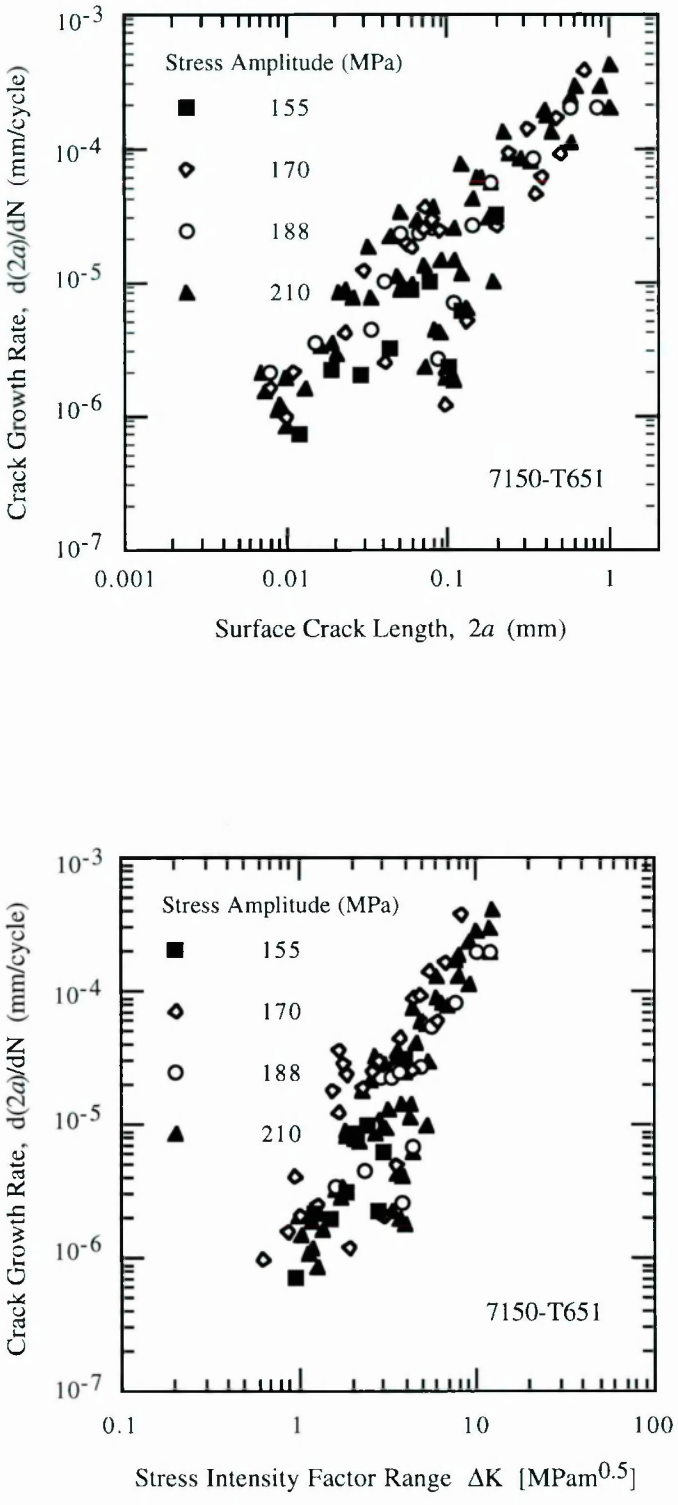

Figure 4-4 Small Fatigue Crack Growths In 7150-T651 Aluminium Alloy

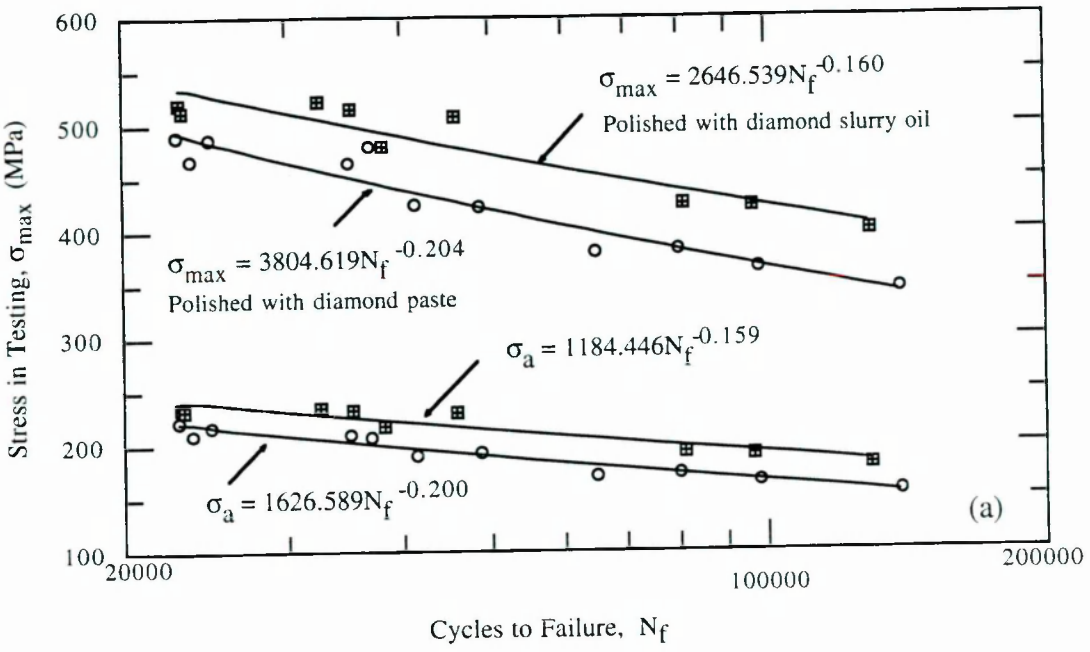

Figure 4-5 Stress-Fatigue Life Relation For 7150-T651 Aluminium Alloy

4.3 DISCUSSION

Discussions in this section are placed on three principal aspects of small fatigue crack growth in the 7×××series aluminium alloys:

(1) Small cracks grow at irregularly fast rates;

(2) Stage I to Stage II crack growth transition;

(3) Convergence of small crack growth into long crack growth.

Acceleration or deceleration of small fatigue crack propagation at early stage of growth was evident in all fatigue tests. The erratic crack growth rates are coupled with a high average crack growth rates at ΔK that is lower than the long crack growth threshold value. This behaviour of propagation also evidences a discontinuous nature of small fatigue cracks growth in the 7×××series aluminium alloys.

4.3.1 The Influence Of Microstructure

The observations confirms that microstructure has a significant influence on microcrack initiation and the early stage of its propagation, especially to small cracks less than a few grain sizes because wherever a small crack initiates grain boundaries act as barriers to crack propagation. There are three interactions of small cracks with grain boundaries.

- The propagation of a small fatigue crack may slow down on approaching a grain boundary.
- Upon contacting a grain boundary between two misorientated grains, the small crack front may deviate towards a favourably crystallographic orientation for slip transmission.
- The first grain boundary does not always causes the severest delay of small fatigue crack propagation in early stage.

There are no clear signs observed in the examination of replicas that indicates a sharp regular reduction of crack growth rate occurred at each grain boundary. However, affected by grain boundaries, a small fatigue crack appears to propagate in a jagged path. This deflection is due to, at least in part, an orientation difference of different slip systems [68]. In other words, the slip planes change direction there, such as from one {111} to another {111} plane [69].

On the other hand, as long as the maximum applied tensile stress is less than the alloy frictional stress, accumulated slips are required to develop a mature plastic zone in the next grain and the crack propagation can not proceed until a critical value for plastic deformation is exceeded. Growth of small fatigue cracks, as a result of interaction with grain boundaries, is therefore not only discontinuous but also sensitive to grain size and grain boundary strength. In addition, as far as the number of grains situated on the periphery of the small crack front is small, the crack tip slip bands will be crystallographic and be blocked at the grain boundary of less favourably oriented grains [69].

In addition to grain size, every microstructural constituent, such as the orientation of slip bands, the mutual misorientation of slip planes in adjacent grains, friction stress in each grain [70], and grain or inclusion size and their spacing [71], has a stochastic nature that leads the small fatigue crack growth to an accelerated and decelerated manner. For instance, a small fatigue crack initiated in the weakest grain decelerates when it approaches a grain with higher deformation resistance. Similarly, the crack accelerates when it approaches a grain with lower deformation resistance.

4.3.2 The Influence Of Plastic Zone

The plastic zone ahead of a small crack tip develops simultaneously as long as the dislocation motion continues at the crack tip. Once the plastic zone meets a grain boundary it may be truncated by the grain boundary resulting in a temporary reduction of crack growth rate. Upon further cycling, the crystallographic slip is initiated in the next grain and the plastic zone quickly develops within the grain, causing a sharp increase in crack growth rate as described in [32]. The truncation, along with subsequent quick development of crack tip plastic zone indicates a noncontinuum nature of crack tip deformation in small crack growth.

4.3.3 The Discrepancy In Crack Growth Rates

Rough comparisons of growth rates of small fatigue cracks in seven sorts of aluminium alloys have been made, and results are shown in Figure 4-6 although some authors did not mention what method was employed to determine the $\frac{da}{dN}$. It can be seen that small crack growth rates recorded for different aluminium alloys are generally within the range from 10^{-7} to 10^{-4} mm/cycle. A large discrepancy at the same ΔK is evident in growth rate. Factors causing such discrepancy may be complicated and difficult to distinguish. However, there may be four possible elements which can partially rationalise the discrepancy in crack growth rate.

- The first element is naturally different alloys investigated and different load levels applied in fatigue tests. The former may be a major factor to cause the discrepancy whilst the latter may incur remarkable fluctuations in crack growth rate [38].

- The second element may be attributed to the fact that there is no well-accepted standard specimens for small fatigue crack tests. So, it is often difficult to compare the experimental results from other laboratories.

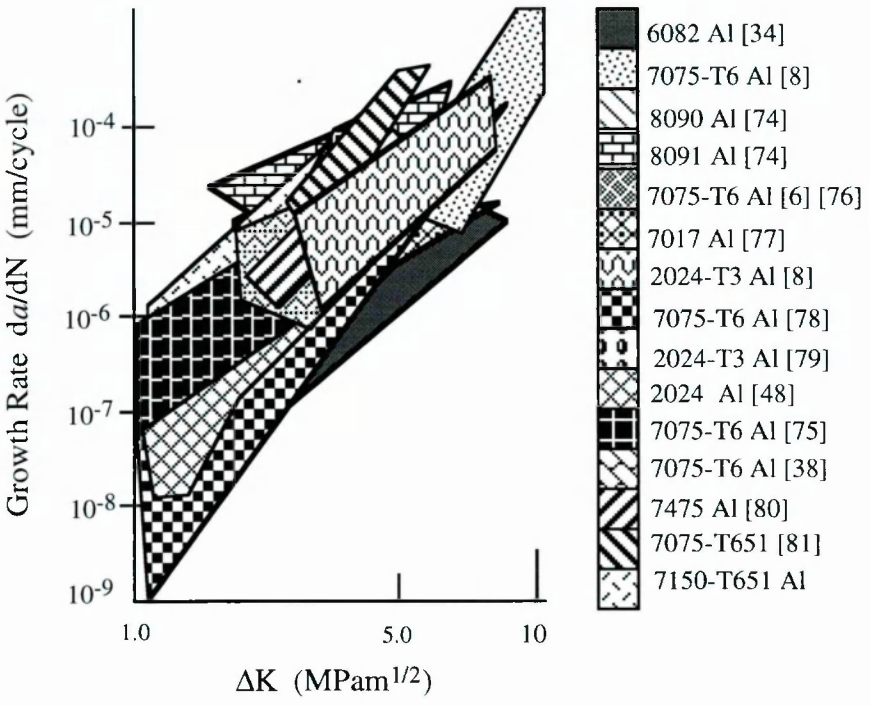

Figure 4-6 Comparisons Of Crack Growth Rates For Aluminium Alloys

- The third element is the technique used to measure the surface crack size. One method is that the small crack size is measured from a projection of the crack on a plane normal to the maximum loading direction. Another way is that the real zigzag cracking path as indicated by Figure 4-7 is measured as the small crack size. It is not possible to say which method is right or wrong to define crack size. However,

different techniques may lead to the discrepancy in the calculated crack growth rates.

- Finally, experimentally recorded data of $a-N$ characteristic relationship for small fatigue cracks are limited in each fatigue test. Even if the data is carefully processed, the resulting crack growth rates seem to be affected by the cycle interval for taking replicas.

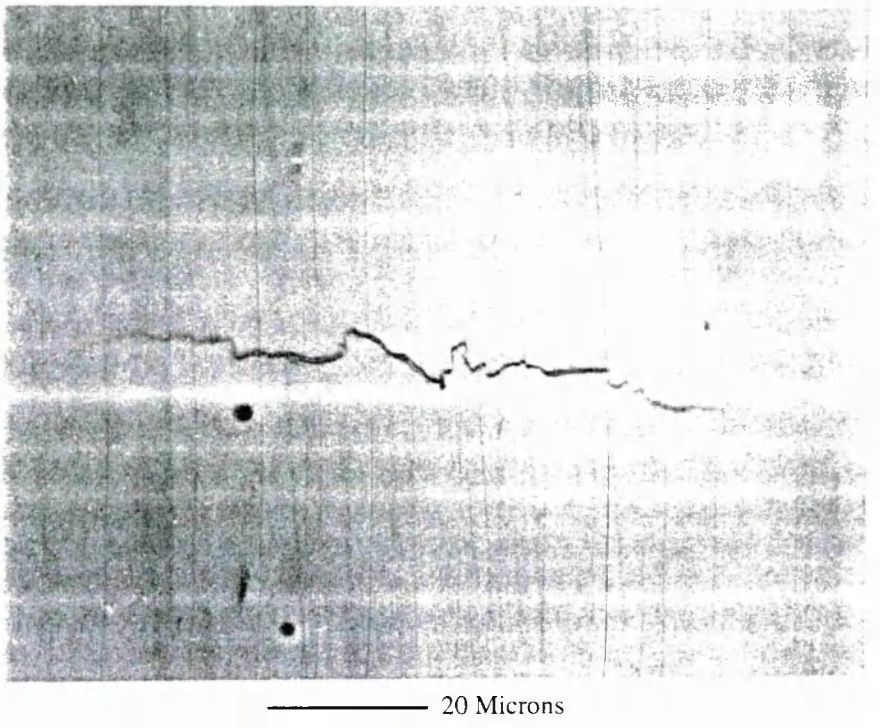

Figure 4-7 Fatigue Cracking In A Zigzag Manner

Possible lowest small crack growth rates at different load levels are of concern since model prediction of fatigue lifetime may involve such information. Figure 4-8 exhibits data comparisons of small crack growth rates. Figure 4-8 together with Figure 4-6 seems to indicate that very lower crack growth rates, particularly those $\left(\frac{d(2a)}{dN}\right)$ far below 10^{-8} mm/cycle [78,124], could be questionable. Re-examination, made by the author, of original experimental work reported in [78,124] seems to disprove the displayed lowest small crack growth rate, particularly those intermittent severe drops of crack growth rate that were attributed to grain boundary blocking [124].

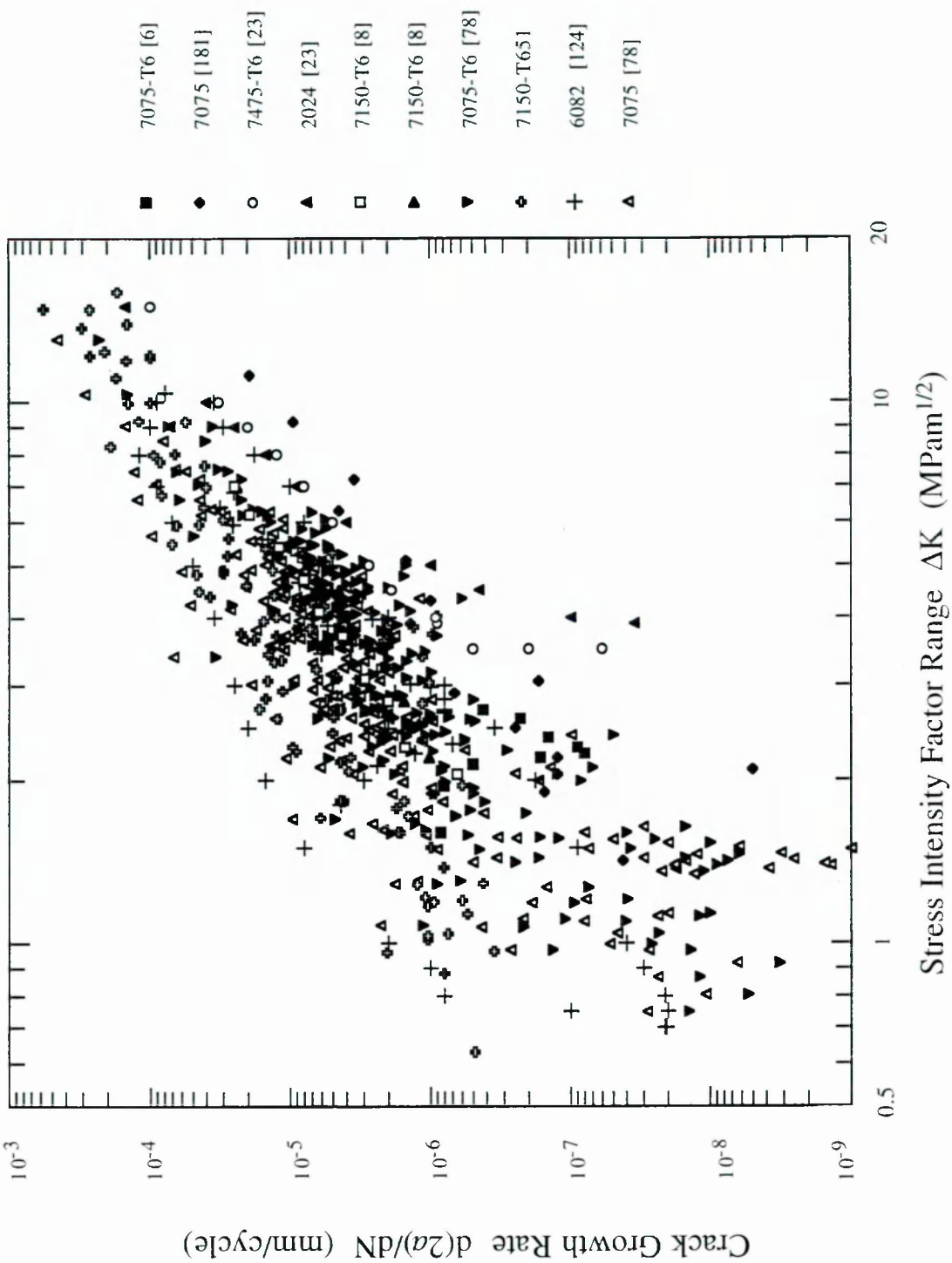

Figure 4-8 Data Display To Compare Reasonable Validity Of Experimental Recordings

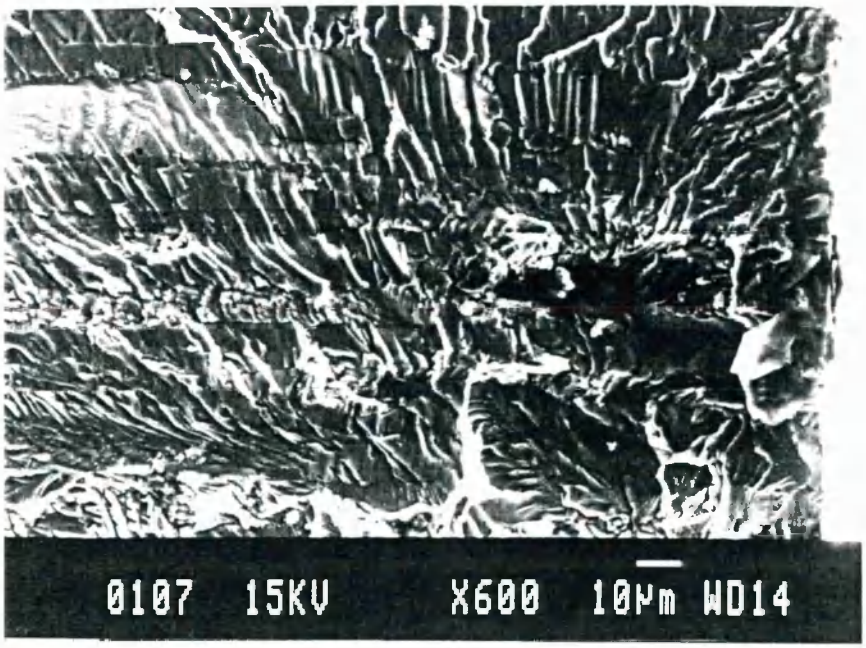

Figure 4-9 Typical Fatigued Area Shown By Scanning Electron Micrograph Of Sample Specimens

Figure 4-10 Fissures In Crack Growth Region

Either the very lower crack growth rates may definitely correspond to an inconceivable longer fatigue lifetime or a very smaller crack increment which seems impossible to be identified by using the replication technique. Conclusively, a well-recognised testing procedure is required indeed for small fatigue crack tests.

It is hereupon suggested that the real surface crack size should be taken as crack length for determining small crack growth rates. This method has three obvious advantages. (1) Firstly, it accurately reflects grain boundary blocking effects on small crack propagation because the zigzag cracking path is primarily due to misorientation between grains. (2) Secondly, it produces real growth rates of small fatigue cracks since the projection method may underestimate crack growth rates when zigzag growth path occurs. (3) Thirdly, it more precisely reflects fatigue damage in materials in comparison to the projection method because the fatigue damage is essentially associated with real cracking in materials. The projection method to determine the small crack size could cause uncertainty to fatigue lifetime estimations.

4.4 CHARACTERISTICS OF FATIGUE CRACKING

In the load-controlled fatigue tests, microcracks initiated either at inclusion or slip bands on the surface of FPB specimens. Fatigue fractures have a common appearance (Figure 4-9) with clear crystallographic type of crack growth. The fracture plane was generally parallel to the transverse direction and fracture was obviously transgranular without any traces of intergranular facets. Fissures were found (Figure 4-10) which extended in the interior towards longitudinal (rolling) direction

Because of continued fatigue cycling, dislocation density progressively increases in the material matrix and dislocation concentration reaches eventually a critical value at which slip band cracks in the matrix along grain boundary or second phase particle-matrix interface [84]. The high stress concentration causes microcracks nucleation at second phase

particle-matrix interface. Since the stress required for microcracks to propagate through the continuous phase (matrix) is larger than that required for them to propagate along grain boundaries [168], fissures in the interior as a result of microcrack coalescence tend to develop along longitudinal (rolling) direction.

4.5 SUMMARY OF THE CHAPTER

(1) Small fatigue cracks initiate either at slip bands or at inclusions in 7150-T651 aluminium alloy and then develop quickly. Grain boundary cracking was not observed in the 7150 aluminium alloys.

(2) Small fatigue cracks grow much faster than do large cracks at approximately the same ΔK and can propagate below the fatigue crack growth threshold ΔK_{th} for long fatigue cracks.

(3) Small fatigue crack propagation may slow down on approaching grain boundaries due to truncation of plastic zone by grain boundaries [32,67]. However, very lower crack growth rates due to grain boundary blocking may need to be carefully studied.

(4) Due to misorientation between two neighbour grains, a small crack front may deviate after penetrating a grain boundary into an adjoining grain. The zigzag crack trajectory is the result of orientation change of new activated slip bands.

(5) The first grain boundary does not always cause the severest drop of growth rate as a small fatigue crack penetrates it. Some grain boundaries have less blockage effect to small fatigue crack growth.

(6) For all load levels investigated, the convergence of a small crack growth into a long crack growth in the 7150-T651 aluminium alloy occurs when the small fatigue crack reaches a size ranging from about 90 to 108 microns.

(7) The macro-plasticity effect, microstructural features of the aluminium alloys, and the stochastic nature of microstructure are considered to be responsible for the accelerating and decelerating growth of small fatigue crack propagation in early stage.

(8) Fatigue damage is primarily due to transgranular cracking other than intergranular cracking. Fatigue failure of FPB specimens is the direct result of individual crack propagation.

In summary, Conclusion (2), (5), (6), (8) and (9) will be particularly of relevance to the micromechanical model which will be presented later in the thesis, whereas other conclusions may be useful for optimising fatigue life prediction methods. Although the present experimental work only reinforces previous experimental observations, made by others, in polycrystalline materials, the author still suggests that

- first grain boundary is not always the most effective barrier to deter small fatigue crack propagation, and
- grain boundary blocking, along with cracking path deflection must be considered in micromechanical simulations of small fatigue crack growth.

Chapter 5 EXPERIMENTAL RESULTS OF LOW-CYCLE FATIGUE TESTS

5.1 INTRODUCTION

It is well known that fatigue failure of plain specimens in push-pull low-cycle fatigue tests is the result of surface small fatigue crack propagation. The propagation of surface small fatigue cracks may be affected by bulk fatigue behaviour. To collect fatigue properties, low-cycle fatigue tests need to be carried out for the 7150 aluminium alloy and the 8090 aluminium-lithium alloy. In addition, different microstructure may lead to different cracking behaviour. Therefore, metallurgical observations and review of the fatigue failure mechanisms associated with the different alloys are needed for properly simulating of cracking behaviour in different microstructure.

The cyclic stress response of materials in fatigue is also important. Continuous hardening or softening behaviour at different load levels reflects a change of bulk fatigue behaviour that may result in change of fatigue properties. An experimentally determined 'stress — fatigue cycle relationship' may be helpful for model predictions of small crack growth. Thus, it is necessary to consider the intrinsic micromechanisms responsible for the hardening or softening behaviour, particularly the role of grain boundaries. These considerations lead to this chapter.

5.2 EXPERIMENTAL RESULTS

Cyclic stress-strain curves can be generated by the companion specimen method which connects the maximum stress of the stabilised half-life hysteresis loops, *i.e.* tips of stable hysteresis loops, from constant amplitude, strain-controlled fatigue tests. However, since a compressive mean stress was present in the fully reversed tests, the stress amplitude $\left[\sigma_a = \frac{\Delta\sigma}{2}\right]$ was used instead of the maximum stress. The cyclic stress-strain curve is modelled mathematically by separating total strain amplitude into elastic and plastic components. Cyclic plastic strain is a measurable quantity that is related to fatigue damage. Figure 5-1 shows experimentally recorded hysteresis loops at different stain ranges and typical hysteresis loops in fatigue tests for 7150-T651 aluminium alloy. Figure 5-2 and Figure 5-3 show experimental results of cyclic strain-stress relations for 7150-T651 aluminium alloy and 8090-T6 aluminium-lithium alloy respectively. Curve fitting indicates that the cyclic plastic strain can be expressed using Equation 5-1.

A vast number of low-cycle fatigue tests on various polycrystalline metal materials have confirmed that stress-strain hysteresis loops can be formulated using elastic strain amplitude and plastic strain amplitude in the form of power function, *i.e.*, Equation 5-1(b), which is illustrated in Figure 3-5. Equation 5-1(a) is an important material property in fatigue design for enhanced fatigue resistance, which depicts the non-linear stress-strain response for the majority of metal materials between cyclic stress and cyclic plastic strain amplitude over the entire life range, and is a very useful aid in understanding the low-cycle fatigue process.

$$\frac{\Delta\varepsilon_p}{2} = \left(\frac{\Delta\sigma}{2K'}\right)^{1/n'} \tag{5-1a}$$

$$\frac{\Delta\varepsilon}{2} = \frac{\Delta\varepsilon_p}{2} + \frac{\Delta\varepsilon_p}{2} = \frac{\Delta\sigma}{2E} + \left(\frac{\Delta\sigma}{2K'}\right)^{1/n'} \tag{5-1b}$$

In Equation 5-1, the cyclic strength coefficient, K', and cyclic strain hardening exponent, n', is determined respectively from log-log linear regression of the half-life stress amplitude versus the corresponding plastic strain amplitude.

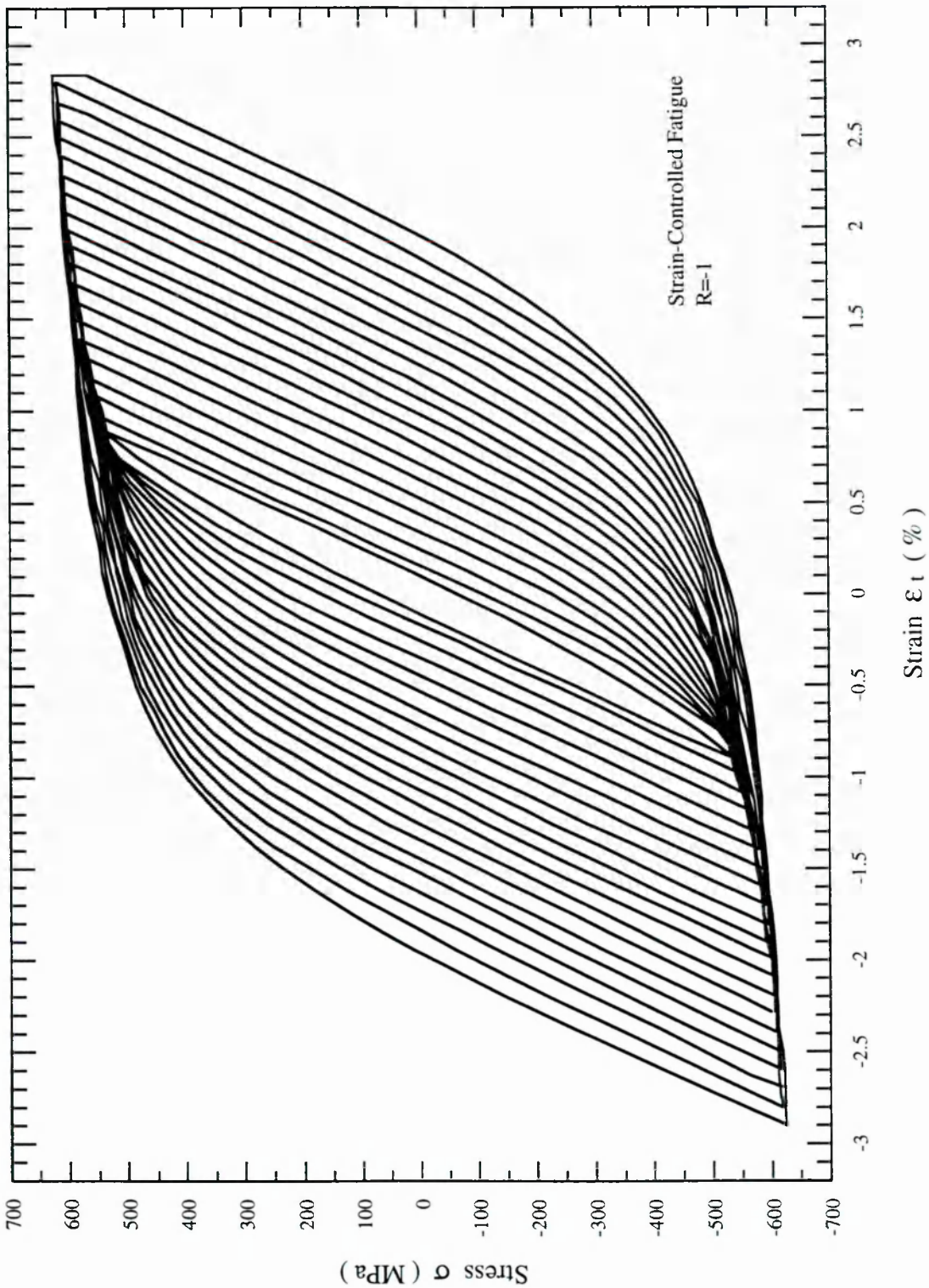

Figure 5-1(a) Experimentally-Recorded Cyclic Hysteresis Loops (7150-T651) In Low-Cycle Fatigue Testing

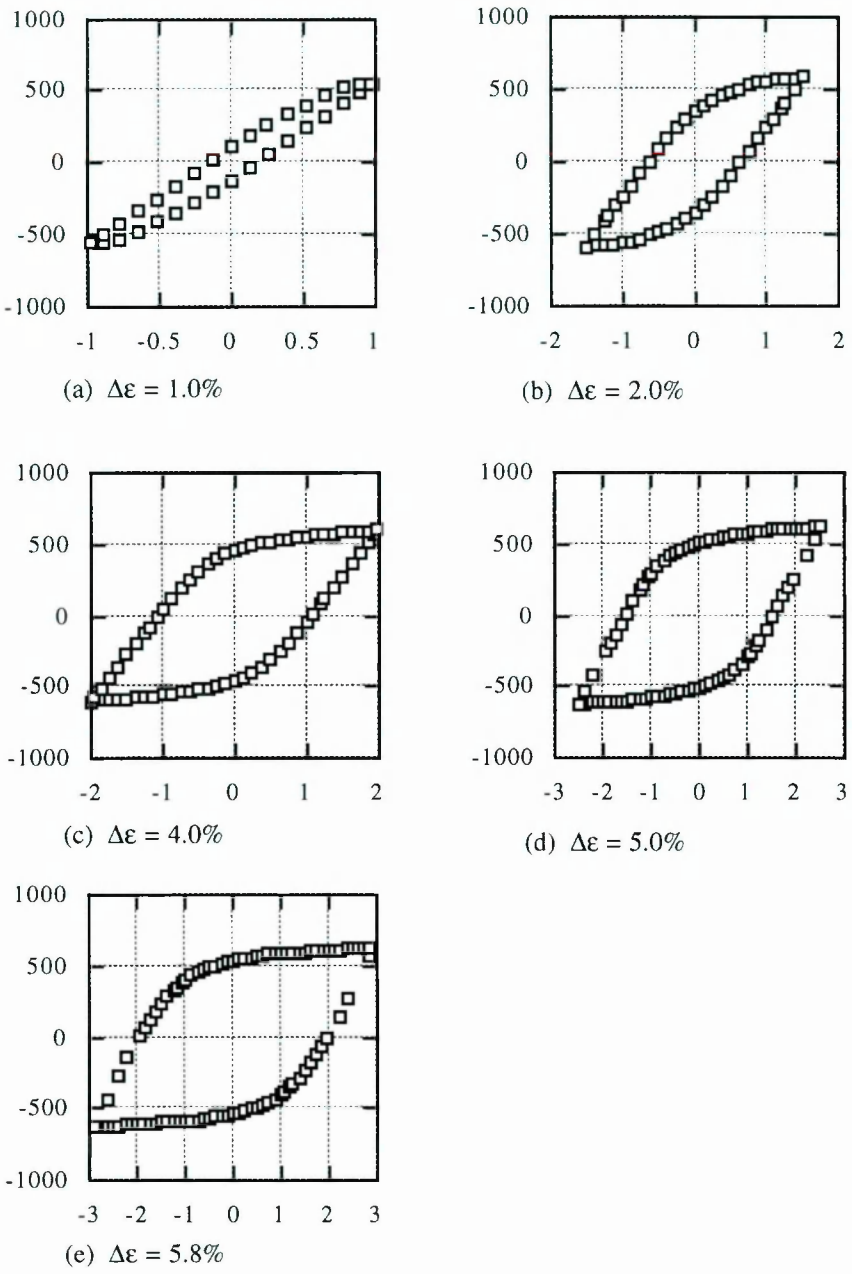

Figure 5-1(b) Typical Hysteresis Loops Of Strain-Stress Response (7150-T651)

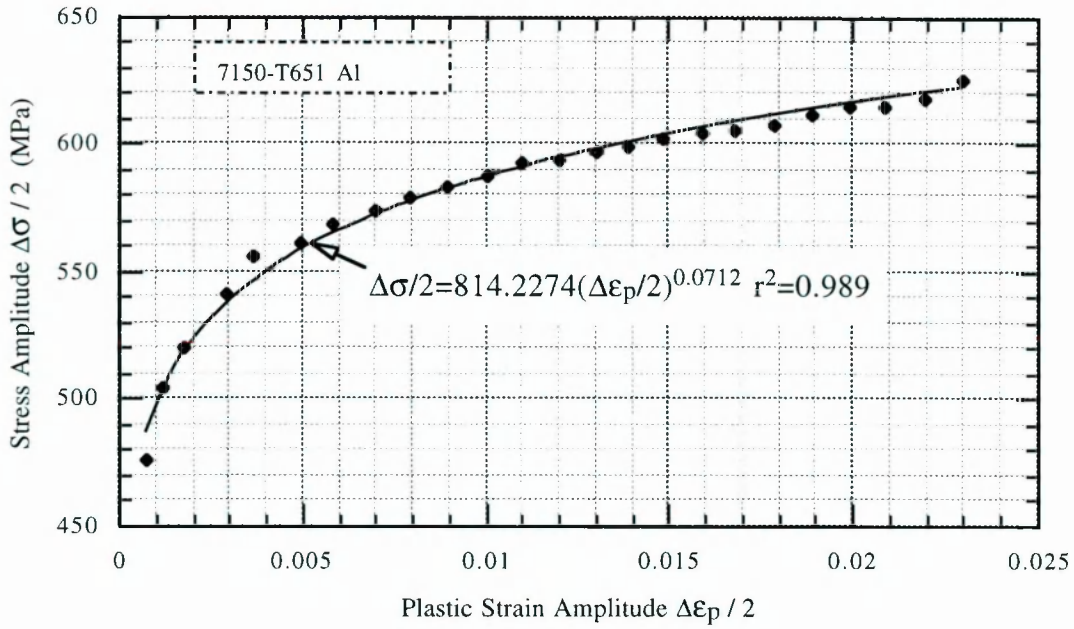

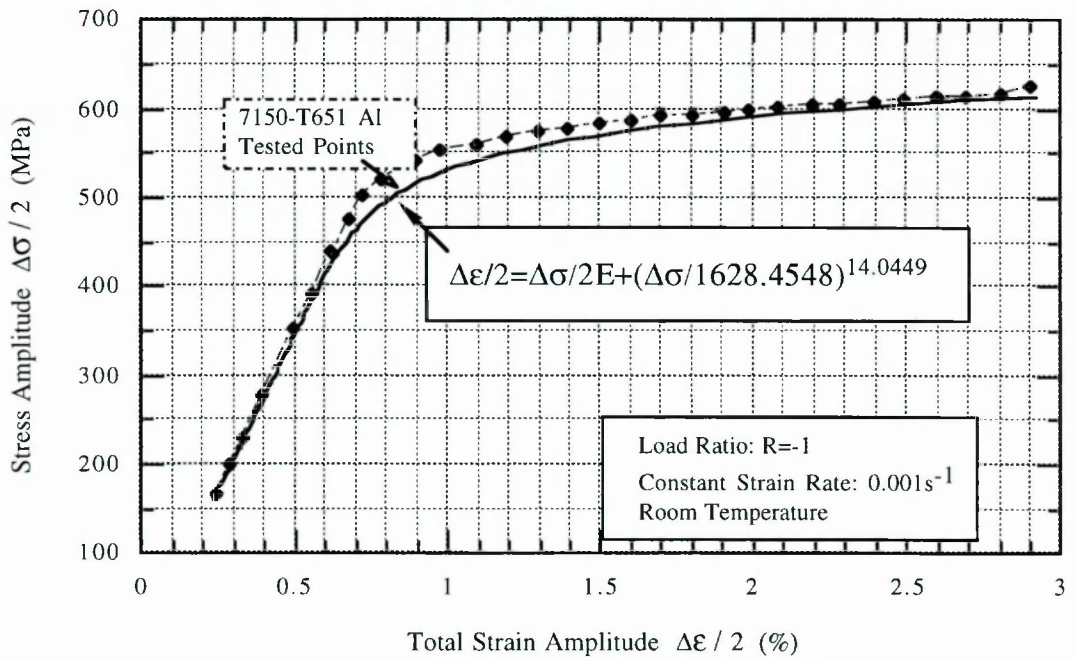

Figure 5-2 Experimental Results Of (a) Cyclic Plastic Strain-Stress Relation; (b) Cyclic Strain-Stress Curve For 7150-T651 Aluminium Alloy

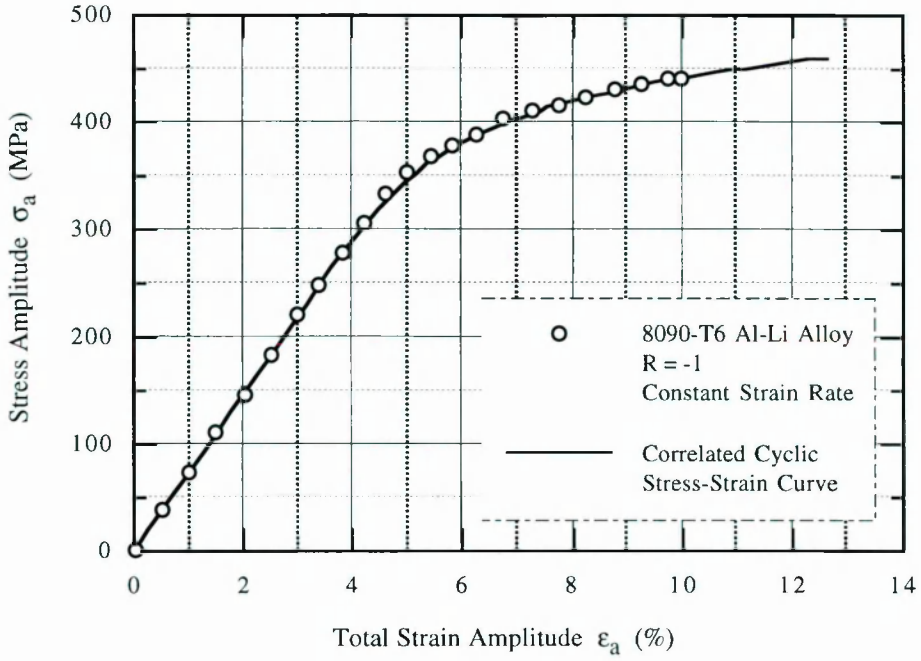

Figure 5-3 Cyclic Strain-Stress Curve For 8090-T6 Aluminium-Lithium Alloy

Fatigue resistance of metal materials is commonly considered consisting of elastic and plastic two parts. The fatigue resistance can be formulated in terms of Coffin-Manson empirical strain-life relation shown in Figure 3-5(b). The Coffin-Manson empirical relation provides a better estimation of fatigue endurance in the low-cycle fatigue regime ($N_f < 10^5$ cycles). The plastic relation is usually plotted on bilogarithmic co-ordinates, on the basis of plastic strain amplitude, $\Delta\varepsilon_p$, and reversals to fatigue failure, $2N_f$ in the form of

$$\log\left(\frac{\Delta\varepsilon_p}{2}\right) = \log\varepsilon_f' + c\log(2N_f) \qquad (5\text{-}2)$$

A best straight-line fit for the Coffin-Manson plot may be attainable by linear regression analysis in which fatigue ductility exponent, c, will be determined. The constant, c, represents the slope of the curve of plastic strain against fatigue life. An extrapolation of this best fit can be made to determine the fatigue ductility coefficient, ε_f' at $2N_f = 1$ that is related to the cyclic ductility of the material. A further extrapolation of the best fit back to $N_f = 1$ gives the plastic strain amplitude at which fatigue failure occurs after first quarter cycle. This represents approximately the fracture strain of the material in a monotonic tensile test, ε_f. A similar process like above was adopted to determine constants, b, $\frac{\sigma_f'}{E}$, and

then $\frac{\Delta\varepsilon_e}{2}$ —$2N_f$ relationship as exhibited in Figure 3-5(b). The elastic Young's modulus, E, of the 7150-T651 aluminium alloy could take an average value, among those as shown in Figure 3-5(a), determined in each test from the first quarter cycle. All recorded data in Low-cycle fatigue tests were processed in terms of Coffin-Manson conventional low-cycle fatigue relations:

$$\frac{\Delta\varepsilon_p}{2} = \varepsilon_f'(2N_f)^c \tag{5-3a}$$

$$\frac{\Delta\varepsilon}{2} = \frac{\Delta\varepsilon_e}{2} + \frac{\Delta\varepsilon_p}{2} = \frac{\sigma_f'}{E}(2N_f)^b + \varepsilon_f'(2N_f)^c. \tag{5-3b}$$

Table 2 Mechanical And Fatigue Properties Of 7150-T651 Aluminium Alloy And 8090-T6 Aluminium-Lithium Alloy

7150-T651	σ_y' (MPa)	n'	σ_u (MPa)	K' (MPa)	E (MPa)
	421	0.0712	600	814.2	69800
	σ_f' (MPa)	b	ε_f'	c	
	1199	-0.108	0.03	-0.49	
8090-T6	σ_y' (MPa)	n'	σ_u (MPa)	K' (MPa)	E (MPa)
	300	0.09	450	590	7300

Figure 5-4 exhibits recorded results of low-cycle fatigue tests which can be taken as an indication of resistance of the alloy microstructure to crack initiation and failure. All fatigue properties relating to cyclic deformation and low-cycle fatigue are listed in Table 2. As it is well known, the mean stress, σ_m, will affect fatigue lifetime if load ratio does not keep R = –1. To take account of this effect, the Coffin-Mansion strain-life relation may be modified by replacing σ_f' with $(\sigma_f' - \sigma_m)$ in Equation 5-3(b). Low-cycle fatigue curves for the 7150-T651 aluminium alloy can be expressed as Equation 5-4(a) whereas the one for 8090-T6 aluminium-lithium alloy can be expressed as Equation 5-4(b).

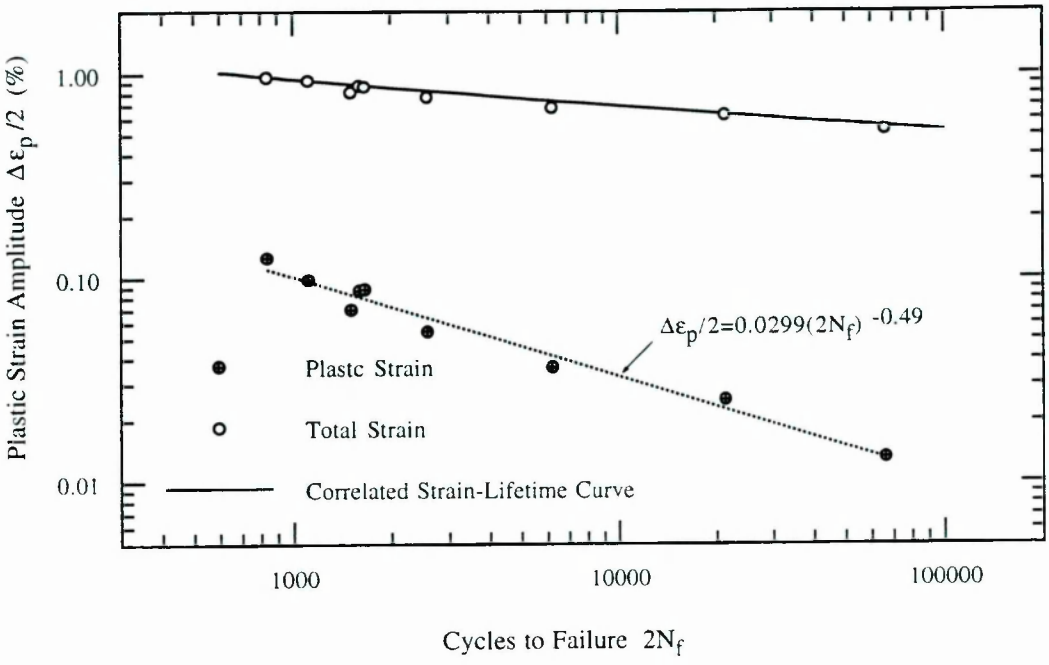

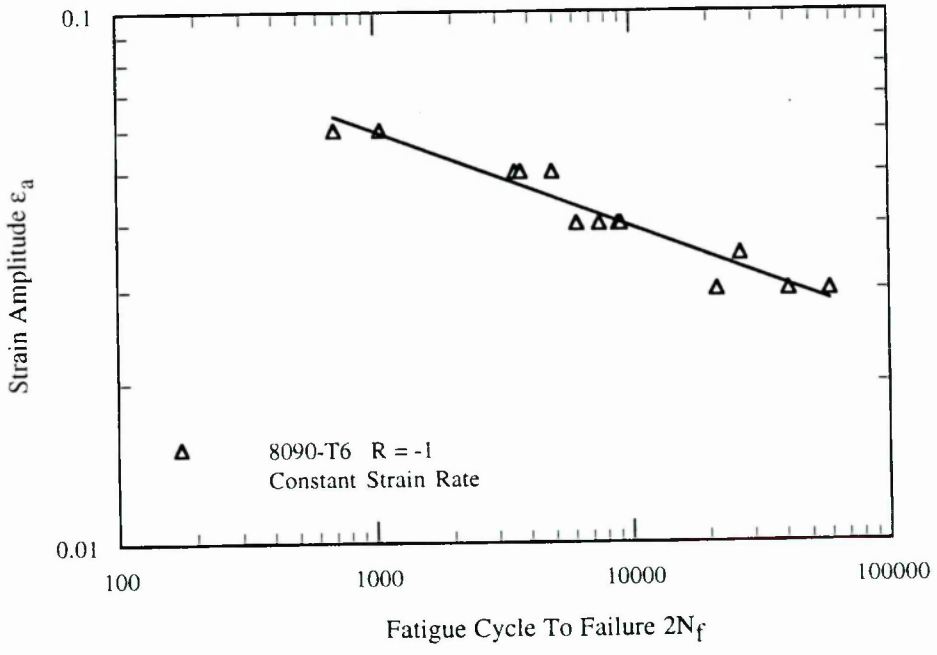

Figure 5-4 Low Cycle Fatigue Curves For (a) 7150-T651 Aluminium Alloy; And (b) 8090-T6 Aluminium-Lithium Alloy

$$\frac{\Delta\varepsilon}{2} = 0.0172\,(2N_f)^{-0.108} + 0.03\,(2N_f)^{-0.49} \qquad (5\text{-}4a)$$

$$\frac{\Delta\varepsilon}{2} = 0.207\,(2N_f)^{-0.18} \qquad (5\text{-}4b)$$

Experimental results prove that 8090-T6 aluminium-lithium alloy exhibits much weak fatigue resistance as compared to 7150T651 aluminium alloy. Data processing on recorded hysteresis loops for 8090-T6 aluminium-lithium alloy indicates that it is impossible to separate a plastic strain component from the total applied strain at low strain range because specimens fractured while the applied nominal strain range remained elastic. This phenomenon demonstrates two fundamental mechanical features associated with the 8090-T6 aluminium-lithium alloy, *i.e.*, a high stress concentration at grain boundaries and a low ductility, which will be explained in the following sections.

5.3 CYCLIC STRESS RESPONSE (7150-T651)

Cyclic-stress response was monitored and is an important feature of the low cycle fatigue process. The mechanical stability of the microstructural features during reverse plastic straining, coupled with the ability of the alloy to distribute plastic strains over the entire volume are two important factors controlling the cyclic response of a material [82-83]. Thus, the cyclic stress response plays an essential roll in all aspects of the fatigue process. Figure 5-5 shows cyclic stress response curves measured for the aluminium alloy 7150-T651. These curves exhibit clearly a tendency of continuous softening with increase in fatigue cycles at all strain ranges.

However, the cyclic softening with increase of cycles is less pronounced at lower strain amplitude than at the higher strain amplitudes, especially during the early lifetime. At the higher stain amplitude the development of material softening continues throughout the entire lifetime. At lower strain amplitudes the development of softening is smooth and

somewhat hindered in early stage of fatigue life, accompanying with a limited duration of material hardening.

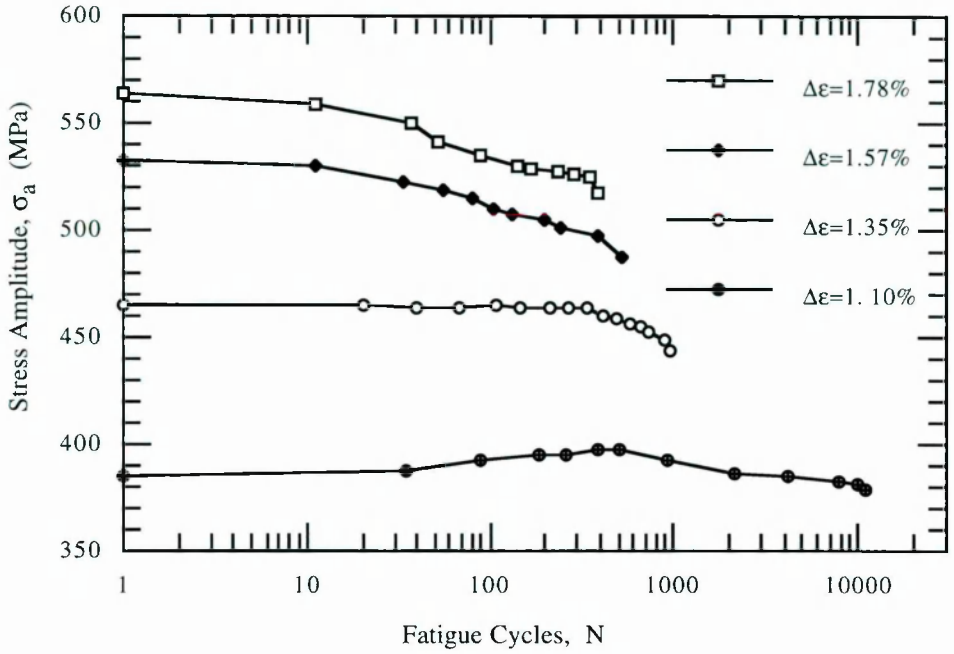

Figure 5-5 Typical Cyclic Stress Response Curves For The 7150-T651 Aluminium Alloy

Since the cyclic deformation plays an important role in crack formation and propagation, it is necessary to understand the intrinsic micromechanisms responsible for the observed softening behaviour. T. S. Srivatsan [84] considered for the same alloy in T77 condition that the precipitates are small, so they do not contribute to cyclic hardening but promote softening from the onset of fatigue. He suggested that with continued cyclic straining dislocations continue to pass on the active slip plane once the matrix precipitates are sheared, which results in a progressive reduction of local work hardening capability. The to-and-fro dislocation motion causes shearing of these small precipitates during cyclic straining no matter whether they are coherent or incoherent [84].

Generally, the cyclic stress response curves of stress amplitude during low cycle tests versus number of cycles at a fixed cyclic strain range illustrate a softening behaviour of 7150-T651 aluminium alloy which has generally some similarities to those found in other Al-Zn-Mg based alloys pertaining to 7××× series [85-87]. However, it is worth noting that the cyclic stress response curve for the lower strain range contains a strain hardening

part, indicating that the alloy in T651 condition seems to behave like strain hardening materials to a some extent for a certain number of fatigue cycles if the applied cyclic strain level does not exceed a specific value.

5.4 CYCLIC DEFORMATION AND FRACTURE CHARACTERISTICS

The fracture surface topographies of fatigued cylindrical specimens were examined under SEM in order to identify

- the initial fatigue and final fracture regions,
- local areas of microcrack initiation and fatigue damage regions, and
- fatigue failure mode.

SEM observation of tested specimens confirms that fracture is transgranular. Fractographic examination to local regions of microcrack initiation indicates that microcracks initiate either at slip bands at the surface or emanate from inclusions at the sub-surface.

5.4.1 Strain-Controlled Fatigue (7150-T651)

At high strain amplitudes above $\Delta\varepsilon$ = 1.8%, microcracks were more likely to initiate at inclusions at the sub-surface [see Figure 5-6(a)]. Observed macroscopic fracture was normal, that is at about 90^{o} to the rolling plane and the stress axis. Macroscopic fracture surfaces were generally flat but with a small portion of slant fracture. The fracture took the form of predominantly ductile transgranular rupture as demonstrated in Figure 5-6(b). The appearance of the transgranular fracture surface showed that the transgranular cracking was perpendicular to the major stress axis. Fatigue crack growth regions were generally smooth without any quasi-cleavage facets. Shallow dimples on the transgranular fracture

(a)

(b)

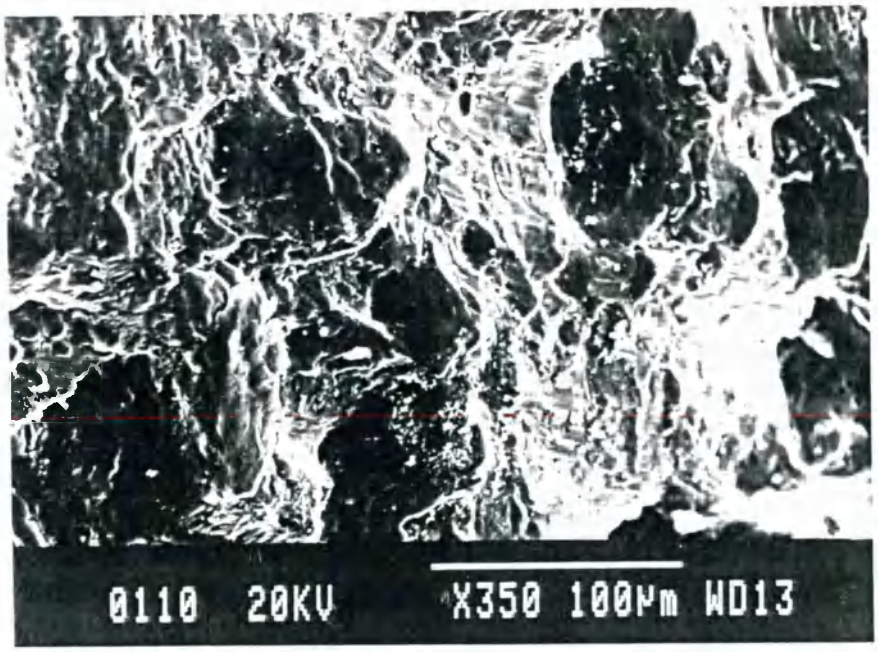

(c)

Figure 5-6 Scanning Electron Micrographs Of Sample Specimen ($\Delta\varepsilon$ = 1.78%). (a) Local Areas Of Crack Initiation And Early Crack Growth; (b) Final Fracture Region; (c) Shallow Dimples On Transgranular Fracture Surface

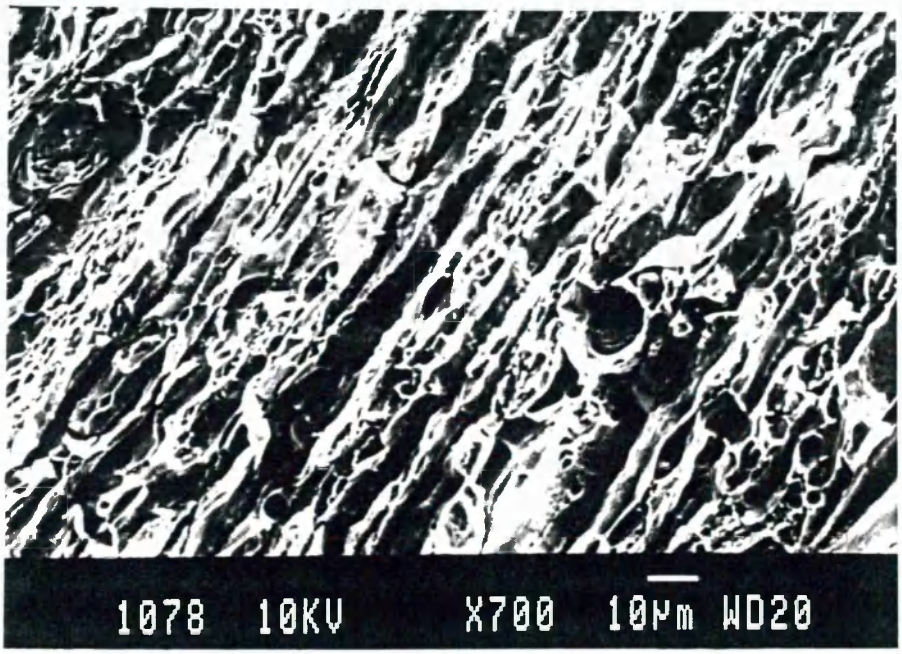

(a)

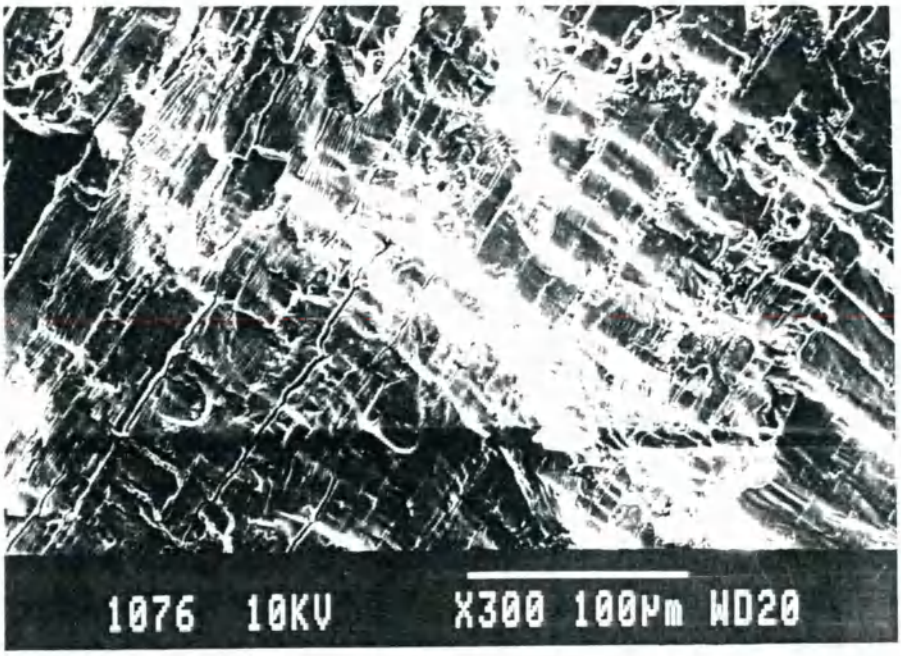

(b)

(c)

Figure 5-7 Scanning Electron Micrographs Of Sample Specimen ($\Delta\varepsilon$ = 1.1%). (a) Final Fracture Region; (b) Intersection Of Slip Planes; (c) Extension Of Fissures Towards Interior

surface [Figure 5-6(c)] could be observed.

At lower strain amplitudes $\Delta\varepsilon = 1.1\%$, microcracks were likely to initiate at slip bands on specimen surface as a result of dislocation concentration at grain boundary and grain boundary triple point. The initiation site has a flat profile. Fractography of specimens indicated that the fracture took a form of predominantly ductile transgranular failure [Figure 5-7(a)] without traces of brittle intergranular regions. Macroscopic fracture surfaces were flat. No slant fracture was observed. Distinctive macroscopic areas for fatigue crack initiation, fatigue crack growth and final fracture were usually observed. The major cracks were perpendicular to the stress axis.

It was also observed that different slip planes intersected in a relatively large area of crack growth [see Figure 5-7(b)] which is more pronounced at the lower strain range than at the higher strain range. Fissures extended down perpendicular to the loading direction. More elapsed fatigue cycles required at lower plastic strain amplitudes results in a great accumulation of strain at grain boundaries and at grain boundary triple points. Consequently, the stress concentration in these regions is high and favours low-energy quasi-cleavage cracking along grain boundary as shown in Figure 5-7(c).

5.4.2 Strain-Controlled Fatigue (8090-T6)

The fracture mode in fracture origin area for 8090-T6 aluminium-lithium alloy consists of transgranular fracture surface, which is the principal fracture surface, plus the intergranular fracture surface, which is perpendicular to principal fracture surface. The stepped appearance (see Figure 5-8) can be observed on the secondary crack surface. Secondary cracks might result from interaction between planar slip and grain boundaries.

Figure 5-9 shows a typical grain boundary region and grain structure after fatigue. 8090-T6 aluminium-lithium alloy has weak grain boundaries and exhibits high stress concentrations at grain boundaries. The weak grain boundaries are attributed to precipitate free zones, and the grain boundary segregation of tramp elements [202, 208, 209]. The

high stress concentration at grain boundaries is attributed to planar slip, precipitates free zones and equilibrium precipitates at grain boundaries [208, 209]. Due to the above two factors, the 8090-T6 aluminium-lithium alloy suffers from a marked tendency to intergranular fracture caused by intergranular secondary cracks. These intergranular secondary cracks grow only in a direction parallel to loading axis because the prominent part of grain boundaries for unrecrystallized grains elongated along deform direction is parallel to loading axis [201,202]. As a result, it shows rapid fatigue crack nucleation at grain boundaries.

8090-T6 aluminium-lithium alloy shows a very rough fracture surface as shown in Figure 5-10. This appearance indicates that cracking can take place along well-defined crystallographic planes, leading to a highly tortuous crack path and a highly faceted fracture surface [200]. SEM Fractography shows

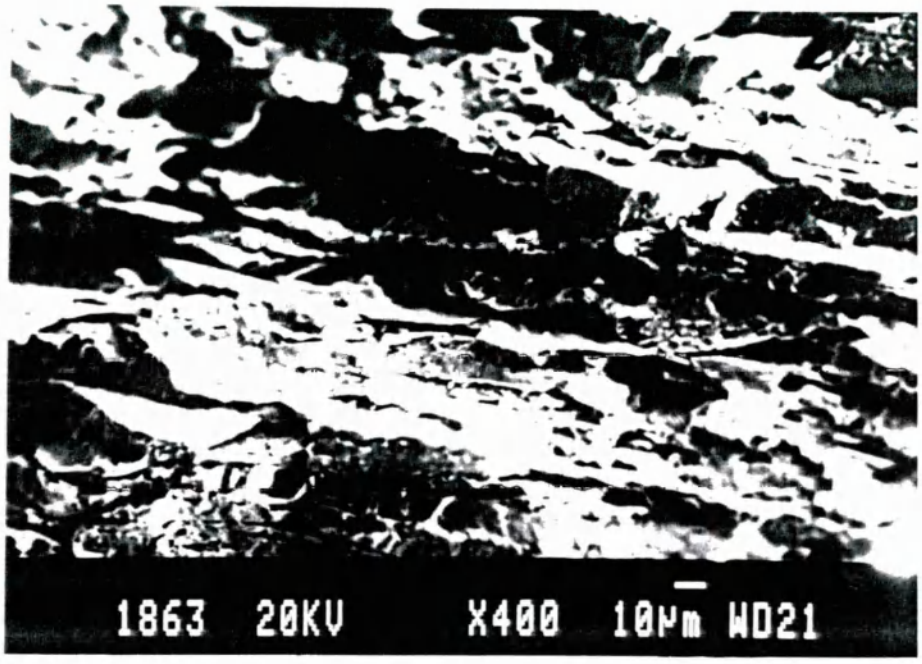

Figure 5-8 Scanning Electron Micrograph Of Step Appearance

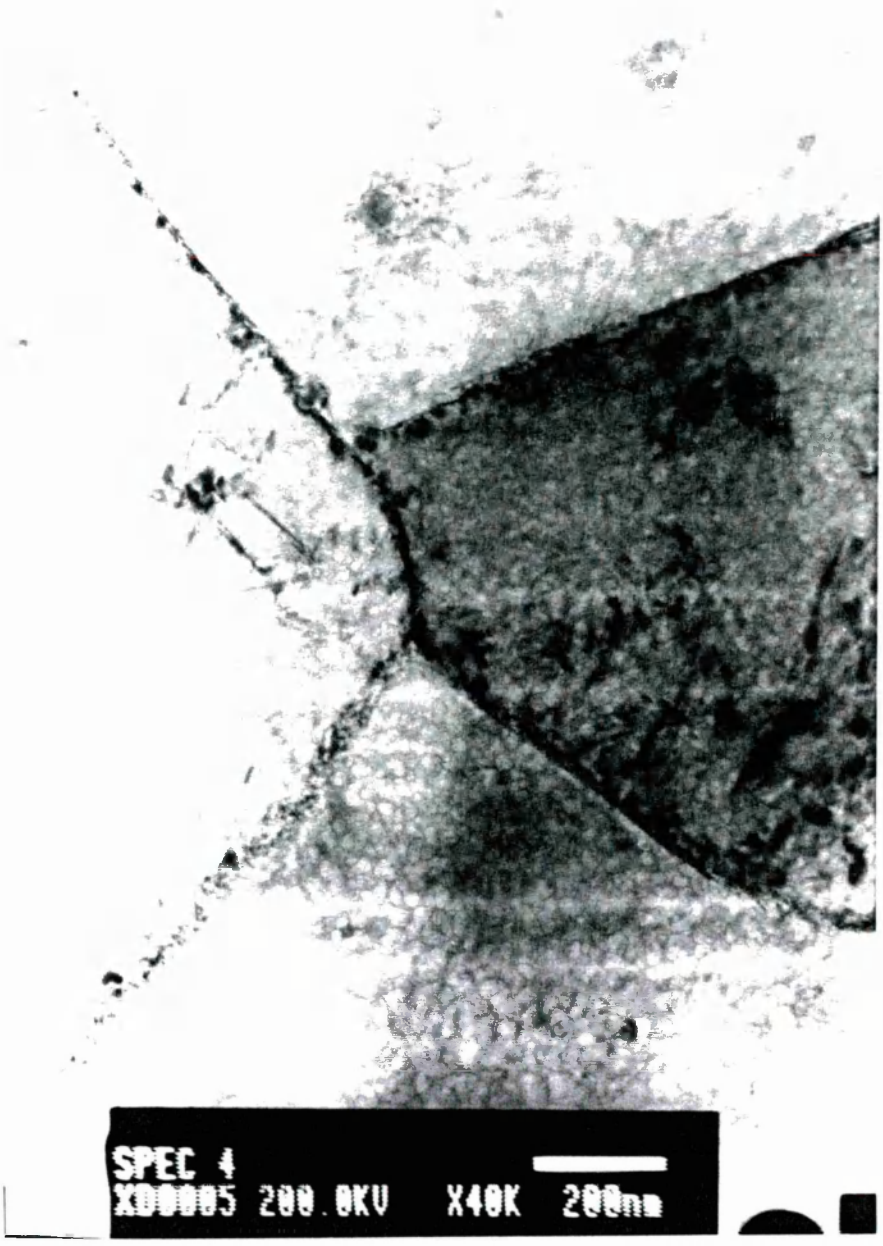

Figure 5-9(a) Transmission Electron Micrograph Of Grain Boundary Region

Figure 5-9(b) Transmission Electron Micrograph Of Grain Structure

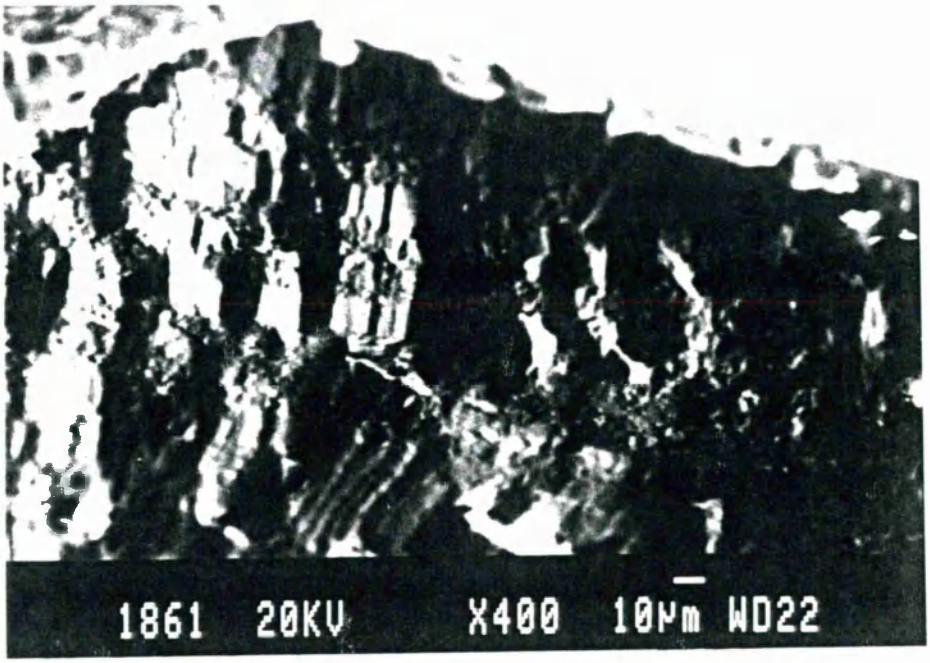

Figure 5-10 Scanning Electron Micrograph Of Rough Fracture Surface With Intergranular Traces

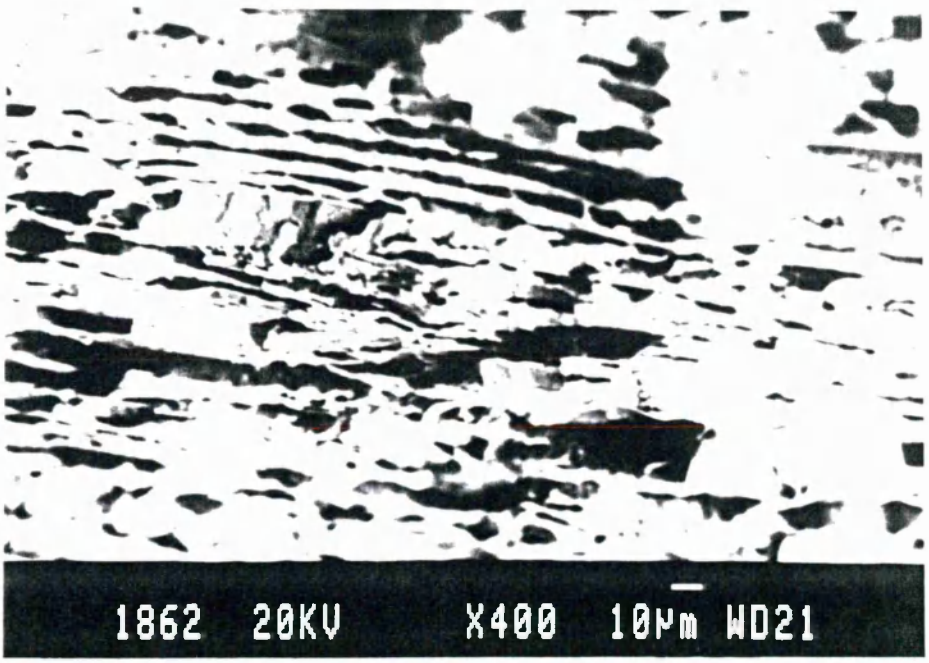

Figure 5-11 Scanning Electron Micrograph Of Longitudinal Fracture Surface

that the growth mode of fatigue cracks for the 8090-T6 aluminium-lithium alloy is transgranular, appearing brittle, wider fracture facets [see Figure 5-11]. This appearance of spatial distribution of the fractographic feature also indicates the weak grain boundary nature associated with the alloy and the low resistance to small fatigue crack propagation.

Generally, the final fracture mode in 8090-T6 aluminium-lithium alloy consists of transgranular coarse slip band splitting, plus transgranular and intergranular tear. The slip stripes and steps can be observed on the fracture surface resulting from transgranular coarse slip band splitting. The tear area includes cleavage surfaces and coarse slip steps. Different to 8090-T6 aluminium-lithium alloy, the final fracture mode for 7150-T651 aluminium alloy is transgranular dimple fracture associated with the mechanism of microvoid coalescence. The difference of final fracture mode between the two alloys indicates that the transgranular coarse slip band splitting, plus transgranular and intergranular tear leads to a multilevel fracture which facilitates fatigue crack propagation in 8090 aluminium-lithium alloy. This explains why the fatigue life of 8090-T6 aluminium-lithium alloy is lower than that of 7150-T651 aluminium alloy.

5.5 SUMMARY OF THE CHAPTER

(1) The cyclic-stress response reveals softening behaviour of the 7150-T651 aluminium alloy at all strain amplitudes examined. The development of softening is not evident at lower strain amplitude ($\Delta\varepsilon$ =1.1%). More pronounced softening is observed at higher strain amplitude ($\Delta\varepsilon$ =1.8%). The degree of softening tends to decrease with decrease of strain amplitude.

(2) Since softening is generally evident at all strain amplitudes, it can be regarded as a mechanical feature of 7150-T651 aluminium alloy.

(3) In strain-controlled fatigue tests for 7150-T651 aluminium alloy, the cyclic fracture morphology either at higher strain amplitudes or at lower strain

amplitudes shows pronounced transgranular cracking, with major cracks perpendicular to the stress axis, rather than intergranular cracking. No evident bimodal fracture or whole grain profile was observed in the fatigue crack initiation and propagation regions although crack path is tortuous with evidence of microstructurally induced deflection of crack path.

(5) The final fracture mode of aluminium alloy 7150-T651 is consisted of transgranular dimple fracture.

(6) The final fracture mode of aluminium-lithium alloy 8090-T6 is consisted of transgranular coarse slip splitting, plus transgranular and intergranular tear in the longitude direction rather than dimple fracture mode. Multilevel fatigue cracking is a pronounced feature.

(7) The 7150 aluminium alloy exhibits a relatively high grain boundary resistance to fatigue crack propagation whereas the 8090 aluminium-lithium alloy exhibits a weak grain boundary resistance to fatigue crack propagation

This chapter along with Chapter 4 confirms that the 7150 aluminium alloy and the 8090 aluminium-lithium alloy experience two different fatigue-fracture mechanisms which need to be identified when one is going to model small fatigue crack growth in these alloys. Transgranular fracture due to fatigue crack propagation is a dominated mechanism for the 7150 while the transgranular fracture plus intergranular cracking is a pronounced mechanism for the 8090.

- Under former circumstance, an advancing small fatigue crack front can be considered experiencing a planar fracture during crack propagation.
- Otherwise, the crack front may experience a multilevel fracture under the later circumstance.

Additionally, both alloys exhibit different grain boundary resistance to small fatigue crack propagation. The blocking effect of grain boundaries could be neglected for 8090 aluminium-lithium alloy.

These diversities between the two alloys lead to a different way not only definitions of microstructure of polycrystalline materials for micromechanical modelling but also understanding of grain boundary blocking to small fatigue crack growth. This is why the two typical alloys are particularly concerned. However, the ongoing work intends to simulate the microstructure with transgranular cracking feature as a first step and model how a small fatigue crack propagates in such microstructure. Chapter 6 and 7 will detail the simulation of microstructure features.

Chapter 6 MICROMECHANICAL MODEL OF SMALL FATIGUE CRACK GROWTH

6.1 INTRODUCTION

Small fatigue cracks have been classified into microstructurally small fatigue cracks (Stage I cracks) and physically small fatigue cracks (Stage II cracks) as illustrated in Figure 6-1. Small fatigue cracks may initiate at slip bands as a result of dislocation motion or emanate from a particle bonded to the matrix due to the stress concentration around it. After microcrack initiation, which is regarded as formation of microcracks, small fatigue cracks may experience two stages of growth [88]. A crack growth transition exists between the two stages of small crack growth.

There are two prominent features associated with Stage I small crack growth: 1) The shear growth mechanism primarily dominates early propagation; 2) Local microstructure significantly affects growth. This effect of local microstructure can not be neglected. In Stage II crack growth the local microstructure still affects small fatigue crack growth to some extent. However, the Stage II small fatigue crack growth is primarily governed by Mode I mechanism and no longer strongly depends upon local microstructure because the metallurgical influence of local microstructure on fatigue crack growth may be averaged. Thus, continuum mechanics may be applicable. As a result, there may exist a coherent connection of microscopic small fatigue growth with macroscopic bulk fatigue properties.

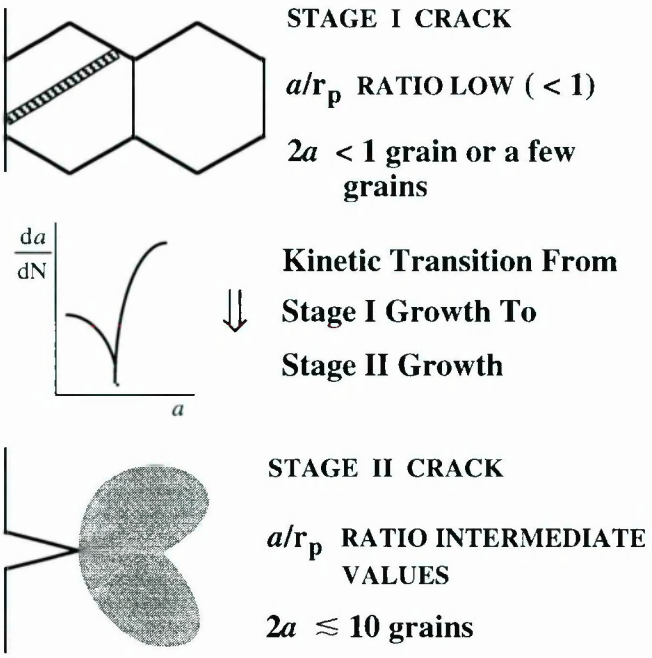

Figure 6-1 Three Distinct Stages Of Microstructurally Small Cracks, Crack Growth Transition And Physically Small Cracks

A number of models [11-13,17-19,24-27,29-31] have been proposed to predict growth rate of small fatigue cracks. Although these models are scientifically elegant, they entail an experimentally-determined expression $\frac{da}{dN}$ for each load level, which is obtained from careful and tedious characterisation of small fatigue cracks. This could limit the engineering application of these models.

6.2 GENERAL BACKGROUND OF PROPOSED MODEL

Three fundamental issues should be addressed when modelling small fatigue crack growth. (1) How is the local microstructure of the material represented? (2) How does plastic zone ahead of an advancing small crack front develop ? (3) What is a coherent connection between the two ?

6.2.1 Microstructural Simulation Of A Polycrystalline Material

Small crack growth may slow down as a result of truncation of the plastic zone and the crack path may deflect due to misorientations at grain boundaries. Local intermetallic particles may also interfere with small crack propagation by changing the direction of dislocations emitted from crack tip. The microstructure of polycrystalline materials affects small fatigue crack propagation in a complex way.

Firstly, it is virtually impossible to kinetically simulate each individual local microstructural feature (such as grain size, grain orientation *etc.*) ahead of a crack front for growing small fatigue cracks. To characterise the microstructure, one usually uses a defined (or fixed) microstructural dimension to reflect the averaged microstructure. The local microstructure features, however, may be ignored as a result. Secondly, it is the lack of an appropriate simulation that draws a coherent link between any defined microstructural dimension affecting microscopic small fatigue crack growth and macroscopic bulk fatigue behaviour. In other words, it is the lack of an engineering representation (approach) of micro-macro mechanical relationship for fatigue cracking. So, an appropriate physical quantity has to be defined to bridge the gap.

Therefore, this work proposes a microstructurally-affected-zone to represent any local microstructure effect on small crack growth. The microstructurally-affected-zone size is therefore regarded as a local dominated microstructural dimension, affecting small crack growth. The question is, how to relate this microstructurally-affected-zone size to a simple physical quantity in the case of small fatigue crack propagation and determine it quantitatively.

P. J. E. Forsyth analysed the idea of an 'elementary block' in a generalised way. He stated "the microstructural features in metals cause break up of the crack front into segments that relate to elementary blocks operating with some degree of independence from their neighbours but under the general influence of the macroscopic crack of which they are a part" [88].

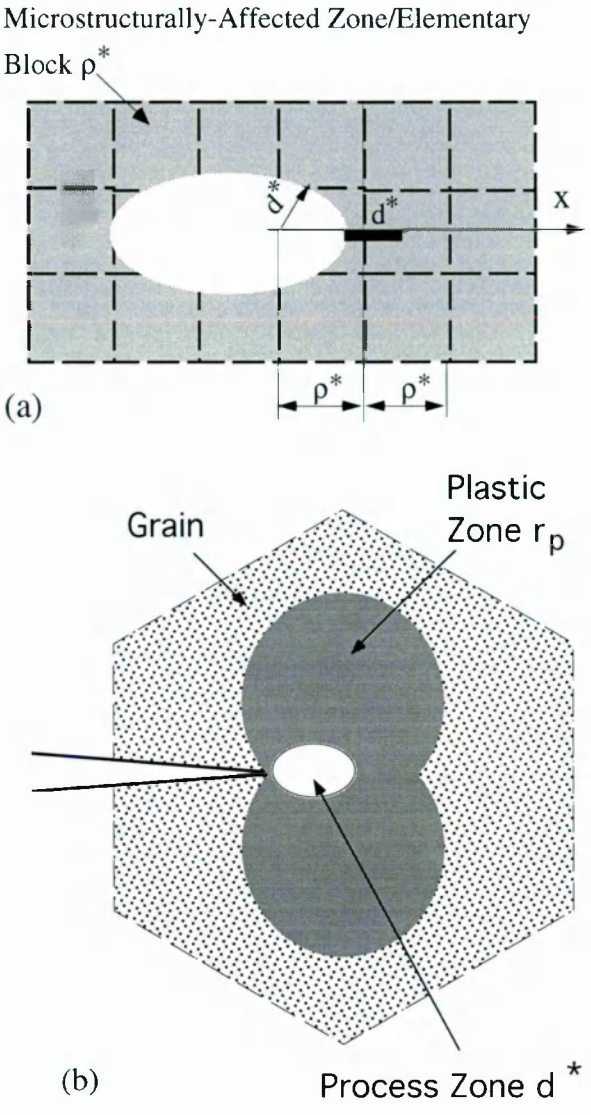

Figure 6-2 Schematic Presentation Of Microcrack Tip (a) In Relation To Microstructurally-affected-zone/Elementary Block And (b) In Relation To Plastic Zone And Grain Size For A Small Fatigue Crack In Stage II Growth

By adopting his concept, it can be suggested that a real polycrystalline material can be conceived to be composed of elementary blocks of finite linear dimension ρ^*. The elementary blocks divide the material into segments. Every segment, from the view point of averaged microstructure, may be identical in size. Since a small fatigue crack may span across elementary blocks, the elementary block can be related to the microstructurally-affected-zone as if the real polycrystalline material would be built up of microstructurally-affected-zones. The local microstructure effect on small fatigue crack propagation is reflected by way of each microstructurally-affected-zone that the small fatigue crack

traverses. Naturally, the microstructurally-affected-zone size can be equated to a simplified physical quantity, *i.e.*, the elementary block size.

Figure 6-2 provides a schematic representation of the microstructurally-affected-zone/elementary block plus crack front representation. The microstructurally-affected-zone is proposed from a microscopic point of view to take account of local microstructural effect whereas the elementary block is proposed from a macroscopic point of view to proceed the with mechanical simulation of polycrystalline materials. It should be noted that every microstructurally-affected-zone/elementary block is not identical but varies in size if taking point of view of localised microstructure for real polycrystalline materials. This point will be eluciated and discussed in Chapter 7

6.2.2 Presentation Of Crack Front And Fatigue Damage At Crack Tip

Consider a physically small fatigue crack which lies in an infinite body subjected to uniform tension stress. No matter how small the crack tip is, it is surrounded by a plastic zone. So, it is practicable to define a process zone as shown in Figure 6-2 on physical grounds at the crack tip. The process zone is dependent upon the plastically deformed zone ahead of the crack front and the local microstructure. Figure 6-3 is a micrograph showing a small crack front which is taken using SEM. The micrograph demonstrates the fact that a small fatigue crack tip may be considered to be a blunted micronotch.

It should be noted that the local stress/strain actually varies throughout each cracked elementary block. But, for mathematical simplicity, it is considered that the stress/strain contributing to the localised driving force for small fatigue crack propagation is uniformly distributed in the process zone. The local stress/strain in the process zone controls small fatigue crack propagation. Each increment d^* is the result of fatigue damage at the crack tip, leading to small fatigue crack propagation. Since the increment d^* is attainable in fatigue cycles, N_f, necessary to fracture element of material contained in the process zone, the crack growth rate at any time will therefore be given by the process zone size divided by its fatigue damage life:

$$\frac{da}{dN} = \frac{d^*}{N_f} \tag{6-1}$$

The physical interpretation to the process zone consists of three aspects:

- The process zone is defined to represent small crack tip blunting. Its size stands for the extent of crack tip blunting;
- The process zone is defined to represent a fully damaged zone at the small crack front;
- The process zone is defined to measure increment of small fatigue crack advance.

6.3 MODELLING PROCESS FOR STAGE II SMALL FATIGUE CRACKS

Before developing the model further, the following assumptions are made:

(1) A polycrystalline material can be treated as an isotropic continuum;

(2) Stress and strain are uniform in the process zone;

(3) The bulk fatigue properties of material are stable during fatigue;

(4) The two tips of a small fatigue crack extend along the surface at approximately the same speed;

(5) Free surface effect due to unusual isotropic (or anisotropic) dislocations [89] on early stage growth of small fatigue cracks is not considered.

6.3.1 Local Strain At Small Fatigue Crack Tip

Consider a microcrack of length $2a$ that lies in an infinite body subjected to uniform tensile loading. The microcrack takes the shape of a quasi-ellipse whose semi-major axis is a. Due to its size, the microcrack can be mathematically treated as a 'line crack'. The displacements of this line crack in an infinite sheet under uniaxial tension stress σ are given for plane strain conditions by the relation [90]

$$v = (1-\upsilon^2)\sigma a\left(\frac{\sin\theta}{E}\right) \tag{6-2}$$

in which each term is defined in "List Of Symbols'. After forward loading, the microcrack opens becoming a micronotch with a blunted tip of radius d^*. A plastic zone of size r_p is formed as a result of the stress concentration at the tip. The opening displacement, δ, of this blunted surface micronotch can be evaluated (See Appendix 1) thus

$$\delta = \frac{2(1-\upsilon^2)}{E}(a+r_p)\left(1-\left(\frac{x-a}{a+r_p}\right)^2\right)^{1/2}\sigma\ . \tag{6-3}$$

To determine the local strain at the microcrack tip, it is necessary to consider a specific crack tip blunting mechanism proposed by others [91-93]. The microcrack tip blunts to a semi-circle of radius d^* after loading. It has been theoretically established and practically demonstrated [94,95] that the normal strain distribution in front of the microcrack tip along the major-axis takes the form:

$$\varepsilon = \frac{\eta}{x-a} \qquad (x > a) \tag{6-4}$$

in which η is the deformation in a yielded zone just at the crack tip. To avoid strain singularity at $x = a$, a process zone is introduced there as mentioned before. In the process zone, the deformation is held constant within a distance d^* from the tip of the microcrack. Therefore, if an elementary block of length ρ^* is initially elongated by δ during forward loading, we have

$$\varepsilon = \frac{\delta}{\rho^*\omega} \tag{6-5}$$

in which ω is a triaxiality factor [96]. To satisfy the requirement of continuity at $x = a + d^*$, η must equal $\delta d^*/(\rho^*\omega)$ in Equation 6-4, leading to the following expression

$$\varepsilon = \frac{\delta\, d^*}{\rho^* \omega\, (x - a)} \tag{6-6}$$

that scales local strain in front of the microcrack tip. Substituting Equation 6-3 into Equation 6-6 yields an expression for the strain distribution in front of the elliptical microcrack tip, thus

$$\varepsilon = \frac{2d^*(1-\upsilon^2)}{\rho^* \omega E\,(x-a)} \left(1 + \frac{r_p}{a}\right) \left[1 - \left(\frac{\frac{x}{a} - 1}{1 + \frac{r_p}{a}}\right)^2\right]^{1/2} \sigma\, a\,. \tag{6-7}$$

At $x = a + r_p$ defines the boundary between the local elastic-plastic region and the elastic region outside. The strain at this boundary can be determined by replacing x with $(a + r_p)$ in Equation 6-7. In the case of cyclic loading, it is assumed that the cyclic strain distribution can be evaluated by means of Equation 6-7 by replacing ε and σ with $\frac{\Delta\varepsilon}{2}$ and $\frac{\Delta\sigma}{2}$. It should be noted that the normalised plastic zone size, $\frac{r_p}{a}$, play essential roles in determining the local strain at a small fatigue crack tip.

6.3.2 Evolution Of The Normalised Plastic Zone And The Normalised Process Zone At An Advancing Small Fatigue Crack Front

Plastic zone size has been found to be an important physical quantity that plays a key role in controlling small fatigue crack growth. Recent novel measurements [37] have confirmed that the plastic zone ahead of a small crack tip is likely to be truncated by grain boundaries due primarily to misorientation between neighbour grains as the small fatigue crack approaches grain boundaries [32,67]. Relatively large plastic zone occurs in front of the advancing small crack front. Initially, the ratio of plastic zone size to crack length $\frac{r_p}{a}$ decreases rapidly with increase of crack length and then decreases gradually until approaching a stable value, which indicates an approach of small fatigue crack propagation to long fatigue crack propagation. This trend is reported in [78]. Applied stress ratio $\frac{\sigma_{max}}{\sigma_y}$ also contributes positively to the comparatively large plastic zone [11,76] although some deforming grains may have not be entirely deformed plastically.

Figure 6-3 illustrates the evolution of normalised plastic zone with respect to small crack size and stress level and shows a general decreasing trend of ratio $\frac{r_p}{a}$ with increasing of crack size. Despite the fact that the measured plastic zone size associated with small fatigue cracks may be different for different aluminium alloys, the pattern of evolution of the normalised plastic zone $\frac{r_p}{a}$ with small fatigue crack size and stress level is likely to be similar. This evolution pattern of normalised plastic zone may be questionable when small fatigue cracks are within a few grains. This point is discussed further in Chapter 7.

As detailed above, the process zone size reflects the extent of crack tip blunting during loading. Once a small fatigue crack grows or its tip deflects, the process zone size changes simultaneously due to local deformation and microstructural constraints. Denoting $\frac{d^*}{\rho^*}$ to be normalised process zone size, the normalised process zone size depends upon the degree of local plastic deformation ahead of the microcrack tip. As a result, the evolution of defined normalised process zone must conform to the co-ordination of local elastic-plastic deformation at the boundary between the plastic zone ahead of crack tip and the elastic region outside. By simply satisfying the requirement for strain equilibrium at the boundary, the evolution pattern of $\frac{d^*}{\rho^*}$ can be revealed.

The local strain just at the boundary can be determined by means of Equation 6-7 which is

$$[\varepsilon]_{(x=a+r_p)} = \frac{2(1-\upsilon^2)d^*\sigma}{\rho^*\omega E}\left(\frac{a}{r_p}\right)\left(1+\frac{2r_p}{a}\right)^{0.5} \tag{6-8}$$

while the elastic strain just beyond the plastic zone conforms to elastic field of the infinite body which can be directly derived by differentiation Equation 6-2, *i.e.*, $\frac{\partial v}{\partial y}$ [see Appendix 2] on the condition that the microcrack is so small that it can be regarded as a line crack. Consequently, an expression can be analytically derived that reveals the evolution of normalised process zone for a growing small fatigue crack.

$$\frac{d^*}{\rho^*} = \frac{\omega}{2}\left(\frac{r_p}{a}\right)\left(1+\frac{2r_p}{a}\right)^{-0.5}. \tag{6-9}$$

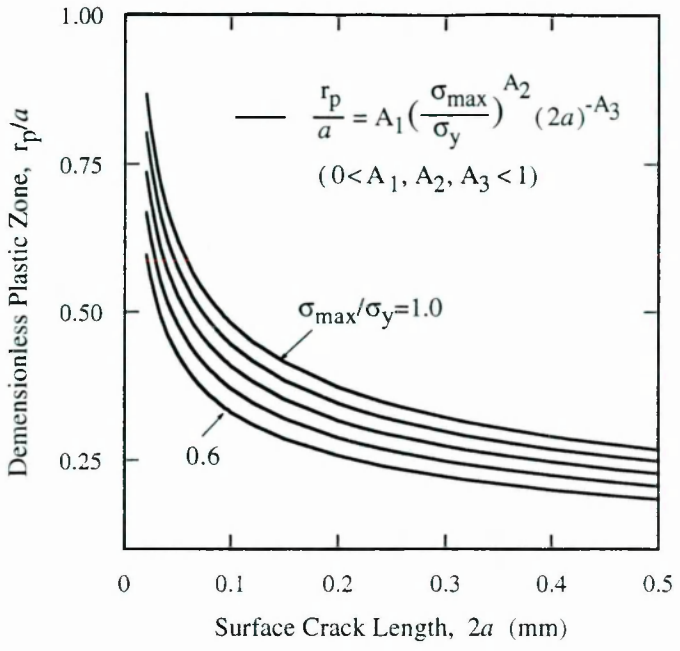

Figure 6-3 An Experimentally-Determined Evolution Pattern Of Normalised Plastic Zone For Growing Small Fatigue Cracks

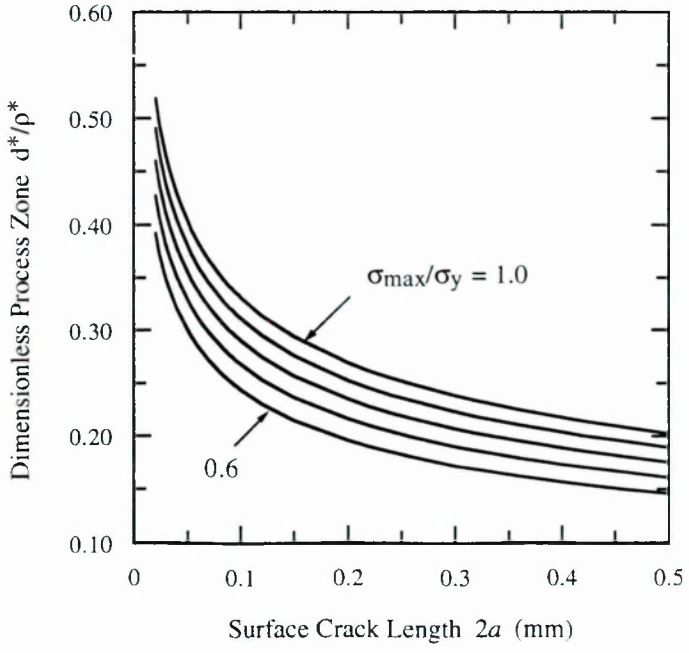

Figure 6-4 Evolution Pattern Of Normalised Process Zone In Conjunction With Small Fatigue Crack Size And Microstructure

This analytical expression shows a coherent micromechanical relationship of the process zone size d^* with the microstructurally-affected-zone size ρ^* and the normalised plastic zone size $\frac{r_p}{a}$. The evolution of normalised process zone $\frac{d^*}{\rho^*}$ is depicted in Figure 6-4.

By comparing Figure 6-3 with Figure 6-4, it is clear that the evolution of the normalised process zone has a similar pattern with that of the normalised plastic zone. This consistency of evolution patterns associated with the normalised plastic zone $\frac{r_p}{a}$ and the normalised process zone $\frac{d^*}{\rho^*}$ is not a phenomenological similarity but establishes a micromechanical basis that the process zone size may be taken as an appropriate unified physical parameter to kinetically correlate small fatigue crack growth. This point will be demonstrated in Chapter 7.

6.3.3 Prediction Of Growth Rate From Macroscopic Fatigue Properties

Successive cracking of material within the process zone results in fatigue crack extension. Crack growth through the process zone can be modelled as strain controlled fatigue damage by the localised strain at the small crack tip. The local cyclic plastic strain in the process zone during fatigue can be analytically determined using Equation 6-7 by letting $x = a + d^*$.

$$\frac{\Delta\varepsilon_p}{2} = \frac{1-\upsilon^2}{\rho^*\omega E}\left(\left(1+\frac{r_p}{a}\right)^2 - \left(\frac{d^*}{a}\right)^2\right)^{0.5} \Delta\sigma\, a \ . \qquad (6\text{-}10)$$

This local cyclic plastic strain depends not only upon plastic deformation but also upon local microstructure as illustrated further in Chapter 7.

From the view point of small crack growth, metal fatigue damage can be equated to crack length and the rate of damage accumulation to the rate of fatigue crack growth [1]. Therefore, the integration of a small crack growth law from initial to final crack length should yield S–N curve [4] because fatigue life to failure is primarily determined by small fatigue crack growth lifetime. This means that the total fatigue lifetime of smooth and cylindrical specimens used in low-cycle fatigue tests consists of fatigue crack growth

lifetime (from small cracks to long cracks) rather than fatigue crack initiation lifetime plus fatigue crack growth lifetime. This fundamental concept makes the Coffin-Manson relation applicable to description of fatigue crack growth. Therefore, any influence of microstructural changes on small fatigue crack growth may be reflected by way of fatigue property changes of macroscopic bulk.

Since the failure of a material element at the crack tip is essentially due to strain-controlled fatigue, the Coffin-Manson relation can be applied to the crack tip to determine the fatigue cycles necessary to rupture the element of material contained in the process zone because relatively large plastic deformation was observed and considered at small surface crack tips [11,32,67,76,97].

Despite the fact that a stress gradient does exist in FPB specimens (or other type of specimens) across whole working section, which is normal to loading direction, the stress gradient in the crack depth direction may be neglected for small fatigue cracks. This stress similitude for using the Coffin-Manson relation can be reasonably accepted. The Coffin-Manson relation is usually consisted of an elastic component, $\frac{\Delta\varepsilon_e}{2}$, and a plstic component $\frac{\Delta\varepsilon_p}{2}$, and expressed to be

$$\frac{\Delta\varepsilon}{2} = \frac{\Delta\varepsilon_e}{2} + \frac{\Delta\varepsilon_p}{2} = \frac{\sigma_f'}{E}(2N_f)^b + \varepsilon_f'(2N_f)^c . \qquad 6\text{-}11$$

For polycrystalline materials which cyclic plastic stress-strain response obeys a well-known power function

$$\frac{\Delta\varepsilon}{2} = \frac{\Delta\varepsilon_e}{2} + \frac{\Delta\varepsilon_p}{2} = \frac{\Delta\sigma}{2E} + \left(\frac{\Delta\sigma}{2K'}\right)^{\frac{1}{n'}} \qquad 6\text{-}12$$

a quantitative relationship can be deduced that links fatigue cycles to failure to the local plastic cyclic strain at the small fatigue crack front:

$$\frac{\Delta\varepsilon_p}{2} = \left(\frac{(\sigma_f' - \sigma_m)\varepsilon_f'}{K'}\right)^{\frac{1}{1+n'}} (2N_f)^{\frac{b+c}{1+n'}} . \qquad (6\text{-}13)$$

in which σ_m takes account of the mean stress effect. Equation 6-13 makes it possible to link the microscopic plastic deformation at an advancing crack front with macroscopic bulk fatigue behaviour, by which along with Equation 6-9 a micro-macro mechanical relationship is established. Defined by Equation 6-1, the small crack growth rate can therefore be formulated in terms of the fatigue damage in the process zone to be

$$\frac{da}{dN} = 2d^* \left(\left(\frac{K'}{(\sigma_f' - \sigma_m)\varepsilon_f'} \right)^{\frac{1}{1+n'}} \frac{\Delta\varepsilon_p}{2} \right)^{\frac{-(1+n')}{b+c}} . \qquad (6\text{-}14)$$

This is a crack growth law equation for a single physically small fatigue crack by which growth rate can be correlated in terms of proposed process zone size and predicted using conventional mechanical and low-cycle fatigue properties along with microscopic quantities, *i.e.*, microstructurally-affected-zone size. Equation 6-14 predicts $\frac{da}{dN} = 0$ as the load level approaches fatigue limit $\Delta\sigma_{FL}$ as explained and detailed in Chapter 7. This equation is applicable only to small fatigue cracks in Stage II propagation.

6.4 MODELLING OF STAGE I CRACK GROWTH

P. J. E. Forsyth suggested that Stage I growth is similar to the process by which a crack is nucleated in an active slip band through the formation of a groove by unequal amounts of forward and reverse slip in neighbouring packets of slip planes [88]. Stage I shear mode growth of a microcrack is attributed to the local damage due to strongly discrete glide edge dislocations at the crack tip. Crack propagation is thus governed by the cyclic shear stress amplitude $\Delta\tau$. Barriers, such as grain boundaries, produce perturbations on growth rate of small fatigue cracks. A theoretically developed alternative model that takes account of blocking effect of dislocations at grain boundaries [98, 13] provides a useful solution to simulate the discontinuous nature of slip band transmission across grain boundaries. For edge dislocations and plane strain conditions, the shear displacement at small fatigue crack tip is given [98,13] as

$$\Delta\delta = \frac{4(1-\upsilon^2)}{E}\,\frac{\sqrt{1-n^2}}{n}\,\Delta\tau a \ . \qquad (6\text{-}15)$$

Here n is a normalised plastic zone size defined by $n = \frac{a}{a + r_p}$. Once the plastic zone extends to the grain boundary, the critical value n_c, at which cracl length the barrier is overcome, can be determined by [13]

$$n_c = \cos\left(\frac{\pi}{2}\left(\frac{\Delta\tau - \tau_{Li}}{\tau_{comp}}\right)\right). \qquad (6\text{-}16)$$

in which $\tau_{Li} = \frac{\tau_{FL}}{\sqrt{i}}$ (i = 1, 3, 5, ...). Here, τ_{FL} is a shear stress corresponding to the fatigue limit [98,13].

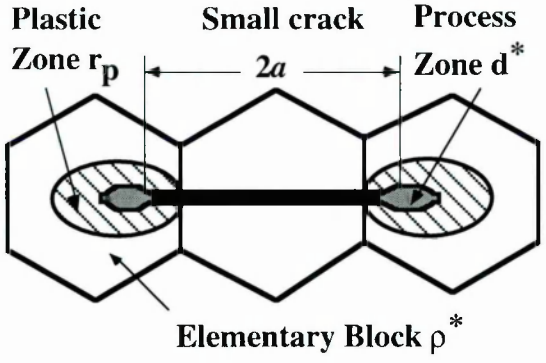

Figure 6-5 Physical Analogue Of Stage I Shear Crack

Equation 6-15 predicts a series of drops of growth rate at every barrier of grain boundaries [13] when small fatigue cracks propagate. However, recent experimental observations [99,100] indicate that the first grain boundary does not always cause the severest fall of growth rates. Some grain boundaries have a little blocking effect on small fatigue crack growth. The Stage I crack growth will terminate at a transition crack length $2a_o$ beyond which the shear mechanism may shift to a Mode I mechanism. Predictions of crack growth rate for Stage I entails a determination of shear strain at the small crack tip.

Despite the different damage mechanisms responsible for Stage I crack growth, the concept of process zone can still be adopted to represent the small fatigue crack front as shown in Figure 6-5. The advancing crack front in this case is still physically modelled as a micronotch with tip radius of $(d^*)_o$ equivalent to the process zone size that corresponds to

the transition crack length $2a_o$. By recalling Equation 6-6 describing the strain distribution in front of a micronotch, the cyclic shear strain can be approximately estimated to be

$$\Delta\gamma = \frac{\Delta\delta\,(d^*)_o}{\rho^*\,\omega\,(x-a)} \tag{6-17}$$

in which ρ^* is still specified as the microstructurally-affected-zone size. If a relation, $\Delta\tau = \frac{1}{2}\Delta\sigma \mathrm{Sin}[2(\frac{\pi}{2}-\varphi)]$ is employed for shear microcracks, which is going to be explained in Chapter 7, the expression for cyclic shear strain at $x = a + (d^*)_o$ can be derived to be

$$\frac{\Delta\gamma}{2} = \frac{(1-\upsilon^2)\sin[2(\frac{\pi}{2}-\varphi)]}{\rho^*\omega E}\,\frac{\sqrt{1-n^2}}{n}\,\Delta\sigma a \ . \tag{6-18}$$

Equation 6-18 shows an oscillating pattern of local shear strain evolution as a result of the blocked plastic zone at the grain boundary. Since shear mechanism dominates crack propagation in Stage I crack growth, the maximum shear strain method [101] can be utilised to estimate strain-controlled fatigue damage in the process zone,

$$\frac{\Delta\gamma_{max}}{2} = 1.30\,\frac{\sigma_f'}{E}\,(2N_f)^b + 1.50\,\varepsilon_f'\,(2N_f)^c \ . \tag{6-19}$$

Valid use of this maximum shear strain criteria entails a prerequisite that shear strain makes a major contribution to fatigue damage.

Although the Stage I small fatigue cracks might be attributed to a surface phenomenon unaffected by the bulk properties, there is still a lack of convincing evidence to prove or disprove this argument. In engineering applications, a 'continuous approach' is still desirable. By using Equation 6-16 as a first approximation, the small crack growth rate can therefore be simulated in terms of the fatigue damage caused by shear strain in the process zone. As a result, the crack growth rate law equation for a single small fatigue crack in Stage I is:

$$\frac{da}{dN} = 2(d^*)_o\left(\left(\frac{K'}{1.95\,(\sigma_f'-\sigma_m)\,\varepsilon_f'}\right)^{\frac{1}{1+n'}}\,\frac{\Delta\gamma_{max}}{2}\right)^{\frac{-(1+n')}{b+c}} \ . \tag{6-20}$$

Combining Equations 6-14 and 6-20 gives a unified crack growth law equation for a single small fatigue crack by which crack growth rates can be correlated using the proposed unified physical parameter, *i.e.*, the process zone size, and quantitatively predicted using mechanical and low-cycle fatigue properties. Microstructure features of polycrystalline materials are incorporated into the unified crack growth law by way of the microstructurally-affected-zone which will be detailed in Chapter 7. The material properties to characterise the material cyclic fatigue behaviour and fatigue resistance are K', n', E, σ_y, σ_f', ε_f', b, c. For polycrystalline materials that exhibit power-law cyclic strain hardening, b and c are not independent parameters. Instead they are can be expressed in terms of the cyclic hardening exponent. Thus, only seven material parameters are required to characterise the small fatigue crack growth.

6.5 DISCUSSION

The modelling process in this chapter exhibits a novel advantage that the growth rate of Stage I and Stage II small fatigue cracks can be predicted using macroscopic low-cycle fatigue properties via the process zone in conjunction with local microstructure without use of regression of experimental data for each load level. Among those fatigue properties (n', K', σ_f', ε_f', b, c) used in the model, the cyclic strain hardening exponent n' is particularly typical because any change of growth rate is primarily dependent upon the cyclic strain hardening exponent. As the n' varies from unity to zero, polycrystalline materials exhibit a change from perfect plasticity to perfect elasticity. However, it is difficult to discriminate each individual effect of those physical quantities on small crack growth rates. Possibly, a self-consistence nature associated with those fatigue properties might exists in fatigue of polycrystalline materials.

Stage I to Stage II crack growth transition is essential in micromechanical modelling of small crack growth rates. Because of the three-dimensional nature of grains, none of slip systems will exactly match the initial crack plane. So, two alternatives are possible. The

initial Stage I crack could meet an internal grain at a critical position, such as a high angle grain boundary, where it will cause a new slip plane to form in the next grain because of high local stress concentration. Alternatively, the crack could induce a local high stress concentration inside the second grain producing an internal crack which will snap back to meet the first crack [182]. No matter how the initial Stage I crack develops, the Stage I to Stage II crack growth transition is closely associated with local stress levels and the local microstructure. Therefore, it seems hard to say whether or not the Stage I crack growth will terminate as the microcrack meets the first grain boundary.

As described in the previous section, the local microstructure has a significant influence over the growth of small fatigue cracks. Grain size is usually considered a factor to influence small crack growth. As a first step of modelling, an average grain size may be used to measure the microstructure effect, which means that the crack growth rates are directly related to grain size. Is it adequate to do so? Experimental investigations on 7091 and 7050 aluminium alloys have revealed that large grain does not definitely result in a fast growth of small fatigue cracks [102]. Comparisons between different aluminium alloys, made by the author, of small crack growth rates in relation to the reported grain sizes, which were found in 2024 [75,48], 2090 [103], 6080 [104], 7075 [67,75,105], 7150, 7017 [77] 7475 [80] aluminium alloys, do not prove any intrinsic relationship between grain size and crack growth rate or show a clear evidence that a large grain structure will definitely result in a higher small crack growth rate.

It is considered that when small fatigue cracks meet grain boundaries, growth rates of small fatigue cracks may be primarily related to two factors, *i.e.*, (1) internal strength bonding grain boundaries together and (2) local metallurgical features around the crack front, such as misorientation between two adjoining grains or grain boundary structure. Either grain boundary blockage or slip band misorientation may cause decelerated growth behaviour [32,69,97,212]. Other obstacles within the grains, such as particles in front of the crack tip, may also interfere with small crack propagation causing the deflection of the crack path or reducing the growth rate.

Therefore, it seems incorrect to directly refer the microstructurally-affected-zone size/the elementary block size, ρ^*, to an average grain size. Moreover, by examining real data of experimental measurements in this work, no clear evidence was found that exhibited the constancy of significant growth rate reduction with grain boundaries. It was also found [100] that the decrease of growth rate at the first grain boundary was not always as much evident as expected even though there is no question in principle to consider the blockage of the first grain boundary. Instead, other grain boundaries may also act as an effective barrier [212] in addition to the first grain boundary to severely deter propagation of small fatigue cracks. In this case, the pile-up behaviour of dislocations ahead of a small fatigue crack tip as a result of the blocking effect by grain boundary may predominantly prevail [106-108] if a small fatigue crack is stemmed at a grain boundary. The blocking effect is particularly evident in the transition regime from Stage I to Stage II crack growth as proved by many previous small fatigue crack tests. Therefore, the microstructurally-affected-zone size ρ^* should be determined in terms of crack growth transition condition rather than given by the average grain size.

On the other hand, the load level is well known to influence small fatigue crack growth, particularly the transition from shear mechanism to tension mechanism. The shear mechanism which dominants the Stage I propagation takes longer to terminate at lower stress levels. This fact has been counted in by means of the defined process zone because the process zone size is strongly dependent upon load level, plastic zone size and microstructurally-affected-zone size. Additionally, the misorientation between two neighbour grains may result in the deflection of cracking path, causing a decrease in growth rate. These factors are going to be studied further.

6.6 SUMMARY OF THE CHAPTER

- The microstructure of a polycrystalline material is interpreted using the microstructurally-affected-zone as if the material would be build up of the

microstructurally-affected-zones. The local microstructure effect on the growth of small fatigue cracks is characterised by the microstructurally-affected-zone size ρ^*. The microstructurally-affected-zone serves as a bridge between microscopic crack growth and macroscopic bulk fatigue behaviour.

- A process zone d^* is defined at a small surface crack front to reflect the interactive effect of the plastic zone, the stress level and the local microstructure on small fatigue crack growth.
- It is suggested that the evolution pattern of normalised plastic zone may be applied to other aluminium alloys.
- For growing small fatigue cracks, the evolution of normalised process zone $\frac{d^*}{\rho^*}$ is remarkably similar to that of the normalised plastic zone $\frac{r_p}{a}$. Associated with crack front advancing, a micromechanical relationship (Equation 6-9) linking the two is established for engineering use, which along with Equation 6-13 draws a coherent micro-macro connection of the microscopic plastic deformation at an advancing crack front with local microstructure.
- It is incorrect to refer the microstructurally-affected-zone size ρ^* to any specific metallurgical size of aluminium alloys. The microstructurally-affected-zone size should be determined in terms of the Stage I to Stage II crack growth transition condition.

The small crack growth transition condition, the microstructurally-affected-zone size, and the kinetics of small fatigue crack growth should be studied further. These are going to be detailed in Chapter 7.

Chapter 7 MODELLING OF KINETICS OF SMALL FATIGUE CRACK GROWTH

7.1 INTRODUCTION

Many experimental studies of small fatigue crack growth have shown that small crack growth rates may drop to a minimum before Stage II crack growth begins. Although the first grain boundary that a small fatigue crack encounters may act as the most effective barrier to block small crack propagation, this observation is not universal. Quantitative comparisons of growth rates with grain sizes [5,6,8,23,78,124,181] do not provide explicit evidence to support the blockage explanation. The minimum growth rate does not always occur once a small fatigue crack meets the first grain boundary and is often also dependent on applied stress levels [100]. Thus, it is unreasonable to take average grain size to simulate Stage I to Stage II crack growth transition.

The Stage I to Stage II crack growth transition is a kinetic process. Applied stress levels and local microstructure influence transition conditions. The non-continuous growth associated with the transition regime (as shown by Figure 1-1 in Chapter 1) can be attributed to some extent to the blocking effect of barriers. Pile-up of dislocations against grain boundaries may occur as a result of the grain boundaries blocking to slip bands that emanate from the advancing small crack front.

Since transition of Stage I crack growth into Stage II crack growth is fundamentally related to local microstructure, the microstructurally-affected-zone size ρ^* must be related to the transition conditions because dominant microstructural barriers control the transition. Obviously, the local orientation of grains, the local orientation of crack tip in relation to far field loading direction will take effect on kinetic growth of small fatigue cracks. The following sections model such a kinetic transition process of small crack growth from Stage I to Stage II and determine the dominant microstructurally-affected-zone size.

7.2 BACKGROUND OF MODEL

Three particular small crack behaviours have been observed in prior experiments [5,69,73,78,100,124, 212] that describes interactions of a small crack tip with grain boundaries. These interactions should be restated.

- Small fatigue crack propagation may slow down on approaching a grain boundary due to truncation of the plastic zone by the grain boundary. Acceleration or deceleration of growth rate is the result of interaction of the crack tip plastic zone with local barriers.
- Due to misorientation between two neighbouring grains, the small crack front may deviate after penetrating grain boundaries into adjoining grains. This crack front deflection is the result of the orientation change of newly activated slip bands.
- The first grain boundary does not always cause the severest drop of growth rate when a small fatigue crack penetrates it. Other grain boundaries may also have some blocking effect on the small fatigue crack propagation.

Due to the change in crystal orientation, grain boundaries are expected to be effective barriers to dislocation glide [106] and the plastic zone extension. Particles bonded in the matrix may also act as obstacles to growth by changing the crack path.

In this work polycrystalline materials are assumed to be originally free of defects that interfere with slip band transmission with the exception of grain boundaries. Small fatigue cracks initiate in shear mode at slip bands as a result of dislocation motion. If the crack size is of the order of a microstructural dimension, the plastic zone ahead of the crack tip essentially consists of crystallographic slip bands emanating from the crack tip. The plastic slip is assumed to be distributed over rectilinear slip bands that extend through the grains. Grain boundaries are considered to be slip barriers.

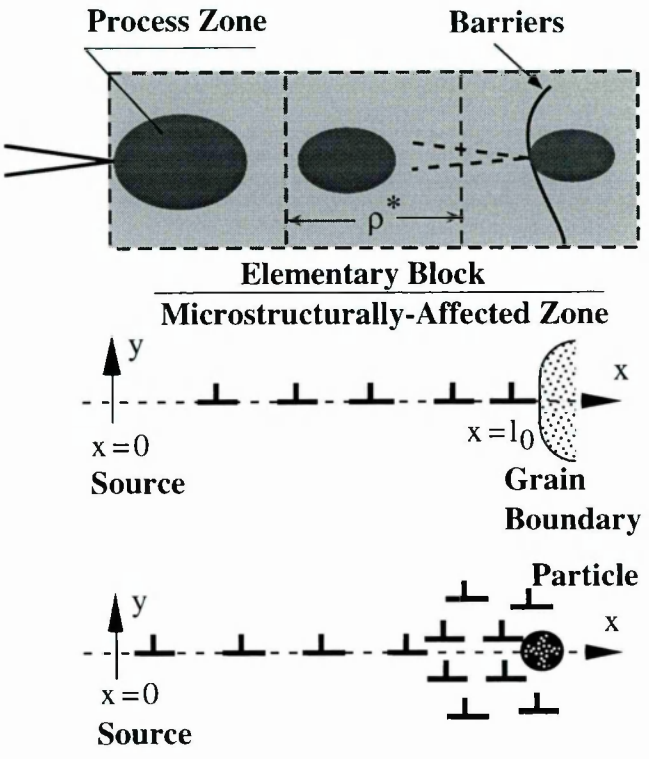

Figure 7-1 Representation Of Kinetics Of A Growing Small Fatigue Crack Over Microstructurally-affected-zones And Dislocation Pile-Up On Contacting Grain Boundary Or Intermetallic Particle

For the sack of review, it is reminded again that the real polycrystalline material in front of a growing small fatigue crack is envisioned to be composed of a series of elementary blocks/microstructurally-affected-zones of finite linear dimension ρ^* (ρ^* is not a constant). The process zone is still defined at the crack tip. Figure 7-1 schematically illustrates the elementary blocks and process zone in relation to the microstructurally-affected-zone for a growing small fatigue crack. As illustrated in Figure 7-1, any blockage

caused by barriers can also be modelled as a dislocation pile-up against an effective barrier to slip transmission.

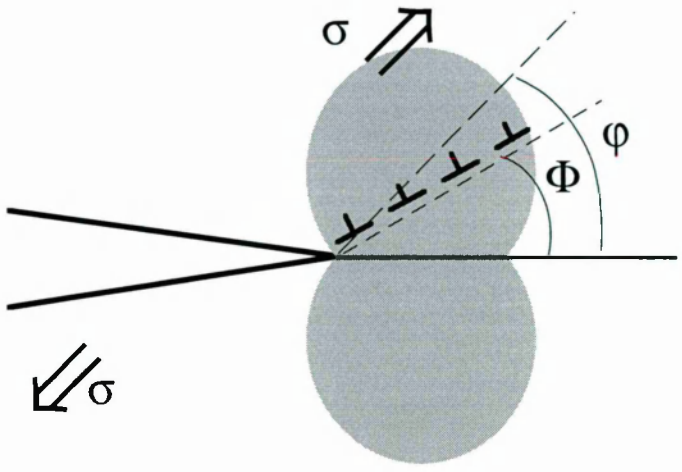

Figure 7-2 Crack Tip Configuration And Its Associated Physical Parameters

Since ρ^* is defined as the microstructurally-affected-zone, it must be related to local microstructural parameters, such as the distance from crack tip to the next grain boundary, the angle φ between the loading direction and the crack plane, the slip band orientation Φ. Figure 7-2 illustrates all parameters used in this study. However, such representation of microstructure features of polycrystalline materials is only suitable to transgranular fatigue cracking. This representation is not explicit enough to reflect the microstructure in the presence of intergranular fatigue cracking.

To model the Stage I to Stage II crack growth transition, small fatigue cracks are considered to initiate at the slip bands or at an inclusion/particle. The small fatigue cracks extend in shear across a few grains before transition from Stage I to Stage II crack growth occurs. To simplify modelling, the small fatigue crack and its associate slip bands are assumed to be coplanar. Local damage at the crack tip is primarily due to strongly discrete glide edge dislocations around the crack tip. The Stage I to Stage II crack growth transition in polycrystalline materials occurs at a transition crack size $2a_0$ beyond which the plastic zone develops its own continually increasing plastic zone size. Once the Stage I crack growth converts into the Stage II crack growth, the plastic zone is the result of the stress

concentration at the crack tip. The mechanism for Stage II crack growth is crack-tip blunting and sharpening by alternating shear on two slip directions. Physically, the transition crack size can be regarded as a transition point in the $2a - \frac{d(2a)}{dN}$ plot at which Stage I propagation terminates and Stage II propagation begins.

7.3 MODELLING PROCEDURES

7.3.1 Crack Tip Sliding Displacement (CTSD) At The Stage I To Stage Crack Growth Transition

A small fatigue crack advances by way of glide edge dislocation emission from the crack tip. When glide dislocation movement spreads to a grain boundary, the grain boundary may block the motion of leading dislocations causing difficulty of dislocation transmission and resulting in a dislocation pile-up. Once the pile-up is strong enough, the leading dislocations initiates new active slip bands in the next grain, leading to crack advance. A similar dislocation pile-up will repeat in next grains before the growing small fatigue crack traverses another grain. In the event of a pile-up, crack tip sliding displacement due to dislocation pile-up controls the Stage I to the Stage II transition. The pile-up ahead of the small fatigue crack tip can be modelled in terms of a continuous distribution of dislocations under a assumption of shear crack analogue [108,109].

Consider a growing small fatigue crack approaching an effective barrier. The slip bands emanate from the crack tip and spread in an infinite body between the crack tip and the barrier ahead of the crack tip. The slip bands are subjected to uniform shear stress τ as shown in Figure 7-3. As τ rises towards a maximum stress τ_{max}, edge dislocations are generated at the small fatigue crack tip [106,107] and run through the remainder of the slip band, stopping at the grain boundary. The question is how to characterise this dislocation pile-up for the growing small fatigue crack at the Stage I to Stage crack growth transition.

It is widely considered that Mode I mechanism primarily dominates the small crack growth after the Stage I to Stage crack growth transition. Obviously, three physical features associated with the transition can be outlined:

- The crack being considered is a growing small fatigue crack, that has traversed a few grains and is about to become a Mode I crack on reaching the transition, rather then a shear crack located within a grain and blocked by grain boundaries;
- The Mode I mechanism begins to prevail over the shear mechanism when the Stage I to Stage II transition occurs;
- Dislocations causing crack tip advancing are emitted from the crack tip [107,183,214,215] and only severely blocked at the transition by the most effective barrier ahead of the advancing crack tip, such as a grain boundary.

On the basis of the three features, it is assumed that the growing small fatigue crack on reaching the transition is a quasi-Mode-I crack with dislocations emitted from its tip at an angle roughly ranging from 63^{o} to 72^{o} [214-216] [as shown by Figure 7-3(a)] and blocked over a distance l_0 by the most effective barrier. The dislocation pile-up, just before the transition, ahead of the small fatigue crack tip within the distance l_0 can be regarded as a stressed single pile-up, being pushed by maximum shear stress τ_{max} against the grain boundary. Consequently, it can be modelled that the crack tip configuration initially consists of the single pile-up along a slip plane in equilibrium with the applied shear stress.

Therefore, the dislocation distribution can be characterised [108,109] by a continuous density function n(x´) replacing the discrete dislocations. For individual dislocations in the pile-up to be equilibrium, the force produced by the external stress and that caused by the interaction with other dislocations must balance, *i.e.*, the external shear stress τ_{max} equilibrates with the stresses at various positions x along the pile-up due to dislocations at $x'\left(=\frac{2x}{l_0}\right)$. The x–axis of the pile-up coincides with the slip direction. This equilibrium

conditions under plane strain condition can be expressed in terms of the continuous distribution function of dislocation $n(x')$ as [106,109]:

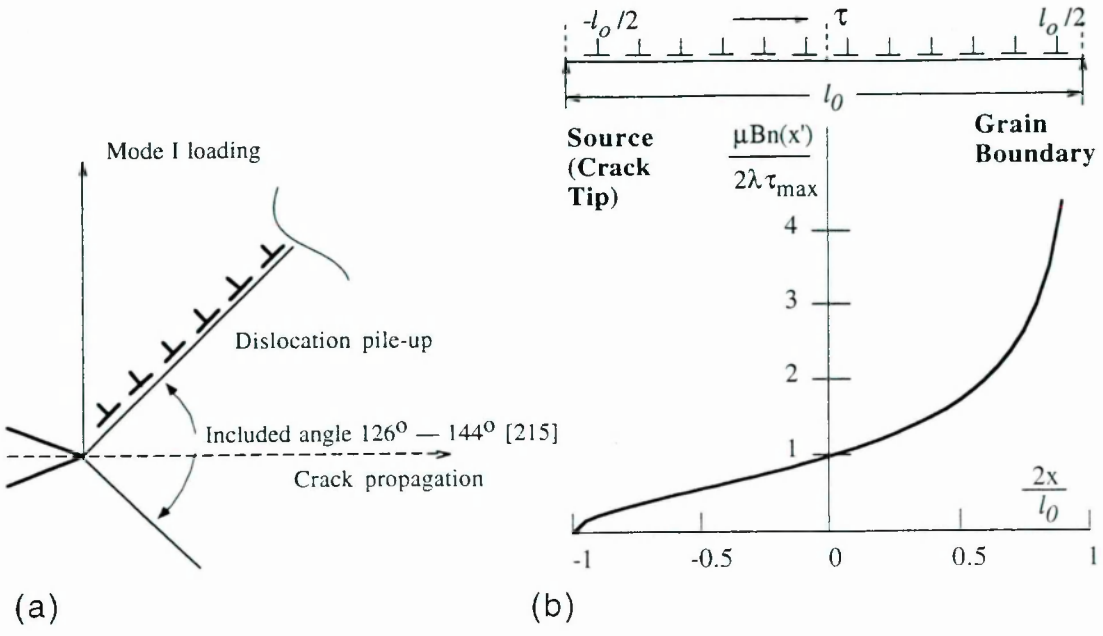

Figure 7-3 Schematic Representation Of (a) The Near-Tip Dislocation Emission; (b) Dislocation Distribution Ahead Of An Advancing Microcrack Tip As A Function Of Normalised Distance

$$\tau_{max}\,\mathbf{B} = \frac{\mu\,\mathbf{B}^2}{2\lambda}\int_{-l_0/2}^{l_0/2}\frac{n(x')dx'}{x'-x} \qquad \left(-\frac{l_0}{2} < x < \frac{l_0}{2}\right) \tag{7-1}$$

where $\mu = \frac{E}{2(1+\upsilon)}$;

$\lambda = (1-\upsilon)$ for edge dislocation.

The configuration originally used in deriving this relation is a double pile-up with dislocations locked at $x = -\frac{l_0}{2}$, $x = \frac{l_0}{2}$ and the dislocation source is located at $x = 0$.

However, in the case of an advancing small crack front, the single pile-up is considered which can be assumed that the dislocations are emitted at $x = -\frac{l_0}{2}$ and form the pile-up at $x = \frac{l_0}{2}$ as illustrated in Figure 7-3. The dislocation density is bounded at the crack tip $\left(x = -\frac{l_0}{2}\right)$ and unbounded at the tip of the slip band $\left(x = \frac{l_0}{2}\right)$. This dislocation pile-up is one that is being pushed at the grain boundary $[n(1) = \infty]$ from the crack tip $[n(-1) = 0]$, which is a

stressed single pile-up and can be treated by superposing a stressed double pile-up with an unstressed single pile-up. Thus, the dislocation distribution in the stressed single pile-up of length l_0 is [107,109]

$$n(x') = \frac{1}{\mathbf{B}}\frac{d\mathbf{B}}{dx} = \frac{2\lambda\tau_{max}}{\mu\mathbf{B}}\left(\frac{1+\frac{2x}{l_0}}{1-\frac{2x}{l_0}}\right)^{1/2}. \tag{7-2}$$

This distribution function predicts accurately how most of the dislocations in the pile-up are arranged [106,108,109]. Thus the total number of edge dislocations in this stressed single pile-up of length l_0 is given

$$N = \int_{-l_0/2}^{l_0/2} n(x')dx = \frac{\pi\lambda\tau_{max}l_0}{\mu\mathbf{B}}. \tag{7-3}$$

The number of dislocations in the single pile-up multiplied by the Burger's vector **B** at a maximum shear stress τ_{max} will be equal to the net maximum displacement along the slip plane at the small crack tip, *i.e.*, $CTSD_{max} = N\mathbf{B}$.

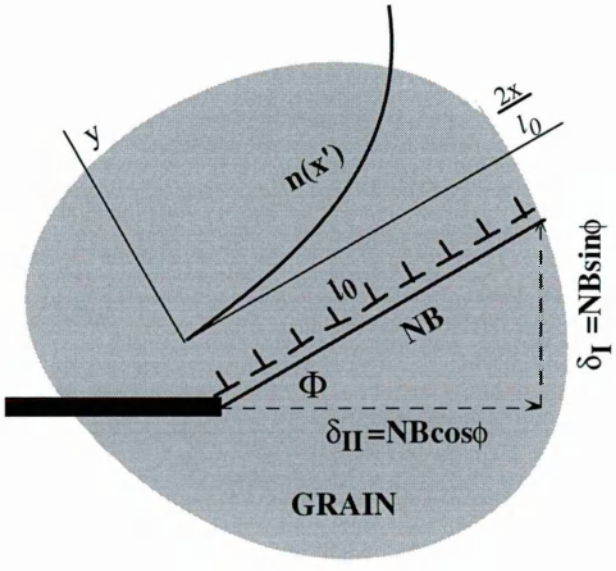

Figure 7-4 Schematic Presentation Of Assumed Edge Dislocation Distribution In Front Of A Crack Tip In A Single Stressed Pile-Up

It is assumed that after forward loading complete slip irreversibility is maintained during unloading. Hence the $CTSD_{max}$ will be the net crack tip displacement corresponding to τ_{max} after unloading. This forward shear displacement produced by τ_{max} will be maintained as a consequence of the unloading process and complete slip irreversibility, resulting in interference of asperities of crack faces at the next positive load. The magnitude of interference between crack faces can be resolved into respective Mode I and Model II components as $(CTSD_{max})_I = NB\sin\Phi$ and $(CTSD_{max})_{II} = NB\cos\Phi$ as defined in Figure 7-4.

Since Stage I growth may terminate when the small fatigue crack reaches the first or subsequent grain boundaries, the growth is considered to become Mode I growth. The applied maximum shear stress τ_{max} can be expressed in terms of a more useful normal stress σ_{max} using the relation, $\tau_{max} = \frac{\sigma_{max}}{2}\sin[2(\frac{\pi}{2}-\varphi)]$ [109,110] for a surface microcrack. As a result, the Mode I component in the maximum crack tip sliding displacement $(CTSD_{max})_I$ due to the pile-up can be derive to be

$$(CTSD_{max})_I = \frac{\pi\lambda\tau_{max}l_0}{\mu}\sin\Phi$$

$$= \frac{\pi(1-\upsilon^2)\sigma_{max}l_0}{E}\sin[2(\frac{\pi}{2}-\varphi)]\sin\Phi\,. \qquad (7\text{-}4)$$

This crack tip sliding displacement is strongly dependent on pile-up length and orientation at a given stress level. The dislocation pile-up builds up against the most effective barrier just before the Stage I small fatigue crack become a Stage II small fatigue crack. Consequently, the small crack growth rate may reach a minimum due to the microstructural barrier.

7.3.2 Determination Of Transition Crack Size

Analysis of the dislocation pile-up makes it possible to determine the transition crack size $2a_o$. However, many metal materials show dramatic cyclic softening or hardening behaviour that may change the material strength and complicates analysis. As it is known,

two opinions were put forward to consider the transition. (1) The period of Stage I small crack growth occurs only whilst the small crack grows across a single grain and therefore crack growth over the subsequent grains no longer relates to microstructure. (2) The Stage I small crack regime extends over several grain diameters.

However, it is unsatisfactory to determine the transition crack size by equating it to one or several grain sizes because the transition is a kinetic process affected by local microstructure and stress level. At lower load levels the Stage I small crack growth period dominated by a shear mechanism may last longer compared to high load levels.

In the present work, it is considered that a mature transition can not occur promptly but gradually. From a point of view of the local driving force at the crack tip, any mature transition from sliding to tension can not proceed until the Mode I component in the crack tip sliding displacement develops sufficiently and becomes dominant. After the transition, the small fatigue crack will (i) become insensitive to microstructural barriers [171] and (ii) develops two mutually perpendicular shear planes through which it will grow owing to equal shear decohension on each shear plane [213]. As a result, the dislocation pile-up may vanishe in subsequent small fatigue crack growth and its effect can be neglected. The CTSD changes to the crack tip opening displacement (CTOD) at the transition crack size and govern the Stage II small crack propagation.

Therefore, the transition crack size $2a_o$ is determined when the Mode I component in the CTSD, which forms due to the pile-up just before the transition, becomes consistent with the CTOD, which is caused by the two mutually perpendicular shear planes just after the transition. In other words, when the $(CTSD_{max})_I$ derived from the dislocation pile-up model equals to the $CTOD_{max}$ calculated from a standard fracture mechanics solution, the Stage I to the Stage II crack growth transition occurs. The crack tip opening displacement for the Stage II small fatigue cracks as a function of stress intensity factor K is given by [111]

$$CTOD_{max} = \frac{0.49\,K_{max}^2}{E\sigma_y} \tag{7-5}$$

in which $K_{max} = Y\sigma_{max}\sqrt{a}$.

Although Equation 7-5 is an elastic solution of fracture mechanics, a plastic zone size $(r_p)_o$ corresponding to the transition crack size can be introduced into the Equation 7-5 by replacing a with $(a+r_p)_o$ (the subscript 'o' stands for the transition point) for taking account of the plastic zone at the crack tip. The r_p can be evaluated in terms of the relationship shown in Figure 6-3. However, this will complicate the determination of the transition crack size, $2a_o$, since the transition crack size will have to be determined in this case by using a numerical computation method. To a first approximation of approach, the transition crack size may be specified to be the real crack size plus the associate plastic zone size at the transition point. More careful computation may be carried out in future to create a correction factor at different load levels for Equation 7-5.

Therefore, when this CTOD solution (Equation 7-5) for Stage II small fatigue cracks equals to the CTSD solution (Equation 7-4) for Stage I small fatigue cracks, the transition crack size, $2a_o$, can be derived to be

$$2a_o = \frac{2\pi(1-\upsilon^2)\,l_0 \sin[2(\frac{\pi}{2}-\varphi)]\sin\Phi}{0.49\,Y^2}\left(\frac{\sigma_{max}}{\sigma_y}\right)^{-1} . \tag{7-6}$$

at which the discrepancy between the non-continuous and continuous nature of small crack growth vanishes. Factors affecting the pile-up length, l_0, will be considered later.

7.3.3 Determination Of Microstructurally-Affected-Zone Size

In Chapter 6, a unified growth rate law equation was derived to predict small crack growth rates using macroscopic low-cycle fatigue properties. The developed $\frac{da}{dN}$ expression can be logically resolved into three components, *i.e.*,

$$\frac{da}{dN} = (\text{macro-related term}) \times (\text{micro-related term}) \times (\text{driving force term}) \tag{7-7}$$

in which each of terms can be expressed respectively as

— macro structurally-related term:

$$2\left(\frac{K'}{(\sigma_f' - \sigma_m)\,\varepsilon_f'}\right)^{\frac{-1}{b+c}}\left(\frac{2(1-\upsilon^2)}{\omega E}\right)^{\frac{-(1+n')}{b+c}} \tag{7-8a}$$

— microstructurally-related term:

$$F(d^*, \rho^*, r_p) = d^*\,(\rho^*)^{\frac{1+n'}{b+c}}\left(\left(1+\frac{r_p}{a}\right)^2 - \left(\frac{d^*}{a}\right)^2\right)^{\frac{-(1+n')}{2(b+c)}} \tag{7-8b}$$

— driving force term:

$$\left(\frac{\Delta\sigma}{2}\sqrt{a}\right)^{\frac{-(1+n')}{b+c}} \tag{7-8c}$$

The resolved microstructurally-related term sets up two conditions for the unified small crack growth law to be applied in the whole range of small fatigue crack growth.

- The valid use of continuum mechanics entails $F(d^*, \rho^*, r_p) \geq 0$ at and just beyond the transition crack size at any load level for the Stage II small fatigue cracks. This requisite can be expressed as

$$\left(\left(1+\frac{2r_p}{a}\right)^{0.5}\left(1+\left(\frac{r_p}{a}\right)^{-1}\right)\frac{2a}{\omega\rho^*}\right)_{(a\to a_o)} \geq 1 \tag{7-9(a)}$$

- $F(d^*, \rho^*, r_p)$ should reaches zero when the load level approaches the fatigure limit to satisfy $\frac{da}{dN} = 0$. This requisite can be expressed as

$$\left(\left(1+\frac{2r_p}{a}\right)^{0.5}\left(1+\left(\frac{r_p}{a}\right)^{-1}\right)\frac{2a}{\omega\rho^*}\right)_{(\Delta\sigma\to\Delta\sigma_{FL})} = 1 \tag{7-9(b)}$$

In other words, the microstructurally-affected-zone size should satisfy the two requisites physically and mathematically. The question is how to determine the microstructurally-affected-zone size by these two requisites.

(1) First of all, it is physically complex to determine a local microstructurally-affected-zone size due to unpredictable local microstructural features. Therefore, the

application of continuum mechanics to a small fatigue crack tip is supposed to be adequate to determine the microstructurally-affected-zone size at the transition crack size $2a_o$. In other words, transition conditions determine the microstructurally-affected-zone size. Otherwise it fails to explain why the Stage I to the Stage II crack growth transition is closely related to microstructure. Substituting Equation 6-9 into Equation 7-8(b) may lead to a determination of the microstructurally-affected-zone size.

By denoting $(\rho^*)_o = \rho^*/a_o$ to be a dimensionless quantity for the microstructurally-affected-zone size, the requisite demanded by the continuum mechanics [Equation 7-9(a)] determines the following condition that is associated with the crack growth transition.

$$(\rho^*)_o \le \frac{2}{\omega}\left(1+\left(\frac{2r_p}{a}\right)_o\right)^{0.5}\left(1+\left(\frac{r_p}{a}\right)_o^{-1}\right) \qquad (7\text{-}10a)$$

where $\left(\frac{r_p}{a}\right)_o$ is the normalised plastic zone size corresponding to the transition crack size $2a_o$ at any load level. Using Equation 7-6 the microstructurally-affected-zone size can be formulated by

$$\begin{aligned}\rho^* &= a_o\,(\rho^*)_o \\ &= \text{Constant}\ \{l_0 \sin[2(\frac{\pi}{2}-\varphi)]\sin\Phi\}\left(\frac{\sigma_{max}}{\sigma_y}\right)^{-1}\end{aligned} \qquad (7\text{-}10b)$$

where $\text{Constant} = \dfrac{2\pi(1-\upsilon^2)}{0.49\omega Y^2}\left(1+\left(\dfrac{2r_p}{a}\right)_o\right)^{0.5}\left(1+\left(\dfrac{r_p}{a}\right)_o^{-1}\right)$.

(2) As the load level approaches the fatigue limit, the microcrack will be completely blocked by grain boundaries and become a non-propagating microcrack. Since it is impossible to know the local grain within which the microcrack forms and the grain size, the transition crack size $(2a_o)_{FL}$, corresponding to the stress level of fatigue limit, should be taken as the non-propagating microcrack size. This approach to $\frac{da}{dN} = 0$ is reasonable because any crack size, smaller or bigger than the transition crack size, dose not ensure attainment of the non-propagating crack. As long as the microstructurally-affected-zone size satisfy this condition, the crack growth rate approaches zero. This condition can be set to be

$$[(\rho^*)_o]_{(\Delta\sigma \to \Delta\sigma_{FL})} = \left(\frac{2}{\omega}\left(1+\left(\frac{2r_p}{a}\right)_o\right)^{0.5}\left(1+\left(\frac{r_p}{a}\right)_o^{-1}\right)\right)_{(\Delta\sigma \to \Delta\sigma_{FL})}. \quad (7\text{-}11)$$

However, physically Equation 7-11 is only a special case of Equation 7-9(a) as the load level reaches the fatigue limit. The microstructurally-affected-zone size attains a maximum at the load level of fatigue limit. This indicates that Equation 7-10 can satisfy the both requisites demanded by Equation 7-9. Therefore, the microstructurally-affected-zone size can be determined using Equation 7-10(b) for polycrystalline materials. As a result, the determined microstructurally-affected-zone size may act as a dominant microstructural dimension affecting small fatigue crack growth. Obviously, corresponding to ρ^*, the evolution of microstructurally-related process zone d^* can be simply computed using the micromechanical relationship (Equation 6-9) as detailed in Chapter 6.

7.4 EVOLUTION OF PLASTIC ZONE AHEAD OF AN ADVANCING CRACK FRONT

As noted in Chapter 6 that the normalised plastic zone size $\frac{r_p}{a}$ increases, following a power function, with smaller crack sizes. This evolution pattern of the normalised plastic zone is questionable when the crack size remains just a few grain sizes because the ratio $\frac{r_p}{a}$ does not really increase rapidly with smaller crack size. By modifying Bilby´s solution for continuous distribution of infinitesimal dislocations, A. Navarro and E. R. de los Rios developed an attractive model to describe progressive evolution of plastic zone for a shear small fatigue crack [13,98]. Their model elegantly described an alternative pattern of evolution of the plastic zone on contacting grain boundaries due to blockage of each grain boundary to the plastic flow. However, their model assumes that the plastic zone ahead of the small fatigue crack frontinstantaneously reaches the grain boundary once the small fatigue crack initiates in a grain and the plastic zone is severely blocked as the growing small fatigue crack approaches each grain boundary. After redevelopment in an adjoining

grain, the plastic zone spreads immediately to another the grain boundary. This pattern is still valid even though the small fatigue crack extends across many grains.

The assumption may be in contradiction to the fact that there is no strong blockage of grain boundaries to small fatigue crack growth after the small fatigue crack propagates over a few grains [76,67]. This is because small fatigue crack growth may be 'continuous' in Stage II and no longer controlled solely by shear mechanisms. The shear crack analogue along with its plastic zone evolution seems inadequate to be extrapolated to Mode II crack regime after the small fatigue crack has spanned a few grains.

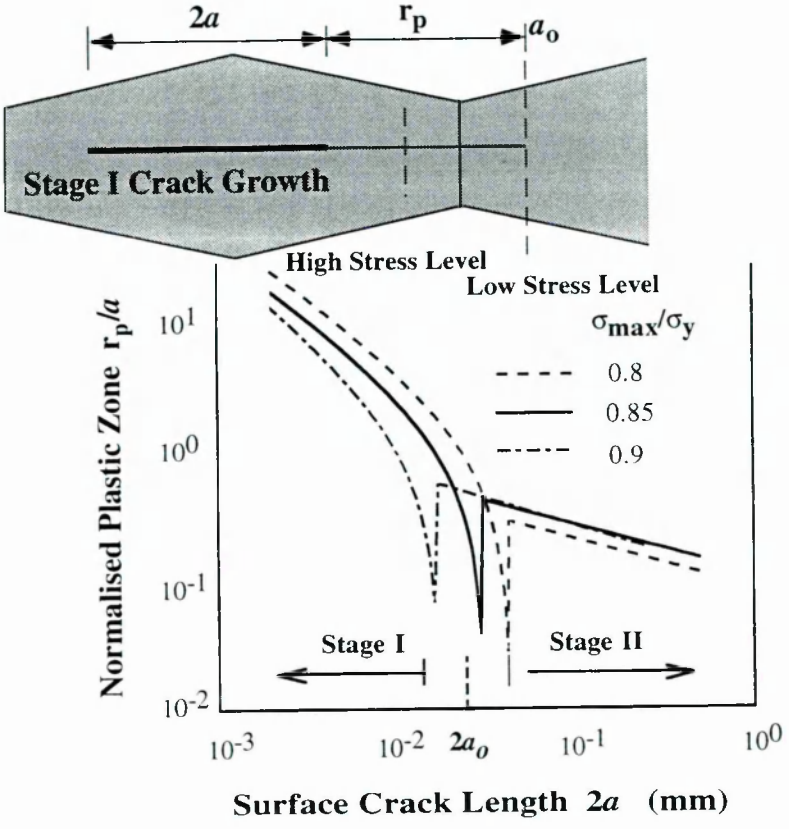

Figure 7-5 Schematic Illustration Of Proposed Evolution Of The Normalised Plastic Zone For Growing Small Fatigue Cracks In Aluminium Alloys

Thus, it is proposed that the evolution of the normalised plastic zone for growing small fatigue cracks follows A. Navarro and E. R. de los Rios´s suggestion before the small fatigue crack size reaches the transition crack size $2a_o$. Afterwards the ratio $\frac{r_p}{a}$ conforms to a continuous decreasing pattern that has been experimentally verified [67] as shown in

Figure 6-3. Figure 7-5 schematically illustrates this evolution of the normalised plastic zone.

This evolution pattern of normalised plastic zone is only applicable to aluminium alloys because the continuously decreasing pattern of $\frac{r_p}{a}$ was only experimentally testified in 7×××series aluminium alloys. For other polycrystalline materials (not composites), the evolution pattern of normalised plastic zone may be similar.

Although the application of continuum mechanics to small fatigue cracks less than a few grain sizes may incur questions in principle, this work still suggests that Equation 6-9 can be applied to the transition crack size because the evolution of normalised process zone has a much closer analogy not only in pattern but also in dimension with that of normalised plastic zone $\frac{r_p}{a}$. A fundamental, in fact, is that the defined process zone is still valid to characterise small crack front. The relation of process zone with the microstructurally-affected-zone is independent of crack growth transition conditions. So, the normalised process zone size at the transition crack size $\frac{(d^*)_o}{\rho^*}$ may reflect the kinetic transition from Stage I to Stage II crack growth.

7.5 CRACK GROWTH RATE PREDICTIONS

7.5.1 Numerical Simulation Of Pile-Up Length

Temporary pile-up of edge dislocations ahead of a growing small fatigue crack is modelled by means of the continuous-dislocation method plus the shear-crack analogue as the crack approaches the grain boundaries. The pile-up length is theoretically defined in terms of Equation 7-3 if only the number of edge dislocations is known. Reported in [203], crack tip dislocation emission arrangements were carefully investigated through *in situ* TEM observations and the dislocations emitted from the crack tip were measured, leading to determination of the number of dislocations. Even so, the total length of the pile-up

involves the last few, widely spaced dislocations which are ill-represented in the continuum model [106].

Since the uniform plastic deformation is assumed mechanically only within the process zone, the dislocation distribution in grain boundary reggion may be inhomogeneous. In spite of this, however, a dislocation density of geometrically necessary dislocation (GND) was defined by M. F. Ashby [204,205,206] to represent the inhomogeneous dislocation near the grain boundary region. The GNDs accumulate in the grain boundary region before the small fatigue crack reaches the grain boundary and causes the grain boundary strengthening which is dependent on grain size [206]. In this case, the piled-up dislocations near the grain boundary region may be substantially comparable to GNDs [204,205] to accommodate the inhomogeneous plastic deformation near the grain boundary region.

Detailed in [207] by Zhonghao Jiang *et al*, a dislocation density approximation for the flow stress-grain size relation of polycrystals was derived in which the flow stress is analysed for polycrystalline materials (Aluminium, Copper and Brass) to be related to the pile-up dislocation density and the pile-up distance from the dislocation source can be analysed. This work adopts their solution with the help of numerical survey of experimental data of small crack growth for 2024, 2124, 6082, 7075, 7150, 7475 series aluminium alloys. As the result of the study, it is found that the pile-up length in front of a small crack front is less dependent upon the load level but more dependent upon alloy strength. Basically, high strength aluminium alloy may exhibit a longer pile-up length due to stronger grain boundary resistance.

Furthermore, investigations of alloy strength in relation to grain size in the transverse direction are also made in this work which covers a wide range of 2×××, 5×××, 6×××, 7××× series aluminium alloys [38,48,56,63,77,78,80,81,104,112-124]. The grain size dependence of 2××× –7××× alloy strength is evident as exhibited in Figure 7-6. General trend of plots in Figure 7-6 is that the bigger the grain size, the lower the alloy strength.

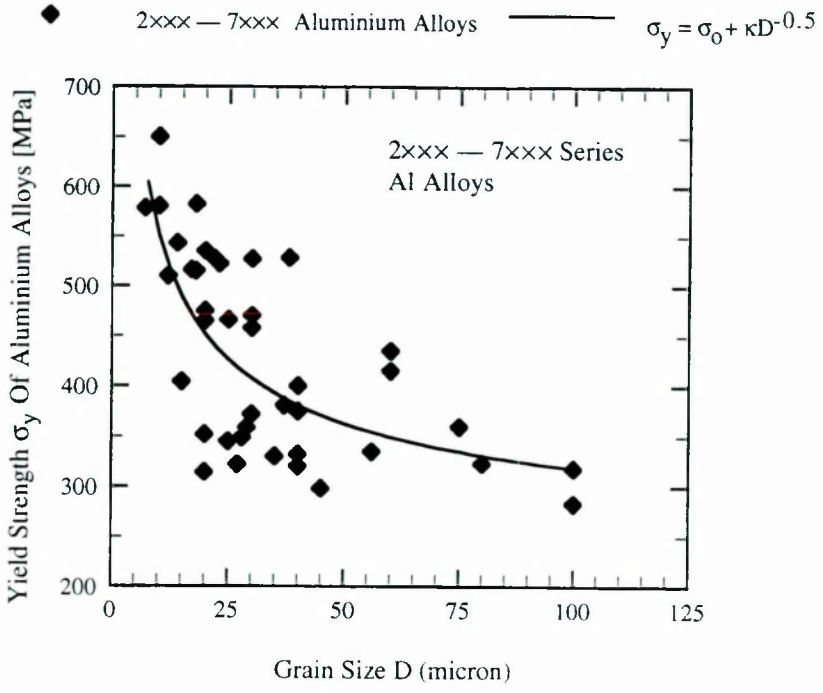

Figure 7-6 Grain Size Dependence Of Aluminium Alloy Yield Strength

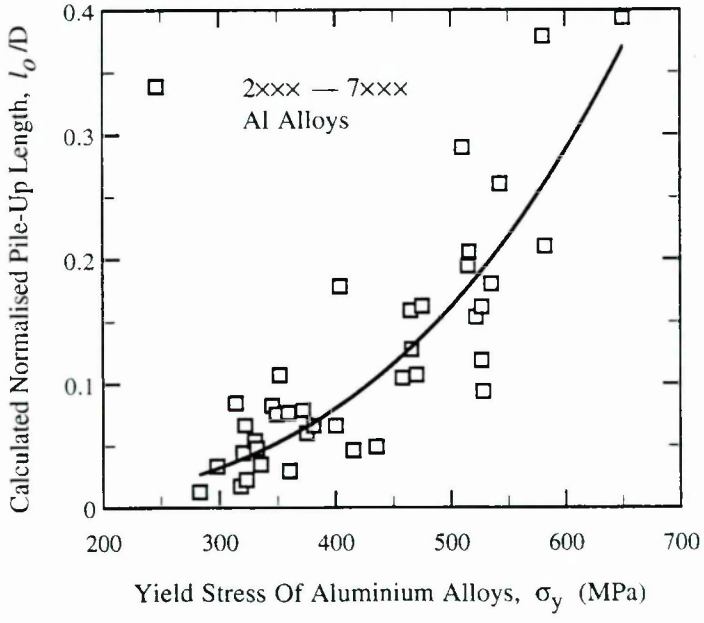

Figure 7-7 Numerical Evaluation Of Normalised Pile-Up Length

Through the analytical study, a good correlation, on the basis of curve fitting, between the normalised pile-up length $\frac{l_0}{D}$ (D stands for grain size) and the yield strength σ_y of 2××× and 7××× series of aluminium alloys is presented as shown in Figure 7-7 to be

$$\frac{l_0}{D} = B_1 [\sigma_y]^{B_2} \tag{7-12}$$

in which B_1 and B_2 are constants. This fitted characteristic curve shows that the analytically numerical evaluation of the pile-up length may be effectively used for most of aluminium alloys to quantify the pile-up effect. The practical use of this evaluation is satisfactory demonstrated by successful predictions of growth rates of small fatigue cracks for a range of aluminium alloys as demonstrated in following section.

7.5.2 Predictions Of $\frac{da}{dN}$ For 7××× Series Aluminium Alloys

A dislocation-based micromechanical model for Stage I small cracks and Stage II small cracks has been described in previous sections. To test the model, predictions of small crack growth rates were compared with experimental results obtained from testing 7075-T6 [78] and 7150-T651 aluminium alloys, shown in Figure 7-8. The pile-up length l_0 was numerically evaluated in terms of alloy strength. All measured mechanical and bulk fatigue properties for both aluminium alloys are listed in Table 3. In the predictions, the material hardening or softening during fatigue cycling was not specifically considered.

Table 3 Mechanical And Low-Cycle Fatigue Properties

Material	7075-T6 [125]	7150-T651	Material	7075-T6 [125]	7150-T651
E (MPa)	71000	69800	n'	0.06	0.0712
σ_y (MPa)	522	582	ε'_f	0.19	0.03
σ'_f (MPa)	1317	1199	b	-0.126	-0.108
K' (MPa)	775	814.2	c	-0.52	-0.49

It should be noted that there are no artificial adjustment to those measured parameters used in the model predictions. Model predictions are well coincided with experimental results, which indicate effective and valid applications of the model.

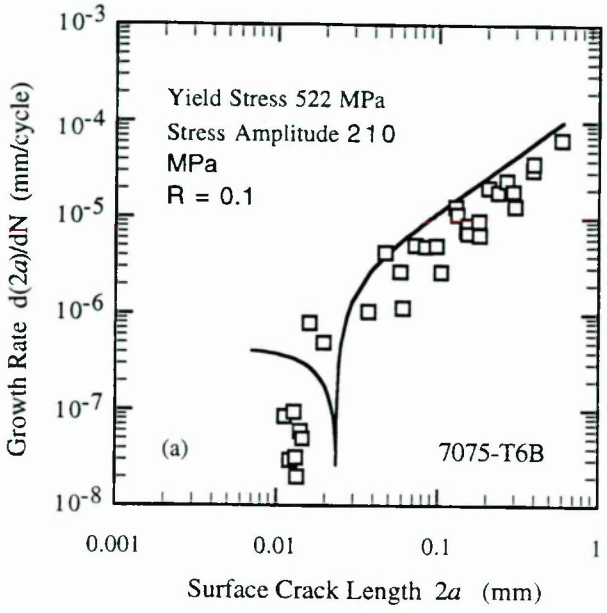
Yield Stress 522 MPa
Stress Amplitude 210 MPa
R = 0.1
(a)
7075-T6B
Growth Rate d(2a)/dN (mm/cycle)
Surface Crack Length 2a (mm)
10-3
10-4
10-5
10-6
10-7
10-8
0.001
0.01
0.1
1

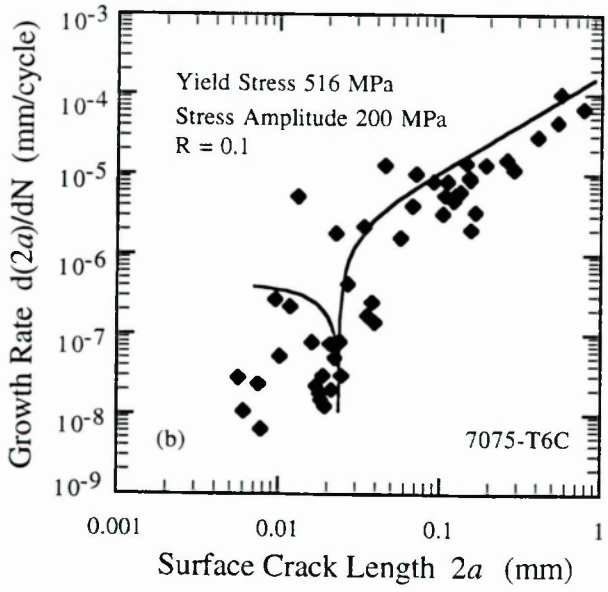
Yield Stress 516 MPa
Stress Amplitude 200 MPa
R = 0.1
(b)
7075-T6C
Growth Rate d(2a)/dN (mm/cycle)
Surface Crack Length 2a (mm)
10-3
10-4
10-5
10-6
10-7
10-8
10-9
0.001
0.01
0.1
1

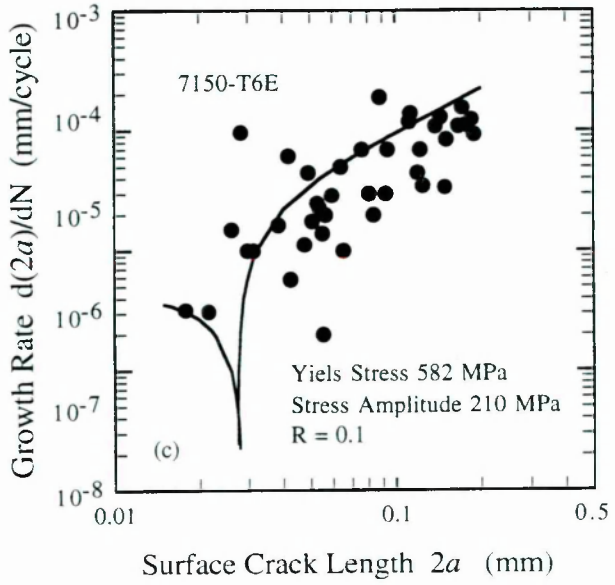

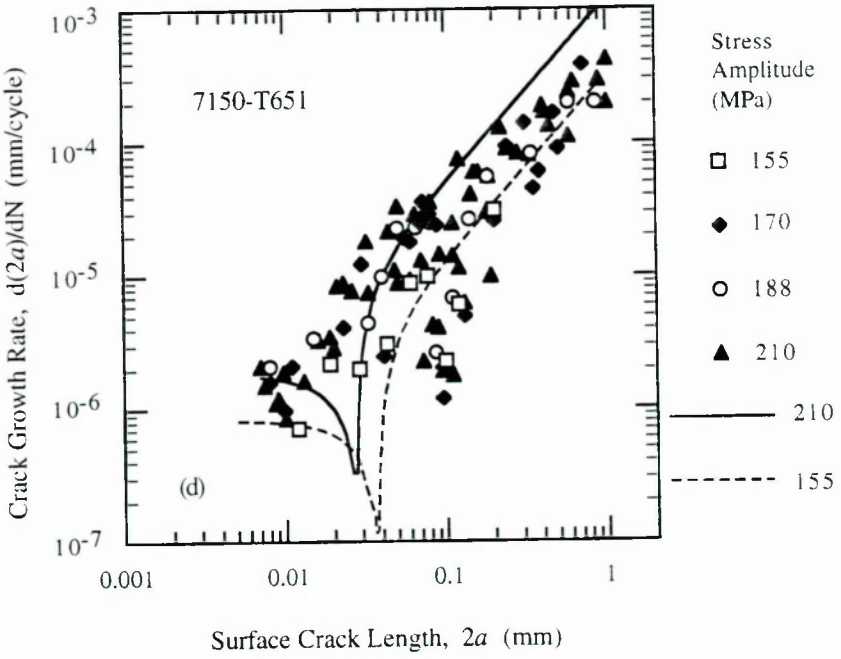

Figure 7-8 Comparisons Of Predicted Crack Growth Rates With Experimental Results (a) 7075-T6B, (b) 7075-T6C, (c) 7150-T6E And (d) 7150-T651

7.5.3 Simulations Of Kinetic Growth And Stage I To Stage II Crack Growth Transition

The kinetic growth of small fatigue cracks in Stage I and Stage II regimes along with transition between the two regimes in 7075-T6 aluminium alloy are simulated in Figure 7-9 using the developed model. The effect of load level is quite clear in all predictions [Figure 7-9(a)]. Small crack growth rates approach a minimum at a shorter transition crack size if the applied load level is higher. The model also predicts that once a small fatigue crack is nucleated, it initially grows at an approximate constant speed insensitive to crack size, and then its growth rate decreases due to the effective blockage of barriers until reaching a minimum. Afterwards the small fatigue crack overcomes the effective barrier, retrieving a fast growth rate quickly. This is a typically pronounced prediction by the developed model. Figure 7-9(b) shows another tendency of orientation dependence of predicted growth rates that the severer the misorientation between two neighbour grains, the lower the predicted growth rates. Figure 7-9(c) exhibits deflection effect of crack front on small crack growth rates. However, it should be noted that the two local orientation parameters, φ and Φ, do not vary independently but relatively in the course of small fatigue crack propagation.

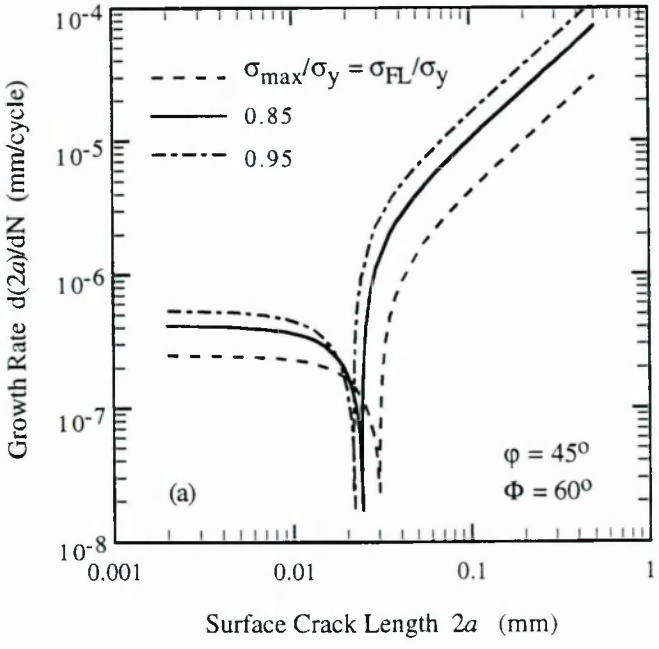

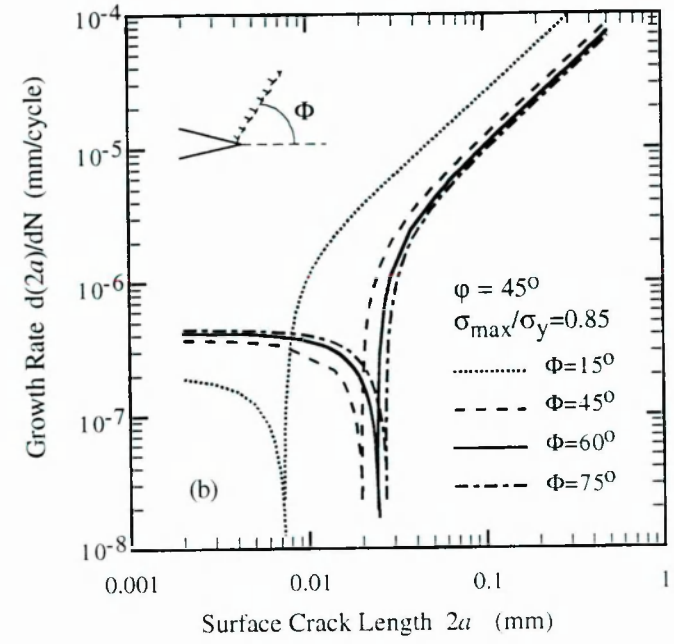

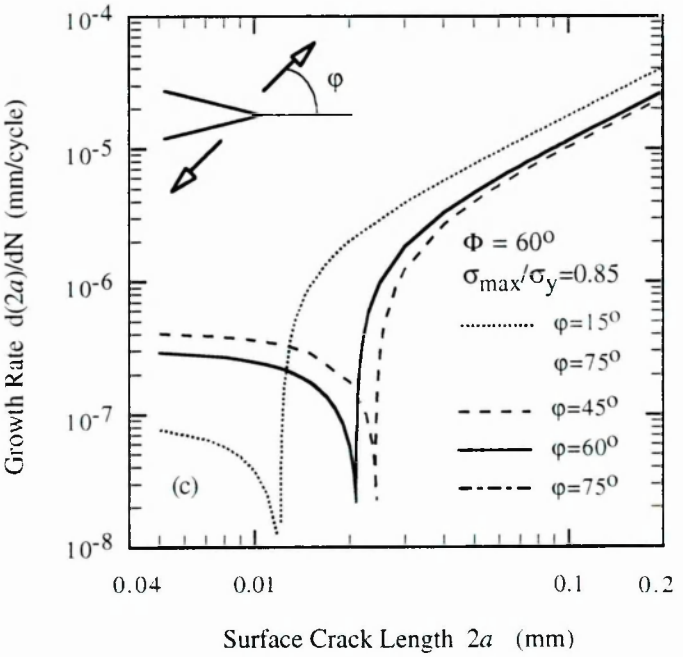

Figure 7-9 Predictions Of Growth Rates Of Small Fatigue Crack In 7075-T6 Aluminium Alloy ($R=\sigma_{min}/\sigma_{max}=0.1$). (a) Stress Level Effect; (b) Orientation Effect Of Slip Bands; (c) Effect Of Crack Front Deflection

7.5.4 Kinetics Of Small Fatigue Crack Growth

A duration of the Stage I to Stage II crack growth transition along the crack-size axis (in a — $\frac{da}{dN}$ coordinate system) commonly occurs either in experiments or in model predictions as shown in Figure 7-9. The causes for the duration are qualitatively explained to be due to the local noncontinuous microstructure, the load level or possible errors incurred in experimental measurements. In this work the transition crack size $2a_0$ is quantitatively related to load level, material strength and local microstructure. The transition crack size plays such a role that distinguishes the Stage II crack growth from the Stage I crack growth. A paradox seems happen that a big transition crack size is predicted as a result by using Equation 7-6 for polycrystalline materials with high strength. It is on the contrary that no unique value linking the transition crack size directly to the material strength can be predicted by Equation 7-6 because it predicts local microstructure-dependence of the crack growth transition.

The slip band orientation Φ affects the transition crack size. Unfavourably orientated slip bands may lead to crack front deflection, resulting in a longer shear dominated behaviour and hereupon a bigger transition crack size. Generally, the model predicts a tendency that an early transition is expected to occur under circumstance of favourably orientated slip bands and/or higher load levels that facilitate the transition from non-continuous crack growth to continuous crack growth. Variation of this transition crack size predicted using Equation 7-6 with respect to slip band orientation is depicted in Figure 7-10(a). It can be seen that a smaller transition crack size is predicted as a result of favourably orientated slip bands.

Further, the orientation-dependence feature of growth rate is embodied in the model by means of the parameters, φ and Φ, which may relatively vary depending upon the activated slip band orientation and crack front deflection. This variation may lead to an oscillating pattern of growth rate plots. Crack front deflection occurring at grain boundaries can be considered to be the result of orientation difference of independent slip systems. When a

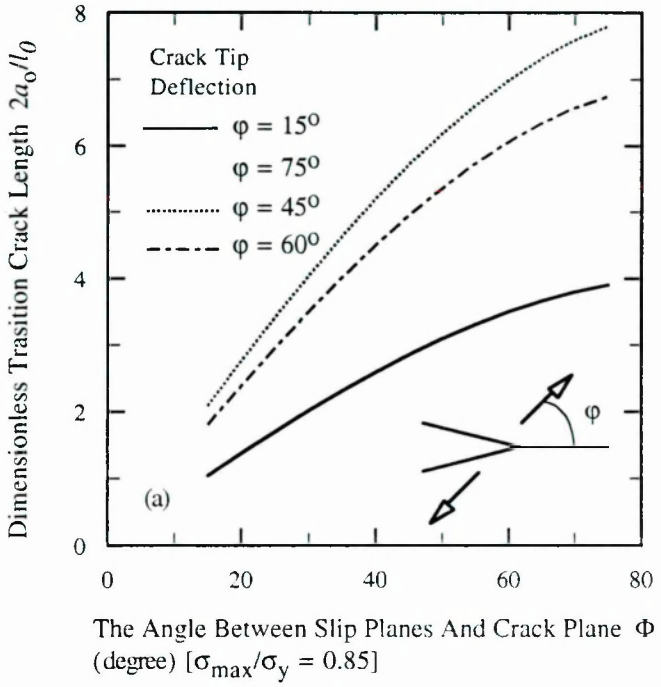

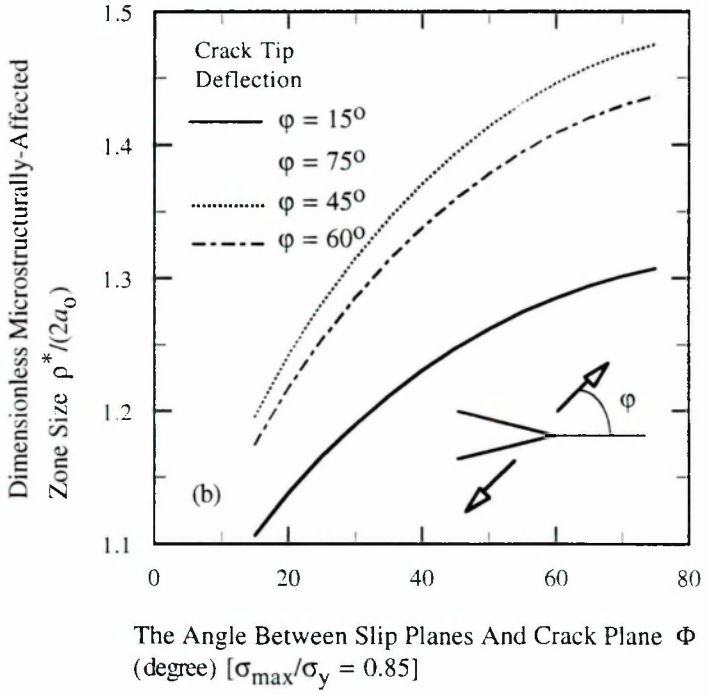

Figure 7-10 Evolution Of Theoretically Predicted (a) Transition Crack Size, And (b) Microstructurally-Affected-Zone Size

growing small fatigue crack penetrates grain boundaries toward a direction of preferred slip bands with a smaller angle of Φ, the model predicts smaller microstructurally-affected-zone size ρ^* as shown in Figure 7-10(b)·

On the other hand, increasing the load level may result in a smaller transition crack size and consequently higher growth rates. Indeed, Equation 7-7 also predicts faster growth of small cracks because the local driving force at crack front is also higher as a result. Either lower load levels or unfavourable slip band orientation may lead to a big microstructurally-affected-zone size, causing crack growth rate reduction. This indicate that it is easier for small fatigue cracks to overcome microstructural barriers and propagate along favourably-orientated slip bands at higher load levels.

The developed model predicts a minimum growth rate to be related to the kinetic transition from Stage I to Stage II crack growth. As it is known, more gliding dislocations may emit from a small crack tip due to presence of local stress concentration. The gliding dislocations are difficult to continue transmission [106-108] as the Stage I small fatigue crack meets an effective barrier, causing a delay to crack propagation and resulting in a minimum of crack growth rate. As long as fatigue cycling continuously proceeds, the dislocation pile-up due to the barrier to dislocation transmission may become strong at the barrier [106-108]. The strong dislocation pile-up may overcome the effective barrier by breaking it up and retrieving to a fast crack growth. Since a real effective barrier with respect to the crack tip driving force may be unpredictable, randomly located in polycrystalline materials, the transition has a kinetic nature.

The degree of delay of the crack propagation seems to be another notable point of concern. This point is certainly associated with the kineticcrack growth transition from Stage I to Stage II. The extent of the minimum of crack growth rate does affect fatigue lifetimes at different load levels. A little of information is available on that point and previous approaches [5,31] taking account of this delay were established on an assumption that the transition occurs at a fixed crack size, such as an average grain size. However, the

transition is a kinetic process as indicated in prior sections in the thesis. The author of this research has been aware of the importance of this point. The load effect on crack growth delay is not discussed in this thesis.

In general, the developed model demonstrates that kinetics of small crack growth can be described properly using the unified physical parameter, *i.e.*, the process zone size d^* because the evolution of the plastic zone associated with a growing small fatigue crack and the local microstructure can be correlated by the proposed physical parameter. However, the process zone size seems difficult to be physically quantified by direct experimental measurement in fatigue tests for a growing small fatigue crack. This is due to unpredictable local microstructure features and a fact that the normalised plastic zone size, $\frac{r_p}{a}$, varies throughout the small crack stage.

In fact, apart from the fatigue cycles, only two parameters can be experimentally measured directly without any physical or mathematical transformation to describe the characteristics of small fatigue crack propagation, *i.e.*, the small crack size and the associate plastic zone size (which may be difficult to measure) at a crack tip. No matter whichever other physical parameter is defined, as detailed in Chapter 2, to apply to small fatigue cracks, either by the small crack size or by the associate plastic zone size small fatigue crack growth rates can anyhow be correlated in a generalised way in the form of $\frac{da}{dN} = A_{small}\,\Pi^M$ as discussed in Chapter 1. This supports use of the process zone size because the established micromechanical relationship (Equation 6-9) quantitatively reflects the interrelation between the normalised process zone and the normalised plastic zone. In spite of uncertainty caused by local microstructure features, the normalised process zone size $\frac{d^*}{\rho^*}$ can still be determined in terms of small fatigue crack size, a, and its associate plastic zone size r_p.

Figure 7-11 shows a space view of Stage II small fatigue crack growth, which draws such an inference that a small fatigue crack front advances through a stochastic environment with a distribution of material properties bearing on different elementary blocks (or segments) of it since the microstructure is stochastic itself. Fluctuations observed in

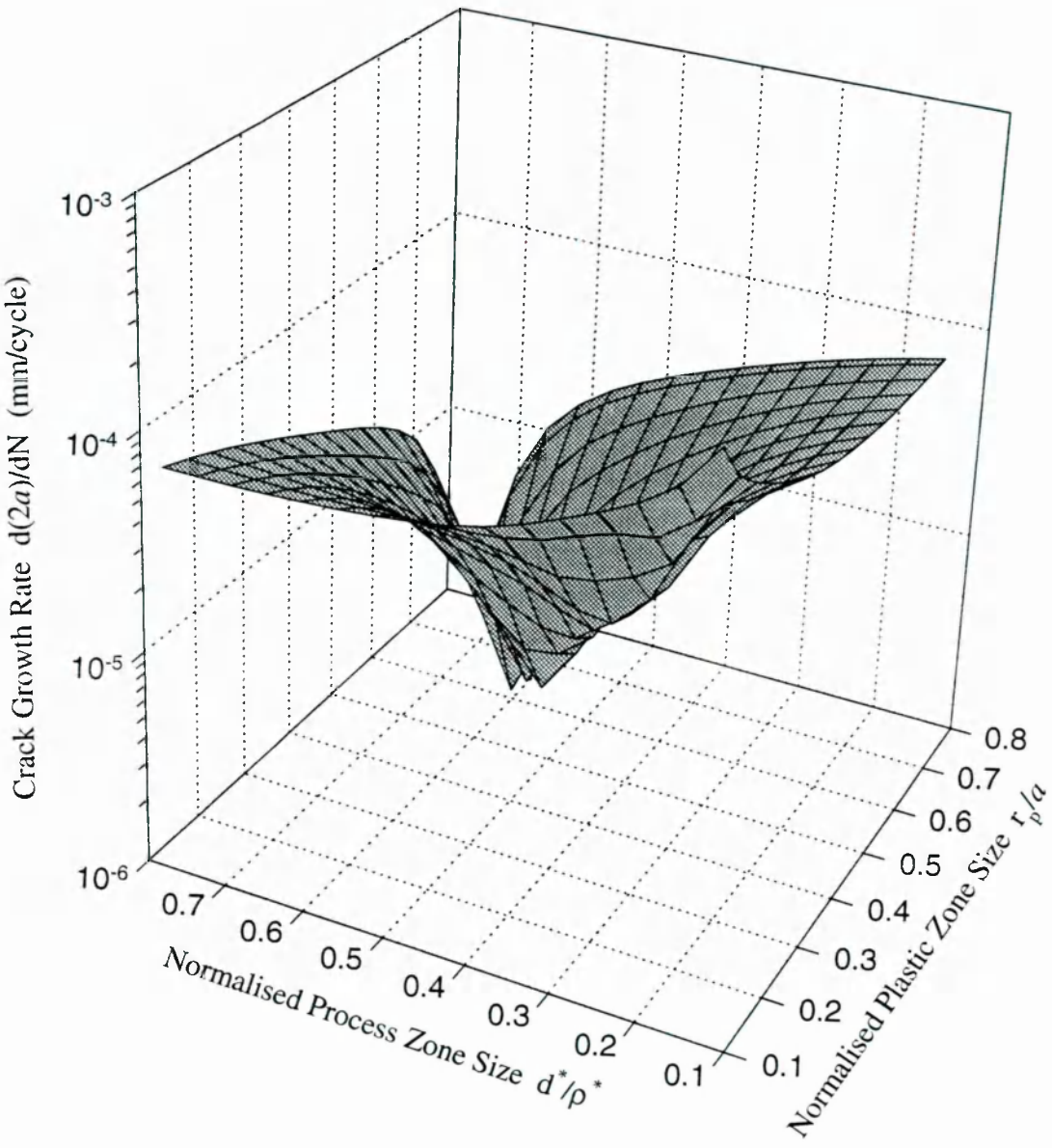

Figure 7-11 Illustration Of Kinetics Of Small Fatigue Crack Growth In Stage II

growth rate data can be directly traced to fluctuations in grains being traversed. Apparently, there exists a limited condition for orientation of both slip bands and the crack front deflection. At limited condition the local strain may reach either a minimum or a maximum at a given load level and a crack size. Consequently, the small fatigue crack growth rate is

not a unique function of the load level and the crack size but varies in a stochastic manner, depending upon the local microstructure.

Finally, the developed model also explains any heat treatment or temperature (fatigue dominated damage) effect on small fatigue crack growth since this effect has been reflected in the model by way of measured fatigue properties. This is another feature of the model.

7.6 SUMMARY OF THE CHAPTER

- The Process zone size d^*, incorporating interactive effect of the plastic zone, the load level and the local microstructure, is found to be a novel unified physical parameter to correlate small crack growth rates.
- The Stage I to Stage II crack growth transition is a kinetic process depending upon the applied load level and the local microstructure. The transition occurs when the Stage I crack tip sliding displacement reaches a value equal to the crack tip opening displacement of Stage II small fatigue crack. The transition crack size is dependent upon both load level and local microstructure.
- Early transition is predicted as the load level increases along with favourable slip band orientation while the later transition is primarily due to misorientation between two adjoining grains.
- Microstructurally-affected-zone is inherently related to the transition crack size rather than the grain size. The microstructurally-affected-zone size can be determined by crack growth transition conditions.
- Pile-up length can be numerically estimated in terms of alloy strength in conjunction with grain size for a wide range of aluminium alloys.

- A dislocation-based micromechanical model has been developed that predicts kinetics of small fatigue crack growth by using the novel unified physical parameter, *i.e.*, the process zone size, in conjunction with microscopic parameters (φ, Φ). An explicit advantage of the developed model is that the small crack growth rates can now be directly predicted using the macroscopic bulk fatigue properties instead of painstaking experimental observations and tedious crack size measurements.

- There exists no one-to-one relationship between $\frac{da}{dN}$ and a for small fatigue cracks due to microstructural dissimilitude. The model explains the origins of scatter in small fatigue crack growth, *i.e.*, slip band orientation dependence and alloy strength dependence of small crack growth and, also explains microstructure dependence and load level dependence of Stage I to Stage II crack growth transition.

It should be noted that the Stage I to Stage II crack growth transition describes a critical condition that the Stage I small fatigue crack overcomes an effective barrier to crack propagation and becomes a Stage II small fatigue crack. The minimum crack growth rate associated with the transition may reduce deeply, even to zero, as the applied load level decreases. Consequently, the applied stress level may reach the microstructural fatigue threshold of polycrystalline materials if the Stage I small fatigue crack is halted completely by the most effective barrier without propagating. This microstructural fatigue threshold can be computationally predicted using the developed model.

On the other hand, fatigue crack growth threshold ΔK_{th} is well known to be the mechanical fatigue threshold which differs from the microstructural fatigue threshold. This mechanical fatigue threshold is also significant to fatigue life predictions. Particularly, the role of the two thresholds and the relevance between them are much concerned. Therefore, following chapter is going to model and predict the fatigue crack growth threshold.

Chapter 8 TWO FATIGUE THRESHOLD CRITERIA

Fatigue crack growth thresholds are particularly of engineering importance in fatigue design and life predictions. The near threshold fatigue crack propagation is known to be greatly sensitive to local microstructure and the fatigue crack growth threshold behaviour is much dependent on load ratio effect (or mean load effect). Although a large number of models are available which predict the fatigue crack growth threshold, threshold nature is not fully understood due to different mechanisms and load ratio effect involved in fatigue crack growth threshold behaviour. Crack closure was overwhelmingly reported in the past twenty-five years. However, the majority of developed models based on crack closure considerations are mostly empirical without convincing explanations because closure arguments are most likely to be qualitative rather than quantitative. Some parameters in those developed models seem adjustable at will or have to be experimentally determined individually.

Recently, on the basis of many investigations of threshold data involving steels, Al-Alloys, ceramics, and metal-matrix composites, A. K. Vasudévan and K. Sadananda [185-187] have summarised a universal rule that two fatigue threshold criteria rather than one must be simultaneously fulfilled to ensure attainment of non crack propagation condition. Experimentally observed fatigue crack growth threshold behaviour (load ratio effect) can only be properly explained by using two fatigue crack growth thresholds that constitute fundamental threshold curves for fatigue failure assessment. Crack closure, no matter

whether it exists or not, does not affect the fundamental threshold curves. These novel interpretations of fatigue crack growth threshold behaviour provide a basis for micromechanical modelling of fatigue crack growth threshold, eliminating uncertainties in understanding fatigue crack growth threshold.

Two fatigue threshold criteria, K^*_{max} and ΔK^*_{th}, are presented to describe fatigue crack growth threshold behaviour and damage at any load ratio without invoking crack closure. Modelled are the two fatigue threshold criteria which demarcate non crack propagation zones from crack propagation zones and constitute fundamental threshold curves at any load ratio for aluminium alloys. By using a continuous configuration of dislocations in a pile-up, the fatigue limit is simulated as pile-up of dislocations against grain boundaries. The fatigue limit is determined in terms of a critical condition at which a fictitious microcrack associated with the pile-up corresponds to the onset of propagation. The two fatigue threshold criteria are attainable as the local stresses at crack front approach the fatigue limit. Microstructure is incorporated in the model to account for its effect on fatigue crack growth threshold behaviour. Quantitative assessment of the two fatigue threshold criteria requires knowledge of only the conventional material properties in conjunction with microstructure. Notably, two fatigue threshold criteria are required to determine fatigue threshold behaviour. The fatigue crack growth threshold can be determined using the two fatigue threshold criteria, K^*_{max} and ΔK^*_{th}, that are coherently related to fatigue limit. Micromechanical modelling of fatigue crack growth threshold exhibits a strong dependence of fatigue crack growth threshold upon local microstructure.

8.1 INTRODUCTION

In engineering design, infinite fatigue life is still required for some crucial parts of structure, which demands a fatigue crack growth threshold below which no fatigue damage (non-propagting crack) is assumed. The threshold phenomenon can therefore be treated

with reference to critical conditions for onset of fatigue crack growth. Two of the assumptions for infinite fatigue life design are as follows:

- Fatigue microcrack initiation should not occur; and
- Existing fatigue cracks or material defects should not grow during fatigue cycling.

The above argument relies on a fatigue limit $\Delta\sigma_{FL}$ below which fatigue lifetime may be regarded as 'infinite'. However, measured fatigue limit by using smooth specimens is likely to be dramatically different from specimen to specimen, depending upon the material surface quality, the material structure at surface, the local stress distribution, the size of the specimen and the environmental condition [126,127]. Fatigue limit could be viewed as a threshold closely related to the critical condition at which microcracks are just about to propagate. On the other hand, a fatigue crack growth threshold could be associated simply with the local driving force that advances the fatigue crack [148]. The former may be related to microcrack propagation due to slip band movement during fatigue while the later to fatigue cracks (or defects). In essence, both of them have to be associated with a given crack size.

Fatigue crack growth threshold conditions for long cracks are still not well understood. Experimentally measured fatigue crack growth threshold ΔK_{th} is debatable [127] because under low crack driving forces the crack growth mechanism becomes different. Mechanisms, such as plasticity-induced crack closure and roughness-induced crack closure, have been proposed to explain fatigue crack growth threshold phenomena. However, available experimental data on crack closure can only account for the total effect on closure as a result of many influences [184]. It is impossible to separate the measured value into individual components that contribute to crack closure.

Proposed in [185-187] are results for a fatigue crack curve consisting of two fatigue threshold criteria K^*_{max} (a parameter that is a critical maximum stress intensity) and ΔK^*_{th} (a parameter that is a critical value in cyclic amplitude) that apply to a variety of materials.

Based on a number of experimental data, this work models the two fatigue thresholds criteria K^*_{max} and ΔK^*_{th}. Fatigue crack growth threshold is viewed as a pile-up of dislocations against grain boundaries during fatigue cycling. A fatigue limit of polycrystalline materials is modelled as a continuous pile-up of dislocations along grain boundaries as observed in [183,190-192]. Their interaction with fatigue crack was analysed in [183,193,194].

To predict the threshold conditions, a number of models or approaches have been proposed which include fatigue limit predictions [128,129] and predictions of fatigue crack growth thresholds [130-133]. This work adopts the concept of the two fatigue threshold criteria in [185-187] and demonstrates that fatigue crack growth thresholds can be predicted using the two fatigue threshold criteria for a wide range of aluminium alloys. Without proving or disproving crack closure, the present work does not build fatigue crack growth threshold model on any closure argument but on fundamental physical phenomena associated with the fatigue crack growth threshold.

8.2 BACKGROUND OF MODEL

8.2.1 Fatigue Crack Growth Threshold

Observation of dislocations at a crack tip for an aluminium alloy shows an array of edge dislocations that were emitted from the crack tip on a plane nearly normal to the crack plane [107,183] as shown schematically in Figure 8-1. The crack tip is hence blunted until microcracks nucleate in a damaged zone ahead of the crack, leading the crack growth process. Prior to crack growth, the material offers resistance to any microcrack propagation. If the crack front is blocked by grain boundaries at load level above the fatigue limit, continuous opening and closing of the crack tip prevails. This process incubates a new plastic zone that precedes renewed crack propagation.

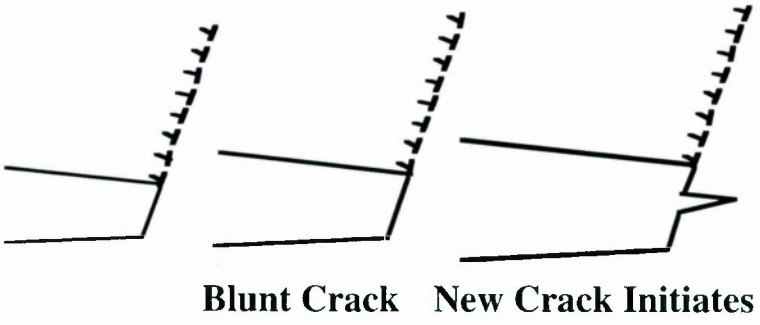

Figure 8-1 Schematic Illustration Of Dislocation Emission From A Fatigue Crack Tip And The Crack Tip Blunting [140]

It is well known that fatigue crack growth is sensitive to microstructure at low stress intensity ranges. This sensitivity is caused by smaller plastic zone sizes less than the relevant controlling microstructural dimensions at the crack tip [141]. The fatigue crack growth threshold has a strong dependence of microstructure controlling dimension for a variety of alloys [142-148]. The relation of the crack growth threshold to other material properties and/or microstructures is not always determinable. Nevertheless, it can be said that the fatigue crack growth threshold tends to decrease with increasing material strength and with increasing grain size for a given class of materials [149,150]. Moreover, experimental data have shown that the fatigue crack growth threshold is less sensitive to load ratio with increase of load ratio. It may approach a constant value at high load ratios.

8.2.2 Two Critical Stress Intensities For Threshold

Two fatigue threshold criteria, ΔK^*_{th} and K^*_{max}, could be proposed[184-189] which are referred to as a critical value in cyclic amplitude and a critical maximum stress intensity respectively. These two fatigue threshold criteria have to be satisfied simultaneously to ensure infinite fatigue lifetime without microcrack propagation. They are independent of any crack closure, load-history or environment. All observed load-ratio effects on fatigue crack growth threshold can be accounted for by the two fatigue threshold criteria without invoking crack closure. From dislocation considerations, crack closure contribution to crack-tip stress intensity reductions is either negligible or absent. Microplasticity originated from the crack tip does not contribute to crack closure.

8.2.3 Definitions And Assumptions In Modelling

Definitions and assumptions involved in the dislocation pile-up model can be stated as follows:

- Edge dislocations emit from a fatigue crack front at onset of fatigue crack growth.
- After emission of dislocations, the fatigue crack front can be mathematically treated as a micronotch with notch radius ρ.
- Two parameters ΔK^*_{th} and K^*_{max} are required to determine fatigue crack growth threshold behaviour to prevent microcrack initiation and threshold fatigue crack propagation.
- ΔK^*_{th} is defined to characterise damage caused by accumulation of cyclic plasticity. It has a critical value below which microcracks can not propagate due to grain boundary blockage and is related to local microstructure. The critical condition is assumed to correspond with the local stresses reaching their fatigue limits.
- K^*_{max} is defined in terms of maximum damage where the peak load to break the bonds at the fatigue crack front can be interpreted as a critical stress intensity below which the bonds remain unbroken at maximum load. Therefore, K^*_{max} is related to the constitutive relations of materials in fatigue. This critical condition may be related to the local strain energy in deformation at the crack front [196-199].
- The two fatigue threshold criteria (ΔK^*_{th} and K^*_{max}) constitute a demarcation that separates the non crack growth region from the crack growth region which are independent from each other.
- These two fatigue threshold parameters, ΔK^*_{th} and K^*_{max}, are in direct connection with threshold behaviour at load ratio R = 0 and are as same in value as K^{max}_{th}, ΔK_{th} respectively at R = 0.

- From the mechanical point of view, at low load ratio, R, threshold fatigue crack advance is prominently (not solely) dominated by breakage of bonds at the crack front while at high load ratio, R, threshold fatigue crack advance is predominantly (not solely) dominated by microcrack initiation due to cyclic fatigue damage in grains in the vicinity of the crack front. So, in low-R range, K^*_{max} controls fatigue crack growth threshold behaviour while in high-R range, ΔK^*_{th} controls fatigue crack growth threshold behaviour. This process can be illustrated by Figure 8-2.

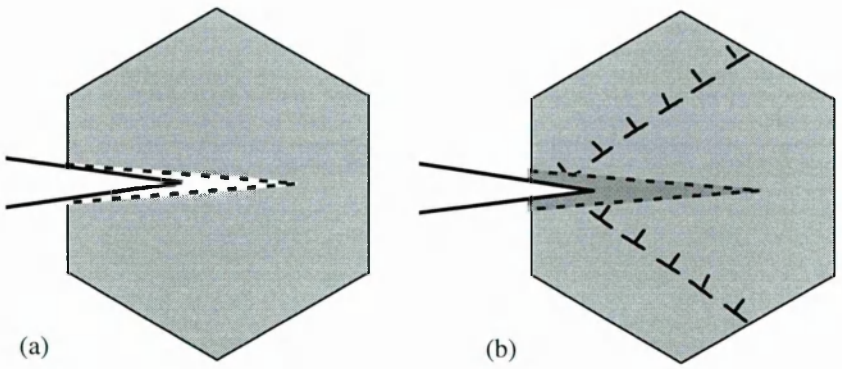

Figure 8-2 Schematic Illustration Of Crack Front Advancing (a) Dominated By Breakage Of Bonds At The Crack Front; (b) Dominated By Microcrack Initiation In The Crack Front

- R^* is defined to be $R^* = 1 - \Delta K^*_{th} / K^*_{max}$ [186] to demarcate the low-R range from the high-R range. In the low-R range $R < R^*$, the fatigue crack growth threshold value ΔK_{th} varies linearly with load ratio R given by [186]

$$\Delta K_{th} = K^*_{max}(1 - R) ; \tag{8-1}$$

In the high-R range $R > R^*$, the maximum stress intensity K^{max}_{th} at the fatigue crack growth threshold is a non-linear function of R and is given by [186]

$$K^{max}_{th} = \frac{\Delta K^*_{th}}{1 - R} ; \tag{8-2}$$

8.3 FATIGUE LIMIT

Surface conditions, harmful particles bonded in matrix have a dramatic influence on fatigue limit which cause a scatter of measured fatigue limits from smooth specimens. Harmful particles may be unshearable during fatigue which brings about a stress concentration in the matrix around it. The influence of particles on fatigue life of smooth specimens has been classified as how big a particle is and where the particle is situated [135,136]. Consequently, scattered distribution of measured fatigue limits from smooth specimens may be fundamentally due to particles of different size and different location in a smooth specimen. Whatever the fatigue limit of smooth specimens is modelled, a key element to interpret the fatigue limit is that how the phenomenon of fatigue limit is characterised . As a first step of approach, the fatigue limit is simulated by adopting an analogue of a fictitious microcrack that nucleates in a slip band within a grain because cyclic slip is essential for fatigue crack nucleation.

8.3.1 Crack Tip Pile-Up Sliding Displacement

This study assumes that a polycrystalline material is originally free of defects that would be otherwise affect the dislocation motion against grain boundaries. Cyclic fatigue loading initially excites sources of glide edge dislocation within a grain. Figure 8-3 shows the distribution of dislocations emitted from a source **S** which is located within a grain. The dislocations then develop across the whole grain without being interfered/hindered until reaching grain boundaries. When the glide dislocation movement spreads to a grain boundary, the grain boundary blocks the motion of the leading dislocation causing difficulty of dislocation transmission and resulting in dislocation pile-up at grain boundary. Since there is no microcrack propagation at the stress level of fatigue limit, the pile-up of dislocation becomes a stressed double pile-up blocked by grain boundaries. In other words, the phenomenon of fatigue limit can be modelled as the stressed double pile-up against grain boundaries. In this process, the grain boundary is taken to be a perfect obstacle and the pile-up is modelled in terms of a continuous distribution of dislocations.

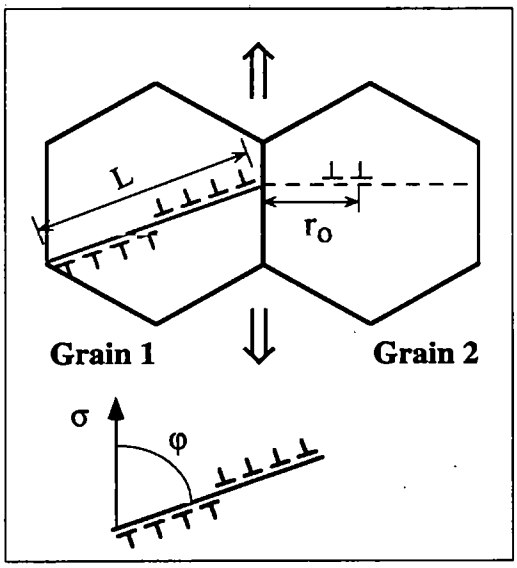

Figure 8-3 Schematic Diagram Of Fictitious Crack Initiation When Dislocations In A Slip Band Of Length L Pile Up Against Grain Boundaries

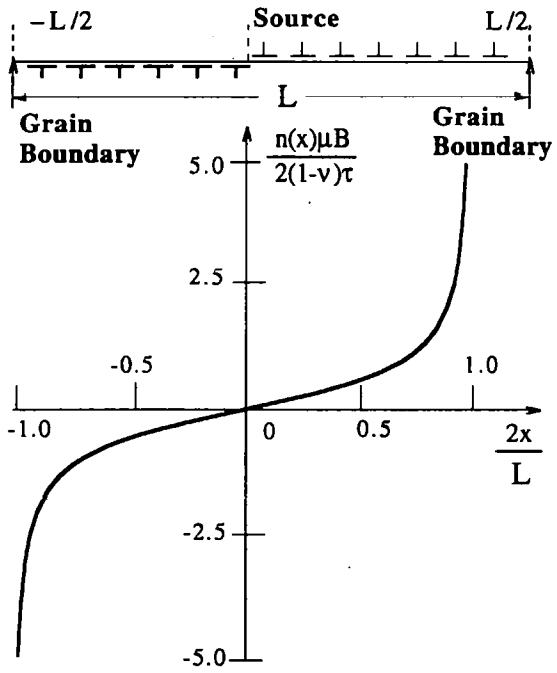

Figure 8-4 Schematic Illustration Of Dislocation Distribution Within A Grain As A Function Of Normalised Distance

The dislocation distribution is characterised [106,108,109] by a continuous density function n(x´) replacing the discrete dislocations. This work adopts the continuous-dislocation method and a shear-crack analogue to deal with the double stressed pile-up (see Figure 8-4). The pile-up is pushed by shear stress τ in forward loading against the grain boundaries. It is assumed that the crack tip configuration initially consists of a single pile-up along a slip plane in equilibrium with applied shear stress. For the individual dislocations in the pile-up to be in equilibrium, the force produced by external stress and that caused by interaction with the other dislocations must balance, *i.e.*, the external shear stress τ equilibrates with the stresses at various positions x along the pile-up due to dislocations at $x'\left(=\frac{2x}{L}\right)$. The x-axis of the pile-up coincides with the slip direction. This equilibrium condition under plane strain condition can be expressed in terms of the continuous distribution function of dislocation n(x´) as [106,108]:

$$\tau \mathbf{B} = \frac{\mu \mathbf{B}^2}{2\lambda} \int_{-L/2}^{L/2} \frac{n(x')dx'}{x' - x} \qquad \left(-\frac{L}{2} < x < \frac{L}{2}\right) \tag{8-3}$$

where $\mu = \frac{E}{2}(1+\upsilon)$;

$\lambda = (1-\upsilon)$ for edge dislocation.

The configuration originally used in deriving this relation is a double pile-up with dislocations locked at $x = -\frac{L}{2}$ and $x = \frac{L}{2}$ and the dislocation source located at $x = 0$. The stressed double pile-up in this case is one that is being pushed at the two grain boundaries, *i.e.*, $[n(-1) = -\infty]$ and $[n(1) = +\infty]$. Thus, the dislocation distribution in the stressed double pile-up of length L is [106,108]:

$$n(x') = \frac{2(1-\upsilon)\tau}{\mu \mathbf{B}} \frac{\frac{2x}{L}}{\left(1 - \left(\frac{2x}{L}\right)^2\right)^{0.5}} \tag{8-4}$$

This distribution function with the pile-up length L predicts accurately how most of the dislocations in the pile-up are arranged [106,108,109]. Thus the total number of edge dislocations in this stressed double pile-up of length L is given by

$$N = \int_{-L/2}^{L/2} n(x')dx = \frac{\lambda \tau L}{\mu \mathbf{B}}. \qquad (8\text{-}5)$$

In the case of screw dislocations, the theory for pile-up of screw dislocations is completely analogous to the above result [137]. Equation 8-3 can be applied to the screw case simply by replacing the factor $1-\upsilon$ with 1. Furthermore, elastic anisotropy can also be included in the analysis directly [137] for both edge pile-up and screw pile-up by using an anisotropic elastic factor Γ instead of μ in Equations 8-3 — 8-5.

When a slip band of length L is formed and the dislocations are piled up against the grain boundaries, the applied shear stress τ is relaxed inside the band by dislocation motion causing a displacement as a result. Therefore, the number of dislocations in the double pile-up multiplied by the Burger's vector **B** at a shear stress τ will be equal to the net displacement along the slip plane, *i.e.*, $\delta = N\mathbf{B}$. It is assumed that after forward loading complete slip irreversibility is maintained during unloading. Hence δ will be the net crack tip displacement corresponding to τ after unloading. This forward shear displacement produced by τ will be maintained as a consequence of purely unloading process and complete slip irreversibility. When the shear stress τ due to external loading lows down to such a level that is equal to a threshold shear stress τ_{FL}, dislocations still form within a grain but they hardly initiate a microcrack in the matrix and they are constrained within the grain without leading dislocations crossing the grain boundary into neighbouring grains. The interpretation is that incipient crack forms when the two leading dislocations in a pile-up are forced to within a distance b of one another [106]. Accordingly, it is assumed that there is no joining up of two leading dislocations in the pile-up at the stress level of fatigue limit.

It has been recognised that the continuum approximation for the pile-up can be equated by analogy to a shear crack [106,108,138]. This assumption enables a first hypothesis to be made in modelling.

Hypothesis I — the surface displacements associated with the pile-up are crack-like.

Accordingly, consider a fictitious shear crack of length L that lies in the surface of an infinite body subjected to a uniform shear stress to replace the stressed double pile-up in the same grain. Both tips of the fictitious crack are located at the grain boundaries. The formation of this shear crack can be envisioned as follows. Make a cut of length L and maintain a shear stress $-\tau$ over the cut surface to balance the external shear stress τ. Next, gradually reduce the internal surface shear stress $-\tau$ to zero, so that the shear crack relaxes to its equilibrium configuration. As a result of such a simulation, the double pile-up of dislocations within a grain at the stress level of fatigue limit is equivalent to a fictitious shear crack at the same stress level, and hence the fatigue limit can be regarded as a stress level that just makes an inception of growth of the fictitious shear microcrack. In parallel to the first hypothesis a second hypothesis can be reasonably made:

Hypothesis II — crack tip displacement controls crack growth in cyclic fatigue.

With this hypothesis it is considered that the blunting/closing mechanism is adequate to characterise propagation of the fictitious crack due to fatigue. Following Equation 8-3 we have a maximum crack tip sliding displacement for cyclic fatigue, $(CTSD)_{max} = \delta_{FL.max}$, due to the dislocations at the applied maximum stress level corresponding to fatigue limit in the pile-up. By defining an angle φ in Figure 8-3 that is an angle between loading direction and the slip plane due to the dislocations, the applied maximum shear stress τ_{max} can be determined in terms of a more useful maximum normal stress σ_{max} using a relation, $\tau_{max} = \frac{\sigma_{max}}{2} \sin[2(\frac{\pi}{2} - \varphi)]$ [110] for the fictitious surface shear microcrack. Hence

$$\delta_{FL.max} = \frac{\lambda \tau_{FL.max} L}{\mu}$$

$$= \frac{(1+\upsilon)\lambda \Delta\sigma_{FL} L}{E} \sin[2(\frac{\pi}{2} - \varphi)] \qquad (8\text{-}6)$$

in which $\delta_{FL.max}$ stands for the maximum crack tip displacement (or the minimum crack tip displacement for propagting a crack) at fatigue limit level to prevent crack propagation. When this fictitious shear crack starts to propagate towards an adjoining grain, the slip

band in the first grain must break the barrier of grain boundary by nucleating new slips in the adjoining grain. This leads to third hypothesis that

Hypothesis III — slips occur in an adjoining grain due to dislocation motion when a dislocation source is created at a distance r_0 away from the fictitious crack tip (or ahaed of the slip band of length L) to enable the transmission of slip across the grain boundary into the adjoining grain.

The third assumption is based on such a fact that if the stress on a dislocation is greater than the lattice friction stress τ, a dislocation will be spontaneously emitted from the crack tip [183]. Obviously, the assumption depicts a critical condition for onset of propagation of the fictitious shear crack. The distance r_0 is numerically assumed to be quarter of the slip band length in the adjoining grain, *i.e.*, $r_0 = \frac{L}{4}$ [130] (see Figure 8-3).

8.3.2 Fatigue Limit

As the fictitious fatigue crack spans the first grain boundary as a result of cyclic fatigue, the crack tip opening displacement (CTOD) of the fictitious crack as a function of stress intensity factor K can be calculated by Rice's approach [111] for plane strain condition. The maximum crack tip opening displacement $\delta_{FL.max}$ at stress level of fatigue limit for the fictitious crack in an infinite body can be determined by

$$\delta_{FL.max} = \frac{0.49\,K_{FL.max}^2}{E\sigma_y'} = \frac{0.49\,\pi\,\sigma_{FL.max}^2 (L+2r_0)}{2E\sigma_y'} \qquad (8\text{-}7)$$

in which $K_{FL.max}$ scales a maximum stress intensity of the fictitious crack at the fatigue limit stress level and σ_y' is the cyclic yield stress of materials. Once the $(CTSD)_{max}$ meets with the $(CTOD)_{max}$, the fictitious crack becomes a real crack. Therefore, by equalising the $(CTSD)_{max}$ to the $(CTOD)_{max}$ in the event of onset of the fictitious crack propagation, the intrinsic maximum stress level σ_{FLmax} at the fatigue limit for polycrystalline materials is obtained as

$$\sigma_{FL.max} = \frac{4(1+\upsilon)\lambda}{1.47\pi} \sin[2(\frac{\pi}{2}-\varphi)]\, \sigma_y' \qquad (8\text{-}8)$$

at any load ratio. As a logical approach we roughly set the angle φ to be 45^o for edge dislocations because the slip plane with an angle of 45^o to loading direction has the maximum shear stress for a given normal stress [110] and hence, the maximum pile-up of dislocations. As a result, the maximum fatigue limit stress level, $\sigma_{FL.max} \approx 0.77\sigma_y'$. A finite element analysis carried by W. J. Baxter and Pei-Chung Wang for high cycle fatigue life of aluminium alloys concluded that, to a first approximation, the fatigue strength σ_f could be a constant fraction of the tensile strength σ_{UTS} which can be expressed as $\sigma_f = 0.26\sigma_{UTS}$ [128]. Practically, their prediction is much useful. Comparisons of Equation 8-8 with their predictions will be carried out for aluminium alloys in future.

At R = 0, $\sigma_{FL.max}$ equals to $\Delta\sigma_{FL}$. Therefore, the cyclic stress range corresponding to fatigue limit can be similarly deduced to be

$$\Delta\sigma_{FL} = \frac{4(1+\upsilon)\lambda}{1.47\pi} \sin[2(\frac{\pi}{2}-\varphi)]\, \sigma_y' \ . \qquad (8\text{-}9)$$

Equations 8-8 and 8-9 show a slip band orientation dependence of the intrinsic fatigue limit. The measured fatigue limit may be lower than this predicted intrinsic fatigue limit in some circumstance due to harmful particles/inclusions contained in the matrix. Present fatigue tests of S—N curve for 7150-T651 aluminium alloy verified that surface harmful particles as well as sub-surface particles often became inevitable sites for small crack initiation which evidently reduced the fatigue lifetime of specimens. These particles may be constituent phases consisted of Al_7Cu_2Fe, Mg_2Si or Al_2CuMg [139] in the 7150-T651 aluminium alloy.

Table 4 lists all predictions of intrinsic fatigue limit of several aluminium alloys. Predictions of fatigue limit based on pure edge dislocation assumption seem more reasonable in comparison with pure screw dislocation assumption. However, the real dislocations would be a mixed type instead of pure one. In addition to that the local

favourable slip band orientation does not always keep 45^{o} in relation to loading direction for all kind of aluminium alloys. These uncertainties should be studied further.

Table 4 Comparison Of Measured And Predicted Fatigue Limit For Aluminium Alloys

Aluminium Alloys	Yield Stress σ_y (MPa)	Load Ratio R	Fatigue Endurance $(\sigma_{FL})_{mea}$ (MPa)		Predicted Fatigue (Screw Type) $(\sigma_{FL})_{pre}$ (MPa)	Endurance (Edge Type) $(\sigma_{FL})_{pre}$ (MPa)
2024	345	0.05	117	[80]	188	126
2024	345	0.5	76	[80]	99	67
7475	449	0.05	115	[80]	245	164
7475	449	0.5	80	[80]	129	86
Wrought MH*	323	0.1	$120^{(1)}$	[78]	167	112
Forged FP*	310	0.1	$120^{(1)}$	[78]	160	108
Squeeze-cast SP*	261	0.1	$100^{(1)}$	[78]	135	91
7075-T6 A	495	0.1	$173^{(2)}$	[124]	256	171
7075-T6 B	522	0.1	$189^{(1,)}$	[124]	270	181
7075-T6 C	527	0.1	$184-194^{(1)}$	[124]	273	183
7075-T6 D	516	0.1	$175^{(2)}$	[124]	267	179
7150-T651	420	0.1	$153^{(3)}$		217	146

(1) 10^7 cycles (2) 10^6 cycles (3) 2.4×10^6 cycles

* 6082 Aluminium Alloy

8.4 FATIGUE CRACK GROWTH THRESHOLD

Regardless of any closure mechanism responsible for the threshold behaviour, two fundamental physical phenomena associated with the fatigue crack growth threshold behaviour can be identified:

- The fatigue crack tip is blunted to a micronotch after emission of dislocations from the tip; and

- There is no longer microcrack propagation at the blunted crack tip, causing crack front advance in further fatigue cycling.

These two basic physical phenomena apply to the micromechanical modelling of fatigue crack growth threshold.

8.4.1 Calculation Of ΔK^*_{th}

In high-R range, any microcrack propagation from the crack front is considered to be the primary factor that leads the crack front to advance. The critical value ΔK^*_{th} plays a key role in threshold fatigue crack propagation dominated by cyclic damage. Since the ΔK^*_{th} scales a damage limit of cyclic fatigue, it must be connected to the fatigue limit and related to local microstructure because crack growth behaviour is sensible to the local microstructure at the fatigue threshold level. The microstructural dimension ρ plays a prominent role in crack growth, connecting the fatigue limit and the fatigue crack growth threshold, which is commonly referred to grain size [195]. This point will be discussed later.

To model the ΔK^*_{th}, let us consider a fatigue crack with a blunted tip. The tip radius can be equated to the dominant microstructural dimension (or dominant grain size) ρ at onset of crack propagation. To prevent microcrack initiation from a grain of size ρ at the crack front, the local stress in the grain (or grains) must be controlled to attain the fatigue limit. For a regular equi-axed grain structure with different angle of orientation between grains, the relation linking the critical threshold value for the fatigue crack with the microstructural dimension can be ideally defined by

$$\Delta K^*_{th} = \Delta\sigma_{FL}\sqrt{\frac{\pi\rho}{2}} \tag{8-10}$$

where $\Delta\sigma_{FL}$ is the stress range at the intrinsic fatigue limit evaluated by Equation 8-9 which is an orientation-related term. For real polycrystalline materials, it is difficult to estimate grain size distribution in the path of crack propagation and the orientation of the grains affected by crack growth process varies in addition to the variation of gain size. However,

since the local orientation effect on intrinsic fatigue limit $\Delta\sigma_{FL}$ have been incorporated into Equation 8-9, Equation 8-10 would predict the microstructure dependence of the critical threshold value ΔK^*_{th} .

8.4.2 Calculation Of K^*_{max} And R^*

In low-R range, any crack front advance is considered to be the result of the material bonds breaking at the crack front. The critical value K^*_{max} sets up a limit that determines whether or not the fatigue crack front advances due to breaking up of bonds at the crack front. Since the maximum loading controls breaking up of bonds, the local stress and strain at the crack front are involved.

Consider the blunted fatigue crack with tip radius ρ again which is subjected to tension stress. To prevent breaking up of bonds at the crack front, the local maximum stress acting on the crack front due to notch effect must be controlled to attain the fatigue limit. The elastic stress distributions ahead of this notch-like crack front were given in [151] for tension mode. Of particular interest is the relevant stress distributions to be included when determining the local stresses at the crack tip. The relevant elastic stress distributions ahead of this notch-like (blunt) fatigue crack tip is formulated by following expression

$$\sigma_{yy} = \frac{K_I}{(2\pi r)^{1/2}} \cos\frac{\theta}{2}\left(1+\sin\frac{\theta}{2}\sin\frac{3\theta}{2}\right)+\frac{K_I}{(2\pi r)^{1/2}}\frac{\rho}{2r}\cos\frac{3\theta}{2} \quad . \tag{8-11}$$

Due to the localisation effect, the stress concentration at the crack tip may result in a relevant large plastic zone appearing ahead of the crack tip no matter where the crack tip is located in a grain or at a grain boundary. It is considered that the inelastic strain amplitude in the plastic zone around the crack tip controls threshold fatigue crack propagation.

By adopting Neuber's rule [152], the local inelastic near-tip stress/strain distribution for mode I crack was derived [134]. Four elementary blocks of linear dimension ρ as shown in Figure 8-5 were used to analyse local stress/strain distribution ahead of the fatigue crack tip. The local stress σ and inelastic strain ε at the fatigue crack tip can be approximated to

be equal to the averages in the first elementary block which are determined in terms of stress intensity K for the notch-like fatigue crack by using cyclic fatigue properties of materials [134].

$$\sigma = \sigma_1 = (2K')^{\frac{1}{1+n'}} \left(\frac{x_1^2(1+n')}{8\pi E}\right)^{\frac{n'}{1+n'}} \left(\frac{K^2}{\rho}\right)^{\frac{n'}{1+n'}} \tag{8-12a}$$

$$\varepsilon = \varepsilon_1 = 2\left(\frac{x_1^2(1+n')}{16\pi EK'}\right)^{\frac{1}{1+n'}} \left(\frac{K^2}{\rho}\right)^{\frac{1}{1+n'}} \tag{8-12b}$$

In Equation 8-12, x_1 =1.633 [134] for tension mode and ρ stands for radius of notch-like crack tip which can be equated to the microstructural dimension.

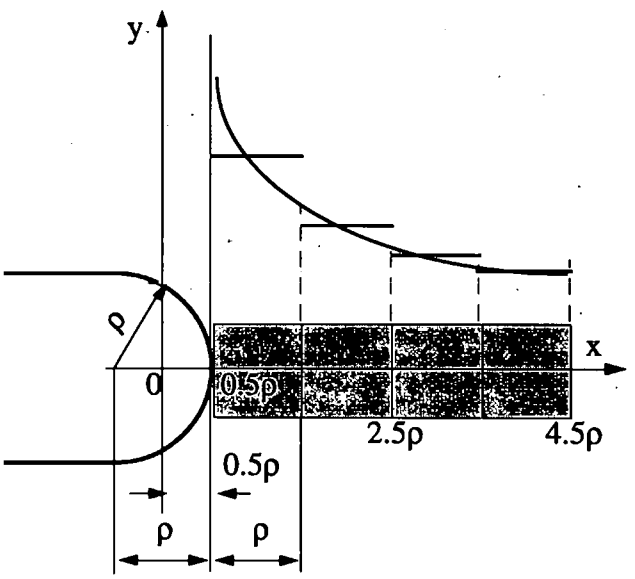

Figure 8-5 Illustration Of Four Elementary Blocks Ahead Of A Blunt Fatigue Crack Front

As the fatigue crack starts growing, the crack must grow at the expense of the strain energy stored in local regions around the crack tip during the fatigue process since energy conservation can not be violated. The driving force for the growth of the fatigue cracks comes from both external loading and elastic energy released from local regions near the crack front. Actually, the local cyclic strain energy density dissipated by the material within

the first elementary block can be approximately evaluated for near threshold crack growth by a product of $\frac{1}{2}(\sigma_1 \varepsilon_1)$. As long as the local stress in front of the fatigue crack front holds the fatigue limitstress level, it is hence ensured attainment of the critical maximum stress intensity K^*_{max}. With this definition coupled with Equation 8-12, the local cyclic strain energy density dissipated by the crack tip material reaches the following equality at the threshold level

$$\frac{1}{2}\sigma_{FL.max}\,\varepsilon_{FL.max} = \frac{1}{2}\left(\frac{x_1^2(1+n')}{4\pi E}\right)\frac{\left(K^*_{max}\right)^2}{\rho} \quad . \tag{8-13}$$

Therefore, using Equations 8-12 and 8-13, a tailored expression for the critical maximum stress intensity K^*_{max} at threshold level can be analytically derived to be

$$K^*_{max} = \frac{2}{x_1}\sigma_{FL.max}\sqrt{\frac{\pi\rho}{1+n'}} \quad . \tag{8-14}$$

In which $\sigma_{FL.max}$ is determined by Equation 8-8 which is also an orientation-related term. This analytical expression indicates that local crystallographic orientation of slip bands and local microstructural dimension primarily determine fatigue crack growth threshold behaviour. With the determination of ΔK^*_{th} and K^*_{max}, the defined R^* to demarcate the low-R region from the high-R region will be only related to material properties and can be expressed to be

$$\begin{aligned} R^* &= 1 - \frac{\Delta K^*_{th}}{K^*_{max}} \\ &= 1 - \frac{x_1}{2}\sqrt{\frac{1+n'}{2}} \end{aligned} \tag{8-15}$$

which is a material-related parameter dependent on cyclic deformation behaviour.

8.5 THRESHOLDS FOR ALUMINIUM ALLOYS

As mentioned already, the near-threshold fatigue crack growth is strongly affected by local microstructures. Referring either the microstructural dimension at the fatigue threshold level to average grain size is a widely adopted way to account for the microstructure influence of materials on the fatigue crack growth threshold. In other words, let ρ in Equations 8-10 and 8-14 be equivalent to grain size D. An implied background for this simulation is supported by such a consideration in principle that a fatigue crack is impeded at a grain boundary without propagating further due to lower stress level at threshold. This simulation may be substantially effective for fine and intermediate grain sizes.

Nevertheless, for those aluminium alloys with large grains, the same simulation, phenomenally, is unsuccessful in predicting fatigue crack growth threshold behaviour because the real plastic zone ahead of the crack tip may be intrinsically small at threshold level if compared to grain size. Empirically, the distance Z, proposed by W. J. Pardee, *et al* [140], from the crack tip to next grain boundary in the case of a large grain size may take over the controlling role as shown in Figure 8-6. This controlling length was numerically assumed to take half or quarter of the size of large grains in Ravichandran's simulation [130]. It is suggested in this work that the grain size in the transverse direction may be adequate to represent the effective microstructural dimension for aluminium alloys.

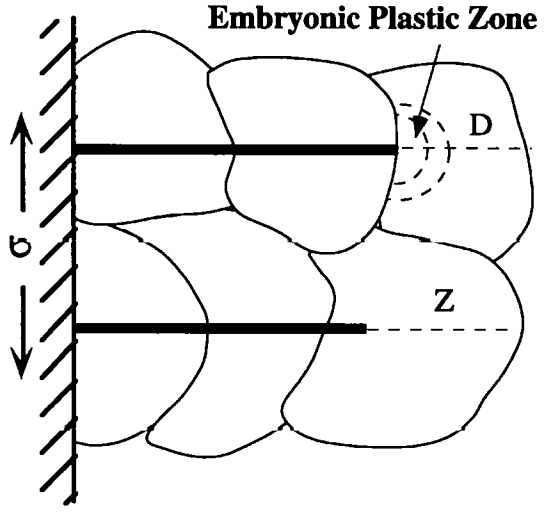

Figure 8-6 Illustration Of Geometrical Parameters Z Controlling Fatigue Crack Closure [140]

Investigations of aluminium alloy strength in relation to grain size in transverse direction have been made which covers a wide range of 2×××, 5×××, 6×××, and 7××× series aluminium alloys, showing a general trend of grain size dependence of alloy yield strength as exhibited in Figure 7-6. A best curve fit shows that for both the 2××× series aluminium alloys and the 7××× series aluminium alloys,

$$\sigma_y = \sigma_0 + \kappa D^{-0.5} \tag{8-16}$$

in which σ_0 and κ are constants. This numerical correlation linking grain size with alloy yield strength determines the microstructural dimension ρ. In this respect the grain size is directly associated with yield strength σ_y. A more detailed correlation of yield strength with grain size can be achieved for 2××× and 7××× series aluminium alloys.

8.5.1 Model Prediction Of Fatigue Crack Growth Thresholds

Experimentally measured data of fatigue crack growth threshold ΔK_{th} [105,122,124,153-164] are plotted in Figure 8-7 for 2××× series and 7××× series aluminium alloys, which generally shows a linear dependence of ΔK_{th} upon load ratio R even though scatter is

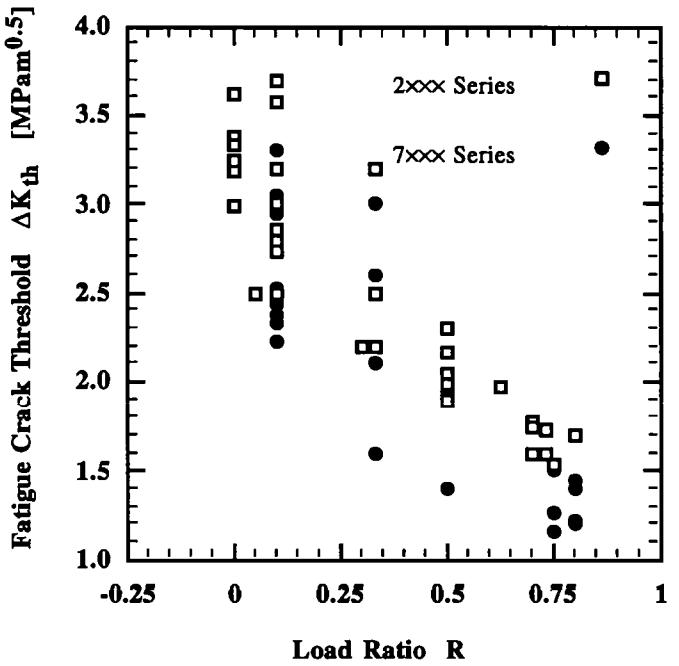

Figure 8-7 Load Ratio Dependence Of Experimentally Measured Fatigue Crack Growth Thresholds [105,122,124,153-164]

evident at low load ratios. To test the micromechanical model, 2××× and 7××× series aluminium alloys are chosen for verifying the model predictions. For both alloys the defined R^* has an approximate value 0.6. It is noted that the defined R^* is only related to material cyclic fatigue behaviour.

Micromechanical model predictions against experimentally measured fatigue crack growth thresholds, using Equations 8-10 and 8-14, are illustrated in Figure 8-9 and Figure 8-9. Figure 8-8(a) demonstrates the constancy of $\Delta K_{th}/(1-R)$ and its equality with K^*_{max} at $R < R^*$, whereas Figure 8-8(b) demonstrates the constancy of K^{max}_{th} and its equality with $\Delta K^*_{th}/(1-R)$ at $R > R^*$. Obviously, the constancy together with the appropriate equality exists at $R < R^*$ if Equation 8-1 is applied and at $R > R^*$ if Equation 8-2 is applied. In essence, Figure 8-8 proves the two fatigue threshold criteria and their valid use. However, it should be noted that only at R = 0 the two fatigue threshold parameters, ΔK^*_{th} and K^*_{max}, depend on a single parameter, *i.e.*, the fatigue limit.

Figure 8-9 shows good correlation of predicted ΔK_{th} with experimentally determined ones for both 2××× series and 7××× series aluminium alloys. In all above model predictions, the grain sizes in transverse direction are assigned to the microstructural dimension ρ which can be determined using material yield strength by means of Equation 8-16. A 45^o angle is assumed to count in the orientation effect between grains which is obviously an ideal assumption for both series aluminium alloys. With the assumption of same orientation of grains, the maximum relevant error caused by the assumption is about 28% and the relevant error is bigger in the low-R range than that in the high-R range.

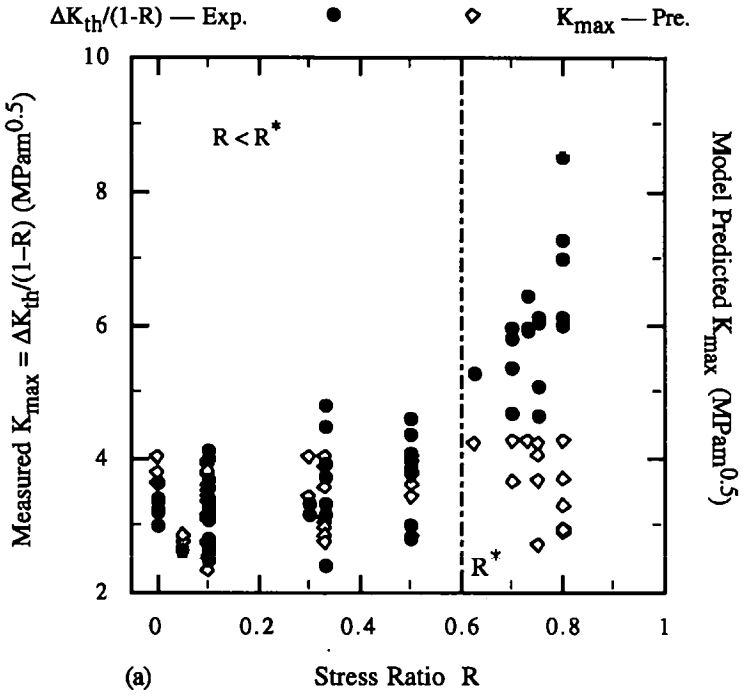

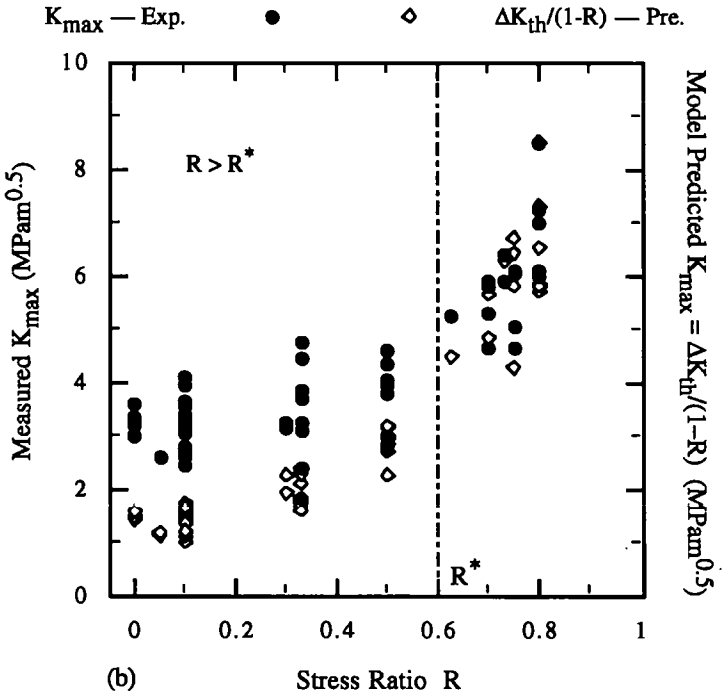

Figure 8-8 Illustrations Of Constancy Of Proposed Models And Their Equality With Experimental Results For (a) $R < R^*$ and (b) $R > R^*$

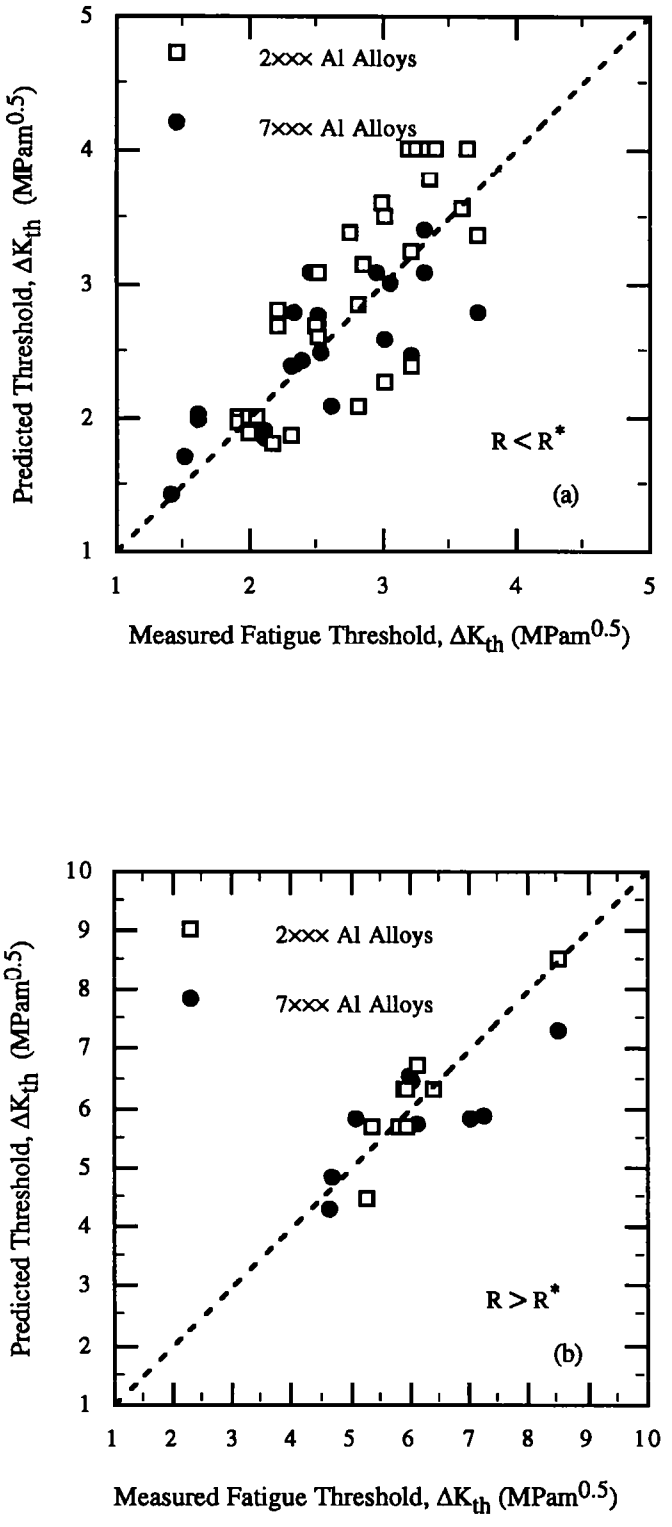

Figure 8-9 Predictions Of Fatigue Crack Growth Thresholds At (a) $R < R^*$ And (b) $R > R^*$ Ranges For 2××× — 7××× Series Aluminium Alloys

8.5.2 Fundamental Fatigue Crack Growth Threshold Curves

Fundamental fatigue crack growth threshold curves are theoretically predicted using Equations 8-1 and 8-2 for 7075-T6 aluminium alloy having grain sizes of 20 micron and 40 micron respectively. The first step is prediction of fatigue crack growth thresholds ΔK_{th} by using Equation 8-1 when the load ratio R is less than R^*. The maximum stress intensity K_{th}^{max} corresponding to this predicted ΔK_{th} simply equals $\frac{\Delta K_{th}}{1-R}$. The second step is to predict the maximum stress intensity K_{th}^{max} by means of Equation 8-2 when load ratio R is greater than R^*. The fatigue crack growth threshold ΔK_{th} corresponding to that predicted maximum stress intensity K_{th}^{max} can be simply determined by $K_{th}^{max}(1-R)$. Using these two sets of predictions at load ratio ranging from 0 to 0.98, the fundamental fatigue crack growth threshold curves are quantitatively established for the aluminium alloy of given grain size, as shown in Figure 8-10. These fundamental fatigue crack growth threshold curves circumvent the stress effect on fatigue crack growth threshold without invoking the crack closure. As a result, each curve demarcates the non-crack growth region from crack

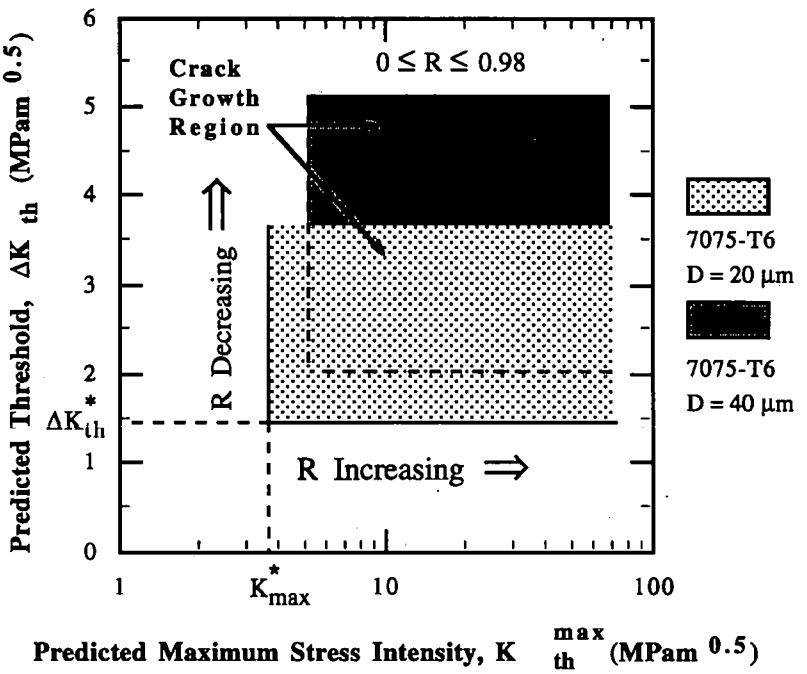

Figure 8-10 Quantitative Predictions Of Fundamental Fatigue Crack Growth Threshold Curves In Terms Of ΔK_{th} *vs.* K_{max} For 7075-T6 Aluminium Alloy

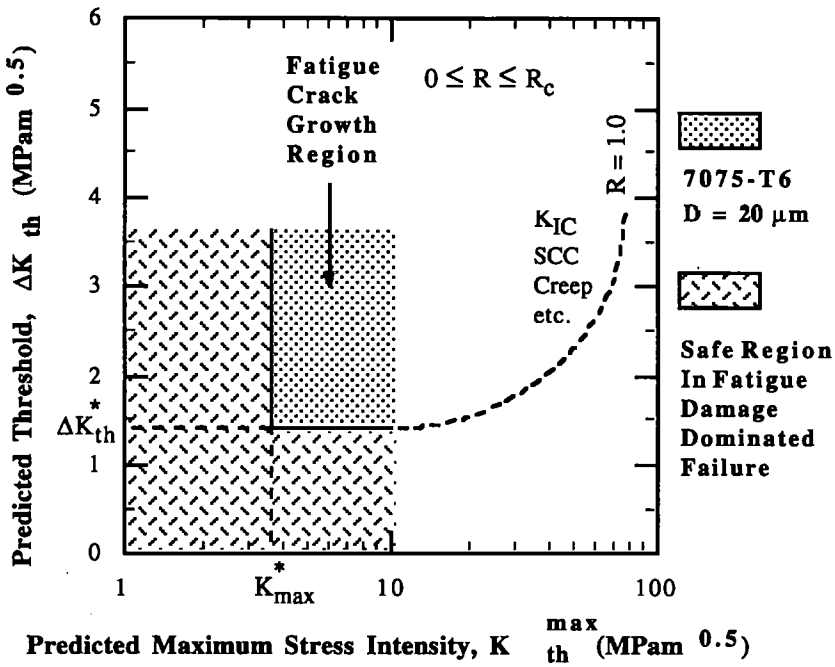

Figure 8-11 Illustration Of Demarcating Safety Zone In Fatigue Dominated Failure From Crack Growth Zones

growth region which lays a basis for risk assessment in structure integrity research.

In real cases, however, other alternative damage processes may supersede fatigue damage process as the load ratio R approaches unity. Physically, a critical load ratio R_c must exist beyond which fatigue damage takes much less effect on failure while other damage mechanisms, such as tensile overload fracture, sustained stress cracking, stress corrosion crack growth or creep crack growth, *etc.*, may dominate the failure. Figure 8-11 shows both non fatigue crack growth region and fatigue crack growth region demarcated by the two fatigue threshold criteria. The uncertainty of thresholds in the range of load ratio $R_c < R \leq 1$ is also schematically illustrated. For 7075-T6 aluminium alloy, no experimentally measured fatigue crack growth thresholds are available at load ratio greater than 0.8 that can be found in open literature. Of course, relevant fundamental fatigue crack growth threshold curves can be similarly predicted for other aluminium alloys.

8.5 DISCUSSION

As demonstrated by analyses, there are two features associated with the modelling of fatigue crack growth threshold. Firstly, in a local region where the crack tip is situated, the local slip band orientation coupled with the local microstructure dimension determines threshold fatigue crack propagation. Secondly, the fatigue crack growth threshold is related to the cyclic strain hardening exponent n'. As n' varies from unity to zero, aluminium alloys exhibit a change from perfect plasticity to perfect elasticity. Any change of cyclic fatigue behaviour of materials will reflected by the cyclic strain hardening exponent n'. However, it is difficult to discriminate the real effect of the cyclic strain hardening exponent n' on fatigue crack growth threshold behaviour because the cyclic strain hardening exponent n' is intrinsically affected by microstructure [165-169].

Certainly, heat treatment conditions (under aged, over aged, peak aged) for those aluminium alloys has dramatic influence on the fatigue crack growth threshold behaviour which results in different threshold values for same kind of aluminium alloy. This effect should be taken account in model predictions. Since the model predictions entail material properties and are dependent upon local microstructure, such as cyclic yield strength σ_y', cyclic strain hardening exponent n' and grain size D, the effect of different aging conditions will be reflected by way of these material bulk properties because different aging may change these material properties. This is a pronounced feature of present micromechanical modelling that incarnates the basic idea of using simple conventional material properties to predict fatigue crack growth thresholds.

Scatter in measured fatigue crack growth threshold values can be primarily attributed to either technique dependence in experiment or microstructure dependence. The most common technique used to experimentally determine the ΔK_{th} in laboratory can be classified into three sorts: 1) the load-shedding technique, 2) the use of precracks produced in compression and 3) the decrease of ΔK at constant K_{max}. A recent experimental investigation of fatigue crack growth threshold of 7020-T5 aluminium alloy [164] testified that using different test procedure led to different ΔK_{th} values even at the same load ratio. The second reason for the scatter is the microstructure as a result of different aging

conditions [105,122,155,156,158,161] which influences the fatigue crack growth threshold. However, in some cases the threshold behaviour corresponding to under aged condition and over aged condition may be identical [170] for given dispersoid content. In spite of observed scatters the model should still properly predict fatigue crack growth thresholds for aluminium alloys because the model entails the cyclic fatigue property n' to account for the difference in material condition and the basis of predictions is laid on the two fundamental physical phenomena rather than crack closure arguments.

It should be noted that this methodology of modelling fatigue crack growth threshold is only applicable to fatigue crack propagation in planar slip mode. In this mode, K^*_{max} increases proportionally with the microstructural dimension ρ (or the grain size) at low stress ratio ($R < R^*$) whereas K^*_{max} increases proportionally with ρ (or the grain size) at high stress ratio ($R > R^*$). However, the maximum stress intensity factor K_{max} dominates fatigue behaviour is only at low R ratios. In addition, the modelled parameter K^*_{max} is more sensitive to microstructure, comparing to the parameter ΔK^*_{th}, because K^*_{max} is affected by cyclic hardening/softening behaviour of polycrystalline materials. The cyclic hardening/softening behaviour is more evident for polycrystalline materials at low R ratios.

Finally, it is stressed here that the present work does not attempt to disprove existence or relevance of fatigue crack closure but only to predict fatigue crack growth thresholds using the two novel threshold criteria without arguing what mechanism is responsible for observed crack closure associated with fatigue threshold behaviour. The developed model relies on two primal physical facts that (1) grain boundaries block dislocation motion in polycrystalline materials, causing pile up of dislocations instead of the dislocations cross through grain boundaries; and (2) no matter whatever mechanism causes crack closure, the fatigue crack tip is blunted in near threshold regime without advancing. Foremost is that the fatigue threshold is determined by the two threshold parameters, i.e., K^*_{max} and ΔK^*_{th}. These two parameters have little to do with crack closure. If the extrinsic crack closure exists and is significant, then it will be a third parameter [217].

It is particularly the qualitative aspect of the modelling that is of engineering significance because fatigue crack growth thresholds can be predicted using simple conventional material properties. In all model predictions of fatigue crack growth thresholds, the local slip band orientation is primarily concerned. A recent publication [97] tried to quantify crystallographic misorientation between neighbouring grains. However, there seems no straightforward method to analytically determine the local crystallographic orientation of slip band between grains for threshold fatigue crack propagation in polycrystalline materials. A probabilistic approach to simulate the local crystallographic orientation may be useful which should be studied further.

8.6 SUMMARY OF THE CHAPTER

- The fatigue limit is modelled as a stressed double pile-up of dislocations against grain boundaries. A fictitious crack analogue is adopted to represent the dislocation pile-up. Onset of incipient growth of the fictitious crack determines the fatigue limit. The maximum stress level at the fatigue limit can be estimated as $\sigma_{FL.max} \approx 0.77\sigma_y$ at any load ratio.

- Two fatigue threshold parameters (ΔK^*_{th} and K^*_{max}) are attainable at load ratio R = 0 as applied load approaches the fatigue limit. The local microstructure and cyclic fatigue property determine the two fatigue threshold criteria.

- Load ratio dependence of measured fatigue crack growth thresholds can be quantitatively predicted in terms of the two fatigue threshold criteria without invoking crack closure. The demarcation between low-R range and high-R range is coherently related to cyclic fatigue properties of materials.

- The developed model takes account of ageing conditions by using material cyclic fatigue properties that are associated with ageing conditions. All model predictions

are reasonably consistent with measured fatigue crack growth thresholds for a range of aluminium alloys.

- A safety zone in fatigue has been quantitatively built up using the two fatigue threshold criteria for aluminium alloys. Using conventional material properties to predict the safety zone is a prominent feature of the developed model.

For systematic modelling of small fatigue crack growth and predictions of fatigue lifetime, it is necessary to explore a upper limit for small crack growth beyond which the small crack propagation converts to long crack propagation and fast crack growth occurs. Chapter 9 details such a determination of the upper limit.

Chapter 9 CONVERGENCE OF SMALL CRACK GROWTH INTO LONG CRACK GROWTH

Small crack growth is very important in fatigue life predictions of polycrystalline material components because long fatigue cracks can spread only in a domain above a certain threshold stress intensity factor range ΔK_{th}, but small fatigue cracks can propagate even below this ΔK_{th} value. Therefore, convergence of growth rate of small fatigue cracks into that of long fatigue cracks is receiving increasing attention since catastrophic fatigue failure may occur after that convergence. Along with the convergence, a smallest crack size at which long fatigue crack growth begins is of technical significance in engineering applications.

Although materials science perspective of metal fatigue resistance has been discussed recently [171,182] in almost every aspect, a few models have been proposed to simulate conversion of small fatigue cracks into long fatigue cracks. A. Navarro and E. R. de los Rios [54,172] proposed a dislocation-based model to predict conversion of small fatigue cracks into long fatigue cracks. They concluded that the conversion happens when the crack tip plastic zone size exceeds the grain diameter. X. Xin, *et al* [173] also considered the effect of strain hardening at small crack front. Chapter 9 establishes quantitative convergence conditions for simulating the small crack to the long crack transition.

9.1 PHYSICAL MODEL AND MATHEMATICAL DESCRIPTION

J. Lankford initially investigated small fatigue crack propagation in 7075-T6 aluminium alloy and generally concluded that "the merge of growth rates of small and long fatigue cracks coincided with the state where the plastic zone size is equal to the relevant microstructural dimension" [5,6]. In other words, when the plastic zone achieves the size of dominant microstructural dimension, the transition from microstructure sensitive to microstructure insensitive of small crack propagation takes place [54]. This explains why small fatigue cracks in some fine-grained microstructures do not exhibit fast growth rates compared with long fatigue cracks. J. Lankford's qualitative criteria has been confirmed by later experiments for the same aluminium alloy.

However, J. Lankford did not specify the relevant microstructural dimension to be any grain size. It seems inconvenient in engineering applications to simulate the convergence of small fatigue crack growth with long fatigue crack growth by measuring or calculating plastic zone size. The plastic zone size is closely related to a maximum crack size to which the small crack growth law is applicable. However, the maximum crack size depends on the specimen size, the applied load level and the microstructure of material [174]. Another reason for the inconvenience is the stochastic nature of all microstructural parameters that affect propagation of the small fatigue cracks, such as crystallographic misorientation of slip planes between adjacent grains, the grain or inclusion size and their spacing [7].

To model Lankford's criteria, an equivalent plastic zone is assumed at the fatigue crack front. Figure 9-1 illustrates a growing small fatigue crack, one of whose tips is located within a grain. Slip bands of length L are emitted from the crack tip due to dislocation motion. Since the plastic zone may be truncated [67] when the small fatigue crack meets a barrier, such as grain boundaries or particles, plastic zone shape alters and plastic zone size varies. It is virtually impossible to judge when and in which direction the plastic zone size achieves the relevant microstructural dimension for the growing small fatigue crack. Therefore, it is proposed that

- The Lankford's criteria can be simulated when the area of the plastic zone ahead of a small crack front coincides with an equivalent circle area which diameter takes the length L of slip bands.
- The length of slip bands is just a half size of controlling microstructural dimension ρ^* by reason that the surface small fatigue crack is embedded in a plastically deformed region.

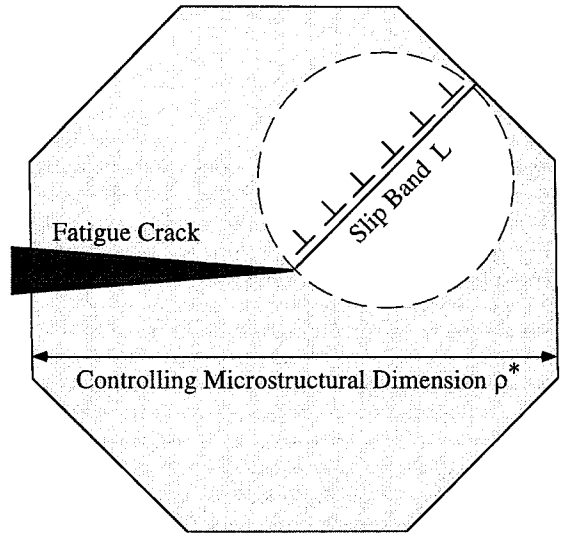

Figure 9-1 Illustration Of Concepts Of Controlling Microstructural Dimension And Equivalent Area As The Conversion Of Small Fatigue Cracks Into Long Fatigue Cracks Occurs

Since the small fatigue crack is still small before it becomes a long fatigue crack, plane strain condition can be assumed to determine the plastic zone size by using Von Mises criterion. Surface effect, analysed in [18], on small fatigue crack growth due to strain localisation or redistribution can be neglected because the small fatigue crack is heading for a long fatigue crack after convergence. The plastic zone size can be calculated [175] by

$$R_p = \frac{[K_{max}]_{con}^2}{4\pi(\sigma_y')^2}\left(\frac{3}{2}\sin^2\beta + (1-2\upsilon)^2[1+\cos\beta]\right). \qquad (9\text{-}1)$$

According to the proposed physical model, on the other hand, the plastic zone area coincides with the equivalent circle area in the form of

$$A_p = \frac{1}{2}\int_0^{2\pi} R_p^2 \, d\beta$$

$$= \frac{1}{2}\left(\frac{[K_{max}]_{con}^2}{4\pi(\sigma_y')^2}\right)^2 \int_0^{2\pi} \left(\frac{3}{2}\sin^2\beta + (1-2\upsilon)^2[1+\cos\beta]\right)^2 d\beta \quad . \tag{9-2}$$

In this case $\int_0^{2\pi} \sin\beta \, d\beta = \int_0^z \frac{\left(z - \frac{1}{z}\right)}{2i} \frac{dz}{i\,z}$

$$\int_0^{2\pi} \cos\beta \, d\beta = \int_0^z \frac{\left(z + \frac{1}{z}\right)}{2i} \frac{dz}{i\,z} .$$

Using the residual theorem, if z_o is the mth order of $f(z_o)$ then the residual $R(z_o)$ is

$$R(z_o) = \frac{1}{(m-1)!} \lim \frac{dm}{dz^m}[(z \cdot z_o)^m f(z)] \tag{9-3}$$

and $\oint_{c-} f(z)dz = 2\pi i \, R(z_o)$,

therefore the area of the plastic zone, A_p, can be directly related to the maximum stress intensity factor and cyclic yield strength σ_y' in the form of

$$A_p = 0.0206\left(\frac{[K_{max}]_{con}}{\sigma_y'}\right)^4 . \tag{9-4}$$

According to the proposed physical model, on the other hand, the plastic zone area coincides with the equivalent circle area, leading to

$$A_p = \frac{\pi}{4}L^2 = \frac{\pi}{4}\left(\frac{\rho^*}{2}\right)^2 . \tag{9-5}$$

Consequently, the stress intensity factor range ΔK_{con} at the conversion of growth rate from small to long crack can be formulated in terms of cyclic yield strength, controlling microstructural dimension and load ratio R as

$$\Delta K_{con} = [K_{max}]_{con} - [K_{min}]_{con} = (1-R)\,[K_{max}]_{con}$$

$$= 0.9913\,(1-R)\,\sigma_y'\sqrt{\pi\rho^*} \qquad (9\text{-}6)$$

Equation 9-6 indicates that the conversion of growth rate of small fatigue crack into that of long fatigue crack is associated with material cyclic properties and the controlling microstructural dimension and the convergence condition is determined by the stress intensity factor range rather than small crack size for a given polycrystalline material.

9.2 DETERMINATION OF CONVERGENCE CONDITIONS

It is recognised that the convergence of small and long small fatigue crack growth rates corresponds to plastic zone size being approximately equal to the relevant microstructural dimension. Under such understanding, the parameter ρ^* in Equation 9-6 will be the controlling microstructural dimension. A recent instance [195] to approach that used a maximum grain size as the controlling microstructural dimension for a C-Mn steel. Unfortunately, no one specifically mentions how to quantify the microstructural controlling dimension in the case that growth rate of small fatigue cracks just merges with that of long fatigue cracks. As a matter of fact, it is difficult to know the local grain size in front of a growing small fatigue crack for polycrystalline materials. The convergence of growth rates may occur when a small fatigue crack just passes through either a large grain or a small grain. This realistic phenomenon indicates that the controlling microstructural dimension other than a specified grain size determines onset of convergence.

Additionally, observed fast growth or slow growth of small fatigue cracks in aluminium alloys is less dependent upon grain size but strongly related to a combinative effect of local

microstructure features, such as grain orientation, grain boundary structure, and load levels. Slow small crack growth in large grain structure and fast small crack growth in small grain structure were reported for the same kind of aluminium alloys [5,8]. In Chapter 6, a microstructurally-affected-zone has been defined that takes into account the combined effect of local microstructure and load level, to represent the controlling microstructural dimension of polycrystalline materials. In Chapter 7, the microstructurally-affected-zone size ρ^* has been quantitatively determined in terms of Stage I to Stage II crack growth transition condition. The microstructurally-affected-zone size ρ^* varies with different load levels and local microstructure features (Equation 7-10) instead of grain size. This reflects the kinetic nature of small fatigue crack growth.

The underlying research work suggests that the microstructurally-affected-zone size ρ^* can be taken as the microstructural controlling dimension to determine the convergence condition.

Apparently, the convergence condition is strongly affected by the cyclic yield strength and the controlling microstructural dimension. As a result, stress intensity factor range ΔK_{con} at convergence is not a constant but a variable since the controlling microstructural dimension, equated to the microstructurally-affected-zone size defined in Chapter 7, is a load level-related parameter.

Interestingly, the grain size of polycrystalline materials is chosen in Chapter 8 as the controlling microstructural dimension to determine the fatigue crack growth threshold ΔK_{th} while the microstructurally-affected-zone size ρ^* is used in this chapter as the same role to determine the convergence condition ΔK_{con}. This distinction between the two microstructural parameters reflects two notable facts, *i.e.*,

(1) The fatigue crack growth threshold ΔK_{th} is physically associated with a non-propagating microcrack, however

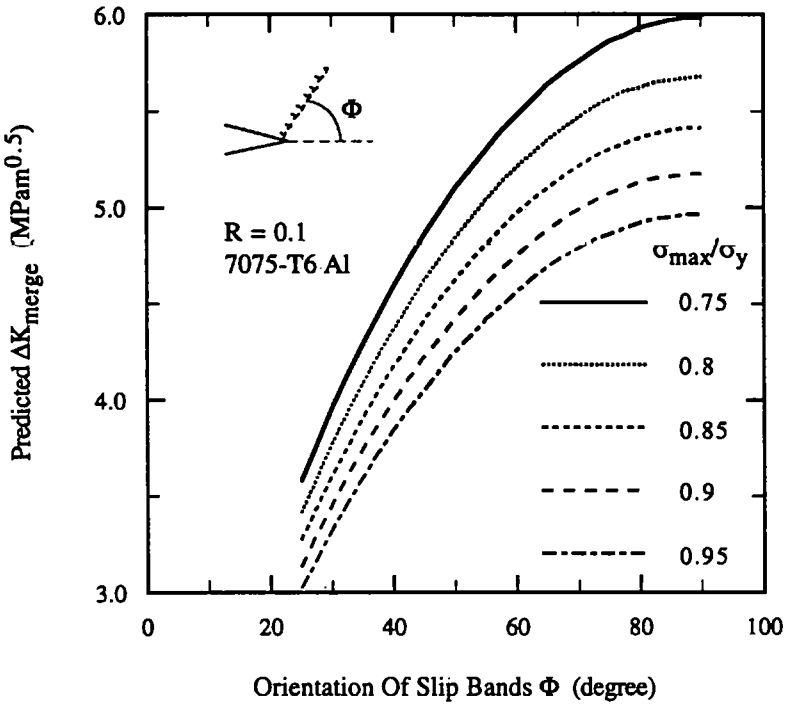

Figure 9-2 Evolution Of ΔK_{con} With Slip Band Orientation And Load Levels

(2) The convergence condition ΔK_{con} is associated with a propagating crack. The later is a kinetic process relating to applied load levels.

These are two reasons why the distinction should be taken into account. Figure 9-2 illustrates evolution of ΔK_{con} with slip band orientation and load levels. Clearly, a higher value of ΔK_{con} is the result of a lower load level or a strong misorientation between two neighbouring grains.

For most types of small fatigue cracks, stress intensity factor can be approximately simplified as $K = Y\sigma\sqrt{a}$ in which Y is a crack shape factor that can be taken as a constant in most cases. Therefore, the fatigue crack size $2a_{con}$ at convergence point of small crack growth rates with long crack growth rates can be estimated by

$$2a_{con} = \frac{1.9654\pi}{Y^2}\left(\frac{\sigma_{max}}{\sigma_y}\right)^{-2}\rho^* \quad . \tag{9-8}$$

Basically, the surface crack size at the convergence from small fatigue crack growth into long fatigue crack growth also depends upon applied load ratios and the microstructural

controlling dimension ρ^*. The surface crack size at the instant of convergence linearly increases with the microstructural controlling dimension. This conclusion is similar to K. Hussain and E. R. de los Rios's result [172]. A difference is that, $2a_{con}$ is linearly proportional to specified grain size in their model.

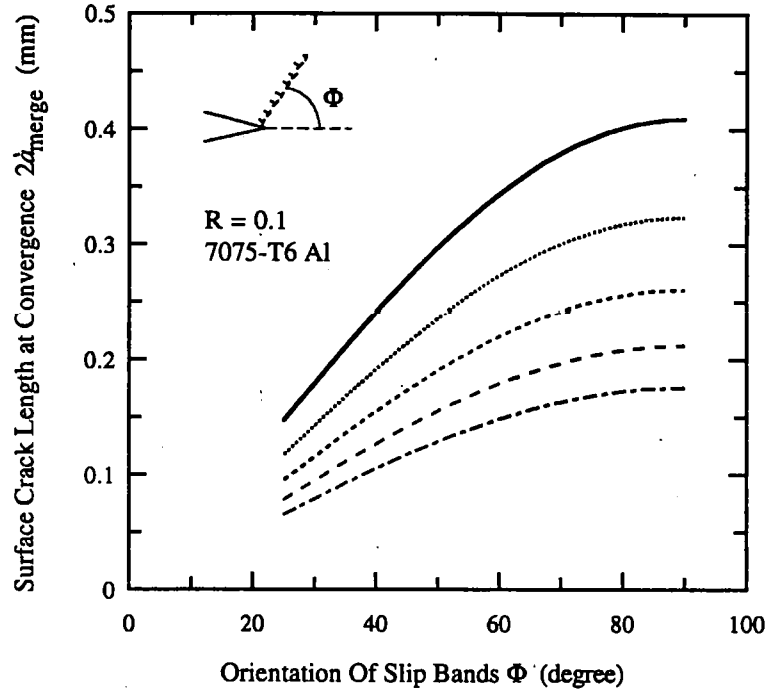

Figure 9-3 Evolution Of $2a_{con}$ With Slip Band Orientation And Load Levels

Figure 9-3 shows predicted surface crack size $2a_{con}$ in relation to load level and orientation of slip bands. Apparently, a lower load level or a strong mismatch between grains may result in a delayed convergence. A pronounced feature of present modelling of convergence is that the convergence condition (either ΔK_{con} or $2a_{con}$) is not a material-related constant but related to local microstructure and load level.

9.3 PREDICTION OF CONVERGENCE

The 7×××× aluminium alloys are chosen for making comparisons of predicted convergence with experimental observed convergence. Small fatigue crack tests were carried out in

The 7×××× aluminium alloys are chosen for making comparisons of predicted convergence with experimental observed convergence. Small fatigue crack tests were carried out in laboratory as described in Chapter 4 and Chapter 5. For the 7150-T651 aluminium alloy, growth rate of small cracks merges with that of long cracks at about $\Delta K_{con} = 4 - 4.5$ MPa$\sqrt{m}$ for all load levels tested. The 7475-T6 aluminium alloy has fine grain structure. The tested ΔK_{con} value at all load levels is ranging from 3.5 – 4 MPa$\sqrt{m}$. In addition, the limited data on plastic zone sizes measured in the 7075T6 aluminium alloy indicated that the plastic zone sizes merged with that of long cracks at about $\Delta K_{con} = 4 - 5$ MPa$\sqrt{m}$ [78].

Table 5 Comparison Of Predicted ΔK_{con} (MPa$\sqrt{m}$) And $2a_{con}$ (μm) With Experimental Measurements

Alloys		CMD^{+} ρ^{*} (μm)	Measured ΔK_{con}	Predicted ΔK_{con}	Observed $2a_{con}$	Predicted $2a_{con}$
7150-T651		42	3.81$^{(1)}$	4.3	118	151
7475-T6		24	3.50$^{(1)}$	3.63	168	171
7075-T6A [78]		37	4.50$^{(2)}$	5.00	224	276
7075-T6B [78]		36	4.48$^{(3)}$	4.96	180	220
7075-T6C [78]		37	4.48$^{(2)}$	5.08	180	230
7075-T6D [78]		35	4.48$^{(2)}$	4.89	180	214

$^{+}$ Controlling Microstructural Dimension;
$^{(1)}$ Stress amplitude σ_a = 210 MPa, R = 0.1;
$^{(2)}$ Stress amplitude σ_a = 180 MPa, R = 0.1; $^{(3)}$ Stress amplitude σ_a = 200 MPa, R = 0.1.

Table 5 shows comparisons of predicted convergence condition with experimental results. In all model predictions, local microstructural parameters, φ and Φ, are averaged out to be 45° and 60° respectively. These presentations of local microstructural parameters have a limitation in the model application that each local feature is still pre-estimated rather than reasonably simulated in terms of local grain and grain structures although computer-assisted simulation of grain structures may provide necessary information for achieving the simulation. In spite of this, the averaged values for local microstructural parameters may be of advantage to characterising microstructure features that affect small fatigue crack growth, if compared with plastic zone size.

9.3 SUMMARY OF THE CHAPTER

- Lankford's qualitative criteria on convergence of growth rate of small fatigue cracks with that of long fatigue cracks is quantitatively modelled to be related to cyclic yield strength and local microstructure.

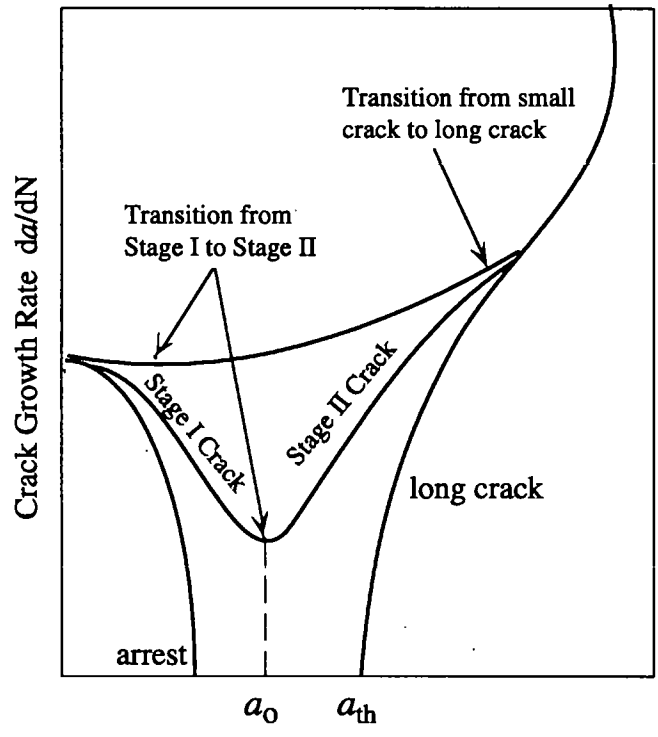

Figure 9-4 Schematic Illustration Of Kinetic Process Of Fatigue Crack Growth

- Convergence of small crack growth into long crack growth occurs when the plastic zone size is comparable to the controlling microstructural dimension which is not a material constant but dependent upon load level and local microstructure.

- Not only may the convergence condition (either ΔK_{con} or $2a_{con}$) determine a limit for preventing catastrophic fatigue failure but also a upper limit for integration of the small fatigue crack growth law to predict safe fatigue lifetime. In this respect,

fatigue damage tolerance may be effectively evaluated in terms of innovative idea of crack growth tolerance design.

- All model predictions for 7×××× aluminium alloys agree well with experimental measurements.

Implementation of predicting crack growth convergence brings to an end the systematic modelling of small fatigue crack propagation as illustrated by Figure 9-4. It is much anticipated to optimise fatigue life prediction method by integrating the developed small crack growth law and hence a rule for fatigue damage accumulation.

Chapter 10 PROMINENT CONCLUSIONS AND RECOMMENDATIONS FOR FUTURE WORK

10.1 PROMINENT CONCLUSIONS

More detailed conclusions have been outlined at the end of each chapter. Only the principal conclusions drawn from the research work for PhD are summarised in this section as follows:

(1) By employing surface replicating technique, it is difficult to judge whether or not growth rate drops to a minimum when small fatigue cracks meet the first grain boundary. There is no clear evidence to prove that the first grain boundary always most severely deters small fatigue crack propagation.

(2) It is suggested that the real crack trajectory should be taken as crack size to quantify fatigue damage in polycrystalline materials. Very lower small crack growth rates caused by blockage of barriers need to be carefully testified for aluminium alloys.

(3) A micromechanical relationship linking the evolution of normalised process zone $\frac{d^*}{\rho^*}$, which reflects local microstructure effect on small crack growth, with that of the normalised plastic zone $\frac{r_p}{a}$, which is associated with an advancing crack front, is decrived for growing small fatigue cracks. A micro-macro mechanical relationship in fatigue is proposed for small fatigue cracks.

(4) The process zone size d^* may be taken as a unified physical parameter to kinetically correlate fatigue crack growth rates.

(5) A dislocation-based micromechanical model is developed that predicts kinetics of small fatigue crack growth by using the novel unified physical parameter, *i.e.*, the process zone size, in conjunction with local microstructure.

(6) The unified model explains the origins of irregular crack growth rates due to slip band orientation and alloy strength dependence of small crack growth and, also explains microstructure dependence and load level dependence of Stage I to Stage II crack growth transition.

(7) The maximum stress level at the fatigue limit can be predicted by $\sigma_{FL.max} \approx 0.77\sigma_y'$. Fatigue crack growth thresholds can be quantitatively predicted in terms of the two fatigue threshold criteria (K^*_{max} and ΔK^*_{th}) that are modelled in Chapter 8. The two fatigue threshold criteria may directly demarcate non crack growth zone from crack growth zone for any load ratio without invoking crack closure.

(8) A upper limit condition for small fatigue crack propagation is quantitatively determined which, along with the modelled fatigue crack growth threshold may be used to quantify damage tolerance for fatigue life predictions.

(9) An engineering significance of all developed models is that predictions of kinetics of small fatigue crack growth in aluminium alloys and associate fatigue thresholds require only conventional bulk mechanical and fatigue properties. The effect of material conditions due to different heat treatments is reflected in the developed models by way of fatigue properties.

(10) All model-based quantitative predictions correlate reasonably with available data of experimental measurements. This indicates that the systematic modelling conducted in the present work may be of practical engineering applications.

10.2 REMARKS AND RECOMMENDATIONS

10.2.1 Remarks To Present Work

Compared with other models reviewed in Chapter 2, the present modelling has following improvements:

- The micro-macro mechanical relationship in connection with small fatigue crack growth is established that may provide convenience for engineering application.
- Slip band oricntation along with small crack front deflection is quantitatively incorporated into the modelling to reflect local microstructural effect.
- Local behaviour at an advancing small crack front is qualitatively and quantitatively interpreted, leading to a kinetic prediction of two crack growth transitions.
- Using conventional mechanical and fatigue properties can make the small crack growth law applicable to different load levels without individual fatigue tests for each load level.
- Fatigue limit and fatigue crack growth threshold phenomenon is coherently related to the non propagation microcracks.
- The present work has accomplished systematic characterisations for computer-assisted simulations which allow to predict the entire small crack growth process (from Stage I small fatigue cracks, Stage II small fatigue cracks, two crack growth transitions, to fatigue crack growth thresholds)

Particularly, the present work is attempted to develop a novel idea to simulate/model the kinetic nature associated with irregular small fatigue crack growth. Of technical and engineering prospect is to extend the fundamental modelling methodology to complex

loading conditions and other polycrystalline materials as a result of successfully systematic modelling of microscopic cracking in solids.

- The basic technical elements to construct this modelling methodology may be likely to be applied to other loading conditions (varying amplitude loading, overloading) and in principle to other fatigue-dominated environments, such as high temperature fatigue environment.

- The fundamental ideas adopted to simulate local microstructure, micro-macro mechanical relationship and dislocation pile-ups may be extended to other polycrystalline materials, such as steels and metal-matrix composites (MMCs) in some cases, because microscopic fatigue cracking behaviour in solids is inevitable to be inherently connected with macroscopic fatigue characteristics that can be determined by known conventional fatigue testing methods.

However, to optimise fatigue life predictions by using a crack growth tolerance technique, more research work on small fatigue cracks, particularly the experimental work that small fatigue cracks propagate across a plastic zone, still needs to be done which will be discussed in the following recommendations.

10.2.2 Recommendations For Future Work

Since fatigue failure is the result of fatigue crack growth, fatigue damage can thereby be equated to fatigue crack propagation, particularly to small fatigue crack propagation. Anyone who involves in this research domain may be aware of three objectives to achieve:

- An original idea is to accumulate fatigue damage by crack growth tolerance method;

- A strong motivation is to develop a well-grounded fatigue damage accumulation rule for engineering use to replace Miner's rule;

- A ultimate mission is to predict fatigue lifetime, particularly the remaining fatigue lifetimes.

Fresh ideas are needed indeed to develop futher reliable methods unaffected by uncertainties and get the small fatigue crack research out of the present awkward predicament. The fundamental problems need to be solved include:

- Seeking a unified physical parameter like ΔK for long fatigue cracks to correlate small fatigue crack growth.

  Seeking a unified physical parameter that links plastic deformation ahead of an advancing small crack front with crack size and a microstructural quantity becomes significant as demonstrated in previous chapters. In other words, if such a physical parameter is found (for instance, the process zone size d^* proposed in this thesis) and optimised, it is expected to establish an integral expression for $\frac{da}{dN}$ to kinetically predict small fatigue crack growth instead of individual small fatigue crack tests for each load level. This is one of reasons why this thesis is conducted in this way.

- Predicting small fatigue crack growth under complex loading conditions (service loading conditions);

  There are two problems here. First of all, standard Coffin-Manson relation is no longer applicable when applied loading varies because the fundamental stress-strain relation (*i.e.*, the shape of hysteresis loops) alters in each fatigue cycle. As a result, there is an interaction between loading cycles. For this reason, constitutive equations applicable to complex loading situation need to be properly developed.

  Secondly, once a high level load applies, such as an overload, it causes a large plastic zone surrounding small fatigue crack front that hinders small fatigue crack growth during a period of certain fatigue cycles. Consequently, small fatigue cracks may experience a fully plastically deformed zone until the plastic zone is

spanned. The retardation effect plus unusual propagation of small fatigue cracks in the plastic zone must be taken account in fatigue lifetime predictions.

- Notch effect on small fatigue crack growth;

  For most engineering components, small fatigue crack initiation and propagation are closely related to notch effect (or stress-raiser effect). Small crack tests of plain specimens do provide necessary crack growth information but fail to simulate notch effect that is more realistic in engineering. Fastener holes in aircraft wing frame, heat-proof grooves on steam turbine rotor shafts *etc.* are absolutely those that produce stress concentration. Unfortunately, inspection period for critical engineering components is to great extent dependent upon whether microcracks initiate at those stress concentration sites.

  With notch effect, small cracks may initiate and then propagate within a fully plastic region in where mechanism for small crack propagation still need to be experimentally and theoretically investigated. Up to today there is still a lack of sound physical models to describe small fatigue crack growth in a fully plastic region. This is a problem that limits application of small fatigue crack research to practical engineering. In general, small crack growth within a plastic zone caused by notch effect should be investigated.

- Statistical estimate of all stochastic microstructural features associated with polycrystalline materials. A probabilistic definition of local features (slip band orientation, crack front deflection) at an advancing fatigue crack front would be necessary.

The importance of structure integrity assessment for key engineering components will still take priority over other matters. To achieve an economic strength/weight ratio, microcracking is still to be a problem that any efficient application of advanced materials to key parts of sophisticated equipment will face on. Complex loading sequence or multiple

environments will be more and more inevitable to be used in space/ocean vehicles. For most materials (particularly the metal matrix composites) constitutive interrelations between microscopic crack growth and macroscopic physical quantities are still something interesting and unclear. Certainly, computational simulations as an effective means will open up a way to handle more complicated situations and provide a powerful assistance for modern fatigue designs.

Of particularly scientific and engineering significance is still to attain two goals, *i.e.*,

- preventing engineering components in service from any risk in premature failure;
- optimising crack growth tolerance methodology to predict fatigue lifetime of high confidence level.

To meet the needs of new challenges in fatigue design of modern structures, the structural integrity research may be directed to data-based computer-assisted simulations.

Appendix 1

It is considered a quasi-ellipse contained in an infinite elastic body subjected to uniform uniaxial tensile stress [see Figure I-1(a)]. The displacement function for this infinite body with an elliptical crack under uniaxial tension σ is given by relation [90]

$$2\mu(u+iv)=\kappa\phi(z)-\overline{\phi'(z)}\quad-\overline{\psi(z)}\quad . \tag{I-1}$$

where $\mu=\frac{E}{2(1+\upsilon)}$;

$\kappa=\frac{3-\upsilon}{1+\upsilon}$ in plain stress and $\kappa=3-4\upsilon$ in plain strain;

$\phi(z)$, $\psi(z)$ — the analytical complex functions.

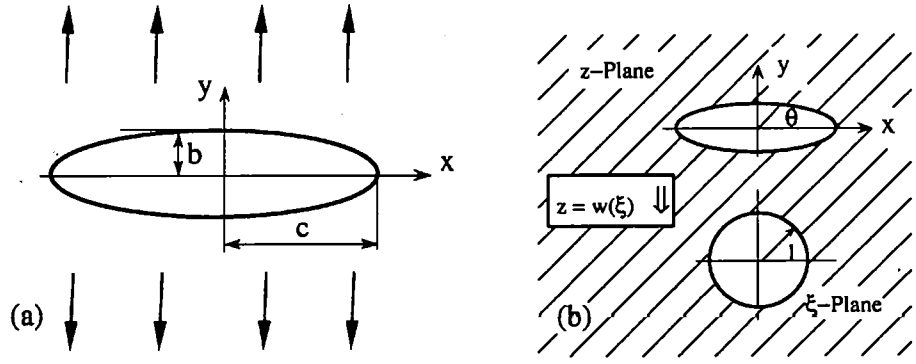

Figure I-1 Presentations Of (a) An Elliptical Microcrack In An Infinite Plate; And (b) Conformal Mapping Of An Ellipse To A Unit Circle

The solution of Equation I-1 is obtained by method of conformal mapping, transferring the ellipse in z–plane into a circle of unit radius in ξ–plane [see Figure I-1(b)] by the transformation

$$z = \omega(\xi) = \vartheta\left(\xi + \frac{M}{\xi}\right) \qquad M < 1. \tag{I-2}$$

where $\vartheta = \frac{c+b}{2}$;

$M = \frac{c-b}{c+b}$;

c, b — the semi-major and semi-minor axis of the ellipse respectively.

After necessary transformation, Equation I-1 becomes

$$2\upsilon\,(u + iv) = \kappa\,\phi(\xi) - \omega(\xi)\,\overline{\phi'(\xi)/\omega'(\xi)} - \overline{\psi(\xi)}\,. \tag{I-3}$$

Above equality can is solved by letting [176]

$$\phi(\xi) = \frac{\sigma\vartheta}{4}\left(\xi - \frac{2+M}{\xi}\right) \tag{I-4a}$$

$$\psi(\xi) = \frac{\sigma\vartheta}{2}\left(\frac{\xi^3 - (M^2 + 2M + 1)\,\xi - \xi^{-1}}{\xi^2 - M}\right). \tag{I-4b}$$

All complex functions, $\omega(\xi)$, $\phi(\xi)$, $\psi(\xi)$ and $\phi'(\xi)/\omega'(\xi)$, can be determined by taking $\xi = e^{i\theta}$ and substituting them into Equation I-4. The values of displacements can be calculated by separating the real part from imaginary part in Equation I-4 that is substituted. The imaginary parts in Equation I-4 is the displacement in y–direction. This displacement is expressed as,

$$v = \frac{\sigma\vartheta}{8\mu}\left(\frac{(3-5M+M^2+M^3)(1+\kappa)\sin\theta + 4(M^2+3M)(\kappa+1)\sin^3\theta}{1 - 2M + M^3 + 4M\sin^2\theta}\right) \tag{I-5}$$

where θ — the angle between any point of interest along the ellipse face and the major axis of the ellipse.

The crack opening displacement, δ, at any point of interest takes the value of 2v. Under plane strain condition ($\kappa=3-4\upsilon$), thus δ can be analytically expressed in the form of

$$\delta = \frac{\sigma\vartheta}{\mu}\left(\frac{(3-5M+M^2+M^3)(1-\upsilon)\sin\theta+2(M^2+3M)(1-\upsilon)\sin^3\theta}{1-2M+M^3+4M\sin^2\theta}\right) \quad \text{(I-6)}$$

Since crack is small it is reasonable to assume that this ellipse can be regarded as a 'line crack'. Thus c becomes the semi-crack length, a and $b\rightarrow 0$, consequently resulting in M= 1 and $\vartheta=\frac{a}{2}$. After these simplicities plus $x=a\cos\theta$, $\sin\theta=[1-(x/a)^2]^{1/2}$ in (x, y) co-ordinate system, the displacement in y-direction and crack opening displacement of this ellipse under plane strain condition ($\kappa=3-4\upsilon$) can be calculated by

$$v = (1-\upsilon^2)\sigma a\left(\frac{\sin\theta}{E}\right) \quad \text{(I-7a)}$$

$$\delta = \frac{2(1-\upsilon^2)}{E}\left(1-\left(\frac{x}{a}\right)^2\right)^{1/2}\sigma a\,. \quad \text{(I-7b)}$$

Equation I-7 is similar with Westergaard's crack opening displacement equation. When plastic zone of size r_p, that is a distance from the crack tip to the edge of the plastic zone, is formed at this elliptical crack tip it is considered an equivalent elastic elliptical crack whose tips in x-direction are located at the edge of the plastic zone. Therefore, δ is defined as the distance of separation of two faces of this equivalent crack due to its notional growth. The corresponding crack opening displacement of this equivalent crack is thus calculated by replacing a with $a+r_p$ in Equation I-7. However, since the crack is very small, the crack is embedded in a local plastically deformed region where the hypothesis of small scale yield is no longer applicable. Plenty of experimental research on notch-like crack [177-180] suggests that a crack mouth opening displacement (CMOP) may be adequate for a fully elastic-plastic condition to represent the actual crack tip opening displacement. To a surface small fatigue crack, this work therefore takes $x-a$ in the Equation I-7 to determine the effective crack tip opening displacement.

Appendix 2

Consider a surface microcrack of ellipse, as specified in Section 6.3.2 and Appendix 1. When a plastic zone of size r_p is generated at the microcrack tip, an equivalent elastic microcrack of size $2(a+r_p)$ is defined, replacing the elastic-plastic microcrack. The opening displacement (in y-direction) v of this equivalent elastic microcrack can be expressed by Equation 6-2. Therefore, the elastic strain at the boundary between the plastic zone and the elastic zone outside can be determined by

$$\left(\frac{\partial v}{\partial y}\right) = \frac{(1-\upsilon^2)\sigma}{E}(a+r_p)\left(\frac{\partial[\sin\theta]}{\partial y}\right)$$

$$= \frac{1}{\sqrt{x^2+y^2}} + \frac{y^2}{(x^2+y^2)^{-3/2}} \quad \text{(II-1)}$$

Since the major axis is relatively longer than the minor axis for the surface microcrack, the surface microcrack can be mathematically treated as a line crack, leading to

$$\left(\frac{\partial v}{\partial y}\right)_{(y\to 0)} = \frac{1}{x} \quad \text{(II-2)}$$

At the boundary, $x = a+r_p$, using Equation II-1, the elastic strain can be derived to be

$$\varepsilon_{(x=a+r_p)} = \frac{(1-\upsilon^2)\sigma}{E}(a+r_p)\left(\left(\frac{\partial v}{\partial y}\right)_{(y\to 0)}\right)_{(x=a+r_p)} = \frac{(1-\upsilon^2)\sigma}{E} \quad \text{(II-3)}$$

which is a constant, dependent upon the load level but independent of the microcrack size.

REFERENCES

1. K. J. Miller, *Proceedings of the Institution of Mechanical Engineers,* **205** 1-14 (1991)

2. K. J. Miller, *Fatigue Fract. Engng. Mater. Struct.*, **10** 75-91 (1987)

3. K. J. Miller, *Fatigue Fract. Engng. Mater. Struct.*, **10** 93-113 (1987)

4. K. Tanaka, *JSME International Journal,* 30 1-13 (1987)

5. J. Lankford, *Fatigue Fract. Engng. Mater. Struct.*, **8** 161-175 (1985)

6. J. Lankford, *Fatigue Fract. Engng. Mater. Struct.*, **5** 233-248 (1982)

7. J. Schijve, *Fatigue* 84, 751-771 (1984)

8. A. K. Zurek, M. R. James & M. L. Morris, *Metall. Trans.*, **14A** 1697-1705 (1984)

9. T. Hoshide, *et al*, *Engng. Fract. Mech.*, **21** 85-101 (1985)

10. M. S. Starkey, & R. P. Skelton, *Fatigue Fract. Engng. Mater. Struct.*, **5** 329-341 (1982)

11. K. S. Chan, & J. Lankford, *Scripta Metallurgica et Materialia*, **17** 529-532 (1983)

12. P. D. Hobson, M. W. Brown & E. R. de los Rios, Symposium on the behaviour of short fatigue cracks, EGF, Publication No.1, Eds. K. J. Miller & E. R. de los Rios, Mechanical Engineering Publications, London, 441-459 (1986)

13. A Navarro & E. R. de los Rios, *Fatigue Fract. Engng. Mater. Struct.*, **10** 169-186 (1987)

14. Z. Shaikh, Ph.D Thesis, University of Sheffield, (1991)

15. A. Navarro & E. R. de los Rios, *Fatigue Fract. Engng. Mater. Struct.*, **11** 383-396 (1988)

16. A. Navarro & E. R. de los Rios, *Fatigue Fract. Engng. Mater. Struct.*, **9** 373-378 (1986)

17. K. Hassan, E. R. de Los Rios & A. Navarro, *Engng. Fract. Mech.*, **44** 425-436 (1993)

18. H. Abdel-Raouf, T. H. Topper & A. Plumtree, *Scripta Metallurgica et Materialia*, **25** 597-602 (1991)

19. E. R. de los Rios, H. J. Mohammed & K. J. Miller, *Fatigue Fract. Engng. Mater. Struct.*, **8** 49-63 (1985)

20. A. Hunsche & P. Neumann, *Acta Metallurgica et Materialia.*, **34** 207-217 (1986)

21. K. Tokaji & T. Ogawa, *Fatigue Fract. Engng. Mater. Struct.*, **11** 331-342 (1988)

22. Z. S. Basinski & S. J. Basinski, *Acta Metallurgica et Materialia.*, **33** 1307-1317 (1985)

23. A. F. Blom, *et al*, Symposium on the behaviour of short fatigue cracks, EGF, Publication No.1, Eds. K. J. Miller & E. R. de los Rios, Mechanical Engineering Publications, London, 37-66 (1986)

24. H. Abdel-Raouf, T. H. Topper & A Plumtree, *Fatigue Fract. Engng. Mater. Struct.*, **15** 895-909 (1992)

25. A. J. McEvily, *JJSME International Journal Series I–Solid Mechanics Strength Of Materials*, **32** 181-191 (1989)

26. A. J. McEvily, *Engng. Fract. Mech.*, **40** 571-584 (1991)

27. M. H. Elhaddad, T. H. Topper & K. N. Smith, *Engng. Fract. Mech.*, **11** 573-584 (1979)

28. A. J. McEvily & K. Minakawa, *Engng. Fract. Mech.*, **28** 519-527 (1988)

29. J. W. Provan & Z. H. Zhai, *Int. J. Fatigue*. **13** 99-109 (1991)

30. J. W. Provan & Z. H. Zhai, *Int. J. Fatigue*, **13** 110-116 (1991)

31. D. Kujawski & F. Ellyin, Short Fatigue Cracks, ESIS13 , Edited by K. J. Miller & E. R. de los Rios , Mechanical Engineering Publications, London, 391-405 (1992)

32. Y. H. Zhang & L. Edwards, *Scripta Metallurgica et Materialia*, **26** 1901-1906 (1992)

33. H. Nisitani, M. Goto & N. Kawagoishi, *Fatigue* 90, 1067-1072 (1990)

34. S. Güngör & L. Edwards, *Mater. Sci. Engng*, **A160** 17-24 (1993)

35. F. Guiu & R. N. Stevens, *Fatigue Fract. Engng. Mater. Struct.*, **13** 625-635 (1990)

36. A. N. Vasjutin, *Fatigue Fract. Engng. Mater. Struct.*, **15** 203-212 (1992)

37. M. L. Bartlett & A. Saxena, *Engng. Fract. Mech.*, **23** 655-665 (1988)

38. K. Tokaji & T. Ogawa, *Fatigue Fract. Engng. Mater. Struct.*, **13** 411-421 (1990)

39. A. Plumtree & B. P. D. O'Connor, *Fatigue Fract. Engng. Mater. Struct.*, **14** 171-184 (1991)

40. N. M. Grinberg, *et al*, *Int. J. Fatigue*, **13** 370-376 (1991)

41. C. Kaynak & A. Ankara, *Engng. Fract. Mech.*, **43** 769-778 (1992)

42. J. C. Jr Newman, P. R. Edwards & H. Zocher, *An AGARD Cooperative Test Programme*, AGARD R-732 (1988)

43. N. H. Carvalho, M. de Freitas, AGARD R-76 (1990)

44. M. H. Swain, *et al*, *Short Crack Growth Behaviour in Various Aircraft Materials*, AGARD R-76 (1990)

45. Yang Jingiun, Pei Hongxun & Ke Wei, *Fatigue Fract. Engng. Mater. Struct.*, **13** 241-252 (1990)

46. T. Christman & S. Suresh, *Engng. Fract. Mech.*, **30** 953-964 (1986)

47. A. J. McEvily & Z. Tang, *Metall. Trans.*, **22** 1079-1082 (1991)

48. M. D. Halliday & C. J. Beevers, *The 3rd International Conference On Aluminium Alloys*, 626-532 (1992)

49. Y. Murakami, *JSME International Journal Series I–Solid Mechanics Strength Of Materials*, **32** 167-180 (1989)

50. Y. Murakami, S. Kofama & S. Konuma, *Int. J. Fatigue*, **11** 291-298 (1989)

51. Y. Murakami, S. Kofama & S. Konuma, *Int. J. Fatigue*, **11** 299-307 (1989)

52. P. Lukas, L. Kunz, B. Weiss & R. Stickler, *Fatigue Fract. Engng. Mater. Struct.*, **10** 187-201 (1987)

53. B. Weiss, R. Stickler & A. F. Blom, Short Fatigue Cracks, ESIS13 , Edited by K. J. Miller & E. R. de los Rios , Mechanical Engineering Publications, London, 423-438 (1992)

54. A Navarro & E. R. de los Rios, *Fatigue Fract. Engng. Mater. Struct.*, **10** 169-186 (1987)

55. A. D. Boyd-Lee & J. E. King, *Fatigue* 90, 1205-1210 (1990)

56. Y. Akiniwa, K. Tanaka & E. Matsui, *Mater. Sci. Engng.* **A104** 105-115 (1988)

57. M. Goto, *Fatigue Fract. Engng. Mater. Struct.*, **15** 953-963 (1992)

58. K. Tanaka, Y Akiniwa & M. Kinefuchi, *Fatigue* 90 2137-2142 (1990)

59. S. Z. Wang, K. J. Miller & E. R. de los Rios, *Fatigue Fract. Engng. Mater. Struct.*, **14** 351-368 (1991)

60. J. L. Bagdanoff & F. Kozin, *ASME Trans. J. Appl. Mech.*, **.49** 37-42 (1982)

61. K. Hassain & E. R. de los Rios, *Scripta Metallurgica et Materialia,* **30** 53-58 (1994)

62. P. Hyspecky & B. Strnadel, *Fatigue Fract. Engng. Mater. Struct.*, **15** 845-854 (1992)

63. E. Zaiken & R. O. Ritchie, *Metall. Trans.*, **16A** 1467-1477 (1985)

64. J. C. Newman, Jr, & I. S. Raju, *Engng. Fract. Mech.*, **15** 185-192 (1981)

65. K. N. Shivakumar & J. C. Newman, *Int. J. Fracture*, **57** R19-R25 (1992)

66. N. A. Mahmoud & A. Hosseini, *Engng. Fract. Mech.*, **24** 207-221 (1986)

67. L. Edwards & Y. H. Zhang, *Acta Metall. Mater.*, **42** 1413-1422 (1994)

68. Fuxing Yin, *et al*, *Trans.Metall*, **21A** 2282-2286 (1990)

69. Z. Mei & J. W. Morris, Jr, *Metall. Trans.*, **24A** 689-700 (1993)

70. J. Lankford, *Fatigue Fract. Engng. Mater. Struct.*, **6** 15-32 (1983)

71. K. Tanaka, Mechanics of small fatigue cracks. *Fatigue 93*. 355-364 (1993)

72. B. N. Leis, A. T. Hopper & J. Ahmad, *Engng. Fract. Mech.*, **23** 883-898 (1986)

73. M. Okazaki, T. Tabata & S. Nohmi, *Metall. Trans.*, **21A** 2201-2208 (1990)

74. D. J. Nicholls & J. W. Martin, *Fatigue Fract. Engng. Mater. Struct.*, **13** 83-94 (1990)

75. C. Kaynak & A. Ankara, *Engng. Fract. Mech.*, **43** 769-778 (1992)

76. J. Lankford, D. L. Davidson & K. S. Chan, *Metall. Trans.*, **15A** 1579-1588 (1984)

77. M. N. James & R. E. Garz, *Int. J. Fatigue*, **13** 169-173 (1991)

78. Y. Zhang, Small fatigue crack growth in high strength aluminium alloys. *Ph.D. Thesis*, The Open University, (1992)

79. Y. Akiniwa & K. Tanaka, *Mater. Sci. Engng.*, **A104** 105-115 (1988)

80. A. F. Blom, *et al*, *Symposium on the behaviour of short fatigue cracks, EGF, Publication No.1, Eds. K. J. Miller & E. R. de los Rios, Mechanical Engineering Publications, London,* 37-65 (1986)

81. M. Hirao, K. Tojo & H. Fukuoka, *Metall. Trans.*, **24A** 1773-1783 (1993)

82. T. S. Srivatsan, *Int. J. Fatigue*, **8** 201-208 (1986)

83. T. S. Srivatsan & E. J. Coyne Jr, *Mater. Sci. Tech.* , **5** 548-558 (1989)

84. T. S. Srivatsan, *Int. J. Fatigue* . **13** 313-321 (1991)

85. T. H. Sanders Jr & E. A. Starke Jr, *Metall Trans.* , **7A** 1407-1418 (1976)

86. T. H. Sanders Jr & E. A. Starke Jr, *Mater Sci. Engng.*, **28** 53-68 (1977)

87. H. C. Heikkenen, F. S. Lin & E. A. Starke Jr, *Mater Sci. Engng.*, **51** 17-23 (1981)

88. P. J. E. Forsyth, *Proceedings Of Crack Propagation Symposium*, Cranfield, The College of Aeronautics, Cranfield, UK, 76-94 (1962)

89. P. M. Hazzledine, Direct observation of anisotropic and surface effects on dislocations, Eds. by B. A. Bilby, K. J. Miller & J. R. Willis, Cambridge University Press, 384-399 (1984)

90. N. I. Muskhelishvili, Some Basic Problems Of The Mathematical Theory Of Elasticity. P. Noordhoff (1963)

91. D. N. Lai & V. Weiss, *Metall. Trans.*, **9A** 413-426 (1978)

92. J. Lanteigne & J. P. Bailon, *Metall. Trans.*, **12A** 459-466 (1981)

93. G. Glinka, *Int. J. Fatigue*, **4** 59-67 (1982)

94. T. R. Wilshaw, *J. Iron Steel Inst.*, **204** 936-942 (1966)

95. J. R. Rice & G. F. Rosengren, *J. Mech. Phys. Solids*, **16** 1-12 (1968)

96. R. Hill, The Mathematical Theory Of Plasticity, First edition, Oxford University Press, London, p.248 (1950)

97. Y. Zhang & L. Edwards, *Mater. Sci. Engng.*, **A188** 121-132 (1994)

98. A. Navarro & E. R. de los Rios, *Phil. Mag.*, **57** 15-36 (1988)

99. Xu-Dong Li & L. Edwards, *Theoretical & Applied Fracture Mechanics*, **23** 187-198 (1995)

100. X. J. Wu, Short fatigue crack behaviour of a submarine hull steel in inert and aggressive environments, Ph.D. Thesis, University Of Sheffield, January (1995)

101. J. W. Fash, D. F. Socie & D. L. McDowell, Multiaxial Fatigue ASTM STP **853** 497-513 (1985)

102. J. Telesman & S. D. Antolovich, *Engng. Fract. Mech.*, **24** 463-477 (1986)

103. K. T. Venkateswara Rao, W. Yu & R. O. Ritchie, *Metall. Trans.*, **19A** 563-569 (1988)

104. S. Güngör & L. Edwards, *7th International Conference on Fracture* in K.Salama etc. eds. **2** 1171-1178 (1989)

105. R. Bu & R. I. Stephens, *Fatigue Fract. Engng. Mater. Struct.*, **9** 35-48 (1986)

106. J. P. Hirth & J. Lothe, Theory Of Dislocations. McGraw-Hill, Inc., p.682 (1968)

107. S. M. Ohr & J. A. Horton, Defects Fracture And Fatigue, Eds. by G. C. Sih & J. W. Provan, Martinus Nijhoff Publishers, 3-15 (1983)

108. I. Kovács & L. Zsoldos, Dislocation And Plastic Deformation, Pergamon Press, p.156 (1973)

109. R. W. Lardner, Mathematical Theory Of Dislocations And Fracture, University of Toronto Press, Toronto, Chapter 6, (1974)

110. G. Venkataraman, Y-W. Chung, Y. Nakasone, & T. Mura, *Acta Metallurgica et Materialia.*, **38** 31-40 (1990)

111. J. R. Rice, Fatigue Crack Propagation, *ASTM STP* **415** P.170 (1967)

112. B. G. Journet, A. Lefrancois & A. Pineau, *Fatigue Fract. Engng. Mater. Struct.*, **12** 237-246 (1989)

113. J. Petit & G. Henaff, *Short Fatigue Cracks,* EGF, Publication, Eds. K. J. Miller & E. R. de los Rios, Mechanical Engineering Publications, London, 135-151 (1990)

114. W. L Morris & M. R. James, *Fatigue Crack Growth Threshold Concepts*, Edited by D. Davdson & S. Suresh, Proc. of the Inter. Symposium on Fatigue Crack Growth Threshold Concepts, 479-495 (1983)

115. J. Telesman & S. D. Antolovich, *Engng. Fract. Mech.*, **24** 453-462 (1986)

116. K. Minakawa, G. Levan & A. J. McEVILV, *Metall. Trans.*, **17A** 1787-1795 (1986)

117. J. R. Pickens, J. R. Gordon & J. A. S. Green, *Metall. Trans.*, **14A** 925-930 (1983)

118. D. Siglev, M. C. Montpetit & W. L. Haworth, *Metall. Trans.*, **14A** 931-938 (1983)

119. P. J. E. Forsyth & A. W. Bowen, *Int. J. Fatigue*, **3** 17-25 (1981)

120. C. Y. Kung & M. E. Dine, *Metall. Trans.*, **10A** 603-610 (1979)

121. S. Hiros & M. E. Fine, *Metall. Trans.*, **14A** 1189-1197 (1983)

122. R. J. H. Wanhill, *Engng. Fract. Mech.*, **30** 233-260 (1988)

123. W. L. Morris, M. R. James & O. Buck, *Metall. Trans.*, **12A** 57-64 (1981)

124. S. Güngör, Fatigue study in Al-Mg-Si alloys, Ph.D. Thesis, The Open University, October (1990)

125. S. S. Manson & U. Muralidharan, *Fatigue Fract. Engng. Mater. Struct.*, **9** 343-356 (1987)

126. J. Schijve, *Fatigue Fract. Engng. Mater. Struct.*, **12** 381-396 (1994)

127. J. Schijve, *JSME International Journal Series I — Solid Mechanics Strength Of Materials,* **34** 269-280 (1991)

128. W. J. Baxter & Pei-Chung Wang, *Metall. Trans.*, **21A** 1151-1159 (1990)

129. T. Mura, *Mater. Sci. Engng.*, **A176** 61-70 (1994)

130. K. S. Ravichandran & E. S. Dwarakadasa, *Acta Metall.. Mater.*, **39** 1343-1357 (1991)

131. L. Bartosiewicz & A. R. Krause, *Engng. Fract. Mech.*, **45** 463-477 (1993)

132. G. Marci, *Fatigue Fract. Engng. Mater. Struct.*, **17** 891-970 (1994)

133. C. R. Chiang, *Engng. Fract. Mech.*, **49** 29-33 (1994)

134. G. Glinka, *Engng. Fract. Mech.*, **21** 145-261 (1985)

135. Y. Murakami, *JSME International Journal Series I–Solid Mechanics Strength Of Materials*, **32** 167-178 (1989)

136, Y. Murakami & M. Endo, *Int. J. Fatigue*, **16** 163-182 (1994)

137, J. P. Hirth & J. Lothe, Theory Of Dislocations, Second edition, John Wiley & Sons, New York, (1982)

138. A. Nica, Mechanics Of Aerospace Materials, Elsevier Scientific Publishing Company, Oxford, (1981)

139. J. T. Staley, *Proceedings Of The 3rd International Conference On Aluminium Alloys*, 107-143 (1992)

140. W. J. Pardee, *et al*, Defects Fracture And Fatigue, Eds. by G. C. Sih & J. W. Provan, Martinus Nijhoff Publishers, 99-111 (1983)

141. K. S. Ravichandran, *Acta Metall.. Mater.* **39** 1331-1341 (1991)

142. D. Taylor, Fatigue Thresholds, Butterworths, London, (1989)

143. Y. Nakai, K. Tanaka & T. Nakanishi, *Engng. Fract. Mech.*, **15** 291-302 (1981)

144. M. Clavel & A. Pineau, *Mater. Sci. Engng.*, **55** 157-171 (1982)

145. R. D. Carter, *et al*, *Metall. Trans.*, **15A** 555-563 (1984)

146. W. L. Morris, M. R. James & A. K. Zurek, *Scripta Metallurgica et Materialia*, **19** 149-153 (1985)

147. J. E. King, *Mater. Sci. Tech.*, **3** 750-764 (1987)

148. P. Lukás & L. Kunz, Fatigue thresholds, *Fatigue 93* Vol.1 493-502 (1993)

149. S. Suresh, Fatigue Of Materials, Cambridge University Press, (1991)

150. R. W. Hertzberg, Deformation And Fracture Mechanics Of Engineering Materials, Third Edition, John Wiley & Sons, New York, (1989)

151. M. Creager & P. Paris, *Int. J. Fract. Mech.*, **3** 247-252 (1967)

152. H. Neuber, *Trans. ASME. J. Appl. Mech.*, **28** 544-550 (1961)

153. J. P. Bailon, M. Elboujdaini & J. I. Dickson, *Fatigue Crack Growth Threshold Concepts*, Edited by D. Davdson & S. Suresh, Proc. of the Inter. Symposium on Fatigue Crack Growth Threshold Concepts, 63-82 (1983)

154. T. Mura & J. Weertman, *Fatigue Crack Growth Threshold Concepts*, Edited by D. Davdson & S. Suresh, Proc. of the Inter. Symposium on Fatigue Crack Growth Threshold Concepts, 531-549 (1983)

155. P. E. Bretz, J. I. Petit & A. K. Vasudevan, *Fatigue Crack Growth Threshold Concepts*, Edited by D. Davdson & S. Suresh, Proc. of the Inter. Symposium on Fatigue Crack Growth Threshold Concepts, 163-183 (1983)

156. E. Zaiken & R. O. Ritchie, *Mater. Sci. Engng.*, **70** 151-160 (1985)

157. R. S. Vecchio, R. W Hertzberg, & R. Jaccard, *Scripta Metall. et Materialia*, **17** 343-346 (1983)

158. S. Suresh, A. K. Vasudévan & P. E. Bretz, *Metall. Trans.*, **15A** 369-379 (1984)

159. R. O. Richie, *et al*, *Fatigue Fract. Engng. Mater. Struct.*, **10** 343-362 (1987)

160. D. L. Chen, B. Weiss & R. Sticker, *Int. J. Fatigue*, **16** 485-491 (1994)

161. S. Suresh, *Fatigue Fract. Engng. Mater. Struct.*, **5** 133-150 (1982)

162. C. Robin & G. Pluvinage, *Fatigue Fract. Engng. Mater. Struct.*, **3** 147-157 (1982)

163. E. P. Phillips, *Mechanics Of Fatigue Crack Closure*, ASTM STP 982 505-515 (1988)

164. R. Pippan, H. P Stüwe & K. Golos, *Int. J. Fatigue* **16** 579-582 (1994)

165. T. S. Srivatsan, *Int. J. Fatigue* **8** 201-208 (1986)

166. T. S. Srivatsan & E. J. Coyne Jr, *Mater. Sci. Tech.* **5** 548-558 (1989)

167. T. S. Srivatsan, *Int. J. Fatigue* **13** 313-321 (1991)

168. T. S. Srivatsan, D. Lanning Jr & K. Soni, *Int. J. Fatigue* **15** 231-242 (1993)

169. T. S. Srivatsan, S. Anand & T. S. Sudarshan, *Mater. Sci. Tech.* **10** 640-646 (1994)

170. L. Edwards, A. K. Bush & J. W. Martin, *Mater. Sci. Tech.* **2** 823-828 (1986)

171. K. J. Miller, *Mater. Sci. Tech.*, **9** 453-461 (1993)

172. K. Hussain & E. R. de los Rios, *Scripta Metall. et Materialia*, **30** 53-58 (1994)

173. X. J. Xin, E. R. de los Rios & A. Navarro, Short Fatigue Cracks, ESIS 13 (*Eds. K. J. Miller & E. R. de los Rios*), *Mechanical Engineering Publications, London,* 369-389 (1992)

174. H. Nishitani & N. Kawagoishi, *JSME International Journal Series I–Solid Mechanics Strength Of Materials,* **35** 1-11 (1992)

175. D. Broek, Elementary Engineering Fracture Mechanics, Fourth revised edition, Kluwer Academic Publisher, 1986 London

176. P. Parker, The Mechanics Of Fracture And Fatigue. E. & F. N. Spon (1981)

177. C. R Pratap & R. K. Pandey, *Engng. Fract. Mech.*, **24** (1986) 539-552

178. C. R Pratap & R. K. Pandey, *Engng. Fract. Mech.*, **26** (1987) 811-824179. W. G. Reuter & W. R. Lloyd, *Surface-crack growth: Model, Experiments, and Structures,* ASTM STP 1060 (1990) 152-176

180. S. Bhattacharya & A. N. Kumar, *Engng. Fract. Mech.*, **40** (1991) 1089-1103

181. R. K. Bolingbroke & J. E. King, Symposium on the behaviour of short fatigue cracks, EGF, Publication No.1, Eds. K. J. Miller & E. R. de los Rios, Mechanical Engineering Publications, London, (1986) 101-120

182. K. J. Miller, *Fatigue Fract. Engng. Mater. Struct.*, **16** 931-939 (1993)

183. S. M. Ohr, *Mater. Sci. Engng.*, **72** (1985) 1-35

184. A. K. Vasudévan, K. Sadananda & N. Louat, *Mater. Sci. Engng.*, **A188** 1-22 (1994)

185. A. K. Vasudévan, K. Sadananda & N. Louat, *Scripta Metall. et Materialia*, **27** 1673-1678 (1992)

186. A. K. Vasudévan, K. Sadananda & N. Louat, *Scripta Metall. et Materialia*, **28** 65-70 (1992)

187. A. K. Vasudévan, K. Sadananda & N. Louat, *Scripta Metall. et Materialia*, **28** 837-842 (1992)

188. A. K. Vasudévan & K. Sadananda, *Metall. Trans.*, **26A** 1221-1234 (1995)

189. N. Louat, *et al*, *Metall. Trans.*, **24A** (1993) 2225-2232

190. Z. Shen, R. H. Wagoner & W. A. T. Clark, *Journal Of Metals*, **37** p.A30 (1985)

191. A. A. Rubinstein, *Mechanics Of Materials* , **5** 145-160 (1986)

192. Sham-Tsong Shiue, Tong-Yi Zhang & Sanboh Lee, *J. Mater. Res.*, **8** 1853-1857 (1993)

193. I. H. Lin, *Mater. Sci. Engng.*, **81** 325-335 (1986)

194. B. S. Majumdarand S. J. Burns, *Int. Fracture*, **21** 229-240 (1983)

195. E. R. de los Rios, A. Navarro & K. Hussain, *Short Fatigue Cracks*, ESIS 13 (Eds. by K. J. Miller & E. R. de los Rios), Mechanical Engineering Publications, London, 115-132 (1992)

196. G. C. Sih & E. T. Moyer, Jr., *Engng. Fract. Mech.*, **17** 269-280 (1983)

197. E. T. Moyer, Jr. & G. C. Sih, *Engng. Fract. Mech.*, **19** 643-652 (1984)

198. G. C. Sih & E. Madenci, Crack growth resistance characterised by the strain energy density function, *Engng. Fract. Mech.*, **18** 1159-1171 (1983)

199. G. C. Sih & D. Y. Jeong, *Theoretical & Applied Fracture Mechanics*, 141-151 (1990)

200. N. Ranganathan, *et al*, *Mater. Sci. Engng.*, **A187** 37-42 (1994)

201. K. J. Park, *et al*, *Mater. Sci. Engng.*, **A190** 99-108 (1995)

202. T. S. Srivatsan & T. A. Place, *J. Mater. Sci.*, **24** 1543-1551 (1889)

203. W. Zielinski, M. J. Li & W. W. Gerberich, *Acta Metall. Mater.*, **40** 2861-2871 (1992)

204. H. Mecking, Deformation Of Polycrystals, Mechanisms And Microstructures, Eds. by N. Hansen, *et al.*) Risø National Lab., Roskilde, p.73 (1981)

205. T. Leffers, Deformation Of Polycrystals, Mechanisms And Microstructures, Eds. by N. Hansen, *et al.*) Risø National Lab., Roskilde, p.55 (1981)

206. M. F. Ashby, Strengthening Methods In Crystals, eds. by A. Kelly and R. B. Nicholson, Elsevier, Amsterdam, p.173 (1971)

207. Zhonghao Jiang, Jianshe Lian & B. Baudelet, *Acta Metall. Mater.*, **43** 3349-3360 (1995)

208. A. K. Vasudévan, *et al*, *Mater. Sci. Tech.* **2** 1205-1209 (1986)

209. W. S. Miller, *et al*, *Mater. Sci. Tech.* **2** 1210-1216 (1986)

210. D. Kujawski & F. Ellyin, *Fatigue Fract. Engng. Mater. Struct.*, **16** 743-752 (1993)

211. H. Kitagawa & S. Takahashi, Proc. Second Int. Conf. on Mechanical Behabiour of Materials, Boston, ASM, p627 (1976)

212. J. R. Yates, W. Chang & K. J. Miller, *Fatigue Fract. Engng. Mater. Struct.*, **16** 351-362 (1993)

213. B. Tomkins, *Phil. Mag.*, **18** 1041-1066 (1968)

214. W. Zielinski, M. J. Lii and W. W. Gerberich, *Acta Metall. Mater.*, **40** 2861-2871 (1992)

215. H. Huang and W. W. Gerberich, *Acta Metall. Mater.*, **40** 2873-2881 (1992)

216. P. G. Mersh, *et al*, *Acta Metall. Mater.*, **40** 2883-2894 (1992)

217. A. K. Vasudévan, K. Sadananda, *Metall. Trans.*, **26A** 3199-3210 (1995)